

Contents

Supernova Remnants (SNR)

Primary particle acceleration above 100 TeV in the shell-type Supernova Remnant RX J1713.7–3946 with deep H.E.S.S. observations	6
H.E.S.S. observations of the supernova remnant RX J0852.0-4622: shell-type morphology and spectrum of a widely extended VHE gamma-ray source	10
H.E.S.S. observations of the supernova remnant RCW 86	14
Discovery of very high energy gamma-ray emission in the W 28 (G6.4–0.1) region, and multi-wavelength comparisons	18
The Monoceros very-high-energy gamma-ray source	22

Pulsar Wind Nebulae (PWN)

Crab nebula spectrum as seen by H.E.S.S.	26
Energy Dependent Morphology in the PWN candidate HESS J1825–137	30
Discovery of the candidate pulsar wind nebula HESS J1718-385 in very-high-energy gamma-rays	34
Morphological Studies of the PWN Candidate HESS J1809-193	38
New VHE emitting middle-age pulsar wind nebula candidates in the extended H.E.S.S. Galactic plane survey data	42
New Companions for the lonely Crab? VHE emission from young pulsar wind nebulae revealed by H.E.S.S.	46
Search for Pulsed VHE Gamma-Ray Emission from Young Pulsars with H.E.S.S.	50

Binaries

Observation of orbital modulation of the VHE emission from the binary system LS 5039 with H.E.S.S.	54
Report on TeV γ -Ray Observations of PSR B1259–63/SS2883 near the 2007 Periastron with the H.E.S.S. Stereoscopic System of Cherenkov Telescopes	58
A search for VHE γ -ray binaries in the H.E.S.S. Galactic Plane Scan	61

A Very High Energy γ-ray Survey of X-ray Binaries with H.E.S.S.	65
 Galactic Center	
Localising the H.E.S.S. Galactic Center point source	69
Simultaneous H.E.S.S. and Chandra observations of Sgr A* during an X-ray flare	73
Search for variability and QPO activity from SgrA* from H.E.S.S observations	77
 Survey	
The H.E.S.S. survey of the inner Galactic plane	80
Establishing a connection between high-power pulsars and very-high-energy gamma-ray sources	84
H.E.S.S. VHE Gamma-ray sources without identified counterparts	88
HESS J1023–575: Non-thermal particle acceleration associated with the young stellar cluster Westerlund 2	92
HESS sources possibly associated with massive star clusters	96
H.E.S.S. Galactic Plane Survey unveils a Milagro Hotspot	100
Search for very high energy gamma-ray emission from parts of the Gould belt with the H.E.S.S. ground based Cherenkov telescopes	104
 Active Galactic Nuclei (AGN)	
Long-Term VHE Gamma-Ray Monitoring of PKS 2155–304 with H.E.S.S. and Multiwavelength measurements, 2002-2005	106
A Spectacular VHE Gamma-Ray Outburst from PKS 2155-304 in 2006	110
Active Atmospheric Calibration for H.E.S.S. Applied to PKS 2155-304	114
Discovery of fast variability of the TeV γ-ray flux from the radio galaxy M 87 with H.E.S.S.	118
Multiwavelength observations of PKS 2005-489 and H 2356-309 with HESS	122
Multi-wavelength Observations of PG 1553+113 with HESS	126
Observations of 1ES 1101–232 with H.E.S.S. and at lower frequencies: A hard spectrum blazar and constraints on the extragalactic background light	130

Discovery of Two New TeV Blazars with the H.E.S.S. Cherenkov Telescope System	134
Discovery of VHE gamma-rays from the BL Lac object PKS 0548-322 with H.E.S.S.	138
Upper Limits from HESS Observations of AGN in 2005-2007	141
A search for Very High Energy γ-rayemission from Passive Super-massive Black Holes	145
Wide-range multiwavelength observations of northern TeV blazars with MAGIC/HESS, Suzaku and KVA	149
 Gamma-Ray Bursts (GRB)	
Simultaneous observation of GRB060602B with the H.E.S.S. Air Cherenkov array	153
Gamma-ray burst observations with the H.E.S.S. Air Cherenkov array	157
 Dark Matter	
Search for a Dark Matter annihilation signal from the Sagittarius dwarf galaxy with H.E.S.S.	161
The γ-radiation from the Galactic Center observed by H.E.S.S. and the possible dark matter interpretation	165
 Cosmic Rays	
Energy spectrum of cosmic iron nuclei measured by H.E.S.S.	169
Measurement of Cosmic Ray Electrons with H.E.S.S.	173
 Extended Extragalactic Objects	
H.E.S.S. observations of galaxy clusters	177
VHE γ-ray observations of starburst galaxies with H.E.S.S.	181



The H.E.S.S. Collaboration

F. AHARONIAN^{1,13}, A.G. AKHPERJANIAN², U. BARRES DE ALMEIDA⁸, A.R. BAZER-BACHI³, B. BEHERA¹⁴, M. BEILICKE⁴, W. BENBOW¹, K. BERNLÖHR^{1,5}, C. BOISSON⁶, O. BOLZ¹, V. BORREL³, I. BRAUN¹, E. BRION⁷, A.M. BROWN⁸, R. BÜHLER¹, T. BULIK²⁴, I. BÜSCHING⁹, T. BOUTELIER¹⁷, S. CARRIGAN¹, P.M. CHADWICK⁸, L.-M. CHOUNET¹⁰, A.C. CLAPSON¹, G. COIGNET¹¹, R. CORNILS⁴, L. COSTAMANTE^{1,28}, M. DALTON⁵, B. DEGRANGE¹⁰, H.J. DICKINSON⁸, A. DJANNATI-ATAÏ¹², W. DOMAINKO¹, L.O'C. DRURY¹³, F. DUBOIS¹¹, G. DUBUS¹⁷, J. DYKS²⁴, K. EGBERTS¹, D. EMMANOULOPOULOS¹⁴, P. ESPIGAT¹², C. FARNIER¹⁵, F. FEINSTEIN¹⁵, A. FIASSON¹⁵, A. FÖRSTER¹, G. FONTAINE¹⁰, M. FÜSSLING⁵, Y.A. GALLANT¹⁵, B. GIEBELS¹⁰, J.F. GLICENSTEIN⁷, B. GLÜCK¹⁶, P. GORET⁷, C. HADJICHRISTIDIS⁸, D. HAUSER¹, M. HAUSER¹⁴, G. HEINZELMANN⁴, G. HENRI¹⁷, G. HERMANN¹, J.A. HINTON²⁵, A. HOFFMANN¹⁸, W. HOFMANN¹, M. HOLLERAN⁹, S. HOPPE¹, D. HORNS¹⁸, A. JACHOLKOWSKA¹⁵, O.C. DE JAGER⁹, I. JUNG¹⁶, K. KATARZYŃSKI²⁷, E. KENDZIORRA¹⁸, M. KERSCHHAGGL⁵, B. KHÉLIFI¹⁰, D. KEOGH⁸, NU. KOMIN¹⁵, K. KOSACK¹, G. LAMANNA¹¹, I.J. LATHAM⁸, M. LEMOINE-GOUMARD¹⁰, J.-P. LENAIN⁶, T. LOHSE⁵, J.M. MARTIN⁶, O. MARTINEAU-HUYNH¹⁹, A. MARCOWITH¹⁵, C. MASTERSON¹³, D. MAURIN¹⁹, T.J.L. MCCOMB⁸, R. MODERSKI²⁴, E. MOULIN⁷, M. NAUMANN-GODO¹⁰, M. DE NAUROIS¹⁹, D. NEDBAL²⁰, D. NEKRASSOV¹, S.J. NOLAN⁸, S. OHM¹, J.-P. OLIVE³, E. DE OÑA WILHELM¹², K.J. ORFORD⁸, J.L. OSBORNE⁸, M. OSTROWSKI²³, M. PANTER¹, G. PEDALETTI¹⁴, G. PELLETIER¹⁷, P.-O. PETRUCCI¹⁷, S. PITA¹², G. PÜHLHOFER¹⁴, M. PUNCH¹², B.C. RAUBENHEIMER⁹, M. RAUE⁴, S.M. RAYNER⁸, M. RENAUD¹, J. RIPKEN⁴, L. ROB²⁰, S. ROSIER-LEES¹¹, G. ROWELL²⁶, B. RUDAK²⁴, J. RUPPEL²¹, V. SAHAKIAN², A. SANTANGELO¹⁸, R. SCHLICKEISER²¹, F.M. SCHÖCK¹⁶, R. SCHRÖDER²¹, U. SCHWANKE⁵, S. SCHWARZBURG¹⁸, S. SCHWEMMER¹⁴, A. SHALCHI²¹, H. SOL⁶, D. SPANGLER⁸, Ł. STAWARZ²³, R. STEENKAMP²², C. STEGMANN¹⁶, G. SUPERINA¹⁰, P.H. TAM¹⁴, J.-P. TAVERNET¹⁹, R. TERRIER¹², C. VAN ELDIK¹, G. VASILEIADIS¹⁵, C. VENTER⁹, J.P. VIALLE¹¹, P. VINCENT¹⁹, M. VIVIER⁷, H.J. VÖLK¹, F. VOLPE^{10,28}, S.J. WAGNER¹⁴, M. WARD⁸, A.A. ZDZIARSKI²⁴, A. ZECH⁶

¹Max-Planck-Institut für Kernphysik, P.O. Box 103980, D 69029 Heidelberg, Germany, ²Yerevan Physics Institute, 2 Alikhanian Brothers St., 375036 Yerevan, Armenia, ³Centre d'Etude Spatiale des Rayonnements, CNRS/UPS, 9 av. du Colonel Roche, BP 4346, F-31029 Toulouse Cedex 4, France, ⁴Universität Hamburg, Institut für Experimentalphysik, Luruper Chaussee 149, D 22761 Hamburg, Germany, ⁵Institut für Physik, Humboldt-Universität zu Berlin, Newtonstr. 15, D 12489 Berlin, Germany, ⁶LUTH, Observatoire de Paris, CNRS, Université Paris Diderot, 5 Place Jules Janssen, 92190 Meudon, France, ⁷DAPNIA/DSM/CEA, CE Saclay, F-91191 Gif-sur-Yvette, Cedex, France, ⁸University of Durham, Department of Physics, South Road, Durham DH1 3LE, U.K., ⁹Unit for Space Physics, North-West University, Potchefstroom 2520, South Africa, ¹⁰Laboratoire Leprince-Ringuet, Ecole Polytechnique, CNRS/IN2P3, F-91128 Palaiseau, France, ¹¹Laboratoire d'Annecy-le-Vieux de Physique des Particules, CNRS/IN2P3, 9 Chemin de Bellevue - BP 110 F-74941 Annecy-le-Vieux Cedex, France, ¹²Astroparticule et Cosmologie (APC), CNRS, Université Paris 7 Denis Diderot, 10, rue Alice Domon et Leonie Duquet, F-75205 Paris Cedex 13, France ¹³Dublin Institute for Advanced Studies, 5 Merrion Square, Dublin 2, Ireland, ¹⁴Landessternwarte, Universität Heidelberg, Königstuhl, D 69117 Heidelberg, Germany, ¹⁵Laboratoire de Physique Théorique et Astroparticules, CNRS/IN2P3, Université Montpellier II, CC 70, Place Eugène Bataillon, F-34095 Montpellier Cedex 5, France, ¹⁶Universität Erlangen-Nürnberg, Physikalisches Institut, Erwin-Rommel-Str. 1, D 91058 Erlangen, Germany, ¹⁷Laboratoire d'Astrophysique de Grenoble, INSU/CNRS, Université Joseph Fourier, BP 53, F-38041 Grenoble Cedex 9, France, ¹⁸Institut für Astronomie und Astrophysik, Universität Tübingen, Sand 1, D 72076 Tübingen, Germany, ¹⁹LPNHE, Université Pierre et Marie Curie Paris 6, Université Denis Diderot Paris 7, CNRS/IN2P3, 4 Place Jussieu, F-75252, Paris Cedex 5, France, ²⁰Institute of Particle and Nuclear Physics, Charles University, V Holesovickach 2, 180 00 Prague 8, Czech Republic, ²¹Institut für Theoretische Physik, Lehrstuhl IV: Weltraum und Astrophysik, Ruhr-Universität Bochum, D 44780 Bochum, Germany, ²²University of Namibia, Private Bag 13301, Windhoek, Namibia, ²³Obserwatorium Astronomiczne, Uniwersytet Jagielloński, Kraków, Poland, ²⁴Nicolaus Copernicus Astronomical Center, Warsaw, Poland, ²⁵School of Physics & Astronomy, University of Leeds, Leeds LS2 9JT, UK, ²⁶School of Chemistry & Physics, University of Adelaide, Adelaide 5005, Australia, ²⁷Toruń Centre for Astronomy, Nicolaus Copernicus University, Toruń, Poland, ²⁸European Associated Laboratory for Gamma-Ray Astronomy, jointly supported by CNRS and MPG



Primary particle acceleration above 100 TeV in the shell-type Supernova Remnant RX J1713.7–3946 with deep H.E.S.S. observations

D. BERGE^{1,2}, F. AHARONIAN^{2,3}, W. HOFMANN², M. LEMOINE-GOUMARD⁴, O. REIMER⁵, G. ROWELL⁶, H.J. VÖLK², FOR THE H.E.S.S. COLLABORATION

¹ CERN PH Department, CH-1211 Geneva 23, Switzerland

² Max-Planck-Institut für Kernphysik, P.O. Box 103980, D-69029 Heidelberg, Germany

³ Dublin Institute for Advanced Studies, 5 Merrion Square, Dublin 2, Ireland

⁴ Laboratoire Leprince-Ringuet, IN2P3/CNRS, Ecole Polytechnique, F-91128 Palaiseau, France

⁵ Stanford University, HEPL & KIPAC, CA 94305-4085, USA

⁶ School of Chemistry & Physics, University of Adelaide, Adelaide 5005, Australia

berge@cern.ch

Abstract: The shell-type supernova remnant RX J1713.7–3946 was observed during three years with the H.E.S.S. Cherenkov telescope system. The first observation campaign in 2003 yielded the first-ever resolved TeV gamma-ray image. Follow-up observations in 2004 and 2005 revealed the very-high-energy gamma-ray morphology with unprecedented precision and enabled spatially resolved spectral studies. Combining the data of three years, we obtain significantly increased statistics and energy coverage of the gamma-ray spectrum as compared to earlier H.E.S.S. results. We present the analysis of the data of different years separately for comparison and demonstrate that the telescope system operates stably over the course of three years. When combining the data sets, a gamma-ray image is obtained with a superb angular resolution of 0.06 degrees. The combined spectrum extends over three orders of magnitude, with significant gamma-ray emission approaching 100 TeV. For realistic scenarios of very-high-energy gamma-ray production, the measured gamma-ray energies imply efficient particle acceleration of primary particles, electrons or protons, to energies exceeding 100 TeV in the shell of RX J1713.7–3946.

Introduction

The energy spectrum of cosmic rays measured at Earth exhibits a power-law dependence over a broad energy range. Starting at a few GeV ($1 \text{ GeV} = 10^9 \text{ eV}$) it continues to energies of at least 10^{20} eV . The power-law index of the spectrum changes at two characteristic energies: in the region around $3 \times 10^{15} \text{ eV}$ – the *knee* region – the spectrum steepens, and at energies beyond 10^{18} eV it hardens again. Up to the knee, cosmic rays are believed to be of Galactic origin, accelerated in shell-type supernova remnants (SNRs) – expanding shock waves initiated by supernova explosions [11]. However, the experimental confirmation of an SNR origin of Galactic cosmic rays is difficult due to the propagation effects of charged particles in the interstellar medium. The most promising way of proving the existence of

high-energy particles in SNR shells is the detection of very-high-energy (VHE) gamma rays ($E > 100 \text{ GeV}$), produced in interactions of cosmic rays close to their acceleration site [9].

Recently the VHE gamma-ray instrument H.E.S.S. has detected two shell-type SNRs, RX J1713.7–3946 [1, 4] and RX J0852.0–4622 [2, 6]. The two objects show an extended morphology and exhibit a shell structure, as expected from the notion of particle acceleration in the expanding shock fronts. While it is difficult to attribute the measured VHE gamma rays unambiguously to nucleonic cosmic rays (rather than to cosmic electrons), the measured spectral shapes favour indeed in both cases a nucleonic cosmic-ray origin of the gamma rays [4, 6].

Apart from the first unambiguous proof of multi-TeV particle acceleration in SNRs, the question

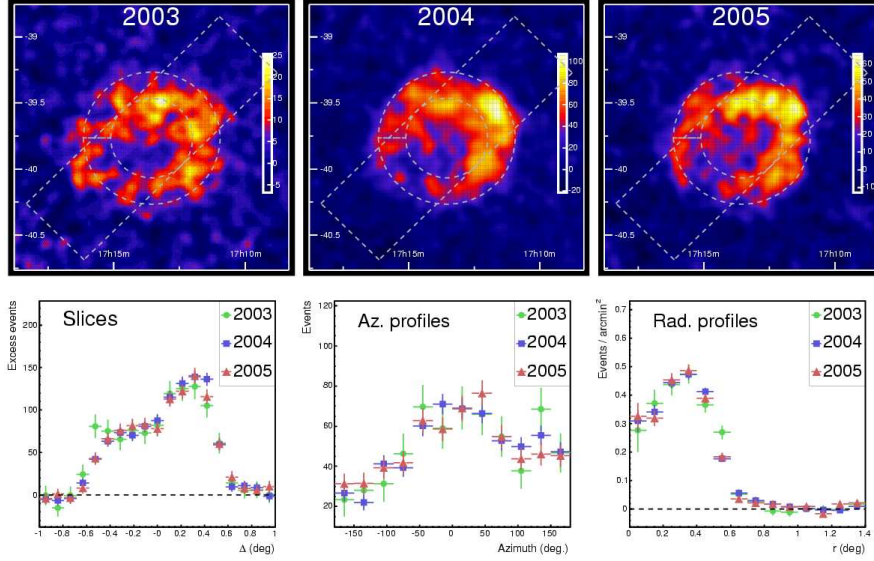


Figure 1: **Upper panel:** H.E.S.S. gamma-ray excess images from the region around RX J1713.7–3946 are shown for three years. **Lower panel:** 1D distributions generated from the non-smoothed, acceptance-corrected gamma-ray excess images.

of the highest observed energies remains an important one. Only the detection of gamma rays with energies of 100 TeV provides experimental proof of acceleration of primary particles, protons or electrons, to the *knee* region (1 PeV). Here we present a combined analysis of H.E.S.S. data of RX J1713.7–3946 of three years, from 2003 to 2005. A comparison of the three data sets demonstrates the expected steady emission of the source as well as the stability of the system. Special emphasis is then devoted to the high-energy end of the combined spectrum.

H.E.S.S. observations

The High Energy Stereoscopic System (H.E.S.S.) consists of four identical Cherenkov telescopes that are operated in the Khomas Highland of Namibia. Its large field of view of $\approx 5^\circ$ make H.E.S.S. the currently best suited experiment in the field for the study of extended VHE gamma-ray sources such as young Galactic SNRs.

The H.E.S.S. observation campaign of RX J1713.7–3946 started in 2003. The data were recorded during the commissioning phase of

the telescope system, with 2 out of the 4 telescopes operational. The data set revealed extended gamma-ray emission resembling a shell structure. It was actually the first ever resolved image of an astronomical source obtained with VHE gamma rays. In 2004, observations were conducted with the full telescope array. The H.E.S.S. data enabled analysis of the gamma-ray morphology and the spectrum of the remnant with unprecedented precision. A very good correlation was found between the X-ray and the gamma-ray image. The differential spectrum showed deviations from a pure power law at high energies. The 2005 observation campaign was aiming at extending the energy coverage of the spectrum to as high energies as possible. Therefore the observations were preferentially pursued at zenith angles larger than in the two years before to make use of the drastically increased effective collection area of the experiment at high energies. The analysis of these data are presented in the following (a more detailed discussion of this analysis can be found in [7]).

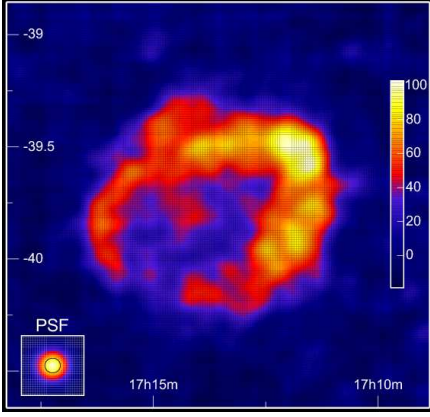


Figure 2: Combined H.E.S.S. image of the SNR RX J1713.7–3946 from the 2004 and 2005 data. A simulated point source (*PSF*) is also shown.

Analysis results

The analysis techniques used here are presented in detail elsewhere ([3, 8]). The gamma-ray morphology measured in three years is seen in the upper panel of Fig. 1. The images are readily comparable. Very similar angular resolutions are achieved for all years. Good agreement is achieved, as can also be seen from the 1D distributions shown in the lower panel, where also the statistical errors are plotted. Shown from left to right are a slice along a thick box (cf. Fig. 1, upper panel), an azimuthal profile of the shell region, and a radial profile. All the distributions are generated from the non-smoothed, acceptance-corrected excess images. Clearly, there is no sign of disagreement or variability, the H.E.S.S. data of three years are well compatible with each other.

The combined H.E.S.S. image is shown in Fig. 2. Data of 2004 and 2005 are used for this Gaussian smoothed ($\sigma = 2'$), acceptance-corrected gamma-ray excess image. In order to obtain optimum angular resolution, a special high-resolution analysis is applied here. Besides choosing only well reconstructed events, the cut on the minimum event multiplicity is raised to three telescopes, disregarding the 2003 data. Moreover, an advanced reconstruction method is chosen, *algorithm 3* of [10]. The image corresponds to 62.7 hours of observation time. 6702 gamma-ray excess events are measured with a statistical significance

of 48σ . An angular resolution of 0.06° ($3.6'$) is achieved. The image confirms nicely the published H.E.S.S. measurements [1, 4], with 20% better angular resolution and increased statistics. The shell of RX J1713.7–3946, somewhat thick and asymmetric, is clearly visible and almost closed. The gamma-ray brightest parts are located in the north and west of the SNR.

The gamma-ray spectra measured with H.E.S.S. in three consecutive years are compared to each other in Fig. 3 (left). In order to compare the data, a correction for the variation of optical efficiency of the telescopes over the years must be applied [5]. After that correction, very good agreement is found. The measured spectral shape remains unchanged over time. The absolute flux levels are well within the systematic uncertainty of 20%. As expected for an object like RX J1713.7–3946, no flux variation is seen on yearly timescales. Clearly, the performance of the telescope system is under good control.

The combined data of three years are shown in Fig. 3 (right). This energy spectrum of the whole SNR region corresponds to 91 hours of H.E.S.S. observations. The combined spectrum extends over almost three decades in energy beyond 30 TeV, and is compatible with previous H.E.S.S. measurements. Taking all events with energies above 30 TeV, the cumulative significance is 4.8σ . Different spectral models can be fit to the data. A pure power law is clearly ruled out, alternative spectral models like a power law with exponential cutoff, a broken power law, or a power law with energy-dependent index, all provide significantly better descriptions of the data, but none of these alternative models is favoured over the other.

Summary

The complete H.E.S.S. data set of the SNR RX J1713.7–3946 recorded from 2003 to 2005 is presented here. Very good agreement is found for both the gamma-ray morphology and the differential energy spectra over the years. The combined analysis confirms the earlier findings nicely: the gamma-ray image reveals a thick, almost circular shell with significant brightness variations. The spectrum follows a hard power law with significant deviations at higher energies (beyond a few TeV).

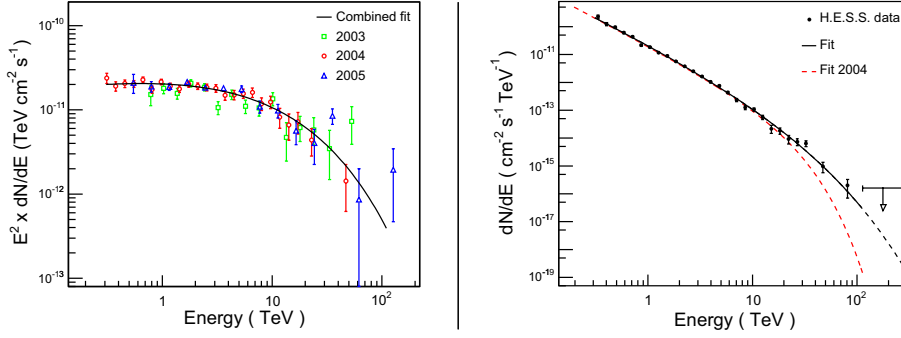


Figure 3: **Left:** Comparison of H.E.S.S. energy-flux spectra of three years. The black curve is the best fit of a power law with exponential cutoff to the combined data, as shown on the **right**, where the combined H.E.S.S. γ -ray spectrum of RX J1713.7–3946 is shown. The data are well described by the fit function, which is continued as dashed line beyond the fit range for illustration. The arrow is a model-independent upper limit, determined in the energy range from 113 to 300 TeV.

In the combined image using ~ 63 hours of H.E.S.S. observations an unprecedented angular resolution of 0.06° is achieved. The high-energy end of the combined spectrum approaches 100 TeV with significant emission (4.8σ) beyond 30 TeV. Given the systematic uncertainties in the spectral determination at these highest energies and comparable statistical uncertainties despite the long exposure time, this measurement is presumably close to what can be studied with the current generation of imaging atmospheric Cherenkov telescopes.

From the largest measured gamma-ray energies one can estimate the corresponding energy of the primary particles. In case of π^0 -decay gamma rays, energies of 30 TeV imply that primary protons are accelerated to $30 \text{ TeV}/0.15 = 200 \text{ TeV}$ in the shell of RX J1713.7–3946. On the other hand, if the gamma rays are due to Inverse Compton scattering of VHE electrons, the electron energies at the current epoch can be estimated in the Thompson regime as $E_e \approx 20 \sqrt{E_\gamma} \text{ TeV} \approx 110 \text{ TeV}$. At these large energies Klein–Nishina effects start to be important and reduce the maximum energy slightly such that $\sim 100 \text{ TeV}$ is a realistic estimate. RX J1713.7–3946 remains an exceptional SNR in respect of its VHE gamma-ray observability, being at present the remnant with the widest possible coverage along the electromagnetic spectrum. The H.E.S.S. measurement of significant gamma-ray emission beyond 30 TeV without indication

of a termination of the high-energy spectrum provides proof of particle acceleration in the shell of RX J1713.7–3946 beyond 10^{14} eV , up to energies which start to approach the region of the cosmic-ray *knee*.

References

- [1] Aharonian et al. (H.E.S.S. Collaboration). *Nature*, 432:75–77, November 2004.
- [2] Aharonian et al. (H.E.S.S. Collaboration). *A&A*, 437:L7, 2005.
- [3] Aharonian et al. (H.E.S.S. Collaboration). *A&A*, 430:865, February 2005.
- [4] Aharonian et al. (H.E.S.S. Collaboration). *A&A*, 449:223–242, 2006.
- [5] Aharonian et al. (H.E.S.S. Collaboration). *A&A*, 457:899–915, 2006.
- [6] Aharonian et al. (H.E.S.S. Collaboration). *ApJ*, 661:236–249, May 2007.
- [7] Aharonian et al. (H.E.S.S. Collaboration). *A&A*, 464:235–243, March 2007.
- [8] D. Berge, S. Funk, and J. Hinton. *A&A*, 466:1219–1229, May 2007.
- [9] L. O. Drury, F. A. Aharonian, and H. J. Voelk. *A&A*, 287:959–971, July 1994.
- [10] Hofmann et al. *Astroparticle Physics*, 12:135–143, November 1999.
- [11] A. M. Hillas. *Journal of Physics G Nuclear Physics*, 31:R95, May 2005.



H.E.S.S. observations of the supernova remnant RX J0852.0-4622: shell-type morphology and spectrum of a widely extended VHE gamma-ray source

M. LEMOINE-GOUMARD¹, F. AHARONIAN^{2,3}, B. DEGRANGE⁴, L. DRURY², U. SCHWANKE⁵, FOR THE H.E.S.S. COLLABORATION

¹*CENBG, Université Bordeaux I, CNRS-IN2P3, Le Haut-Vigneau, 33175 Gradignan, France*

²*Dublin Institute for Advanced Studies, 5 Merrion Square, Dublin, Ireland*

³*Max-Planck-Institut für Kernphysik, P.O. Box 103980, Heidelberg, Germany*

⁴*LLR, Ecole Polytechnique, CNRS-IN2P3, 91128 Palaiseau, France*

⁵*Institut für Physik, Humboldt-Universität zu Berlin, D 12489 Berlin, Germany*

lemoine@cenbg.in2p3.fr

Abstract: The shell-type supernova remnant RX J0852.0-4622 was detected in 2004 and re-observed between December 2004 and May 2005 with the High Energy Stereoscopic System (H.E.S.S.), an array of four Imaging Cherenkov Telescopes located in Namibia and dedicated to the observations of γ -rays above 100 GeV. The angular resolution of $< 0.1^\circ$ and the large field of view of H.E.S.S. (5° diameter) are well adapted to studying the morphology of the object in very high energy gamma-rays, which exhibits a remarkably thin shell very similar to the features observed in the radio range and in X-rays. The spectral analysis of the source from 300 GeV to 20 TeV will be presented. Finally, the possible origins of the very high energy gamma-ray emission (Inverse Compton scattering by electrons or the decay of neutral pions produced by proton interactions) will be discussed, on the basis of morphological and spectral features obtained at different wavelengths.

Introduction

Shell-type supernova remnants (SNR) are widely believed to be the prime candidates for accelerating cosmic rays up to 10^{15} eV, but until recently, this statement was only supported by indirect evidence, namely non-thermal X-ray emission interpreted as synchrotron radiation from very high energy electrons from a few objects. A more direct proof is provided by the detection of very high energy γ -rays, produced in nucleonic interactions with ambient matter or by inverse Compton scattering of accelerated electrons off ambient photons.

Here, we present recent data on RX J0852.0-4622 obtained with H.E.S.S. in 2004 and 2005.

The H.E.S.S. detector and the analysis technique

H.E.S.S. is an array of four 13 m diameter imaging Cherenkov telescopes located in the Khomas High-

lands in Namibia, 1800 m above sea level [11]. Each telescope has a tessellated mirror with an area of 107 m^2 [5] and is equipped with a camera comprising 960 photomultipliers [13] covering a field of view of 5° diameter. Due to the powerful rejection of hadronic showers provided by stereoscopy, the complete system (operational since December 2003) can detect point sources at flux levels of about 1% of the Crab nebula flux near zenith with a significance of 5σ in 25 hours of observation. This high sensitivity, the angular resolution of a few arc minutes and the large field of view make H.E.S.S. ideally suited for the study of the γ -ray morphology of extended sources. During the observations, an array level hardware trigger required each shower to be observed by at least two telescopes within a coincidence window of 60 ns [9]. The data were recorded in runs of typical 28 minute duration in the so-called “wobble mode”, where the source is offset from the center of the field of view, and were calibrated as described in detail in [4]. In a first stage, a standard image cleaning

was applied to shower images to remove the pollution due to the night sky background. The results presented in this paper were obtained using a 3D-modeling of the light-emitting region of an electromagnetic air shower, a method referred to as “the 3D-model analysis” [12], and were also cross-checked with the standard H.E.S.S. stereoscopic analysis based on the Hillas parameters of showers images [2]. The excess skymap was produced with a background subtraction called the “Weighting Method” [11]. In this method, the signal and the background are estimated simultaneously in the same portion of the sky. In each sky bin (treated independently), the signal and the background are estimated from those events originating from this bin exclusively; this is done by means of a likelihood fit in which each event is characterized by a discriminating parameter whose distribution is fairly different for γ -rays and hadrons. In the case of the 3D-Model, this discriminating parameter is the 3D-width of the electromagnetic shower.

H.E.S.S. results

RX J0852.0–4622 is a shell-type SNR discovered in the ROSAT all-sky survey. Its X-ray emission is mostly non-thermal [5]. Indeed, up to now no thermal X-rays were detected from this source, which could imply a limit on the density of the material in the remnant $n_0 < 2.9 \times 10^{-2} (D/1 \text{ kpc})^{-1/2} f^{-1/2} \text{ cm}^{-3}$, where f is the filling factor of a sphere taken as the emitting volume in the region chosen [14]. The X-ray non-thermal spectrum of the whole remnant in the 2–10 keV energy band is well described by a power law with a spectral index of 2.7 ± 0.2 and a flux $F_X = 13.8 \times 10^{-11} \text{ erg cm}^{-2} \text{ s}^{-1}$ [3]. In the TeV range, the announcement of a signal from the North-Western part of the remnant by CAN-GAROO was rapidly followed by the publication of a complete γ -ray map by H.E.S.S. obtained from a short period of observation (3.2 hours) [2]. The study of this source is really complex due to several points: its extension (it is the largest extended source ever detected by a Cherenkov telescope), its location at the South-Eastern corner of the Vela remnant and the uncertainty on its distance and age. Indeed, RX J0852.0–4622 could be as close as Vela ($\sim 250 \text{ pc}$) and possibly in in-

teraction with Vela, or as far as the Vela Molecular Ridge ($\sim 1 \text{ kpc}$). Figure 1 presents the γ -ray image of RX J0852.0–4622 obtained with the 3D-Model from a long observation in 2005 (corresponding to 20 hours live time). The morphology appearing from this skymap reveals a very thin shell of 1° radius and thickness smaller than 0.22° . Another interesting feature is the remarkably circular shape of this shell, even if the Southern part shows a more diffuse emission. Keeping all events inside a radius of 1° around the center of the remnant, the cumulative significance is about 19σ and the cumulative excess is ~ 5200 events. The overall γ -ray morphology seems to be similar to the one seen in the X-ray band, especially in the Northern part of the remnant where a brightening is seen in both wavebands. The correlation coefficient between the γ -ray counts and the X-ray counts in bins of $0.2^\circ \times 0.2^\circ$ is found to be equal to 0.60 and comprised between 0.54 and 0.67 at 95% confidence level. The differential energy spectrum (Fig. 2) extends from 300 GeV up to 20 TeV. The spectral parameters were obtained from a maximum likelihood fit of a power law hypothesis $dN/dE = N_0 (E/1 \text{ TeV})^{-\Gamma}$ to the data, resulting in an integral flux above 1 TeV of $(15.2 \pm 0.7_{\text{stat}} \pm 3.20_{\text{syst}}) \times 10^{-12} \text{ cm}^{-2} \text{ s}^{-1}$ and a spectral index of $2.24 \pm 0.04_{\text{stat}} \pm 0.15_{\text{syst}}$. An indication of curvature at high energy can be noticed.

Emission processes

One of the key issues is the interpretation of the γ -ray signal in terms of an electronic or a hadronic scenario. Despite the large uncertainty on the distance and age of the remnant, the multi-wavelength data already give some strong constraints. In a leptonic scenario, where γ -rays are produced by Inverse Compton scattering of high energy electrons off ambient photons, the ratio of the X-ray flux and the γ -ray flux determines the magnetic field to be close to $7 \mu\text{G}$. This value is completely independent of the distance and only assumes a filling factor (fraction of the Inverse Compton emitting electrons containing the magnetic field responsible for the synchrotron emission) of 1; this low magnetic field seems hardly compatible with the amplification suggested by the thin filaments resolved by

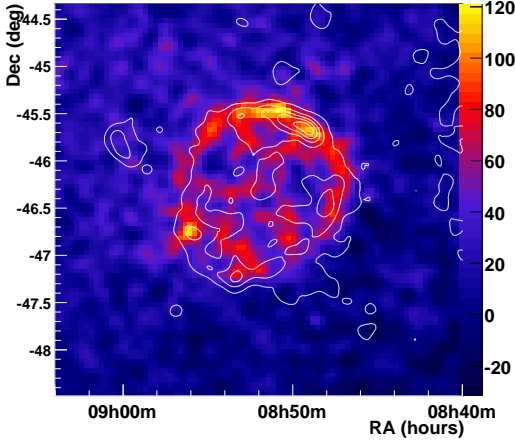


Figure 1: Excess skymap of RX J0852.0–4622 smoothed with a Gaussian of 0.06° standard deviation, obtained with the 3D-Model. The white lines are the contours of the X-ray data from the ROSAT All Sky Survey for energies higher than 1.3 keV (smoothed with a Gaussian of 0.06° standard deviation to enable direct comparison of the two images).

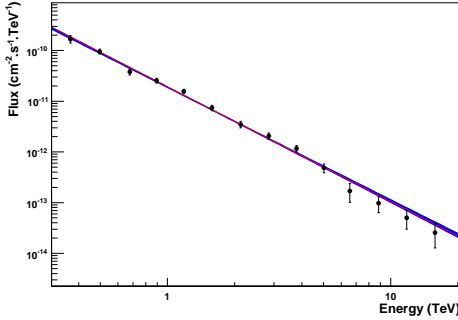


Figure 2: Differential energy spectrum of RX J0852.0–4622, for the whole region of the SNR. The shaded area gives the 1σ confidence region for the spectral shape under the assumption of a power law. The spectrum ranges from 300 GeV to 20 TeV.

Chandra [6]. In the nearby case (~ 200 pc), the limit on the width of the shell ΔR obtained by the morphological analysis of the H.E.S.S. data is $\Delta R < 0.7$ pc, which leads to an escape time by diffusion and by convection lower than both the age of the remnant and the synchrotron cooling time for energies higher than ~ 10 TeV. Therefore, one would expect to see a variation of the width of the shell with the energy, which is not observed by H.E.S.S. [3] and disfavours the electronic scenario at this distance. In a hadronic scenario, in which we assume that the γ -ray flux is entirely due to proton-proton interactions, one can estimate the total energy in accelerated protons in the range 10 – 100 TeV required to produce the γ -ray luminosity observed by H.E.S.S.:

$$\begin{aligned} L_\gamma(1 - 10 \text{ TeV}) &= 4\pi D^2 \int_{1 \text{ TeV}}^{10 \text{ TeV}} E \phi(E) dE \\ &= 2.6 \times 10^{32} \left(\frac{D}{200 \text{ pc}} \right)^2 \text{ erg s}^{-1} \end{aligned}$$

In this energy range, the characteristic cooling time of protons through the π^0 production channel is approximately independent of the energy and can be estimated to be: $\tau_\gamma = 4.4 \times 10^{15} \left(\frac{n}{1 \text{ cm}^{-3}} \right)^{-1}$. Assuming that the proton spectrum continues down to $E \approx 1$ GeV with the same spectral slope as that of the photon spectrum, the total energy injected into protons is estimated to be:

$$W_p^{\text{tot}} \approx 10^{49} \left(\frac{D}{200 \text{ pc}} \right)^2 \left(\frac{n}{1 \text{ cm}^{-3}} \right)^{-1} \text{ erg}$$

Therefore, for densities compatible with the absence of thermal X-rays, the only way to explain the entire γ -ray flux by proton-proton interactions in a homogeneous medium is to assume that RX J0852.0–4622 is a nearby supernova remnant ($D < 600$ pc). Indeed, for larger distances and a typical energy of the supernova explosion of 10^{51} erg, the acceleration efficiency would be excessive. Nevertheless, a distance of 1 kpc should also be considered if one assumes that RX J0852.0–4622 is the result of a core collapse supernova which exploded inside a bubble created by the wind of a massive progenitor star [7]. According to stellar wind theory, the size of the bubble evolves according to the formula: $R = 45 \left(\frac{n_0}{1 \text{ cm}^{-3}} \right)^{-0.2} \text{ pc}$. For a density of

1 cm^{-3} , the radius of this bubble would be equal to 45 pc. In the case of a close supernova remnant, its size would be significantly lower than the size of the bubble and the hypothesis of a homogeneous medium would be satisfactory. In the opposite, for larger distances ($D \sim 1 \text{ kpc}$), the presence of the Vela Molecular Ridge can produce a sudden increase of the density leading to a smaller bubble (15.6 pc for a density of 200 cm^{-3}), which would make the proton-proton interactions efficient at the outer shock.

Summary

We have firmly established that the shell-type supernova remnant RX J0852.0–4622 is a TeV emitter and for the first time we have resolved its morphology in the γ -ray range, which is highly correlated with the emission observed in X-rays. Its overall γ -ray energy spectrum extends over two orders of magnitude, providing the direct proof that particles of $\sim 100 \text{ TeV}$ are accelerated at the shock.

The question of the nature of the particles producing the γ -ray signal observed by H.E.S.S. was also addressed. In the case of a close remnant, the results of the morphological study combined with our spectral modeling highly disfavour the leptonic scenario which is unable to reproduce the thin shell observed by H.E.S.S. and the thin filaments resolved by Chandra. In the case of a medium distance, the explosion energy needed to explain the γ -ray flux observed by H.E.S.S., taking into account the limit on the density implied by the absence of thermal X-rays, would highly disfavour the hadronic process. At larger distances, both the leptonic and the hadronic scenario are possible, at the expense, for the leptonic process, of a low magnetic field of $\approx 7 \mu\text{G}$. Such a small magnetic field exceeds typical interstellar values only slightly and is difficult to reconcile with the theory of magnetic field amplification at the region of the shock.

However, at present, no firm conclusions can be drawn from the spectral shape. The results which should hopefully be obtained by GLAST or H.E.S.S. II at lower energies will therefore have a great interest for the domain.

Acknowledgements

The support of the Namibian authorities and of the University of Namibia in facilitating the construction and operation of H.E.S.S. is gratefully acknowledged, as is the support by the German Ministry for Education and Research (BMBF), the Max Planck Society, the French Ministry for Research, the CNRS-IN2P3 and the Astroparticle Interdisciplinary Programme of the CNRS, the U.K. Science and Technology Facilities Council (STFC), the IPNP of the Charles University, the Polish Ministry of Science and Higher Education, the South African Department of Science and Technology and National Research Foundation, and by the University of Namibia. We appreciate the excellent work of the technical support staff in Berlin, Durham, Hamburg, Heidelberg, Palaiseau, Paris, Saclay, and in Namibia in the construction and operation of the equipment.

References

- [1] F. Aharonian et al. (*H.E.S.S. Collaboration*). *Aph*, 22:109, 2004.
- [2] F. Aharonian et al. (*H.E.S.S. Collaboration*). *A&A*, 436:L7, 2005.
- [3] F. Aharonian et al. (*H.E.S.S. Collaboration*). *ApJ*, 661:236–249, 2007.
- [4] F. Aharonian (*H.E.S.S. Collaboration*). *Aph*, 22:109, 2004.
- [5] B. Aschenbach et al. *Nature*, 396:141, 1998.
- [6] A. Bamba, R. Yamazaki, and J.S. Hiraga. *ApJ*, 632:294, 2005.
- [7] E. G. Berezhko and H. J. Völk. *A&A*, 451:981, 2006.
- [8] K. Bernlöhr et al. *Aph*, 20:111, 2003.
- [9] S. Funk et al. *Aph*, 22:285, 2004.
- [10] J. A. Hinton. *NewAR*, 48:331, 2004.
- [11] M. Lemoine-Goumard and B. Degrange. In *Proceedings of “Towards a Network of Atmospheric Cherenkov Detectors VII”*, 2005.
- [12] M. Lemoine-Goumard et al. *Aph*, 25:195, 2006.
- [13] P. Slane et al. *ApJ*, 548:614, 2001.
- [14] P. Vincent (*H.E.S.S. Collaboration*). In *Proceedings of the 28th ICRC, T. Kajita et al., Eds. (Universal Academy Press, Tokyo, page 2887, 2003.*



H.E.S.S. observations of the supernova remnant RCW 86

S. HOPPE¹ & M. LEMOINE-GOUMARD² FOR THE H.E.S.S. COLLABORATION

¹*Max-Planck-Institut für Kernphysik, P.O. Box 103980, Heidelberg, Germany*

²*CENBG, Université Bordeaux I, CNRS-IN2P3, Chemin du Solarium, 33175 Gradignan, France*

hoppe@mpi-hd.mpg.de, lemoine@cenbg.in2p3.fr

Abstract: The shell-type supernova remnant (SNR) RCW 86 - possibly associated with the historical supernova SN 185 - was observed during the past three years with the High Energy Stereoscopic System (H.E.S.S.), an array of four atmospheric-Cherenkov telescopes located in Namibia. The multi-wavelength properties of RCW 86, e.g. weak radio emission and North-East X-ray emission almost entirely consisting of synchrotron radiation, resemble those of two very-high energy (VHE; > 100 GeV) γ -ray emitting SNRs RX J1713.7-3946 and RX J0852-4622. The H.E.S.S. observations reveal a new extended source of VHE γ -ray emission. The morphological and spectral properties of this new source will be presented.

Introduction

Shell-type supernova remnants are widely believed to be the prime candidates for accelerating cosmic rays up to 10^{15} eV. The most promising way of proving the existence of high energy particles accelerated in SNR shells is the detection of VHE γ -rays produced in nucleonic interactions with ambient matter. Recently, the H.E.S.S. instrument has detected VHE γ -ray emission from two shell-type SNRs, RX J1713.7-3946 [3] and RX J0852.0-4622 [1]. They both show an extended morphology highly correlated with the structures seen in X-rays. Although a hadronic origin is highly probable in the above cases, a leptonic origin can not be ruled out.

Another young shell-type SNR is RCW 86 (also known as G315.4-2.3 and MSH14-63). It has a complete shell in radio [9], optical [12] and X-rays [10], with a nearly circular shape of 40' diameter. It received substantial attention because of its possible association with SN 185, the first historical galactic supernova. However, strong evidence for this connection is still missing: using optical observations, Rosado et al. [11] found an apparent kinematic distance of 2.8 kpc and an age of 10 000 years, whereas recent observations of the North-East part of the remnant with the Chandra and XMM-Newton satellites strengthen the case

that the event recorded by the Chinese was a supernova and that RCW 86 is its remnant [14]. These observations also reveal that RCW 86 has properties resembling the already established TeV emitting SNRs mentioned above: weak radio emission and X-ray emission (almost) entirely consisting of synchrotron radiation, which could be due to the expansion of the shock in a wind blown bubble. The South-Western rim seems to be completely different, with hard X-ray emission, observed by ROSAT [6], mainly coming from stellar ejecta possibly interacting with circumstellar layers ejected before the SN explosion. The relatively large size of the remnant - about 40' in diameter - and the observation of non-thermal X-rays make it a promising target for γ -ray observations, aiming at increasing the currently modest number of remnants where the shells are resolved in VHE γ -rays. Hints for γ -ray emission from RCW 86 were seen with the CANGAROO-II instrument [16], but no firm detection was claimed. Here, we present recent data on RCW 86 obtained with the full H.E.S.S. array in 2005 and 2006.

The H.E.S.S. detector and the analysis technique

H.E.S.S. is an array of four imaging Cherenkov telescopes located 1800 m above sea level in the Khomas Highlands in Namibia [11]. Each telescope has a tessellated mirror with an area of 107 m² [5] and is equipped with a camera comprising 960 photomultipliers [13] covering a field of view of 5° diameter. Due to the effective rejection of hadronic showers provided by its stereoscopy, the complete system (operational since December 2003) can detect point sources at flux levels of about 1% of the Crab nebula flux near zenith with a statistical significance of 5 σ in 25 hours of observation [3]. This high sensitivity, the angular resolution of a few arc minutes and the large field of view make H.E.S.S. ideally suited for morphology studies of extended VHE γ -ray sources.

The data on RCW 86 were recorded in runs of typically 28 minutes duration in the so-called “wobble mode”, where the source is slightly offset from the center of the field of view. As a cross-check, the obtained data were analysed using two independent analysis chains, which share only the raw data. The first one is based on the combination of a semi-analytical shower model and a parametrisation based on the moment method of Hillas to yield the combined likelihood of the event being initiated by a γ -ray [7]. We will call this method the “Combined Model analysis” in the following. The second analysis method is the standard stereoscopic analysis based on the Hillas parameters of the shower images [10].

H.E.S.S. results

RCW 86 was observed for about 30 hours with the H.E.S.S. instrument with a mean zenith angle of 41°. Within a circular region of 27' radius (defined a priori so that it encompasses the whole remnant) around the centre of the SNR ($\alpha_{J2000} = 14^h42^m43^s$, $\delta_{J2000} = -62^\circ29'$), a clear VHE γ -ray signal with more than 9 standard deviations is detected with both analysis methods described above. The exact morphology of the gamma-ray emission is still under study: whereas one type of data analysis shows hints of a 3/4 shell re-

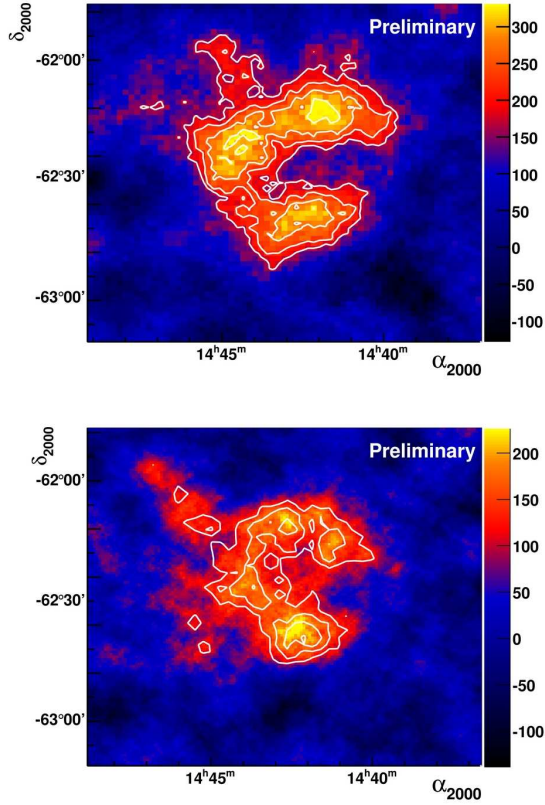


Figure 1: VHE γ -ray emission from RCW 86, as seen with H.E.S.S.. The top image shows the excess skymap obtained with the Combined Model analysis where shower images are matched against image templates, whereas the bottom image results from the classical, slightly less sensitive Hillas analysis technique. White contours correspond to 3, 4, 5, 6 sigma significance, obtained by counting gamma rays within 0.11° from a given location.

sembling the shape of the X-ray emission (Fig. 1 top, Fig 2), this morphology is not quite as evident with the other analysis technique (Fig. 1 bottom), and more data may be required to fully settle this issue. The differential energy spectrum of RCW 86, $\phi(E)$, was extracted from a circular region of diameter 22' around the position $\alpha_{J2000} = 14^h42^m12^s$, $\delta_{J2000} = -62^\circ24'$ which is – different from the region for which the detection significance was determined – adjusted to the H.E.S.S. data to include $\sim 90\%$ of the γ -ray excess. It is

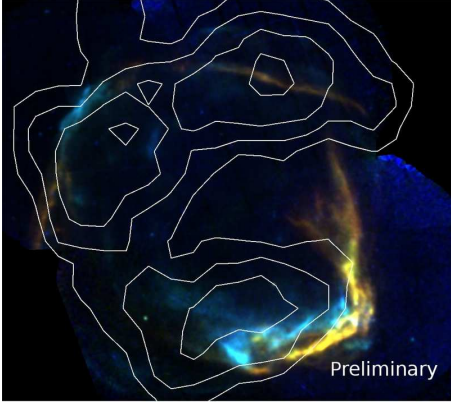


Figure 2: Significance contours of gamma-ray emission (from the Combined Model analysis; 3, 4, 5, 6 sigma) superimposed onto the XMM X-ray image of the remnant [14].

well described by a power-law with a spectral index of $\Gamma = 2.5 \pm 0.1_{\text{stat}}$ and a flux normalisation at 1 TeV of $\phi(1\text{TeV}) = (2.71 \pm 0.35_{\text{stat}}) \times 10^{-12} \text{cm}^{-2} \text{s}^{-1} \text{TeV}^{-1}$. The integral flux in the energy range 1 - 10 TeV is $\sim 8\%$ of the integrated flux of the Crab nebula within the same range. However, at this level of data statistics, a power-law with index $\Gamma \sim 1.9$ and an exponential cut-off at $E_c^\gamma \sim 5 \text{ TeV}$ is also a good fit to the data.

Discussion

There are two basic mechanisms for γ -ray production in young supernova remnants, inverse Compton scattering of high energy electrons off ambient photons (leptonic scenario) and π^0 mesons produced in inelastic interactions of accelerated protons with ambient gas decaying into γ -rays (hadronic scenario). The measured γ -ray flux spectrum from RCW 86 translates into an energy flux between 2 and 10 TeV of $3.4 \times 10^{-12} \text{erg cm}^{-2} \text{s}^{-1}$. In a leptonic scenario, the ratio of this energy flux and the X-ray flux between 2 and 10 keV ($1.7 \times 10^{-10} \text{erg cm}^{-2} \text{s}^{-1}$, see Winkler [17]) determines the magnetic field to be close to $22 \mu\text{G}$. This value, completely independent of the distance and age of the SNR, is compatible with the calculation made by J. Vink et al. [14] based on the thin filaments resolved by Chandra for a dis-

tance of 2.5 kpc in which he also deduces a high speed of the blast wave ($\sim 2700 \text{ km s}^{-1}$). However, it is more than ten times lower than the value proposed by H. J. Voelk and his colleagues [15] for the same distance using a much lower velocity of the shock of 800 km s^{-1} as suggested by optical data in the Southern region of the SNR [11].

In a hadronic scenario, one can estimate the total energy in accelerated protons W_p in the range 10 - 100 TeV required to produce the γ -ray luminosity L_γ observed by H.E.S.S. using the relation:

$$W_p(10 - 100\text{TeV}) \approx \tau_\gamma \times L_\gamma(1 - 10\text{TeV}) \quad (1)$$

in which $\tau_\gamma \approx 4.4 \times 10^{15} \left(\frac{n}{1 \text{ cm}^{-3}}\right)^{-1}$ is the characteristic cooling time of protons through the π^0 production channel. The corresponding L_γ can be calculated using:

$$\begin{aligned} L_\gamma(1 - 10 \text{ TeV}) &= 4\pi D^2 \int_{1 \text{ TeV}}^{10 \text{ TeV}} E \phi(E) dE \\ &= 2.8 \times 10^{31} \left(\frac{D}{200 \text{ pc}}\right)^2 \text{erg s}^{-1} \end{aligned}$$

Finally, the total energy injected in protons is calculated by extrapolating the proton spectrum with the same spectral shape as the photon spectrum down to 1 GeV. Therefore, this estimation is highly dependent on the shape of the γ -ray spectrum. Assuming that the proton spectrum is a power-law with index $\Gamma = 2.5$, one would obtain a total energy injected into protons of $W_p(\text{tot}) = 3 \times 10^{51} \left(\frac{D}{2.5 \text{ kpc}}\right)^2 \left(\frac{n}{1 \text{ cm}^{-3}}\right)^{-1} \text{erg}$. For densities of $\sim 1 \text{ cm}^{-3}$, the only way to explain the entire γ -ray flux by proton-proton interactions in a homogeneous medium is to assume that RCW 86 is a close supernova remnant ($\sim 1 \text{ kpc}$). Indeed, for larger distances and a typical energy of the supernova explosion of 10^{51} erg , the acceleration efficiency would be excessive. For an exponential cut-off power-law with $\Gamma = 1.9$ and $E_c = 10 \times E_c^\gamma = 50 \text{ TeV}$, the total energy injected into protons would be $10^{50} \left(\frac{D}{2.5 \text{ kpc}}\right)^2 \left(\frac{n}{1 \text{ cm}^{-3}}\right)^{-1} \text{erg}$ which would make the hadronic scenario possible even at larger distances. However, the observation of TeV gamma-rays from the remnant up to more than 10 TeV favors somewhat the scenario of a young - and therefore close-by - remnant with high expansion speed, easing the acceleration of high-energy particles.

Summary

H.E.S.S. observations have led to the discovery of the shell-type SNR RCW 86 in VHE γ -rays. The γ -ray signal is extended but the exact morphology of the emission region is still under study. The flux from the remnant is $\sim 8\%$ of the flux from the Crab nebula, with a similar spectral index of 2.5, but the spectrum is also well described by a power law with index 1.9 and a cutoff around 5 TeV. The question of the nature of the particles producing the γ -ray signal observed by H.E.S.S. was also addressed. However, at present, no firm conclusions can be drawn from the spectral shape.

Acknowledgements

The support of the Namibian authorities and of the University of Namibia in facilitating the construction and operation of H.E.S.S. is gratefully acknowledged, as is the support by the German Ministry for Education and Research (BMBF), the Max Planck Society, the French Ministry for Research, the CNRS-IN2P3 and the Astroparticle Interdisciplinary Programme of the CNRS, the U.K. Science and Technology Facilities Council (STFC), the IPNP of the Charles University, the Polish Ministry of Science and Higher Education, the South African Department of Science and Technology and National Research Foundation, and by the University of Namibia. We appreciate the excellent work of the technical support staff in Berlin, Durham, Hamburg, Heidelberg, Palaiseau, Paris, Saclay, and in Namibia in the construction and operation of the equipment.

References

- [1] F. Aharonian et al. *A&A*, 437:L7–L10, 2005.
- [2] F. Aharonian et al. *A&A*, 457:899–915, 2006.
- [3] F. Aharonian et al. *A&A*, 464:235–243, 2007.
- [4] F. Aharonian et al. (*H.E.S.S. Collaboration*). *A&A*, 430:865, 2005.
- [5] K. Bernlöhr et al. *APh*, 20:111, 2003.
- [6] F. Bocchino et al. *A&A*, 360:671, 2000.
- [7] M. de Naurois. In *Proceedings of “Towards a Network of Atmospheric Cherenkov Detectors VII”*, 2005.
- [8] J. A. Hinton. *NewAR*, 48:331, 2004.
- [9] M. J. Kesteven and J. L. Caswell. *A&A*, 183:118, 1987.
- [10] P. L. Pisarski et al. *ApJ*, 277:710, 1984.
- [11] M. Rosado et al. *A&A*, 315:243, 1996.
- [12] R. C. Smith. *AJ*, 114:2664, 1997.
- [13] P. Vincent (*H.E.S.S. Collaboration*). In *Proceedings of the 28th ICRC, T. Kajita et al., Eds. (Universal Academy Press)*, page 2887, 2003.
- [14] J. Vink et al. *ApJL*, 648:33, 2006.
- [15] H. J. Völk et al. *A&A*, 433:229, 2005.
- [16] S. Watanabe (*CANGAROO Collaboration*). In *Proceedings of the 28th ICRC, T. Kajita et al., Eds. (Universal Academy Press)*, 2003.
- [17] P. F. Winkler Jr. *ApJ*, 221:220, 1978.



Discovery of very high energy gamma-ray emission in the W 28 (G6.4–0.1) region, and multiwavelength comparisons

G. ROWELL^{1†}, E. BRION^{2†}, O. REIMER^{3†}, Y. MORIGUCHI⁴, Y. FUKUI⁴, A. DJANNATI-ATAÏ^{5†}, S. FUNK^{3†}

¹ *School of Chemistry & Physics, University of Adelaide, Adelaide 5005, Australia*

² *DAPNIA/DSM/CEA, CE Saclay, F-91191 Gif-sur-Yvette, Cedex, France*

³ *Stanford University, HEPL & KIPAC, Stanford, CA 94305-4085, USA*

⁴ *Department of Astrophysics, Nagoya University, Chikusa-ku, Nagoya 464-8602, Japan*

⁵ *APC, 11 Place Marcelin Berthelot, F-75231 Paris Cedex 05, France*

† *for the H.E.S.S. Collaboration www.mpi-hd.mpg.de/hfm/HESS*

growell@physics.adelaide.edu.au

Abstract: H.E.S.S. observations of the old-age ($>10^4$ yr; $\sim 0.5^\circ$ diameter) composite supernova remnant (SNR) W 28 reveal very high energy (VHE) γ -ray emission situated at its northeastern and southern boundaries. The northeastern VHE source (HESS J1801–233) is in an area where W 28 is interacting with a dense molecular cloud, containing OH masers, local radio and X-ray peaks. The southern VHE sources (HESS J1800–240 with components labelled A, B and C) are found in a region occupied by several HII regions, including the ultracompact HII region W 28A2. Our analysis of NANTEN CO data reveals a dense molecular cloud enveloping this southern region, and our reanalysis of EGRET data reveals MeV/GeV emission centred on HESS J1801–233 and the northeastern interaction region.

Introduction & H.E.S.S. Results

The study of shell-type SNRs at γ -ray energies is motivated by the idea that they are the dominant sites of hadronic Galactic cosmic-ray (CR) acceleration to energies approaching the *knee* ($\sim 10^{15}$ eV) and beyond, e.g. [34]. CRs are then accelerated via the diffusive shock acceleration (DSA) process (eg. [3, 31]). Gamma-ray production from the interaction of these CRs with ambient matter and/or electromagnetic fields is a tracer of such particle acceleration, and establishing the hadronic or electronic nature of the parent CRs in any γ -ray source is a key issue. Already, two shell-type SNRs, RX J1713.7–3946 and RX J0852.0–4622, exhibit shell-like morphology in VHE γ -rays [16, 18, 19] to 20 TeV and above. Although a hadronic origin of the VHE γ -ray emission is highly likely in the above cases, an electronic origin is not ruled out.

W 28 (G6.4–0.1) is a composite or mixed-morphology SNR, with dimensions $50' \times 45'$ and an estimated distance between 1.8 and 3.3 kpc (eg.

[4, 33]). It is an old-age SNR (age 3.5×10^4 to 15×10^4 yr [11]), thought to have entered its radiative phase of evolution [33]. The shell-like radio emission [27, 23] peaks at the northern and northeastern boundaries where interaction with a molecular cloud [2] is established [35, 36]. The X-ray emission, which overall is well-explained by a thermal model, peaks in the SNR centre but has local enhancements in the northeastern SNR/molecular cloud interaction region [25]. Additional SNRs in the vicinity of W 28 have also been identified: G6.67–0.42 and G7.06–0.12 [21]. The pulsar PSR J1801–23 with spin-down luminosity $\dot{E} \sim 6.2 \times 10^{34}$ erg s $^{-1}$ and distance $d \geq 9.4$ kpc [28], is at the northern radio edge.

Given its interaction with a molecular cloud, W 28 is an ideal target for VHE observations. This interaction is traced by the high concentration of 1720 MHz OH masers [6, 5, 29], and also the location of very high-density ($n > 10^3$ cm $^{-3}$) shocked gas [36, 35]. Previous observations of the W 28 region at VHE energies by the CANGAROO-I tele-

scope revealed no evidence for such emission [13] from this and nearby regions.

The High Energy Stereoscopic System (H.E.S.S.: see [24] for details and performance) has observed the W 28 region over the 2004, 2005 and 2006 seasons. After quality selection, a total of ~ 42 hr observations were available for analysis. Data were analysed using the moment-based Hillas analysis procedure employing *hard cuts* (image size > 200 p.e.), the same used in the analysis of the inner Galactic Plane Scan datasets [15, 17]. An energy threshold of ~ 320 GeV results from this analysis. The VHE γ -ray image in Fig. 1 shows that two source of VHE γ -ray emission are located at the northeastern and southern boundaries of W 28. The VHE sources are labelled HESS J1801–233 and HESS J1801–240 where the latter can be further subdivided into three components A, B, and C. The excess significances of both sources exceed $\sim 8\sigma$ after integrating events within their fitted, arcminute-scale sizes. Similar results were also obtained using an alternative analysis [7].

W 28: The Multiwavelength View

We have revisited EGRET MeV/GeV data, including data from the CGRO observation cycles (OC) 1 to 6, which slightly expands on the dataset of the 3rd EGRET catalogue (using OCs 1 to 4; [9], revealing the source 3EG J1800–2338. We find a pointlike $E > 100$ MeV source in the W 28 region, labelled GRO J1801–2320 in Fig 1. The 68% and 95% location contours of GRO J1801–2320 match well the location of HESS J1801–233. However we cannot rule out a connection to HESS J1800–240 due to the degree-scale EGRET PSF.

Fig. 2 presents ^{12}CO ($J=1-0$) observations from the NANTEN [1] Galactic Plane survey [12] covering the line-of-sight velocity ranges $V_{\text{LSR}} = 0$ to 10 km s^{-1} and 10 to 20 km s^{-1} . These ranges represent distances 0 to ~ 2.5 kpc and 2.5 to ~ 4 kpc respectively and encompass the distance estimates for W 28. We cannot rule out however, distances ~ 4 kpc for the $V_{\text{LSR}} > 10 \text{ km s}^{-1}$ cloud components. It is clear that molecular clouds coincide well with the VHE sources. The northeast-

ern cloud $V_{\text{LSR}} < 10 \text{ km s}^{-1}$ component near HESS J1801–233, is already well-studied [35, 36]. Contributions from the $V_{\text{LSR}} > 10 \text{ km s}^{-1}$ cloud components are also likely. The molecular cloud to the south of W 28 coincides well with HESS J1800–240 and its three VHE components. The $V_{\text{LSR}} < 10 \text{ km s}^{-1}$ component of this cloud coincides well with HESS J1800–240B, and may represent the dense molecular matter surrounding the ultra-compact HII region W 28A2. This cloud also extends to $V_{\text{LSR}} \sim 20 \text{ km s}^{-1}$ and thus, similar to HESS J1801–233, the total VHE emission in HESS J1800–240 may result from several molecular cloud components in projection.

Fig. 3 compares the radio (left panel — VLA 90 cm [8]), infrared and X-ray views (right panel MSX 8.28 μm and ROSAT PSPC 0.5 to 2.4 keV [25]) with the VHE results. HESS J1801–233 overlaps the northeastern shell of the SNR, coinciding with a strong peak in the 90 cm continuum emission. Additional SNRs G6.67–0.42 and G7.06–0.12 [21, 10] are indicated. The non-thermal radio arc G5.71–0.08 is a SNR candidate [8], and is possibly a counterpart to HESS J1801–240C. The distances to G6.67–0.42 and G5.71–0.08 are presently unknown. The unusual, ultracompact HII region W 28A2, is positioned within 0.1° of the centroid of HESS J1800–240B. W 28A2, at a distance $d \sim 2$ kpc, exhibits energetic bipolar molecular outflows [30, 26, 14] and may therefore be an energy source for particle acceleration in the region. The other HII regions G6.1–0.6 [32] and G6.225–0.569 [22] are also associated with radio emission.

The X-ray morphology (Fig. 3 right panel) shows the central concentration of X-ray emission. A local X-ray peak or *Ear* is seen at the northeastern W 28 boundary. The HII regions, W 28A2 and G6.1–0.6 are prominent in the MSX 8.28 μm image (Fig. 3 right panel), indicating that a high concentration of heated dust still surrounds these very young stellar objects.

Discussion and Conclusions

H.E.S.S. and NANTEN observations reveal VHE emission in the W 28 region spatially coincident with molecular clouds. The VHE emission and

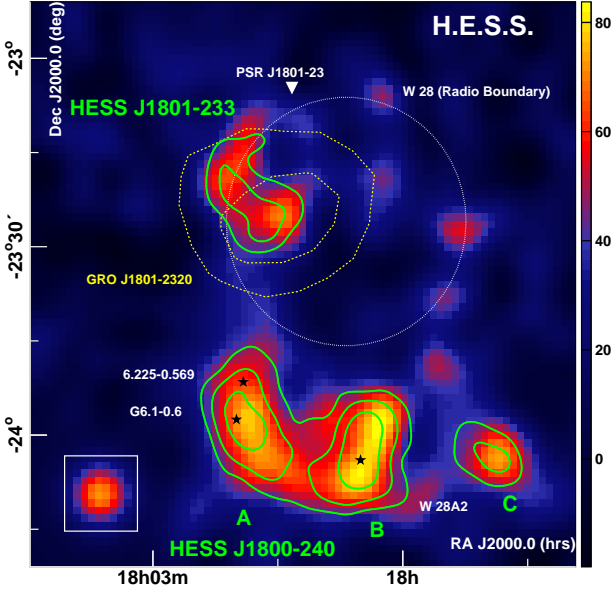


Figure 1: H.E.S.S. VHE γ -ray excess counts, corrected for exposure and Gaussian smoothed (with 4.2' std. dev.). Solid green contours represent excess significance levels of 4, 5, and 6 σ , for an integrating radius $\theta=0.1^\circ$. The VHE sources HESS J1801–233 and a complex of sources HESS J1800–240 (A, B & C) are indicated. The thin-dashed circle depicts the approximate radio boundary of the SNR W 28 [23, 8]. Additional objects indicated are: HII regions (black stars); W 28A2, G6.1–0.6 6.225–0.569; The 68% and 95% location contours (thick-dashed yellow lines) of the $E > 100$ MeV EGRET source GRO J1801–2320; the pulsar PSR J1801–23 (white triangle). The inset depicts a pointlike source under identical analysis and smoothing as for the main image.

molecular clouds are found at the northeastern boundary, and $\sim 0.5^\circ$ south of W 28 respectively. The SNR W 28 may be a source of power for the VHE sources, although there are additional potential particle accelerators in the region such as other SNR/SNR-candidates, HII regions and open clusters. Further details concerning these results and discussion are presented in [20].

Acknowledgements

The support of the Namibian authorities and of the University of Namibia in facilitating the construction and operation of H.E.S.S. is gratefully acknowledged, as is the support by the German Ministry for Education and Research (BMBF), the Max Planck Society, the French Ministry for Research, the CNRS-IN2P3 and the Astroparticle Interdisciplinary Programme of the CNRS, the U.K. Particle Physics and Astronomy Research Council (PPARC), the IPNP of the Charles University, the Polish Ministry of Science and Higher Education, the South African Department of Science and Technology and National Research Foundation, and by the University of Namibia. We appreciate the excellent work of the technical support staff in Berlin, Durham, Hamburg, Heidelberg, Palaiseau, Paris, Saclay, and in Namibia in the construction and operation of the equipment. The NANTEN project is financially supported from JSPS (Japan Society for the Promotion of Science) Core-to-Core Program, MEXT Grant-in-Aid for Scientific Research on Priority Areas, and SORST-JST (Solution Oriented Research for Science and Technology: Japan Science and Technology Agency). We also thank Crystal Brogan for the VLA 90 cm image.

References

- [1] Mizuno A. and Fukui Y. *ASP Conf. Proc.*, 317:59, 2004.
- [2] Wootten A. *ApJ*, 245:105, 1981.
- [3] Bell A.R. *MNRAS*, 182:443, 1978.
- [4] Goudis C. *Ap&SS*, 40:91, 1976.
- [5] Claussen M.J. and Frail D.A., Goss W.M., and Gaume R.A. *ApJ*, 489:143, 1997.
- [6] Frail D.A., Goss W.M., and Slysh V.I. *ApJ*, 424:L111, 1994.
- [7] de Naurois M. *arXiv:astro-ph/0607247*, 2006.
- [8] Brogan C.L. et al. *ApJ*, 639:L25, 2006.
- [9] Hartman R.C. et al. *ApJ (Supp)*, 123:79, 1999.
- [10] Helfand D.J. et al. *AJ*, 131:2525, 2006.
- [11] Kaspi V.M. et al. *ApJ*, 409:L57, 1993.
- [12] Matsunaga K. et al. *PASJ*, 53:1003, 2001.
- [13] Rowell G.P. et al. *A&A*, 359:337, 2000.
- [14] Sollins P.K. et al. *ApJ*, 616: L35, 2004.
- [15] Aharonian F. et al. (H.E.S.S. Collab.). *Science*, 307:1938, 2005.
- [16] Aharonian F. et al. (H.E.S.S. Collab.). *A&A*, 449:223, 2006.
- [17] Aharonian F. et al. (H.E.S.S. Collab.). *ApJ*, 636:777, 2006.
- [18] Aharonian F. et al. (H.E.S.S. Collab.). *ApJ*, 661:236, 2007.
- [19] Aharonian F. et al. (H.E.S.S. Collab.). *A&A*, 464:235, 2007.
- [20] Aharonian F. et al. (H.E.S.S. Collab.). *A&A*, submitted, 2007.
- [21] Yusef-Zadeh F., Shure M., Wardle M., and Kassim N. *ApJ*, 540:842, 2000.
- [22] Lockman F.J. *ApJ (Supp)*, 71:469, 1989.
- [23] Dubner G.M., Velázquez P.F., and Holdaway M.A. Goss W.M. *AJ*, 120:1933, 2000.
- [24] Hinton J.A. *New Astron. Rev.*, 48:331, 2004.
- [25] Rho J.H. and Borkowski K. *ApJ*, 575:201, 2002.
- [26] Acord J.M., Walmsley C.M., and Churchwell E. *ApJ*, 475:693, 1997.
- [27] Long K.S., Blair W.P., White R.L., and Matsui Y. *ApJ*, 373:567, 1991.
- [28] Claussen M.J., W.M. Goss, Desai K.M., and Brogan C.L. *ApJ*, 580:909, 2002.
- [29] Claussen M.J., Goss W.M., Frail D.A., and Desai K. *ApJ*, 522:349, 1999.
- [30] Harvey P.M. and Forveille T. *A&A*, 197:L19, 1988.
- [31] Blandford R.D. and Ostriker J.P. *ApJ*, 221:L29, 1978.
- [32] Kuchar T.A. and Clark F.O. *ApJ*, 488:224, 1997.
- [33] Lozinskaya T.A. *Sov. Astron. Lett.*, 7:17, 1981.
- [34] Ginzburg V.L. and S.I. Syrovatskii. *The Origin of Cosmic Rays*. (New York: Macmillan), 1964.
- [35] Reach W.T., Rho J., and Jarrett T.H. *ApJ*, 618:297, 2005.
- [36] Arikawa Y., Tatematsu K., Sekimoto Y., and Takahashi T., 1999.

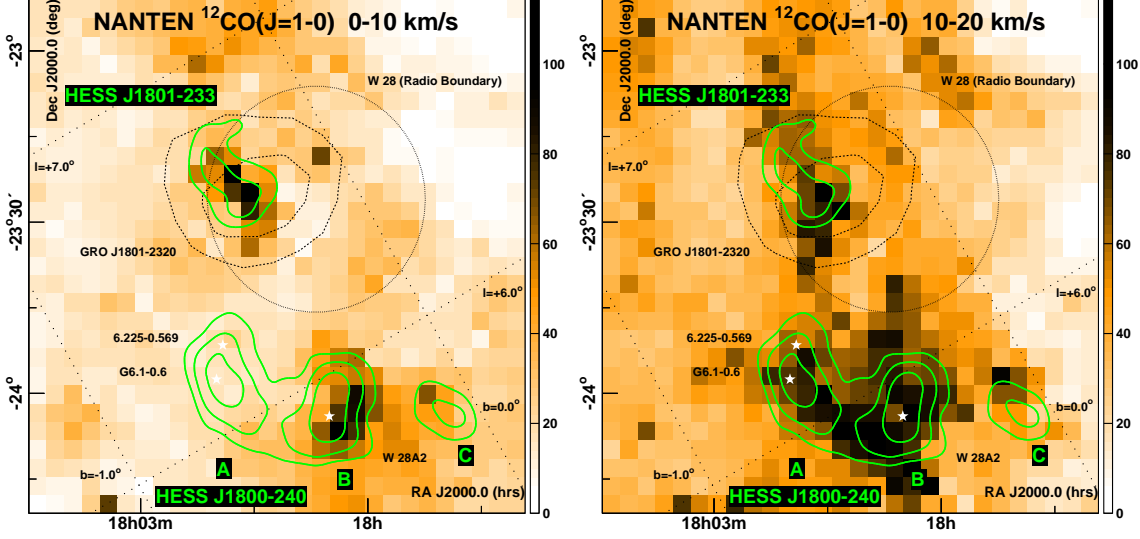


Figure 2: **Left:** NANTEN $^{12}\text{CO}(J=1-0)$ image (linear scale in K km s^{-1}) for $V_{\text{LSR}}=0$ to 10 km s^{-1} with VHE γ -ray significance contours overlaid (green) — levels $4, 5, 6\sigma$ and other features as in Fig. 1. **Right:** NANTEN $^{12}\text{CO}(J=1-0)$ image for $V_{\text{LSR}}=10$ to 20 km s^{-1} (linear scale and same maximum as for left panel).

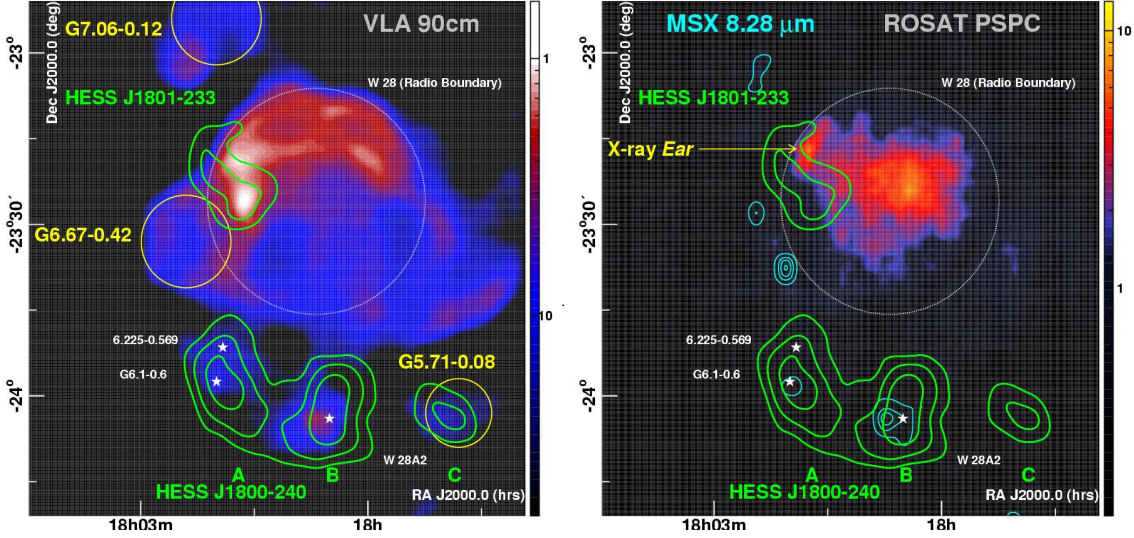


Figure 3: **Left:** VLA 90cm radio image [8] in Jy beam^{-1} . The VHE significance contours (green) from Fig. 1 are overlaid along with the HII regions (white stars) and the additional SNRs and SNR candidates (with yellow circles indicating their location and approximate dimensions) discussed in text. **Right:** ROSAT PSPC image — 0.5 to 2.4 keV (smoothed counts per bin [25]). Overlaid are contours (cyan — 10 linear levels up to $5 \times 10^{-4} \text{ W m}^{-2} \text{ sr}^{-1}$) from the MSX 8.28 μm image. Other contours and objects are as for the left panel. The X-ray *Ear* representing a peak at the northeastern edge is indicated.



The Monoceros very-high-energy gamma-ray source

A. FIASSON¹, J. A. HINTON², Y. GALLANT¹, A. MARCOWITH¹, O. REIMER³, G. ROWELL⁴, FOR THE H.E.S.S. COLLABORATION

¹*Laboratoire de Physique Théorique et Astroparticules, IN2P2/CNRS, Université Montpellier II, CC 70, Place Eugène Bataillon, F-34095 Montpellier Cedex 5, France*

²*School of Physics & Astronomy, University of Leeds, Leeds LS2 9JT, UK*

³*Stanford University, HEPL & KIPAC, Stanford, CA 94305-4085, USA*

⁴*School of Chemistry & Physics, University of Adelaide, Adelaide 5005, Australia*

Armand.Fiasson@lpta.in2p3.fr, J.A.Hinton@leeds.ac.uk

Abstract: The H.E.S.S. telescope array has observed the complex Monoceros Loop SNR/Rosette Nebula region which contains unidentified high energy EGRET sources and potential very-high-energy (VHE) γ -ray source. We announce the discovery of a new point-like VHE γ -ray sources, HESS J0632+057. It is located close to the rim of the Monoceros SNR and has no clear counterpart at other wavelengths. Data from the NANTEN telescope have been used to investigate hadronic interactions with nearby molecular clouds. We found no evidence for a clear association. The VHE γ -ray emission is possibly associated with the lower energy γ -ray source 3EG J0634+0521, a weak X-ray source 1RXS J063258.3+054857 and the Be-star MWC 148.

Introduction

Shell type supernova remnants (SNRs) are believed to be particle accelerator to energy up to a few hundred TeV. Observations of very high energy γ -ray (VHE; $E \geq 100$ GeV) from these objects (Aharonian et al. 2006) confirm the presence of particles with energy higher than 10 TeV in these regions. The presence of molecular clouds in the vicinity of SNRs could reveal the nature of such particles as they would interact and produce VHE γ rays. The Monoceros SNR (G205.5+0.5), situated at ~ 1.6 kpc (Graham et al. 1982), apparently interacting with the Rosette Nebula (a young stellar cluster/molecular cloud complex situated at 1.4 ± 0.1 kpc (Heinsberger et al. 2000)) is a candidate.

In the case of interaction of accelerated particles with interstellar medium producing neutral pions which decays in two γ rays, we expect a correlation between γ -ray emission and matter concentration. We used NANTEN data to trace target material. The NANTEN 4m diameter sub-mm telescope at Las Campanas observatory, Chile, has been con-

ducting a ^{12}CO ($J=1 \rightarrow 0$) survey of the galactic plane since 1996, including the Monoceros region (Mizuno & Fukui 2004).

H.E.S.S. observations and results

The H.E.S.S. experiment is an array of four Cherenkov telescope installed in Namibia which detects γ rays with energy in the 100 GeV to 50 TeV range. A more complete description of the H.E.S.S. experiment is given in Aharonian et al. 2004. The Monoceros loop region has been observed between March 2004 and March 2006 (Aharonian et al. 2007). The dataset includes 13.5 hours of data after quality selection and dead-time correction and was taken at zenith angles ranging between 29° and 59° . It corresponds to a mean energy threshold of 400 GeV with standard cuts used in spectral analysis and 750 GeV with hard cuts used for the source search and position fitting.

We made a search for a point-like source on this dataset using a source size of 0.11° and a ring of radius 0.5° for background estimation. We

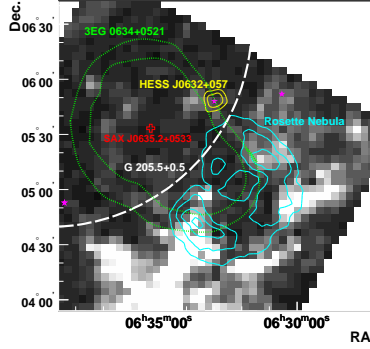


Figure 1: ^{12}CO ($J=1\rightarrow 0$) emission from the Monoceros SNR / Rosette Nebula region. The gray-scale corresponds to velocity integrated ($0\text{--}30\text{ km.s}^{-1}$) emission from the NANTEN Galactic Plane Survey (white areas mean highest flux). The 4σ and 6σ levels for the statistical significance of a point-like VHE γ -ray source are shown as yellow contours. Extended cyan contours are radio observations at 8.35 GHz of the Rosette Nebula. The white dashed circle is the Green catalog nominal position and size of the Monoceros SNR. The dotted green contours are 95% and 99% confidence level for the position of the EGRET source 3EG J0634+0521. And last, the position of the binary pulsar SAX J0635.2+053 is marked as a red square and the position of Be-stars with pink stars.

found an excess corresponding to a statistical significance of 7.1σ . Fig. 1 shows the NANTEN ^{12}CO map with 4 and 6σ levels of statistical confidence contours for the VHE γ -ray excess (yellow contours). As we made a blind search for a point-like source, the probability we get an excess at this position is increased by the number of positions in the field of view, here $\approx 10^5$. This leads to a post-trials statistical significance of 5.3σ . The excess is confirmed by an independent analysis based on a fit of camera images to a shower model (*Model Analysis*, see de Naurois 2006), which yields to a significance of 7.3σ (5.6σ post-trials).

The fitted position of this new source HESS J0632+057, is $6^{\text{h}}32^{\text{m}}58.3^{\text{s}}$, $+5^{\circ}48'20''$ (RA/Dec. J2000) with $28''$ statistical errors on each axis (fig. 2). We estimated systematics errors at $20''$ on each axis. The fig. 3 represents

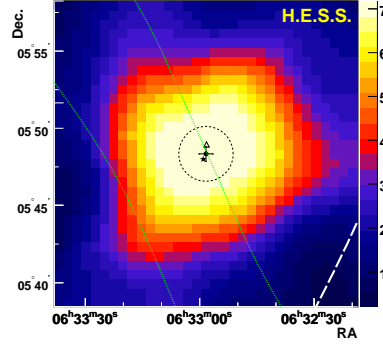


Figure 2: Statistical significance map of the H.E.S.S. VHE γ -ray source. The rms size limit is shown as a dotted circle. Dotted green contours are 95% and 99% confidence level for the position of the EGRET source 3EG J0634+0521. The unidentified X-ray source 1RXS J063258.3+054857 is marked with a triangle and the Be-star MCW 148 with a star.

the distribution of signal in function of the angular distance around the fitted position. The distribution is fully compatible with the point spread function (red curve). We derived an upper limit on the size of the source of $2'$ at 95% confidence assuming a Gaussian profile for the source.

The reconstructed energy spectrum of the excess is consistent with a power-law of index $\Gamma = 2.53 \pm 0.26 \pm 0.20$ and differential flux at 1 TeV $\Phi_{TeV} = 9.1 \pm 1.7 \pm 3.0 \times 10^{-13}\text{ cm}^{-2}\text{ s}^{-1}\text{ TeV}^{-1}$. The first errors are statistical errors and the second are estimated systematic errors. Fig.4 represents the VHE γ -ray reconstructed flux together with that for the EGRET sources 3EG0634+0521 and the upper limit derived by the HEGRA telescope array for the EGRET source position (converted to differential flux assuming the spectral shape observed by H.E.S.S.). There is no evidence of flux variability in our dataset but the sparse sampling of data together with the weakness of the source do not permit to constrain strongly intrinsic variability of the source.

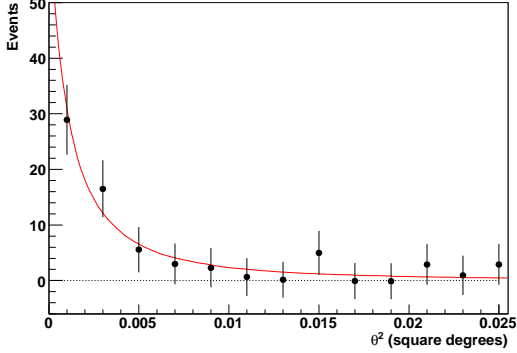


Figure 3: Distribution of γ -ray candidate events as function of squared angular distance from the best fit position of HESS J0632+057. The red line is the point spread function corresponding to this dataset obtained with Monte-Carlo simulations.

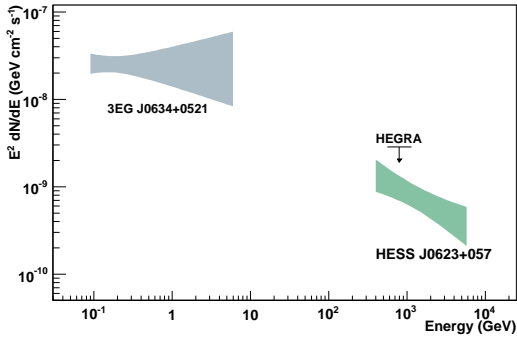


Figure 4: Reconstructed VHE γ -ray spectrum of HESS J0632+057 compared to the EGRET source 3EG J0634+0521. The upper limit obtained using the HEGRA instrument for the EGRET source position is shown.

Possible associations

The region where lies HESS J0632+057 is a complex region and although there is no clear counterpart, it may be associated with various objects known at other wavelengths.

3EG J0634+0521

In the same region lies also an EGRET source, 3EG J0634+0521 (Hartman et al., 1999). Considering that the source is flagged as confused and possibly extended, our measurement, which lies between 95% and 99% confidence region, is compatible with its position. Furthermore, the reported third EGRET catalogue flux above 100 MeV is consistent with an extrapolation of the H.E.S.S. spectrum. A global fit of the two spectra gives a photon index of 2.41 ± 0.06 (fig.4).

The Monoceros Loop SNR

The possible association of spectra in the GeV and TeV band is an argument in favor of an hadronic interpretation of the VHE γ -ray emission. In this case, the Monoceros loop SNR is a good candidate for acceleration of particles. This remnant, which has an age of $\sim 3 \times 10^4$ years, is rather old in comparison to known shell type SNRs emitting VHE γ rays (~ 2000 years). However, cosmic rays acceleration may occur even at later evolutionary phase (late Sedov or Radiative, see Yamazaki et al. 2006). Given the point-like nature of the VHE γ -ray emission, to explain VHE γ rays as a product of accelerated cosmic rays interacting with interstellar medium requires the presence of a dense molecular cloud coincident with the emission. An unresolved molecular cloud listed in CO survey at 115 GHz (Oliver et al. 1996) lies rather close to HESS J0632+057. The distance estimate for this cloud (1.6 kpc) is consistent with that for the Monoceros SNR. NANTEN survey shows that the intensity peak of this cloud is significantly shifted to the east of the H.E.S.S. source (fig. 1). There is no evidence of other dense clouds along the line of sight in the NANTEN data.

1 RXS J063258.3+054857

1 RXS J063258.3+054857 is a faint ROSAT source which is potential counterpart of HESS J0632+057, given the uncertainty of the position of the two objects. Given the number of sources in the field of view, the chance probability of coincidence of the two source is 0.1%. X rays are useful to discriminate between scenario of VHE γ -ray emission. If γ -rays are due to inverse Compton scattering from a population of accelerated electrons, X rays are expected to come from synchrotron emission of the same population. In this case, the weakness of this source ($\sim 10^{-13} \text{ erg cm}^{-2} \text{ s}^{-1}$) compared to the TeV flux ($\sim 10^{-12} \text{ erg cm}^{-2} \text{ s}^{-1}$) required a very low magnetic field ($\ll 3 \mu\text{G}$), unless a strong radiation source exists in the neighbourhood of the emission region. Important absorption of the X-ray emission may also explain weakness of the ROSAT source. In the case of a hadronic scenario, production of pions leads to secondary electrons which produce a weaker X-ray source, probably compatible with the measured ROSAT flux.

MWC 148

A massive emission-line Be-star lies within the H.E.S.S. error circle. Given the fact that there are only three stars of this type in the field of view, the chance probability of the association is $\approx 10^{-4}$. Stars of this spectral type have winds with typical velocities and mass loss rates of 1000 km.s^{-1} and $10^{-7} M_{\odot}$. Stellar winds may induce internal or external shocks where particles can be accelerated, but no association of VHE γ -ray emission with similar stars have been already detected and seems unlikely. Another hypothesis is that this star is a part of a binary system with a compact companion not already detected. Further observations are required to constrain this scenario.

Acknowledgments

The support of the Namibian authorities and of the University of Namibia in facilitating the construction and operation of H.E.S.S. is gratefully acknowledged, as is the support by the German Ministry for Education and Research, the CNRS-IN2P3 and the Astroparticle Interdisciplinary Pro-

gramme of the CNRS, the U.K. Particle Physics and Astronomy Research Council (PPARC), the IPNP of the Charles University, the South African Department of Science and Technology and National Research Foundation, and by the University of Namibia. We appreciate the excellent work of the technical support staff in Berlin, Durham, Hamburg, Heidelberg, Palaiseau, Paris, Saclay, and in Namibia in the construction and operation of the equipment. The NANTEN project is financially supported from JSPS (Japan Society for the Promotion of Science) Core-to-Core Program, MEXT Grant-in-Aid for Scientific Research on Priority Areas, and SORST-JST (Solution Oriented Research for Science and Technology: Japan science and Technology Agency). We would also like to thank Stan Owocki and James Urquhart for very useful discussions.

References

- [1] F. A. Aharonian et al. *Nature*, 432:75, 2004.
- [2] F. A. Aharonian et al. *A&A*, 249:223, 2006.
- [3] F. A. Aharonian et al. Discovery of a point-like very-high-energy γ -ray source in Monoceros. *to appear in A&A*, 2007.
- [4] M. de Naurois. *astro-ph/0607247*. 2006.
- [5] D. A. Graham, C.G.T. Haslam, C. J. Salter, and W. E. Wilson. *A&A*, 109:145, 1982.
- [6] H. Hensberge, K. Pavlovski, and W. Verschueren. *A&A*, 358:553, 1999.
- [7] A. Mizuno and Y. Fukui. *ASP Conf. Ser.*, page 59, 2004.
- [8] R. J. Oliver, M. R. W.. Masheder, and P. Thaddeus. *A&A*, 315:578, 1996.
- [9] R. Yamazaki, K. Kohri, and A. Bamba. *MNRAS*, 371:1975, 2006.



Crab nebula spectrum as seen by H.E.S.S.

B. KHÉLIFI¹, C. MASTERSON², S. PITA³, E. OÑA-WILHELMI³ FOR THE H.E.S.S. COLLABORATION

¹*Laboratoire Leprince-Ringuet, Ecole Polytechnique/IN2P3/CNRS, Palaiseau, France*

²*Dublin Institute for Advanced Studies, 5 Merrion Square, Dublin 2, Ireland*

³*AstroParticule et Cosmologie, Paris VII/IN2P3/CNRS, Paris, France*

khelifi@llr.in2p3.fr

Abstract: The H.E.S.S. stereoscopic Cherenkov telescope system has observed the Crab nebula since December 2003 with the complete four-telescope array. The stable signal from this pulsar wind nebula (PWN) has been used to verify the performance and calibration of the instrument thanks to its high flux compared to the H.E.S.S. sensitivity. These observations allow us also to study the radiation mechanisms of this PWN, in particular by focusing on the high energy part of its energy spectrum, where gamma-ray emission at energies above 30 TeV has been detected.

Introduction

The Crab nebula was discovered at very high energies (VHE; >100 GeV) in 1989 [1] and the emission has been confirmed by a number of other experiments (e.g. [2, 3, 4]). This pulsar wind nebula (PWN) has a high flux relative to other known VHE sources and its emission is expected to be stable. As a result, the Crab nebula is commonly used as a standard ‘calibration candle’ for the ground-based gamma-ray detectors, and a particular attention is paid here to the control of the analysis chain accuracy. Indeed, the detector ageing results from a decrease of the overall optical efficiency (a combination of mirrors, light-cones, and photomultipliers degradation) and from ageing of electronics components of cameras. The detector response is measured, calibrated [5] and used for the data analysis [5].

Important questions on the origin of the non-thermal emission of the Crab nebula remain. It is commonly admitted that its spectral energy distribution (SED) can be well-reproduced with a mechanism based on a synchrotron self-Compton (SSC) emission of high energy electrons/positrons (e.g. [7]) even if a contribution from proton radiation is not excluded at high energies (e.g. [8]). However, the acceleration mechanisms of these leptons and hadrons are still under investigation (Cf. [9] for a

recent review). Thus, multi-wavelength observations are still necessary to understand the underlying physics, in particular observations of VHE gamma-rays above 30 TeV.

H.E.S.S. observations and data analysis

The Crab nebula has been observed with the complete array for 58.4 hours from December 2003 to December 2006. After data-quality selection based on good weather conditions and good detector operation, an exposure of 29.4 hours live-time is obtained. The periods of the Crab observations suffer sometimes of poor weather conditions in Namibia. All observations were taken in *wobble* mode whereby the source is alternately offset by a fixed distance within the field of view, alternating between 28 minutes runs in positive and negative declination (or right ascension) directions.

In table 1 we present, for each observation period considered, the live-time (in hours), mean zenith angle (in degrees), mean position (in degrees) of the Crab pulsar position relative to the centre of the field of view and mean optical efficiency (in percent) of the detection system.

The data are processed with the HAP (H.E.S.S. Analysis Package) software as follows. In order

Year	2004	2005	2006	All
Live-time [h]	20.6	5.4	3.4	29.4
Zenith Angle [deg]	52.2	47.7	49.2	51.1
Offset [deg]	0.65	0.58	0.70	0.65
OptEff [%]	8.3	7.8	7.0	8.1

Table 1: Summary of the Crab observations. The row descriptions are given in the text.

to reject the overwhelming background of night-sky diffuse light and hadronic showers, a two-level image cleaning is performed to remove pixels containing only background noise. After image cleaning, the Hillas parameters [10] are computed. For comparison, two methods are used to reconstruct the characteristics of the atmospheric showers, i.e. the impact parameter (D), the shower maximum (H) and the shower direction. The first method [5], called hereafter *Hillas*, is based on a geometrical reconstruction of the shower characteristics from the Hillas parameters (tracks of the projected direction of the shower in the field of view). The second one, called *Model3D* [11], uses a model of the atmospheric shower as a ‘Cherenkov ellipsoid’ and its parameters are adjusted to the camera images. Cuts are applied to the parameters derived by these methods to improve the signal to (hadronic) noise ratio. For the *Model3D* analysis, the standard cuts of the *Hillas* analysis are applied together with cuts on the ‘Cherenkov ellipsoid’ size. The remaining background is estimated from regions at same distance from the field of view centre as the Crab pulsar position for the observations (cf. fig. 9 of [5]).

The energy of each event is estimated from D , H and the images charges within the Hillas ellipses (Q). Look-up tables given the image charges as a function of energy (E), D and H ($Q = f(E, D, H)$) are derived from gamma-ray simulations made with Kaskade [12] for different fixed energies, zenith angles, offsets and optical efficiencies. Given the measured Q , D and H , inverting the tables provides an estimation of the event energy. To determine the energy spectrum, the instrument response functions (effective areas and energy resolutions) are derived from the same gamma-ray simulations, and a forward-folding algorithm developed by the CAT collaboration [13] is used. A likelihood fit is used to adjust different spectral shape hypotheses. A test of the hypotheses with a likelihood ratio is made to determine the spectrum shape that best adjusts to the data.

H.E.S.S. results

The main results of the analysis of the Crab observations are given in table 2. For each method of shower reconstruction and for each year, the number of gamma-rays above the analysis energy threshold, the significance and the integral flux above 1 TeV are listed. A strong signal is detected and, independently of the year and the analysis method, the integral flux is basically constant, illustrating the good correction for the effects of the detector ageing.

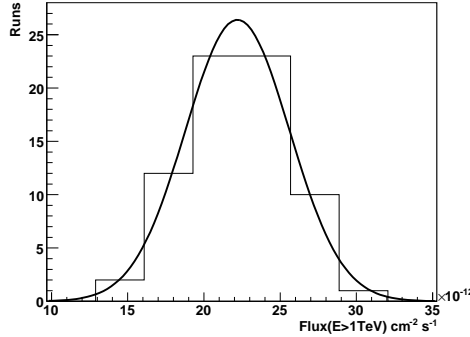


Figure 1: Distribution of the run-wise integral fluxes above 1 TeV for the *Hillas* analysis.

The run-wise fluxes are also computed and their distribution is given in fig. 1 for the *Hillas* analysis. It follows a Gaussian distribution (black line) with a χ^2/dof of 0.50/3. The best-fit parameters are Mean = 2.22 ± 0.04 and Sigma = 0.34 ± 0.02 in units of $10^{-11} \text{cm}^{-2} \text{s}^{-1}$. The flux derived is thus compatible with a steady flux with Gaussian fluctuations of $\sim 15\%$.

	<i>Hillas</i>	<i>Model3D</i>
Φ_0^{PL}	3.52 ± 0.04	3.46 ± 0.04
Γ^{PL}	2.60 ± 0.01	2.61 ± 0.01
Φ_0^{EC}	3.53 ± 0.04	3.48 ± 0.04
Γ^{EC}	2.40 ± 0.03	2.42 ± 0.03
E_c^{EC}	16.7 ± 2.5	16.1 ± 2.5
λ^{EC}	74.4	66.6

Table 3: Summary of spectrum fits. The row descriptions are given in the text.

For both analyses, the energy spectrum is computed for two different spectral hypotheses: a pure power-law \mathcal{H}_0 ($dN/dE_{\text{PL}} = \Phi_0 \times E^{-\Gamma}$) and a power-law with an exponential cut-off \mathcal{H}_1

Method	Year	Excess [γ]	Significance [σ]	$F_{>1\text{ TeV}}$ [$\times 10^{-11}\text{ cm}^{-2}\text{ s}^{-1}$]
<i>Hillas</i>	2004	5788	122	2.22 ± 0.07
	2005	1674	70	2.18 ± 0.06
	2006	1069	57	2.41 ± 0.10
	All	8531	151	2.22 ± 0.04
<i>Model3D</i>	2004	5208	130	2.20 ± 0.06
	2005	1612	74	2.13 ± 0.18
	2006	1008	59	2.37 ± 0.12
	All	7828	161	2.22 ± 0.05

Table 2: Results of the observations. The column descriptions are given in the text.

($dN/dE_{\text{EC}} = \Phi_0 \times E^{-\Gamma} \times e^{-E/E_c}$). The fit results are listed in table 3. The parameter Φ_0 is in units of $10^{-11}\text{ cm}^{-2}\text{ s}^{-1}\text{ TeV}^{-1}$, E_c in TeV. λ is the ratio between the maximum likelihood of the \mathcal{H}_1 fit over the \mathcal{H}_0 fit and its distribution follows asymptotically a χ^2 law with one degree of freedom. From this parameter and independently of the analysis method used, it can clearly be seen that the fitted spectrum shape is not compatible with a pure power-law with a probability less than 10^{-6} . The use of a ‘parabolic’ spectrum shape ($E^{-\alpha-\beta \log(E)}$) fits the data equally well as a power-law with an exponential cut-off. Note that the fit results are compatible between the different analyses.

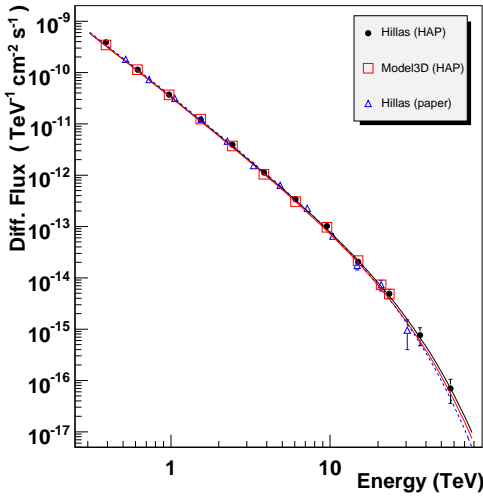


Figure 2: Comparison of the Crab spectrum fits between this analysis and that published in [5]. The lines are the best-fit shapes.

Figure 2 shows the Crab spectrum derived with these two analyses carried out with the HAP software, together with the H.E.S.S. spectrum pub-

lished in [5]. In the following, the results of the \mathcal{H}_1 fit for the *Hillas* analysis are used and the flux measurements for each energy bin (differential flux) are given in table 4. Here, the measurements on high energy bins above 30 TeV should be emphasised in which a signal is detected at the level of $\sim 6\sigma$. A signal is detected significantly at the highest energies which allows the spectrum curvature to be measured more accurately. Figure 3 shows the comparison of the best-fit parameters Γ and $1/E_c$ between these analyses and the results from [5]. The parameters are quite compatible between these and the exponential cut-off energy, E_c , is compatible with ~ 15 TeV.

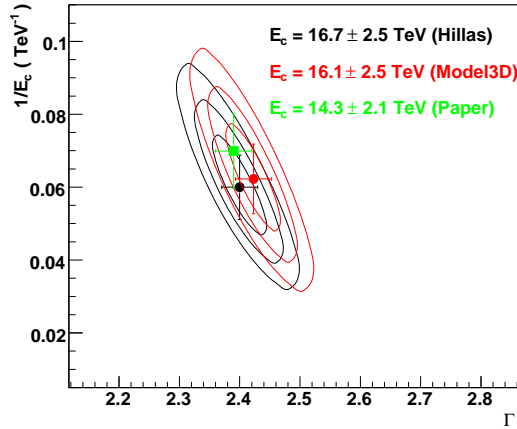


Figure 3: Comparison of the best-fit parameters between this analysis and those published in [5].

Conclusions

Analysis of Crab data carried out with the new software framework HAP yields results which are consistent with those published previously by H.E.S.S. in [5]. The measured Crab flux is compatible with a steady flux between December 2003 and Decem-

Mean Energy	Significance	$\frac{dN}{dE}$
	$[\sigma]$	$[\text{cm}^{-2}\text{s}^{-1}\text{TeV}^{-1}]$
0.39	16.7	$(3.87 \pm 0.38) \times 10^{-10}$
0.62	73.4	$(1.14 \pm 0.03) \times 10^{-10}$
0.97	78.4	$(3.72 \pm 0.08) \times 10^{-11}$
1.54	67.7	$(1.21 \pm 0.03) \times 10^{-11}$
2.43	55.9	$(3.93 \pm 0.12) \times 10^{-12}$
3.84	41.3	$(1.13 \pm 0.05) \times 10^{-12}$
6.06	30.2	$(3.40 \pm 0.19) \times 10^{-13}$
9.54	22.4	$(1.01 \pm 0.07) \times 10^{-13}$
15.0	12.4	$(2.05 \pm 0.27) \times 10^{-14}$
23.5	7.9	$(4.91 \pm 1.00) \times 10^{-15}$
36.7	4.1	$(7.56 \pm 2.84) \times 10^{-16}$
57.0	3.8	$(7.22 \pm 3.40) \times 10^{-17}$

Table 4: Flux measurements for each energy bin for the *Hillas* analysis.

ber 2006, indicating that all effects of the detector ageing are correctly taken into account. The integral flux above 1 TeV is $F(> 1 \text{ TeV}) = (2.22 \pm 0.07) \times 10^{-11} \text{ cm}^{-2}\text{s}^{-1}$. Its energy spectrum is not compatible with a pure power-law shape and is well-represented by a power-law with an exponential cut-off ($E_c = 16.7 \pm 2.5 \text{ TeV}$).

Comparing the results of different analyses presented here, one finds that the differences of flux and spectrum index estimated are well within the systematics detailed in [5].

A clear signal is detected above 30 TeV which allows the curved nature of the Crab nebula spectrum to be clearly confirmed. This measured spectrum seems to be still compatible with a SSC scenario in the Klein-Nishina regime as described in [7]. An adjustment of the fit parameters of this radiation model on our data is still necessary to confirm this scenario.

Acknowledgements

The support of the Namibian authorities and of the University of Namibia in facilitating the construction and operation of H.E.S.S. is gratefully acknowledged, as is the support by the German Ministry for Education and Research (BMBF), the Max Planck Society, the French Ministry for Research, the CNRS-IN2P3 and the Astroparticle Interdisciplinary Programme of the CNRS, the U.K. Science and Technology Facilities Council (STFC), the IPNP of the Charles University, the Polish Ministry of Science and Higher Education, the South African Department of Science and Technology

and National Research Foundation, and by the University of Namibia. We appreciate the excellent work of the technical support staff in Berlin, Durham, Hamburg, Heidelberg, Palaiseau, Paris, Saclay, and in Namibia in the construction and operation of the equipment.

References

- [1] Weekes T.C. *et al.*, 1989, ApJ 342, 379
- [2] Aharonian F.A. *et al.* (HEGRA coll.), 2000, ApJ 539, 317
- [3] Masterson C. *et al.*, 2001, High Energy Gamma-Ray Astronomy, AIP 558, 753
- [4] Albert J. *et al.* (MAGIC coll.), 2007, astro-ph/07053244
- [5] Aharonian F.A. *et al.* (H.E.S.S. coll.), 2004, APh 22, 119
- [6] Aharonian F.A. *et al.* (H.E.S.S. coll.), 2006, A&A 457, 899
- [7] Horns D. and Aharonian F.A., 2004, ESASP 552, 439
- [8] Amato E., Guetta D. and Blasi P., 2003, A&A 402, 827
- [9] Kirk J.G., Lyubarsky Y. and Pétri J., 2007, astro-ph/0703116v2
- [10] Hillas A., 1985, Proc. 19nd I.C.R.C., Vol. 3, 445
- [11] Lemoine M. *et al.*, 2006, APh 25, 195
- [12] Kertzman M. P. and Sembroski G. H., 1994, NIM A 343, 629
- [13] Piron F. *et al.*, 2001, A&A 374, 895



Energy Dependent Morphology in the PWN candidate HESS J1825–137

S. FUNK¹, J. A. HINTON², O. C. DEJAGER³ FOR THE H.E.S.S. COLLABORATION

¹Kavli Institute for Particle Astrophysics and Cosmology, SLAC, Menlo Park, CA-94025, USA

²School of Physics and Astronomy, University of Leeds, Leeds LS2 9JT, UK

³Unit for Space Physics, North-West University, Potchefstroom 2520, South Africa

Stefan.Funk@slac.stanford.edu

Abstract: Observations with H.E.S.S. revealed a new source of very high-energy (VHE) gamma-rays above 100 GeV – HESS J1825–137 – extending mainly to the south of the energetic pulsar PSR B1823–13. A detailed spectral and morphological analysis of HESS J1825–137 reveals for the first time in VHE gamma-ray astronomy a steepening of the energy spectrum with increasing distance from the pulsar. This behaviour can be understood by invoking radiative cooling of the IC-Compton gamma-ray emitting electrons during their propagation. In this scenario the vastly different sizes between the VHE gamma-ray emitting region and the X-ray PWN associated with PSR B1823–13 can be naturally explained by different cooling timescales for the radiating electron populations. If this scenario is correct, HESS J1825–137 can serve as a prototype for a whole class of asymmetric PWN in which the X-rays are extended over a much smaller angular scales than the gamma-rays and can help understanding recent detections of X-ray PWN in systems such as HESS J1640–465 and HESS J1813–178. The future GLAST satellite will probe lower electron energies shedding further light on cooling and diffusion processes in this source.

Introduction

The pulsar PSR B1823–13 and its surrounding X-ray pulsar wind nebula (PWN) G18.0–0.2 is a system that has been studied by H.E.S.S. in very high-energy gamma-rays above 200 GeV in unprecedented detail [1]. PWNe seem to constitute a significant fraction of the population of identified Galactic VHE gamma-ray sources detected by H.E.S.S. [2] and as also suggested by a statistical assessment of the correlation between Galactic VHE γ -ray sources and energetic pulsars (see Carrigan et al., these proceedings). The gamma-ray emission in these objects is typically thought to be generated by Inverse Compton scattering of relativistic electrons accelerated in the termination shock of the PWN.

Considering the population of VHE gamma-ray PWNe, HESS J1825–137 is probably thus far the best example of the emerging class of so-called *offset Pulsar Wind nebulae* in which an extended VHE gamma-ray emission surrounding an energetic pulsar is offset into one direction of the pulsar. This offset is generally thought to arise from

dense molecular material in one direction of the pulsar that prevents an symmetric expansion of the PWN (see e.g. [3] for a hydro-dynamical simulation and discussion of this effect).

As one of the best studied objects in VHE gamma-rays with an observation time of nearly 70 hours, HESS J1825–137 has been used as a template for the association of asymmetric PWN in VHE γ -rays and X-rays [2, 4]. In HESS J1825–137 the claimed association between the VHE γ -ray source and the X-ray PWN rests on the following properties of the source:

- Same morphology (i.e. asymmetric extension to the south) in both bands but X-ray nebula much smaller ($\sim 5''$) than γ -ray ($\sim 0.5^\circ$) emission region
- Spectral steepening of the VHE gamma-ray source away from the pulsar (i.e. decrease of gamma-ray extension with increasing energy). Interestingly the maximum of the VHE γ -ray emission is not coincident with the pulsar position but is shifted $\sim 17'$ to the south-west.

The vastly different sizes of the emission region in the two wavebands prevents at first glance a direct identification as a counterpart, since the morphology can not be matched between X-rays and gamma-rays. As will be explained in the following, the different sizes can be explained in a time-dependent leptonic model by different cooling timescales of the X-ray and of the VHE gamma-ray emitting regions. Caution should however be used, if such an association serves as a template for other unidentified H.E.S.S. VHE gamma-ray sources with an energetic pulsar in the vicinity, in cases in which no X-ray PWN has been detected so far.

Observational data

CO-Observations performed in the composite survey [7] show a dense molecular cloud in the distance band between 3.5 and 4 kpc to the north of PSR B1823–13 (located at ~ 4 kpc) [6]. This cloud seems to support the picture of an offset PWN and could explain why the X-ray and VHE emission is shifted to the south of the pulsar. Given the relatively high gamma-ray flux and the rather large distance of the system of 4 kpc (in comparison to the Crab), the required gamma-ray luminosity $L_\gamma \sim 3 \times 10^{35}$ erg/s is comparable to the Crab luminosity. The spin-down luminosity of the pulsar is, however, two orders of magnitude lower than the Crab spin-down luminosity. Assuming the distance of ~ 4 kpc is correct this shows that the efficiency of converting spin-down power to gamma-ray luminosity must be much higher than in the Crab Nebula, not unexpected, given the large magnetic field in the Crab Nebula. Detailed time-dependent modelling of the source shows indeed that (especially below ~ 1 TeV) the energy injection into the system must have been about an order of magnitude higher in the past. Potentially the spin-down power of the pulsar was significantly higher in the early stage of the pulsar evolution. For the lower energy end of the H.E.S.S. spectrum and for modest magnetic fields of a few μ G as suggested by the large VHE gamma-ray flux, the electron lifetimes become comparable to the pulsar age and therefore “relic” electrons released in the early history of the pulsar can survive until today and provide the required luminosity. It should

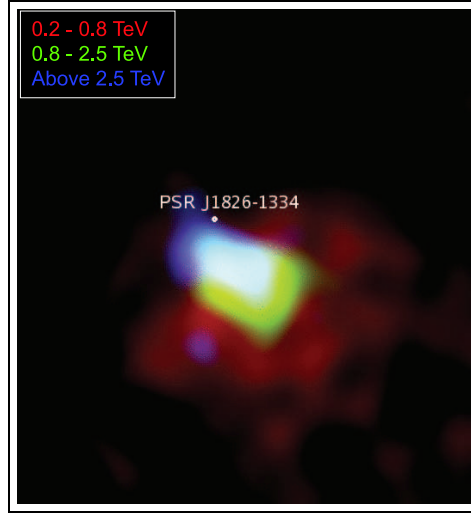


Figure 1: Three-colour image showing the gamma-ray emission in different energy bands (red: 0.2–0.8 TeV, green 0.8–2.5 TeV and blue: above 2.5 TeV). The different gamma-ray energy bands show a shrinking with increasing energy away from the pulsar PSR B1823–13.

be noted that to this date no sensitive X-ray observation of the region coinciding with the peak of the VHE gamma-ray emission has been performed and a low surface-brightness extension to the south of the X-ray PWN found by Gaensler et al. [7] remains an interesting possibility that should eventually be tested.

Energy dependent morphology

Given the large data set with nearly 20,000 γ -ray excess events, a spatially resolved spectral analysis of HESS J1825–137 could be performed. For the first time VHE γ -ray astronomy an energy dependent morphology (see Figure 1) was established [1] in which the size of the emission region decreases with increasing energy. This shrinking size with increasing energy is equivalent to the statement of a steepening of the spectral index away from the pulsar. The spectrum in HESS J1825–137 changes from a rather hard photon index ~ 2 close to the pulsar to a softer value of ~ 2.5 at a distance of 1° away from the pulsar.

Figure 2 shows the surface brightness as a function of the distance from the pulsar for different energy bands. Two clear trends are apparent in this figure: a) the peak of the surface brightness shifts to lower energies (as already suggested by the steepening of the energy spectrum away from the pulsar) b) at low energies the surface brightness is nearly independent of the distance whereas at the higher energies the surface brightness drops rapidly with increasing distance from the pulsar. The right panel of Figure 2 shows the derived radius R_{50} corresponding to the 50% containment of the surface brightness. This radius R_{50} drops with increasing energy as already apparent in Figure 1.

The steepening of the energy spectrum away from a central pulsar is a property commonly observed in X-ray studies of PWNe other than the Crab. For most of these system the total change in the photon index is close to ~ 0.5 similar to what is seen in HESS J1825–137. It should be noted that the results shown here represent the first unambiguous detection of a spectral steepening at a fixed electron energy (since the synchrotron emission seen in X-rays depends on the magnetic field) in a PWN system. Spectral variation with distance from the pulsar could result from (1) energy loss of particles during propagation, with radiative cooling of electrons as the main loss mechanism, from (2) energy dependent diffusion or convection speeds, and from (3) variation of the shape of the injection spectrum with age of the pulsar. Concerning (1): Loss mechanisms include amongst others adiabatic expansion, ionisation loss, bremsstrahlung, synchrotron losses and inverse Compton losses. Only synchrotron and IC losses can result in a electron lifetime that decreases with increasing energy. A source decreasing source size with increasing energy is therefore generally seen as indicative of electrons as the radiating particles.

For continuous injection and short radiative lifetimes of the electrons (in comparison to the age of the source), the spectral index of the electrons changes by one unit as a result of the cooling, yielding in a change of 0.5 in the photon index. This matches roughly what is seen in HESS J1825–137 when comparing the inner and the outer nebula. The lower energy gamma-rays (i.e. below ~ 0.6 TeV) correspond to mostly un-cooled low energy electrons (i.e. the spectral index consistent

with the injection spectral index). At these low energies the electron lifetime becomes comparable to the age of the source and the size is rather independent of the energy. At higher energies the cooling break takes effect and the source size shrinks with increasing energy as expected from electron cooling. The XMM-Newton X-ray emitting electrons typically have much higher energies (~ 100 TeV) than the γ -ray emitting electrons (~ 10 TeV), assuming a typical magnetic field of $5 \mu\text{G}$. The synchrotron cooling lifetime of X-ray emitting electrons is therefore expected to be much smaller, resulting in a smaller spatial extension in X-rays.

For systems like HESS J1825–137 a detailed study in X-rays trying to detect the low surface brightness nebula in the soft X-ray band would be very beneficial, is however very hard to achieve given the absorption of soft X-rays. The upcoming GLAST-satellite will observe this object in a thus far rather unexplored energy regime especially above ~ 10 GeV, where the angular resolution of the instrument becomes comparable to the angular resolution of the ground-based instrument. In this energy range GLAST will probe even lower energy electrons and it will be interesting to compare the sizes of the GLAST and the H.E.S.S. emission region. The H.E.S.S. results have shown that a wealth of detail exists in gamma-rays at an angular scale of $\sim 0.1^\circ$. Future instruments like CTA or AGIS might improve this angular resolution even further.

Acknowledgements

”The support of the Namibian authorities and of the University of Namibia in facilitating the construction and operation of H.E.S.S. is gratefully acknowledged, as is the support by the German Ministry for Education and Research (BMBF), the Max Planck Society, the French Ministry for Research, the CNRS-IN2P3 and the Astroparticle Interdisciplinary Programme of the CNRS, the U.K. Science and Technology Facilities Council (STFC), the IPNP of the Charles University, the Polish Ministry of Science and Higher Education, the South African Department of Science and Technology and National Research Foundation, and by the University of Namibia. We appreciate the excel-

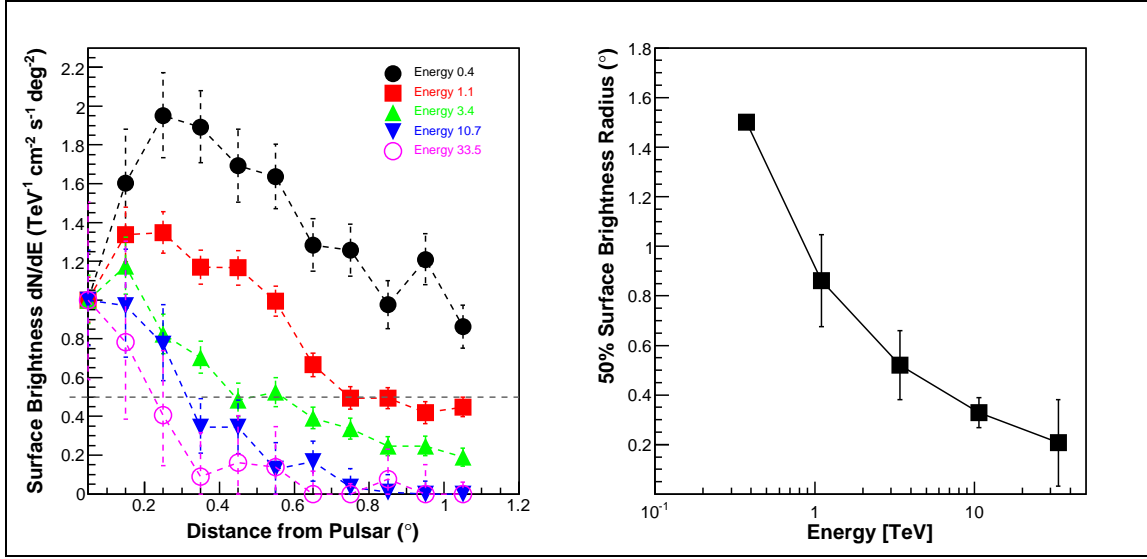


Figure 2: **Left:** Surface brightness as a function of distance from the pulsar for different energy bands (derived from Figure 4 in Aharonian et al [1]. The surface brightness is defined as the differential gamma-ray flux at a given energy scaled by the area of the extraction region and normalised by the flux for that energy at the pulsar position $r = 0$. **Right:** Distance from the pulsar at which the surface brightness drops to 50% of the flux at the pulsar position. The error bars are derived by fitting the falling points of the left plot, varying the fit parameters within the errors and recalculating the 50% containment radius.

lent work of the technical support staff in Berlin, Durham, Hamburg, Heidelberg, Palaiseau, Paris, Saclay, and in Namibia in the construction and operation of the equipment.”

References

- [1] Aharonian, F., et al. (H.E.S.S. collaboration), 2006, A&A 460, 365
- [2] Funk, S. (for the H.E.S.S. collaboration), 2007, ApSS, in press (astro-ph/0609586)
- [3] Blondin, J.M., Chevalier, R.A., & Frierson, D.M. 2001, ApJ 563, 806
- [4] Gallant, Y. (for the H.E.S.S. collaboration), 2007, ApSS, in press (astro-ph/0611720)
- [5] Dame, T. M., et al, 2001, ApJ 547, 792
- [6] Lemi re, A., for the H.E.S.S. Collaboration, To appear in the Proceedings of the 29th ICRC, Pune (2005)
- [7] Gaensler, B. M., et al., 2003, ApJ 588, 441



Discovery of the candidate pulsar wind nebula HESS J1718-385 in very-high-energy gamma-rays

S. CARRIGAN¹, Y.A. GALLANT², J.A. HINTON^{1,3}, NU. KOMIN², K. KOSACK¹ AND C. STEGMANN⁴
FOR THE H.E.S.S. COLLABORATION

¹Max-Planck-Institut für Kernphysik, P.O. Box 103980, D 69029 Heidelberg, Germany

²Laboratoire de Physique Théorique et Astroparticules, IN2P3/CNRS, Université Montpellier II, CC 70, Place Eugène Bataillon, F-34095 Montpellier Cedex 5, France

³Landessternwarte, Universität Heidelberg, Königstuhl, D 69117 Heidelberg, Germany

⁴Universität Erlangen-Nürnberg, Physikalisches Institut, Erwin-Rommel-Str. 1, D 91058 Erlangen, Germany
svenja.carrigan@mpi-hd.mpg.de

Abstract: Motivated by recent detections of pulsar wind nebulae in very-high-energy (VHE) gamma rays, a systematic search for VHE gamma-ray sources associated with energetic pulsars was performed, using data obtained with the H.E.S.S. (High Energy Stereoscopic System) instrument. The search for VHE gamma-ray sources near the pulsar PSR J1718-3825 revealed the new VHE gamma-ray source HESS J1718-385. We report on the results from the HESS data analysis of this source and on possible associations with the pulsar and at other wavelengths. We investigate the energy spectrum of HESS J1718-385 that shows a clear peak. This is only the second time a VHE gamma-ray spectral maximum from a cosmic source was observed, the first being the Vela X pulsar wind nebula.

Introduction

It has long been known that pulsars can drive powerful winds of highly relativistic particles. Confinement of these winds leads to the formation of strong shocks, which may accelerate particles to \sim PeV energies.

The best studied example of a pulsar wind nebula (PWN) is the Crab nebula, which exhibits strong non-thermal emission across most of the electromagnetic spectrum from radio to >50 TeV γ -rays [10]. More recently, VHE γ -ray emission has been detected from the Vela X PWN [4], which is an order of magnitude older (~ 11 kyr) than the Crab nebula, and its nebula is significantly offset from the pulsar position, both in X-rays and VHE γ -rays. Offset nebulae in both X-rays and VHE γ -rays have also been observed in the Kookaburra Complex [2] and for the PWN associated with the γ -ray source HESS J1825-137 [7, 3]. The latter source appears much brighter and more extended in VHE γ -rays than in keV X-rays. This suggests

that searches at TeV energies are a powerful tool for detecting PWNe.

Motivated by these detections, a systematic search for VHE γ -ray sources associated with high spin-down energy loss rate pulsars was performed, using data obtained with the H.E.S.S. instrument. The VHE γ -ray data set used in the search includes all data used in the H.E.S.S. Galactic plane survey [3], an extension of the survey to $-60^\circ < l < -30^\circ$, dedicated observations of Galactic targets and re-observations of H.E.S.S. survey sources. It spans Galactic longitudes $-60^\circ < l < 30^\circ$ and Galactic latitudes $-2^\circ < b < 2^\circ$, a region covered with high sensitivity in the survey. These data are being searched for VHE emission from pulsars from the Parkes Multibeam Pulsar Survey [11]. The search for a possible γ -ray excess is done in a circular region with radius $\theta = 0.22^\circ$ (as in [3]) around each pulsar position, sufficient to encompass a large fraction of a possible PWN. The statistical significance of the resulting associations of the VHE γ -ray source with the pulsar is evaluated by repeating the procedure for randomly gen-

erated pulsar samples, modelled after the above-mentioned parent population.

In this search, it is found that pulsars with high spin-down energy loss rates are on a statistical basis accompanied by VHE emission. The search for VHE γ -ray emission near the pulsar PSR J1718–3825 revealed the new VHE γ -ray source HESS J1718–385. This paper deals with the results from the HESS data analysis of HESS J1718–385 and with its possible associations with PSR J1718–3825 and other objects seen in radio and X-ray wavelengths.

H.E.S.S. Observations and Analysis

The data on HESS J1718–385 are composed primarily from dedicated observations of the supernova remnant RX J1713.7–3946 [1], which is located at about 1.6° south-west of HESS J1718–385. After passing the H.E.S.S. standard data quality criteria based on hardware and weather conditions, the data set for HESS J1718–385 has a total live time of ~ 82 hours. The standard H.E.S.S. analysis scheme [2] is applied to the data, including optical efficiency corrections. In this analysis, *hard cuts* are applied, which include a rather tight cut on the shower image brightness of 200 photo-electrons and are suitable for extended, hard-spectrum sources such as PWN. These cuts also improve the angular resolution and therefore suppress contamination from the nearby RX J1713.7–3946. To produce a sky map, the background at each test position in the sky is derived from a ring surrounding this position with a mean radius of 1° and a width scaled to provide a background area that is about 7 times larger than the area of the on-source region.

For spectral studies, only observations in which the camera centre is offset by less than 2° from the best-fit source position are used to reduce systematic effects due to reconstructed γ -ray directions falling close to edge of the field of view. The remaining live time of the data sample is ~ 73 hours. The spectral significance is calculated by counting events within a circle of radius 0.2° from the best-fit position, chosen to enclose the whole emission region while reducing systematic effects arising from morphology assumptions. The proximity

of the strong source makes it necessary to choose the background data from off-source observations (matched to the zenith angle and offset distribution of the on-source data) instead of from areas in the same field of view. For a more detailed description of methods for background estimation, see [8].

Results

The detection significance from the search for VHE γ -ray emission within 0.22° of the location of PSR J1718–3825 is 7.9σ . A very conservative estimate of the number of trials involved ([3]) leads to a corrected significance of 6.2σ .

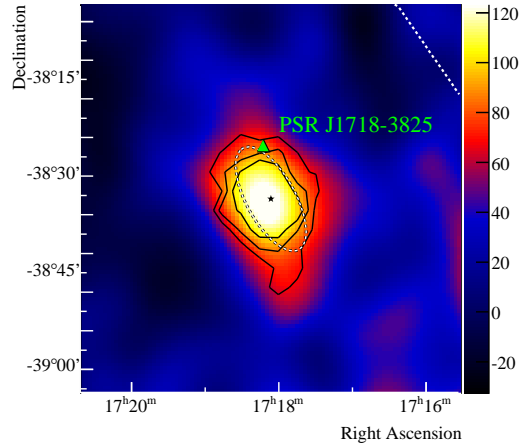


Figure 1: An image of the VHE γ -ray excess counts of HESS J1718–385, smoothed with a Gaussian of width 0.06° . The colour scale is set such that the blue/red transition occurs at approximately the 3σ significance level. The black contours are the 4 , 5 and 6σ significance contours. The position of the pulsar PSR J1718–3825 is marked with a green triangle and the Galactic plane is shown as a white dotted line. The best-fit position for the γ -ray source is marked with a black star and the fit ellipse with a dashed line.

Figure 1 shows the smoothed excess count map of the $1^\circ \times 1^\circ$ region around HESS J1718–385. A two-dimensional Gaussian brightness profile, folded with the H.E.S.S. point-spread function, is fit to the distribution before smoothing. Its parameters are the width in two dimensions and the orientation angle, defined counter-clockwise from North. The intrinsic widths (with the effect of

the point-spread function removed) for the fit are $9' \pm 2'$ and $4' \pm 1'$ and the orientation angle is $\sim 33^\circ$. The best-fit position for the centre of the excess is RA = $17^h 18^m 7^s \pm 5^s$, Dec = $-38^\circ 33' \pm 2'$ (epoch J2000). H.E.S.S. has a systematic pointing error of $\sim 20''$.

For the spectral analysis, a statistical significance of 6.8σ (with 343 excess counts) is derived. Figure 2 shows the measured spectral energy distribution for HESS J1718-385 (in $E^2 dN/dE$ representation).

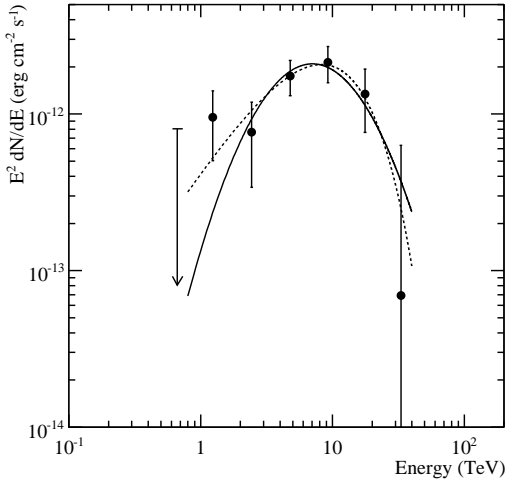


Figure 2: The energy spectrum of HESS J1718-385, which is fit by a curved profile (solid line). Alternatively, the fit of an exponentially cut-off power law is shown (dashed line, refer to the text for details on both fits). The first point in the spectrum lacks statistics due to lower exposure at small zenith angles and is plotted as an upper limit with a confidence level of 2σ .

The spectrum is fit by a curved profile (shown as the solid line):

$$\frac{dN}{dE} = N_0 \left(\frac{E_{\text{peak}}}{1 \text{ TeV}} \right)^{-2} \left(\frac{E}{E_{\text{peak}}} \right)^{\beta \cdot \ln(E/E_{\text{peak}}) - 2} \quad (1)$$

The peak energy E_{peak} is $(7 \pm 1_{\text{stat}} \pm 1_{\text{sys}})$ TeV, the differential flux normalisation $N_0 = (1.3 \pm 0.3_{\text{stat}} \pm 0.5_{\text{sys}}) \times 10^{-12} \text{ TeV}^{-1} \text{ cm}^{-2} \text{ s}^{-1}$ and $\beta = -0.7 \pm 0.3_{\text{stat}} \pm 0.4_{\text{sys}}$. This fit has a $\chi^2/d.o.f.$ of 3.2/3. The integral flux between 1 – 10 TeV is about 2 % of the flux of the Crab nebula in the same energy range [2].

Alternatively, fitting the spectrum by an exponentially cut-off power law ($dN/dE = N_0 E^{-\Gamma} e^{-E/E_{\text{cut}}}$) gives $N_0 = (3.0 \pm 1.9_{\text{stat}} \pm 0.9_{\text{sys}}) \times 10^{-13} \text{ TeV}^{-1} \text{ cm}^{-2} \text{ s}^{-1}$, photon index $\Gamma = 0.7 \pm 0.6_{\text{stat}} \pm 0.2_{\text{sys}}$ and a cut-off in the spectrum at an energy of $E_{\text{cut}} = (6 \pm 3_{\text{stat}} \pm 1_{\text{sys}}) \text{ TeV}$. This fit, which is shown as a dashed line in Figure 2, has a $\chi^2/d.o.f.$ of 1.6/3.

Both the curved and exponentially cut-off power law profiles fit the data well; the former has the advantage of showing explicitly the peak energy of the spectrum, which has to date only been resolved in one other VHE source, Vela X [4].

Possible Associations

The γ -ray source HESS J1718-385 is located $\sim 0.14^\circ$ south of the pulsar PSR J1718-3825. PSR J1718-3825 appears to be a Vela-like pulsar, as it is of comparable age, 90 kyr, and has a similar spin period, 75 ms. From the spectral fit of a curved profile, the energy flux of HESS J1718-385 between (1 – 10) TeV is estimated to $2.9 \times 10^{-12} \text{ erg cm}^{-2} \text{ s}^{-1}$. With a distance of $\sim 4 \text{ kpc}$ and a spin-down luminosity of $\dot{E} = 1.3 \times 10^{36} \text{ erg s}^{-1}$, PSR J1718-3825 is energetic enough to power HESS J1718-385, with an implied efficiency of $\epsilon_\gamma \equiv L_\gamma/\dot{E} = 0.5\%$.

As can be seen in Figure 3, no obvious X-ray counterpart is visible for HESS J1718-385. There is diffuse extended radio emission, which is partially coincident with the VHE emission. However, this emission seems to be correlated with thermal dust emission visible in the IRAS Sky Survey Atlas [12], suggesting that the radio emission is thermal and is thus not likely associated with a possible PWN. The brightest part of this diffuse feature is catalogued as PMN J1717-3846 [14]. From the point of view of positional coincidence, energetics, and lack of other counterparts, the association of HESS J1718-385 with PSR J1718-3825 seems plausible. To confirm this, additional evidence from spectral and morphological studies in VHE γ -rays and from data at other wavelengths is needed.

HESS J1718-385 may well represent the first VHE γ -ray PWN found in a systematic search for pulsar associations, despite the present lack

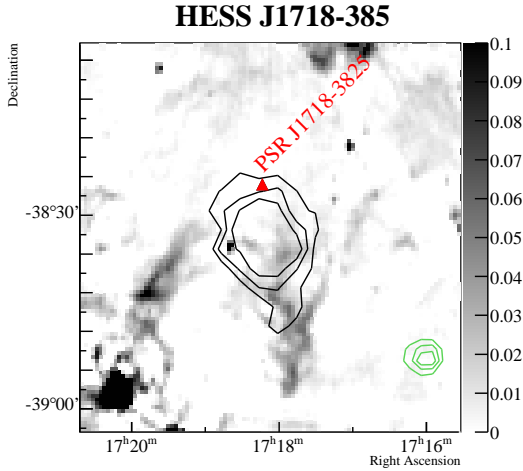


Figure 3: Radio image from the Molonglo Galactic Plane Survey at 843 MHz [11] (in Jy/beam). The H.E.S.S. significance contours are overlaid in black and the pulsar position is marked with a red triangle. Adaptively smoothed ROSAT hard-band X-ray contours are shown in green [19].

of a PWN detection in other wave bands. The remarkable similarity between HESS J1718–385 and other known VHE PWNe, together with the lack of other probable counterparts, gives additional confidence. The detection of an X-ray PWN would provide confirmation.

Acknowledgements

The support of the Namibian authorities and of the University of Namibia in facilitating the construction and operation of H.E.S.S. is gratefully acknowledged, as is the support by the German Ministry for Education and Research (BMBF), the Max Planck Society, the French Ministry for Research, the CNRS-IN2P3 and the Astroparticle Interdisciplinary Programme of the CNRS, the U.K. Science and Technology Facilities Council (STFC), the IPNP of the Charles University, the Polish Ministry of Science and Higher Education, the South African Department of Science and Technology and National Research Foundation, and by the University of Namibia. We appreciate the excellent work of the technical support staff in Berlin, Durham, Hamburg, Heidelberg, Palaiseau, Paris, Saclay, and in Namibia in the construction and operation of the equipment. We have made use of the ROSAT Data Archive of the Max-Planck-Institut fuer extraterrestrische Physik (MPE) at Garching, Germany.

References

- [1] F. Aharonian et al. A detailed spectral and morphological study of the gamma-ray supernova remnant RX J1713.7–3946 with HESS. *A&A*, 449:223–242, April 2006.
- [2] F. Aharonian et al. Discovery of the two “wings” of the Kookaburra complex in VHE γ -rays with HESS. *A&A*, 456:245–251, September 2006.
- [3] F. Aharonian et al. Energy dependent γ -ray morphology in the pulsar wind nebula HESS J1825–137. *A&A*, 460:365–374, December 2006.
- [4] F. Aharonian et al. First detection of a VHE gamma-ray spectral maximum from a cosmic source: HESS discovery of the Vela X nebula. *A&A*, 448:L43–L47, March 2006.
- [5] F. Aharonian et al. Observations of the Crab nebula with HESS. *A&A*, 457:899–915, October 2006.
- [6] F. Aharonian et al. The H.E.S.S. Survey of the Inner Galaxy in Very High Energy Gamma Rays. *ApJ*, 636:777–797, January 2006.
- [7] F. A. Aharonian et al. A possible association of the new VHE γ -ray source HESS J1825 137 with the pulsar wind nebula G 18.0 0.7. *A&A*, 442:L25–L29, November 2005.
- [8] D. Berge, S. Funk, and J. Hinton. Background modelling in very-high-energy γ -ray astronomy. *A&A*, 466:1219–1229, May 2007.
- [9] A. J. Green, L. E. Cram, M. I. Large, and T. Ye. The Molonglo Galactic Plane Survey. I. Overview and Images. *ApJS*, 122:207–219, May 1999.
- [10] A. M. Hillas et al. The Spectrum of TeV Gamma Rays from the Crab Nebula. *ApJ*, 503:744, August 1998.
- [11] R. N. Manchester et al. The Parkes multi-beam pulsar survey - I. Observing and data analysis systems, discovery and timing of 100 pulsars. *MNRAS*, 328:17–35, November 2001.
- [12] G. Neugebauer et al. The Infrared Astronomical Satellite (IRAS) mission. *ApJL*, 278:L1–L6, March 1984.
- [13] W. Voges, T. Boller, J. Englhauser, M. Freyberg, and R. Supper. The ROSAT X-ray Database from All-Sky Survey and Pointed Observations. In R. J. Brunner, S. G. Djorgovski, and A. S. Szalay, editors, *ASP Conf. Ser. 225: Virtual Observatories of the Future*, page 234, 2001.
- [14] A. E. Wright, M. R. Griffith, B. F. Burke, and R. D. Ekers. The Parkes-MIT-NRAO (PMN) surveys. 2: Source catalog for the southern survey (delta greater than -87.5 deg and less than -37 deg). *ApJS*, 91:111–308, March 1994.



Morphological Studies of the PWN Candidate HESS J1809-193

NU. KOMIN¹, S. CARRIGAN², A. DJANNATI-ATAÏ³, Y.A. GALLANT¹,
K. KOSACK², G. PUEHLHOFFER⁴, S. SCHWEMMER⁴, FOR THE H.E.S.S. COLLABORATION⁵

¹ *LPTA, Université Montpellier 2, CNRS/IN2P3, Montpellier, France*

² *Max-Planck-Institut für Kernphysik, Heidelberg, Germany*

³ *APC (CNRS, Université Paris VII, CEA, Observatoire de Paris), Paris, France*

⁴ *Landessternwarte, Universität Heidelberg, Germany*

⁵ *www.mpi-hd.mpg.de/HESS*

komin@lpta.in2p3.fr

Abstract: The source HESS J1809–193 was discovered in 2006 in data of the Galactic Plane survey, followed by several re-observations. It shows a hard gamma-ray spectrum and the emission is clearly extended. Its vicinity to PSR J1809-1917, a high spin-down luminosity pulsar powerful enough to drive the observed gamma-ray emission, makes it a plausible candidate for a TeV Pulsar Wind Nebula (PWN). On the other hand, in this region of the sky a number of faint, radio-emitting supernova remnants can be found, making a firm conclusion on the source type difficult.

Here we present a detailed morphological study of recent H.E.S.S. data and compare the result with X-ray measurements taken with *Chandra* and radio data. The association with a PWN is likely, but contributions from supernova remnants cannot be ruled out.

Introduction

Since the beginning of observations with H.E.S.S. (High Energy Stereoscopic System) in 2003 the number of known TeV gamma-ray emitting sources has increased drastically. The ongoing scan of the Galactic plane revealed several bright and extended sources for which no clear association with objects in other wavelength could be found [1, 3].

Pulsars, rapidly rotating neutron stars, are widely believed to be able to accelerate particles up to PeV energies. Those objects loose their rotational energy in winds of relativistic particles. The confinement of the wind in the interaction with the ambient interstellar material forms shocks; the particles accelerated there are visible as a Pulsar Wind Nebula (PWN) (see [9] for a review). Synchrotron radiation seen in radio and X-rays prove the existence of relativistic electrons in the PWN. These electrons undergo inverse Compton (IC) scattering off ambient radiation fields, like the Cosmic Microwave Background, Galactic infrared back-

ground and optical star light, leading to the production of TeV gamma-rays.

Here we present the observation of one TeV source, HESS J1809–193, which is located close to a powerful pulsar and thus a good PWN candidate. X-ray emission from the direction of the pulsar support the theory of being a PWN. However, confusion with other sources cannot be ruled out.

TeV observations of HESS J1809–193

H.E.S.S. is a system of four Imaging Atmospheric Cherenkov telescopes (IACTs) dedicated to the observation of TeV gamma-rays. Its high sensitivity allows the detection of point sources with a flux of 1% of that of the Crab nebula within 25 h [3]. Its large field of view and an angular resolution of better than 0.1° makes it an ideal tool for observations of extended objects and for the conduction of sky surveys.

In the original Galactic plane survey conducted with H.E.S.S., TeV emission from

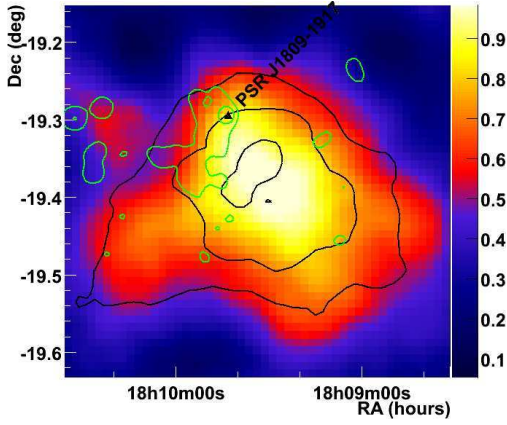


Figure 1: TeV gamma-ray excess counts from the direction of HESS J1809–193 (colour scale). The image is smoothed with the point-spread function. Overlaid are 5, 7 and 9σ significance contours, oversampled with a circle with radius 0.1° . The position of the pulsar is marked with a black triangle. The green contours denote the diffuse X-ray emission from Fig. 2.

HESS J1809–193 was only marginally detected. Further re-observations confirmed the existence of gamma-ray emission [6]. Further observations were performed in autumn 2006; in total data with a live time of 32 h is available.

The gamma-ray excess map of the source HESS J1809–193 is shown in Fig. 2. The emission is clearly extended lying south-west of the pulsar. In addition faint emission can be seen to the south-east. In total, an excess of 3600 events with a significance of 19σ was detected. The source shows an energy spectrum consistent with a power law with an index of $2.2 \pm 0.1_{\text{stat}} \pm 0.2_{\text{syst}}$ and an energy flux between 1 and 10 TeV of roughly $1.3 \times 10^{-11} \text{ erg cm}^{-2} \text{ s}^{-1}$ [6]. If this energy flux is projected to the distance of the pulsar, only 1.2% of the pulsar’s spin down luminosity of $1.8 \times 10^{36} \text{ erg s}^{-1}$ is needed to power the H.E.S.S. source. Therefore it seems to be plausible that HESS J1809–193 is indeed a Pulsar Wind Nebula.

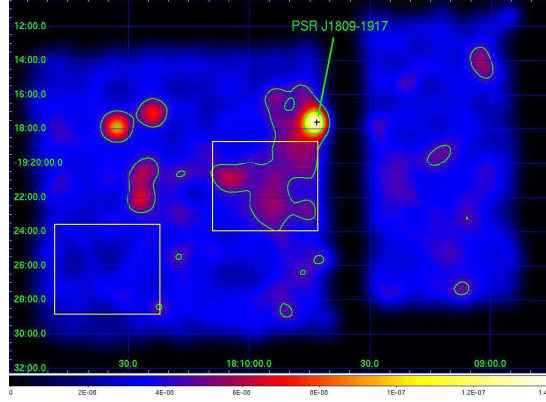


Figure 2: Chandra X-ray excess of the field of view of HESS J1809–193. The map is exposure-corrected and smoothed with a Gaussian with $32''$.

X-Ray Observations

In the data of the Galactic plane scan performed with the ASCA satellite diffuse emission was detected [7], which turned out to be coincident with the TeV source. The X-ray source G11.0 + 0.0 has been discussed to be either a young shell-type supernova remnant (SNR) or a plerionic SNR.

High-resolution observations with the *Chandra* satellite revealed a compact X-ray nebula north of the pulsar and additional faint emission south [12]. Here we present *Chandra* data which was taken in February 2007 (ObsID 6720). Figure 2 shows the exposure-corrected and smoothed X-ray excess map. It shows a strong X-ray nebula, high resolution images show its extension to the north of the pulsar [12]. Further faint emission can be seen to the south.

The significance of the diffuse emission was tested by comparing the on-source region with an off-source region in the same field of view (these regions are indicated by the yellow rectangles in Fig. 2). Taking into account the small acceptance difference of 4% (estimated from the exposure map at 2 keV), the source region shows an excess of about 900 events with a statistical significance of 10σ .

The contour of the diffuse X-ray emission is overlaid in the TeV excess map in Fig. 2. It should be noted that due to the gap between the chips of

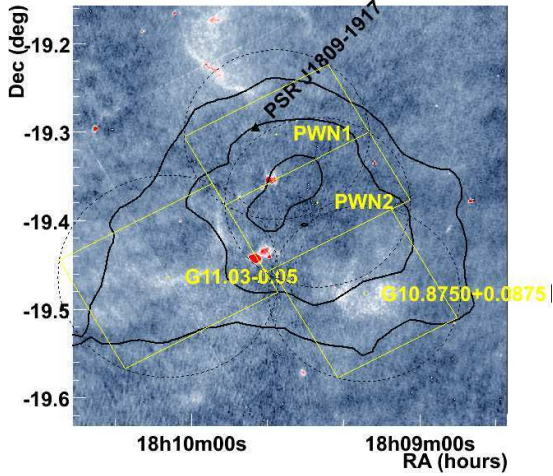


Figure 3: MAGPIS radio image. Overlaid are the 5, 7 and 9σ H.E.S.S. significance contours. The yellow rectangles indicate the test regions for the spectral analysis of the H.E.S.S. data.

the X-ray detector and the different nature of the chips on the right hand side, no conclusions can be drawn on the existence of diffuse emission to the west. However, it can be seen that the X-ray nebula's extension to the south is far smaller than the extension of the TeV emission.

Radio Data of the Field of View

We compared the region of HESS J1809–193 with radio data of the Multi-Array Galactic Plane Imaging Survey [11] shown in Fig. 3. North of the pulsar is the SNR G11.18 + 0.11 [8, 7], not coincident with the H.E.S.S. excess. Located south-east of the pulsar and coincident with the H.E.S.S. excess is the SNR G11.03 – 0.05 [8, 7]. Further south-west of the pulsar is the supernova remnant candidate 10.8750 + 0.0875 [11]. In the region between the latter two SNRs and the pulsar no diffuse radio emission can be found.

For a spectral analysis different regions according to the radio data have been chosen. Two regions for the SNRs G11.03 – 0.05 and 10.8750 + 0.0875 and another two regions for the possible pulsar wind nebula (PWN1, PWN2). These regions are indicated in Fig. 3.

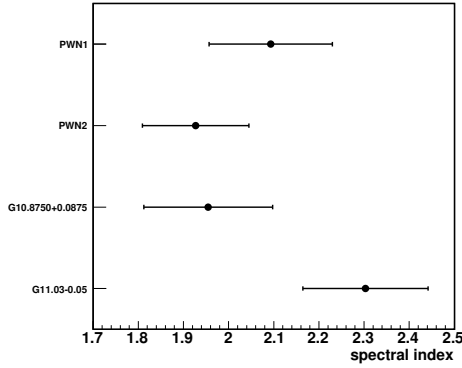


Figure 4: Spectral indices for the test regions indicated in Fig. 3.

Spectral Analysis

The TeV energy spectra of each region were fitted with a power law. The spectral indices are shown in Fig. 4. The regions PWN1, PWN2 and 10.8750 + 0.0875 are with increasing distance to the pulsar. A steepening of the spectrum with increasing distance would be a clear indication for a PWN (see [5]). A significant different energy spectrum between the region of the SNR G11.03 – 0.05 and the rest of the emission region would be a hint for different source associations. However, due to the large statistic uncertainties no conclusion on spectral variations over the extension of the source can be drawn.

Discussion

The existence of the powerful pulsar PSR J1809 – 1917 which can easily power the TeV emission suggests that the TeV emission is a PWN associated with the pulsar. The association with a PWN is further supported by a compact X-ray nebula and diffuse X-ray emission coincident with the H.E.S.S. source. The X-ray emission is significantly smaller than the TeV source. This has been already seen for the PWN HESS J1825 – 137 [2].

On the other hand, two supernova remnants coincide with the TeV emission. They do not show X-ray emission, however, TeV emission can still be

expected, in particular if they are associated with dense molecular clouds [13, 14]. Further studies will include the search for dense molecular clouds in the region.

Conclusion

Detailed studies of the source HESS J1809 – 193 and comparison with objects in other wavelength show that this source is likely a PWN powered by the pulsar PSR J1809 – 1917. The number of TeV emitting PWNe is increasing, showing that TeV PWN constitute a significant fraction of the Galactic TeV gamma-ray source population.

Contribution of gamma-ray emission from faint radio supernova remnants cannot be ruled out. Radio-emitting, X-ray quiet SNRs, possibly in connection with dense molecular clouds, remain interesting targets for gamma-ray observations.

Acknowledgements

The support of the Namibian authorities and of the University of Namibia in facilitating the construction and operation of H.E.S.S. is gratefully acknowledged, as is the support by the German Ministry for Education and Research (BMBF), the Max Planck Society, the French Ministry for Research, the CNRS-IN2P3 and the Astroparticle Interdisciplinary Programme of the CNRS, the U.K. Science and Technology Facilities Council (STFC), the IPNP of the Charles University, the Polish Ministry of Science and Higher Education, the South African Department of Science and Technology and National Research Foundation, and by the University of Namibia. We appreciate the excellent work of the technical support staff in Berlin, Durham, Hamburg, Heidelberg, Palaiseau, Paris, Saclay, and in Namibia in the construction and operation of the equipment.

References

- [1] Aharonian F. et al. (H.E.S.S. collaboration). *Science*, 307:1938–1942, March 2005.
- [2] Aharonian F. et al. (H.E.S.S. collaboration). *A&A*, 442:L25–L29, November 2005.
- [3] Aharonian F. et al. (H.E.S.S. collaboration). *ApJ*, 636:777–797, January 2006.
- [4] Aharonian F. et al. (H.E.S.S. collaboration). *A&A*, 457:899–915, October 2006.
- [5] Aharonian F. et al. (H.E.S.S. collaboration). *A&A*, 460:365–374, December 2006.
- [6] Aharonian F. et al. (H.E.S.S. collaboration). *A&A*, 472:489–495, September 2007.
- [7] A. Bamba, M. Ueno, K. Koyama, and S. Yamauchi. *ApJ*, 589:253–260, May 2003.
- [8] C. L. Brogan, J. D. Gelfand, B. M. Gaensler, N. E. Kassim, and T. J. W. Lazio. *ApJ*, 639:L25–L29, March 2006.
- [9] B. M. Gaensler and P. O. Slane. *ARA&A*, 44:17–47, September 2006.
- [10] D. A. Green. *Bulletin of the Astronomical Society of India*, 32:335–370, December 2004.
- [11] D. J. Helfand, R. H. Becker, R. L. White, A. Fallon, and S. Tuttle. *AJ*, 131:2525–2537, May 2006.
- [12] O. Kargaltsev and G. G. Pavlov. *submitted to ApJ, ArXiv e-prints 0705.2378*, 705, May 2007.
- [13] Rowell, G. et al. for the H.E.S.S. collaboration. Discovery of TeV Gamma-Ray Emission in the W28 Region from HESS Observations, and Multiwavelength Comparisons. In *ICRC 2007*, 2007.
- [14] R. Yamazaki, K. Kohri, A. Bamba, T. Yoshida, T. Tsuribe, and F. Takahara. *MNRAS*, 371:1975–1982, October 2006.



New VHE emitting middle-age pulsar wind nebula candidates in the extended H.E.S.S. Galactic plane survey data

A. LEMIERE^{1,3}, A. DJANNATI¹, O. DEJAGER², R. TERRIER¹

⁽¹⁾ *APC - Astroparticule et Cosmologie - CNRS Université Paris VII, Paris.*

⁽²⁾ *Unit for Space Physics, North-West University, Potchefstroom 2520, South Africa.*

⁽³⁾ *Center for Astrophysics, Smithsonian-Harvard Observatory 60 Garden street, Cambridge MA, USA.*

alemiere@head.cfa.harvard.edu

Abstract: The H.E.S.S. 2004-2005 survey of the Galactic Plane at energies above 200 GeV had revealed a number of pulsar wind nebulae candidates, including the remarkable source HESS J1825-137. Spatially resolved spectral measurements of this source gave the first evidence of an energy-dependent morphology which was interpreted as being due to the cooling of relic electrons cumulated throughout pulsar's history. Also for a few number of sources the asymmetry of the pulsar with respect to the nebula could be attributed to an asymmetric reverse shock from the associated supernova remnant due to inhomogeneities in the interstellar matter. Subsequently a class of large offset and relic nebulae emerged as an outstanding new type of VHE γ -ray source.

We discuss here the cases of such nebulae in the extended H.E.S.S. Galactic Plane survey data through an energetic criterion taking into account earlier epochs of pulsar injection as well as through investigation of CO data to search for inhomogeneities.

Introduction

During 2004-2006 H.E.S.S. (High energy stereoscopic system) performed a Survey of the inner part of the Galaxy [3] where its excellent capability allowed to mark a breakthrough in the field of Pulsar wind nebula (PWN) study : for the first time the morphological structure of many PWN was resolved in the γ -ray band and many of them appears to belong to the middle-age Vela-like pulsar class. HESS J1825-137 is the archetypal example of this population. For this source, a detailed spectral and morphological analysis [2] revealed for the first time in γ -ray a steepening of the energy spectrum with increasing distance from the pulsar. This fact was interpreted as due to the radiative cooling of the emitting electrons during their propagation. Indeed very high energy (VHE) Inverse Compton (IC) flux typically provide information on lower energy electrons than those of the keV synchrotron flux and imply a larger life-time for IC emitters. For the middle-age PWN, electrons emitting at TeV energies consist of cooled particles cumulated during few tenth of kyrs (called

relic electrons thereafter). HESS J1825-137 can also be taken as a prototype by its asymmetrical configuration with respect to the pulsar, a morphological characteristic observed in many of the middle-age candidates. The similar morphology of HESS J1825-137 to that of the X-ray nebula G18.0-0.7 [8] suggested an asymmetric reverse shock to have happened in the 10 first kyrs of the pulsar life, consisting of the interaction of a supernova remnant (SNR) with an inhomogeneous surrounding material implying different colliding times of the reverse shock with the PWN, and resulting in a one-sided morphology [1]. To examine this hypothesis, [12] probed the interstellar matter density near G18.0-0.7 through ^{12}CO line emissions. Two molecular structures were discovered and their characteristics were found compatible with the observed offset of the VHE nebula HESS J1825-137 within the framework of the simulations by [5].

Here, we propose to extend this study to the large set of asymmetric middle-age PWN candidates found in the 2004-2007 H.E.S.S. data. In one first step, the association between the TeV sources and

the pulsars will be tested by the calculation of a new energy criterion. It will result in the first catalogue of middle-age PWN at VHE γ -ray. For the selected candidates which exhibit an asymmetric shape, the pulsar configuration with respect to the H_2 density profile and the high energy emissions will be considered and compared to the numerical model of [5], as it has been done in [12].

Build a catalogue of PWN candidates

Method

During the first part of the H.E.S.S. scan of the Galactic Plane, we built a list of six VHE sources for which the spectral and morphological characteristics together with the proximity of an energetic pulsar placed them as potential PWN candidates. With the extended scan performed during 2006-2007, 3 new sources have been added to the list : HESS J1718-385 and HESS J1809-193 [3], and HESS J1912+101 [9]. All the sources of this list have ages between few to few hundred of kyrs (middle-age class) and the high energetic pulsars are closer than 7 kpc from us.

To evaluate the likelihood of an association between the TeV sources and the nearby pulsars, the power available for γ -ray production must be assessed. Since pulsar's rotational energy \dot{E} is the source for most of the emission seen from PWNe, it is used to consider the actual spin evolution of pulsars with respect to the PWN flux. But since the sources we consider have middle-ages, and given the fact that TeV electrons emitters are cooled particles in the nebula, we must consider also the earlier stages of the system if we want to get a true estimation of the TeV flux (contrary to the X-ray nebulae for which the actual \dot{E} is relevant).

Our solution is to take into account the electrons injected by the pulsar in the nebula along the pulsar life-time, and the radiative losses dominated by the synchrotron component. The model assumes a power law electron injection spectrum with index of 2.02 and a fixed minimum energy $E_{\min} = 1$ TeV. The maximum energy is constrained by the acceleration condition that the gyroradius must not exceed the terminal shock radius and the normalization is determined by \dot{E} at each time and by the ratio between particles and field σ defined in [11]

and fixed at 0.003 (similar to Crab Nebula's). The time evolution of the spin down power of the pulsar is written $\dot{E}(t) = \frac{\dot{E}_o}{(1+t/\tau_o)^2}$, with \dot{E}_o , the initial spin down power of the pulsar, τ_o the characteristic pulsar time scale (we fix it at the standard value of 400 years) and a braking index of 3. The total injected energy by the pulsar during the time dt is:

$$dW = \frac{1}{\sigma + 1} \dot{E}(t) dt \quad (1)$$

The synchrotron losses are calculated with a typical average magnetic field of $5 \mu\text{G}$:

$$dP_{\text{losses}} = k.E^2.B^2 dt \quad (2)$$

The energetic balance for the electrons in the nebula can then be written at each time :

$$dU = dW - dP_{\text{losses}} \quad (3)$$

After integration of this equation over the pulsar life-time, we obtain the actual total electron spectrum in the nebula. These electrons produce Inverse Compton photons that can be seen in the γ -ray band. We use an average value for the targets density of 0.25 eV.cm^{-3} for the CMB and 0.5 eV.cm^{-3} for the star and dust light. We define as ϵ an equivalent percentage of the ratio between the measured and predicted (this calculation) flux and propose to use it as an energetic criterion to estimate the credibility of an association between the VHE sources and corresponding pulsars.

Results

Table 1 shows the complete selected sources list, with the corresponding pulsars characteristics, the measured and predicted γ -ray luminosity and the γ -ray efficiency. A 30% efficiency criterion of acceptance looks reasonable, since it gives the insurance that the pulsar generated enough power to reproduce the observed flux, even if the conversion efficiency at the shock radius is low. Using this criterion, a first class of 9 good candidates appears clearly in the upper part of the table, whereas the two last sources are definitely rejected. All the selected candidates are extended and have a spectral index between 2 and 2.5, in good agreement with the known X-ray nebula. Six of them have an X-ray nebula detected but only one has a counterpart

in radio (mostly due to the faint radio emission of such extended object).

One of the most remarkable characteristic of these sources is that almost all of them show an asymmetric shape. We now propose to investigate possible reasons of this asymmetry by exploring the Interstellar medium (ISM).

Search for inhomogeneity in the ISM

Data and Method

The ^{12}CO observations used here are taken from the Composite CO Survey from [7]. This survey compiles observations from 37 individual surveys with a resolution of 0.2° and a FWHM velocity resolution of 2 km.s^{-1} [7].

As a first step, clouds are searched for through the scan of the CO intensity in the (l, b) plane as a function of the radial velocity in the vicinity of the associated pulsar. If some structures are detected, the average CO velocity profiles are made in the line of sight of these structures and they are extracted by detecting CO pics. We take the fit (gaussian) centroid of the ^{12}CO peak to establish the kinematic distance to the clouds using the empirical Galactic rotation curve models [6]. Only molecular clouds with a compatible distance with the pulsar are selected. In order to compare the compatibility of the interstellar matter distribution with the one by [5], we analyze the average gradient of molecular matter along the vector defined from the pulsar position, in the direction of the TeV emission's center of gravity. The CO emission is spatially averaged for each band and integrated over the cloud's velocity range. These values (usually called $\langle W(\text{CO}) \rangle$) are converted into average H_2 column density using the conversion coefficient by [10]. We consider here the total average gradient of each distribution by defining the contrast as the ratio between the maximum and minimum values of the density and the characteristic scale as the distance needed for the density to decrease by a factor two. These numbers are given for each sources in Table .

Results

Half of the cases seems to have a configuration compatible with the simulations of [5]. Only one case is rejected (HESSJ 1420-607) due to the geometric configuration incompatible with the reverse shock hypothesis. The major conclusion of this study is that the asymmetric reverse shock is a credible hypothesis if we consider the ISM distribution around most of the middle-age PWN VHE candidates. However it remains difficult to get a strong conclusion on this study, firstly because of the distance near-far ambiguity and secondly because of the effect of projection in the line of sight.

Conclusion

We established a list of potential PWNe candidates in the H.E.S.S. data and calculated an energetic criterion for each of them, taking into account the pulsar spindown power evolution over time together with average synchrotron losses. This study allowed to build the first VHE catalogue of middle-age PWN candidates consisting of 9 sources. Many of these candidates show an asymmetric shape around the putative associated pulsar. By probing the ISM through CO data, we showed that for many of them, the hypothesis of an asymmetric reverse shock is not to exclude, given the ISM density distribution.

References

- [1] F. Aharonian et al. *A&A*, 442:L25, 2005.
- [2] F. Aharonian et al. *A&A*, 460:365, 2006.
- [3] F. Aharonian et al. . *submitted to A&A* , astro-ph/0705.1605v1, 2007.
- [4] F. Aharonian et al. *ApJ*, 636:777, 2006.
- [5] J. M. Blondin et al. *ApJ*, 563:806, 2001.
- [6] D. P. Clemens et al. *ApJ*, 295:422, 1985.
- [7] T. M. Dame et al. *ApJ*, 547:792, 2001.
- [8] B. M. Gaensler et al. *ApJ*, 588:441, 2003.
- [9] HESS source of the month <http://www.mpi-mpg.de/hfm/HESS/public/>.
- [10] S. D. Hunter et al. *ApJ*, 481, 1997.
- [11] C.F. Kennel et al. *ApJ*, 283:710, 1984.
- [12] A. Lemi re et al. (*in preparation*), 2007.

Name HESS	Pulsar PSR	Age (yrs)	Dist (kpc)	\dot{E} 10^{36} (erg/s)	$L_{\gamma\text{mes}}(\theta)$ 10^{35} (erg/s)(deg)	$L_{\gamma\text{theo}}$ 10^{35} (erg/s)	ϵ (%)	RX	A
J1303-631	J1301-6305	11 000	6.6	1.7	1.80(0.32)	6.78	27.00	x	Y
J1420-607	J1420-6048	13 000	5.6	10	0.61(0.16)	61.37	1.01	rx	Y
J1616-508	J1617-5055	8 100	6.5	18	1.59(0.4)	5.04	3.16	–	Y
J1702-420	J1702-4128	55 000	5.2	0.34	0.57(0.35)	10.8	5.30	–	Y
J1718-385	J1718-3825	89 500	4.2	1.3	0.14(0.18)	62.75	0.22	–	Y
J1804-216	J1803-2137	15 800	3.9	2.2	0.70(0.49)	16.79	4.20	x	Y
J1809-193	J1809-1917	51 000	3.7	1.8	0.33(0.5)	54.78	0.59	x	Y
J1825-137	J1823-13	21 000	3.9	2.8	1.96(0.8)	31.74	6.10	x	Y
J1912+101	J1913+1011	170 000	4.48	2.9	0.87(0.5)	199.2	0.43	–	Y
J1632-478	J1632-4818	19 800	7	0.05	2.67(0.36)	0.42	534	–	–
J1745-303	B1742-30	546 000	2.1	0.008	0.12(0.4)	0.32	32.77	–	–

Table 1: This table shows the complete selected sources list, with the corresponding pulsars characteristics, the measured (with the associated radius of intergration) and predicted γ -ray luminosity in the [200 GeV - 10 TeV] energy band and the γ -ray efficiency. The detection of a radio (r) or X-ray(x) nebula around the pulsar and an asymmetric shape of the VHE nebula (A) are also indicated.

Source name HESS	Cloud name MC	M_{CO} 10^3 (M_{sol})	density mol cm^{-3}	D_{Cl} kpc	Offset % R_{SNR}	H 10^{19} cm	Cont pc	D	G	Gr	RC
J1303-631	304.1+0.3	62	18	6.2	19.2	4	2	Y	Y	Y	Y
J1420-607	314+0.0	225	75	3.5/8	14	—	–	Y	N	N	N
J1616-508	332.7-0.6	222	164	3.9	10	12.2	2	Y	Y	Y	Y
J1718-385	348.8-0.4	11	16	4	20	—	–	Y	?	?	?
	348.8-0.5	13	40	3.5	20	—	–	Y	?	?	?
J1804-216	8.3+0.25	71	129	3	23	11.2	1.3	Y	Y	?	?
	8.7-0.6	132	107	4	23	—	–	N	–	–	–
J1809-193	11.1+0.12	80	67	3.7	25	13	2	Y	Y	Y	Y
J1825-137	18.15-0.32	80 000	150	4	20	4.2	3.6	Y	Y	Y	Y
	18.32-0.75	16 000	200	4	20	4.2	3.6	Y	Y	Y	Y

Table 2: Summary of the asymmetric PWNe candidates observed by H.E.S.S. for which we have detected one or several molecular clouds with distance compatible with the associated pulsar. The name, mass, density and approximate distance of the clouds are summarized. The offset between the pulsar and center of gravity of the source in percentage of the SNR radius, the contrast and the scale of the gradient of matter are calculated. Finally the distance (D), geometric configuration (G) and gradient (Gr) compatibility are compared with the simulations of [5](Y:compatible, N:not compatible).The final conclusion of the study is given in the last column (RC : reverse shock) (Y:compatible with the RC hypothesis, N:not compatible with the RC hypothesis).



New Companions for the lonely Crab? VHE emission from young pulsar wind nebulae revealed by H.E.S.S.

A. DJANNATI-ATAÏ¹, O.C. DE JAGER², R. TERRIER¹, Y.A. GALLANT³ & S. HOPPE⁴ FOR THE H.E.S.S. COLLABORATION⁵

¹ APC (CNRS, Université Paris VII, CEA, Observatoire de Paris), Paris, France

² Unit for Space Physics, North-West University, Potchefstroom 2520, South Africa

³ LPTA, Université Montpellier 2, IN2P3/CNRS, Montpellier, France

⁴ Max-Planck-Institut für Kernphysik, PO box 103980, D69029 Heidelberg, Germany

⁵ www.mpi-hd.mpg.de/HESS

djannati@apc.univ-paris7.fr

Abstract: The deeper and more extended survey of the central parts of the Galactic Plane by H.E.S.S. during 2005-2007 has revealed a number of new point-like, as well as, extended sources. Two point-like sources can be associated to two remarkable objects around “Crab-like” young and energetic pulsars in our Galaxy : G21.5-0.9 and Kes 75. The characteristics of each of the sources are presented and possible interpretations are briefly discussed.

Introduction

The standard candle of VHE astronomy, the Crab Nebula, has served for decades as a yardstick in almost all wavelengths, and yet it is a very peculiar object, harbouring the most energetic and one of the youngest pulsars of our Galaxy. Since the early days, where the similarities of the historical trio Crab/3C 58/G 21.5-0.9 were under debate [19], radio and X-ray astronomy have provided a wealth of information by detecting and characterizing nebulae around rotation-powered pulsars. In the VHE domain, H.E.S.S. has revealed more than a dozen pulsar wind nebulae (PWN), either firmly established as such or compelling candidates [16], almost all of which are middle-aged (at least few kyrs up to ~ 100 kyrs, except MSH 15-52) and exhibit an offset between the pulsar position and the nebula center. We report here on the VHE emission discovery of two remarkable objects, G 21.5-0.9 and Kes75, which also harbor very young and energetic pulsars and which on some aspects, especially their plerionic nebular emission due to an energetic pulsar, can be considered as Crab-like.

G21.5-0.9 [7], recently revealed as a composite SNR consisting of a centrally peaked PWN and a

4' shell [8, 10], was previously classified as one of the about ten Crab-like SNR [4]. Its flat spectrum PWN is polarised in radio [2] with a spectral break above 500 GHz [20]. The non-thermal X-ray PWN with radius $\sim 40''$ shows significant evidence of cooling [18], with the power-law photon index steepening from 1.43 ± 0.02 near the pulsar to 2.13 ± 0.06 at the edge of the PWN. There appears to be a synchrotron X-ray halo at a radius of $140''$ from the pulsar which could originate in the shell [8, 10], with a contribution of scattering off dust grains as proposed by Bocchino et al. [8]. The 61.8 ms pulsar PSR J1833-1034, with a spin-down power of $\dot{E} = 3.3 \times 10^{37}$ erg/s and a characteristic age of 4.9 kyr was discovered only recently through its faint radio pulsed emission [14, 9]. Given the derived distance of 4.7 ± 0.4 kpc, the age of G 21.5-0.9 was revised downwards by a factor of ~ 10 to force consistency with the freely expanding SNR shell [9]. PSR J1833-1034 in G 21.5-0.9 is the second most energetic pulsar known in the Galaxy.

Kes 75 (SNR G29.70.3) is also a prototypical example of a composite remnant for which the distance of 19 kpc was estimated through neutral hydrogen absorption measurements [1]. Its 3.5' radio

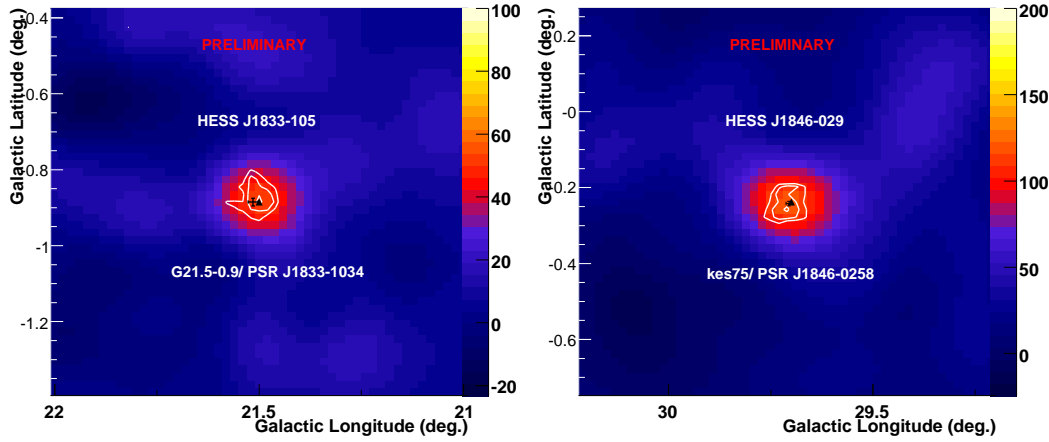


Figure 1: Smoothed excess maps ($\sigma = 0.08^\circ$) of the $0.5^\circ \times 0.5^\circ$ field of view around the positions of HESS J1833-105 (left) and HESS J1846-029 (right). The white contours show the pre-trials significance levels for 4, 5, 6 σ , and 7, 8, 9 σ , respectively. The black triangle marks the position of the pulsars. The best-fit positions of the two sources are marked with an error cross (for HESS J1846-029 the latter overlaps with the triangle).

shell surrounds a flat-spectrum highly polarized radio core, and harbors, at its center, the 325 ms X-ray Pulsar, PSR J1846-258 [13]. The latter has the shortest known characteristic age $\tau_c = 723$ yr and a large inferred magnetar-like magnetic field of $B = 4.9 \times 10^{13}$ G. The pulsar lies within a $25'' \times 20''$ X-ray nebula which exhibits an photon index of 1.92 ± 0.04 , but no evidence of cooling as a function of the distance to the pulsar. Like in G 21.5-0.9 there is an X-ray halo, in this case due mostly to dust scattering, but a non-thermal contribution from electrons accelerated in the shell remains possible [15].

Observations, Analysis & Results

Results presented in this section should be considered as preliminary.

The first H.E.S.S. observations of G 21.5-0.9 and Kes 75 were performed during 2004 and 2005 as part of the systematic survey of the inner Galactic plane within the longitude range $l \in [-30^\circ, +30^\circ]$ and latitude band $b \in [-3^\circ, +3^\circ]$. Kes 75, at the edge of the first survey, was covered in the extension to $l \in [+30^\circ, +60^\circ]$ of the survey in the years

2005-2007. The data obtained through the systematic survey was completed with followup observations of promising candidates in wobble mode, hence the two sources are offset at various angular distances with respect to the center of the field of view. The total quality-selected and dead-time corrected data-set includes 19.7 hours of data on G 21.5-0.9 and 24.1 hours on Kes 75, with average offsets of 1.33° and 1.1° , for each source, respectively.

The standard scheme for the reconstruction of events was applied to the data [4]. Cuts on the scaled width and length of images (optimised on γ -ray simulations and off-source data) were used to suppress the hadronic background. As described e.g. in [5], sky-maps and morphological analyses are made with a tight cut on the image size of 200 p.e. (photoelectrons) to achieve a maximum signal-to-noise ratio and a narrow PSF (point spread function). For the spectral analysis, the image size cut is loosened to 80 p.e. in order to cover the maximum energy range. The background estimation for each position in the two-dimensional sky map is made in the same way as for search of extended sources [12], i.e. computed from a ring with a radius of 1.0° . For a point-like source

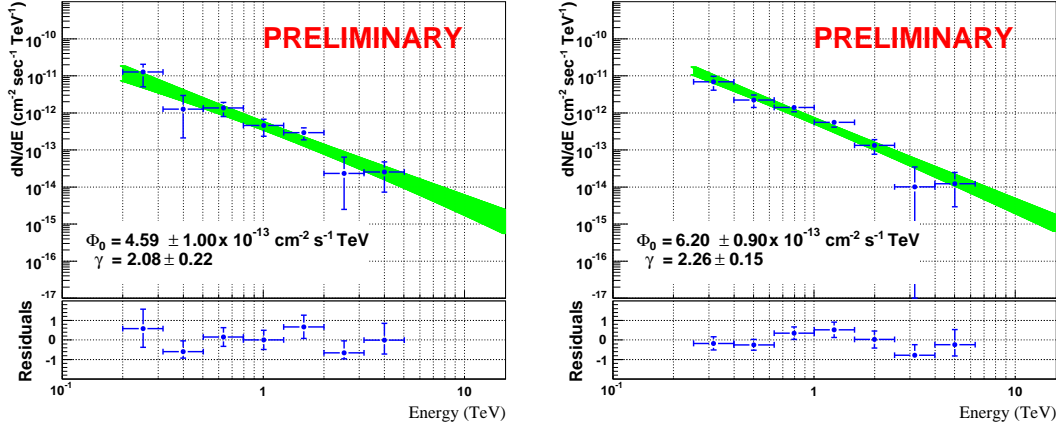


Figure 2: Differential energy spectra above for HESS J1833-105 (left) and HESS J1846-029 (right). The shaded area shows the 1σ confidence region for the fit parameters.

this radius yields seven times a larger area for the background estimation than the on-source region. The background used for the derivation of the spectrum, is evaluated from circular regions in the field of view with the same radius and same offset from the pointing direction as that of the source region. Finally, to avoid contamination of the background, events coming from known sources were excluded.

Fig. 1 shows the Gaussian-smoothed excess maps for HESS J1833-105 and HESS J1846-029 where the white contours mark the pre-trials significance levels. Both sources were first discovered as hot-spots within the analysis scheme described above and then confirmed through additional followup data at pre-trials significance of 6.4 and 9.9 standard deviations, respectively. A conservative estimate of the trials yields post-trials significance of 4.0σ and 8.3σ for HESS J1833-105 and HESS J1846-029, respectively.

The extension and the position of the sources were evaluated by adjusting to the images a symmetrical two-dimensional Gaussian function, convolved with the instrument PSF ($5'$ for this analysis). The best-fit positions lie at $18^{\text{h}}33^{\text{m}}32.5^{\text{s}} \pm 0.9^{\text{s}}, -10^{\text{d}}33'19'' \pm 55''$ and $18^{\text{h}}46^{\text{m}}24.1^{\text{s}} \pm 0.5^{\text{s}}, -02^{\text{d}}58'53'' \pm 34''$. The intrinsic extensions are compatible with a point-like source for both sources and their positions are in a quite good agreement with the pulsars associated

to each supernova remnant, i.e. PSR J1833-1036 ($18^{\text{h}}33^{\text{m}}33.57^{\text{s}}, -10^{\text{d}}34'7.5''$) and PSR J1846-0258 ($18^{\text{h}}46^{\text{m}}24.5^{\text{s}}, -02^{\text{d}}58'28''$).

The energy spectra of the two sources are derived using the forward-folding maximum likelihood fit of a power-law [12]. The fluxes are at a level of $\sim 2\%$ of that of the Crab Nebula and the spectra are rather hard (Fig. 2): the photon indices are $2.08 \pm 0.22_{\text{stat}}$ and $2.26 \pm 0.15_{\text{stat}}$ for HESS J1833-105 and HESS J1846-029, respectively, with a systematic error of ± 0.1 .

Discussion

It is remarkable that de Jager et al. [11] predicted that plerionic VHE γ -rays from G21.5-0.9 would be detectable at a level of $4 \times 10^{-13} \text{ cm}^{-2} \text{ s}^{-1}$ at 1 TeV with an electron spectral index of ~ 2.8 , which would give a photon index near 2.0 at VHE energies (after including KN effects given the contributions from dust and CMBR). Their prediction was based on an assumed equipartition field strength of $22 \mu\text{G}$ which is close to the value of $\sim 15 \mu\text{G}$ implied from γ -ray observations reported here (assuming IC scattering on CMB photons only, and using the ratio of the X-ray to the γ -ray luminosities: $L_X/L_\gamma \sim 30$). The equipartition field strength was afterwards increased to 0.3 mG following the revision of the maximum spectral

range of the radio PWN to 500 GHz [20, 9]. However, the detection of VHE γ -rays by H.E.S.S. from PWN tends to confirm the suggestion of Chevalier [3] that some PWN may be particle dominated, so that the true PWN field strength may be significantly lower than equipartition for some objects. In the case of Kes 75, $L_X/L_\gamma \sim 10$ yields also a lower than equipartition nebular magnetic field strength of $\sim 10 \mu\text{G}$. It should be noted that Kes 75 shows the highest conversion efficiency in X-rays ($\sim 15\%$) as compared to other “Crab-like” pulsars ($\sim 3\%$ and $\sim 0.6\%$ for the Crab and G 21.5-0.9, respectively) and a 100 times larger γ -ray efficiency ($\sim 2\%$) than the Crab and G 21.5-0.9 which are similar in that respect ($\sim 0.02\%$). However, the latter object’s $L_X/L_\gamma \sim 30$ is 4 times smaller than that of the Crab Nebula $L_X/L_\gamma \sim 120$. These numbers together with the spin parameters and high surface magnetic field in the case of PSR J1846-0258, show that these objects, although “Crab-like” in some aspects, do possess peculiar properties.

Given the evidence for synchrotron emission in the SNR shell, an alternative interpretation of the VHE emissions of G 21.5-0.9 and Kes75 would be radiation from particles accelerated at the non-relativistic forward shock of the freely expanding SNR. However the required field strength in the shell to explain the H.E.S.S. detection in terms of IC scattering should be much lower than $10 \mu\text{G}$, value which may be unreasonably low for typical expanding SNR shells. Deeper observations of both sources could help to constrain the size of the VHE emission region and to ascertain whether it is compatible with this scenario.

*

Acknowledgments The support of the Namibia authorities and of the University of Namibia in facilitating the construction and operation of H.E.S.S. is gratefully acknowledged, as is the support by the German Ministry for Education and Research (BMBF), the Max Planck Society, the French Ministry for Research, the CNRS-IN2P3 and the Astroparticle Interdisciplinary Programme of the CNRS, the U.K. Particle Physics and Astronomy Research Council (PPARC), the IPNP of the

Charles University, the Polish Ministry of Science and Higher Education, the South African Department of Science and Technology and National Research Foundation, and by the University of Namibia. We appreciate the excellent work of the technical support staff in Berlin, Durham, Hamburg, Heidelberg, Palaiseau, Paris, Saclay, and in Namibia in the construction and operation of the equipment.

References

- [1] R.H. Becker and D.J. Helfand. *ApJ*, 283:154, 1984.
- [2] R.H. Becker and A.E. Szymkowiak. *ApJ*, 248:L23, 1981.
- [3] R.A. Chevalier. *Adv. Space. Res.*, 33:456, 2004.
- [4] D.A. Green. *Bull. of the Astr. Soc. of India*, 32:335, 2004.
- [5] F.A. Aharonian et al. (H.E.S.S. Collaboration). *A&A*, 457:899–915, 2006.
- [6] F.A. Aharonian et al. (H.E.S.S. Collaboration). *A&A*, 456:245–251, 2006.
- [7] W.J. Altenhoff et al. *A&AS*, 1:319, 1970.
- [8] F. Bocchino et al. *A&A*, 442:539, 2005.
- [9] F. Camilo et al. *ApJ*, 637:456, 2006.
- [10] Matheson D.A. and S. Safi-Harb. *Adv. Space Res.*, 35:109, 2005.
- [11] O.C. de Jager et al. In *24th ICRC, Roma, Italy*, page 528, 1995.
- [12] A. Djannati-Ataï for the H.E.S.S. Collaboration. In *30th ICRC, Merida, Mexico*, 2007.
- [13] E.V. Gotthelf et al. *ApJ*, 552:L37, 2000.
- [14] Y. Gupta et al. *Current Science*, 89:853, 2005.
- [15] B.F. Helfand, D.J. Collins and Gotthelf E.V. *ApJ*, 582:783:792, 2003.
- [16] A. Lemi re for the H.E.S.S. Collaboration. In *30th ICRC, Merida, Mexico*, 2007.
- [17] F. Piron et al. *A&A*, 374:895, 2001.
- [18] P. Slane et al. *ApJ*, 533:L29, 2000.
- [19] A. S. Wilson and K. W. Weiler. *A&A*, 53:89–92, November 1976.
- [20] Gallant Y.A. and R.J. Tuffs. *Mem. Soc. Astron. Italiana*, 69:963, 1998.



Search for Pulsed VHE Gamma-Ray Emission from Young Pulsars with H.E.S.S.

M. FÜSSLING¹, S. SCHLENKER² AND C. VENTER³ FOR THE H.E.S.S. COLLABORATION, T. EIFERT⁴, R. MANCHESTER⁵ AND F. SCHMIDT⁶

¹*Institut für Physik, Humboldt-Universität zu Berlin, Newtonstr. 15, D 12489 Berlin, Germany*

²*CERN PH Department, CH-1211 Geneva 23, Switzerland*

³*Unit for Space Physics, North-West University, Potchefstroom 2520, South Africa*

⁴*Université de Genève, Section de physique, 24 Quai Ernest-Ansermet, CH-1211 Geneva 4, Switzerland*

⁵*Australia Telescope National Facility, CSIRO, PO Box 76, Epping NSW 1710, Australia*

⁶*Department of Astronomy and Astrophysics, The University of Chicago, IL 60637, USA*

fuessling@physik.hu-berlin.de

Abstract: We present the results of a search for pulsed very-high-energy (VHE) γ -ray emission from young pulsars using data taken with the H.E.S.S. imaging atmospheric Cherenkov telescope system. Data on eleven pulsars, selected according to their spin-down luminosity relative to distance, are searched for γ -ray signals with periodicity at the respective pulsar spin period. Special analysis efforts were made to improve the sensitivity in the 100 GeV γ -ray energy domain in an attempt to reduce the gap between satellite and ground-based γ -ray instruments. No significant evidence for pulsed emission is found in any data set. Differential upper limits on pulsed energy flux are determined for all selected pulsars in the approximate γ -ray energy range between 100 GeV and 50 TeV, using different limit determination methods, testing a wide range of possible pulsar light curves and energy spectra. The limits derived here imply that the magnetospheric VHE γ -ray production efficiency in young pulsars is less than 10^{-4} of the pulsar spin-down luminosity, requiring spectral turnovers for the high-energy emission of four established γ -ray pulsars, and constrain the inverse Compton radiation component predicted by several outer gap models.

Introduction

Rotating neutron stars are known to convert a significant part of their rotational energy into radiation that originates from within the magnetosphere. This emission is observable as a periodic signal at the neutron star rotation frequency (the *pulsar* phenomenon). For many of the known young and energetic pulsars, the emitted luminosity peaks at X-ray or γ -ray energies [12] and is usually attributed to curvature radiation of accelerated electrons in the strong magnetic fields pervading the pulsar magnetosphere. The luminosity of the pulsed high-energy emission was found to correlate significantly with the energy loss rate of the pulsar, i.e. its spin-down power \dot{E} [4, 3]. For most of the pulsars with established γ -ray emission [5], there is evidence for a turnover in the pulsed spectrum at a critical energy E_c in the sub-GeV to 10 GeV range.

The two most commonly discussed scenarios for magnetospheric γ -ray emission place the emission regions either near the magnetic poles of the neutron star (*polar cap* model), or near the null surface in the outer magnetosphere of the pulsar (*outer gap* model). Both models predict a cutoff in the curvature radiation spectrum at γ -ray energies of the order of GeV up to several tens of GeV. Additionally, in some outer gap model calculations, a spectral component in the TeV range due to inverse Compton (IC) up-scattering of soft ambient seed photons by the accelerated electrons is predicted [6, 11].

The prime candidates for the search for very-high-energy (VHE, energies above ~ 100 GeV) γ -ray emission are the pulsars with established γ -ray emission at energies below ~ 10 GeV which have been detected by CGRO instruments. Some of them have been subject to intensive searches for pulsed VHE γ -ray emission by ground-based in-

Table 1: The characteristics of the selected pulsars taken from [9]. Period, P , distance, D , spin-down age, spin-down luminosity, \dot{E} , and the corresponding value for \dot{E}/D^2 , and calculated magnetic field strength at the neutron star surface, B_{surf} , and the light cylinder, B_{LC} , are listed. The last column shows the rank in \dot{E}/D^2 within the ATNF catalogue.

Pulsar name	P	D	Age	$\log_{10} \left(\frac{\dot{E}}{\text{erg s}^{-1}} \right)$	$\log_{10} \left(\frac{\dot{E}/\text{erg s}^{-1}}{D^2/\text{kpc}^2} \right)$	B_{surf}	B_{LC}	Rank	
PSR	[ms]	[kpc]	[kyears]			[10^{11} G]	[10^4 G]	\dot{E}/D^2	
B0531+21*	J0534+2200	33.1	2	1.24	38.7	38.1	37.8	98.0	1
B0833−45*	J0835−4510	89.3	0.29	11.3	36.8	37.9	33.8	4.45	2
B1706−44*	J1709−4429	102	1.8	17.5	36.5	36.0	31.2	2.72	6
B1509−58*	J1513−5908	151	4.4	1.55	37.3	36.0	154	4.22	7
B1259−63	J1747−2958	98.8	2.5	25.5	36.4	35.6	24.9	2.42	13
	J1302−6350	47.8	1.5	332	35.9	35.5	3.3	2.87	15
	J1811−1925	64.7	5	23.3	36.8	35.4	17.1	5.92	18
	J1524−5625	78.2	3.8	31.8	36.5	35.3	17.7	3.46	19
	J1420−6048	68.2	7.7	13	37.0	35.3	24.1	7.13	22
	J1826−1334	101	4.1	21.4	36.4	35.2	27.9	2.51	23
	J1801−2451	125	4.6	15.5	36.4	35.1	40.4	1.95	30

* established as γ -ray pulsars below ~ 10 GeV by EGRET

struments. Up to now, no evidence for pulsed emission has been found in these observations, and upper limits on the pulsed VHE γ -ray flux have been derived under various assumptions on the characteristics of the pulsed emission. However, the IC component predicted by outer gap models has not yet been significantly constrained.

H.E.S.S. Observations and Analysis

The High Energy Stereoscopic System (H.E.S.S.) [8], an array of imaging atmospheric Cherenkov telescopes located in the Khomas Highland of Namibia, detects cosmic VHE γ -rays by imaging the Cherenkov emission of their air showers in the atmosphere using optical telescopes. The superior sensitivity of H.E.S.S. with respect to previous ground-based instruments puts the predicted pulsed IC component from outer gap models within reach of testability.

Apart from the known γ -ray pulsars, other candidates for which H.E.S.S. data were available were selected from the ATNF pulsar catalogue [9] if their spin-down flux \dot{E}/D^2 was greater than $10^{35} \text{ erg s}^{-1} \text{ kpc}^{-2}$. Table 1 lists all candidates chosen along with selected measured and derived characteristics collected from the literature.

The data used in this search for pulsed VHE emission were either obtained in pointed observations or accumulated in the Galactic Plane survey and were analysed using the standard method as de-

scribed in detail in [1]. Since observational data indicate steep cut-offs in high-energy (GeV) γ -rays, special *low energy* cuts have been applied in addition to the standard cuts to reduce the gap in observational coverage between satellite and ground-based γ -ray observations of young pulsars.

Search for Pulsed Emission

In order to test for pulsed γ -ray emission at the pulsar position, the timestamps of each recorded shower passing selection cuts were transformed from the observer's frame into the pulsar frame and then folded with the pulsar spin period taken from observations in other energy domains. The resulting distribution of pulsar phases corresponding to each shower event was tested for variability using several statistical tests (χ^2 -, Z_m^2 -, H - and Kuiper-test).

As an example, the distribution of event phases from observations of the Vela Pulsar (PSR B0833-45) is shown in Fig. 1 for the signal (*on*) and background (*off*) region, obtained using the standard cuts. The difference between on and off results from the known γ -ray excess from HESS J0835-456 at the position of the pulsar.

No conclusive evidence for pulsed emission has been found with any of the statistical tests for pulsations for any data set of the complete sample of pulsars. The distribution of the test statistic H of the H-test is compatible with the expected distri-

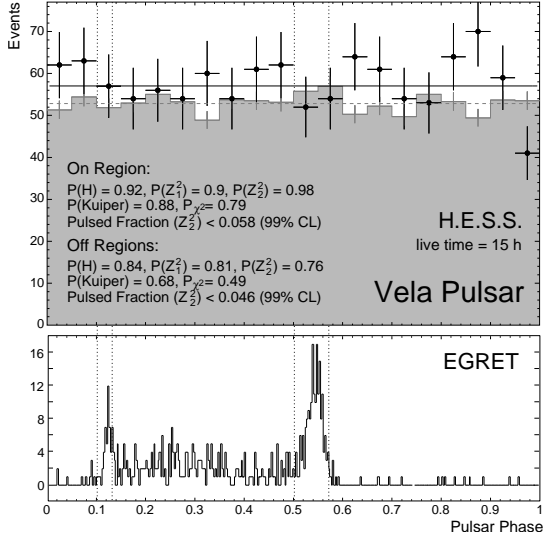


Figure 1: *Upper plot*: Distribution of event phases for the Vela pulsar (PSR B0833–45). The points represent the events in the on-region at the pulsar position and the histogram the normalised off-region events. For both regions the probabilities for being consistent with a uniform distribution according to the statistical tests on pulsations are listed. No significant deviation from uniformity was found within any of the statistical tests for pulsations. *Lower plot*: Phase distribution for γ -rays with energies between 2 and 10 GeV as measured by EGRET [5].

bution of H for the case when no pulsed signal is present in any data set, see Fig. 2.

Several methods were applied to obtain upper limits on the γ -ray flux from the selected pulsars. They differ in the assumptions made concerning the characteristics of the pulsed emission. The *on-off-pulse* method assumes similar characteristics of the pulse position and shape as measured in other energy domains for the hypothetical VHE γ -ray emission whereas the *pulsed fraction* method only assumes a certain pulse shape. As an example, the calculated differential flux limits are shown for Crab and Vela, two of the four observed γ -ray pulsars, in Fig. 3 and 4, respectively. For more details on the analysis and the limits derived for all selected pulsars refer to [2].

For the complete sample of pulsars, the absence of pulsed VHE γ -ray emission already disfavors a significant contribution of the IC component to the

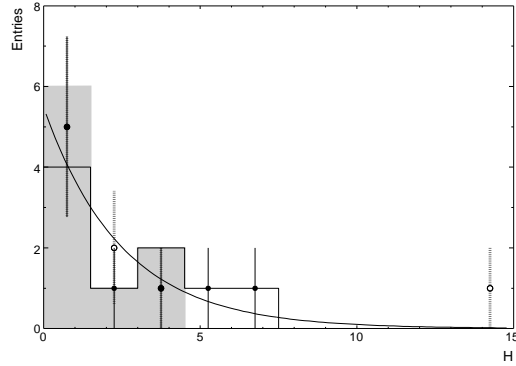


Figure 2: Ensemble distributions of the H-test statistic for the selected pulsars and their corresponding background control samples. The results for the on-region are shown as open and closed circles for the low energy and standard cut analysis, respectively. The distributions for the off-regions are displayed as grey filled and outlined histograms, respectively. The solid curve shows the expected distribution $N_H(H) = N_0 \exp(-\lambda H) |_{\lambda=0.4}$ if no pulsed signals are present.

energy loss mechanism of these pulsars. The flux limits shown here for Crab and Vela significantly constrain the IC component of selected outer gap models for flux predictions in the TeV range.

Conclusions

No conclusive evidence for pulsed emission has been found and differential upper limits on the pulsed flux were derived, constraining the pulsed flux for a wide range of possible pulse shapes and spectra in the VHE γ -ray range.

Although in several cases there is spatial coincidence with extended TeV γ -ray emission, pulsed emission is not detected in VHE γ -rays. In particular, the flux upper limits derived are of the order of 10^{-4} to 10^{-6} of the pulsar spin-down flux, underlining the non-magnetospheric origin of the TeV radiation component and supporting the widely accepted scenario of an effective energy transport mechanism to, and strong particle acceleration in, the pulsar wind nebula.

The upper limits imply a steep turnover of the pulsed high-energy spectrum at energies of a few tens of GeV. As the pulsar models differ sig-

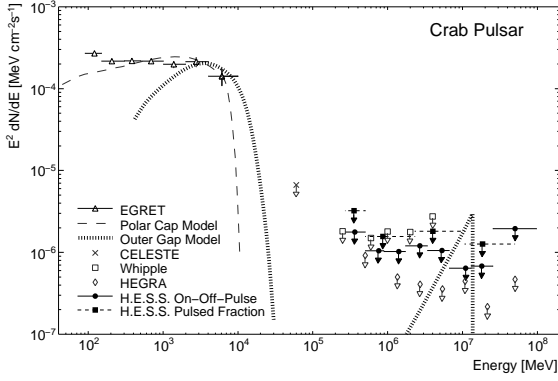


Figure 3: H.E.S.S. energy flux limits (99% c.l.) for pulsed emission of the Crab pulsar. The full circles and full squares correspond to the on-off-pulse and pulsed fraction limit determination methods, respectively. Below energies of 0.5 TeV the results were obtained with the low energy selection cuts, otherwise the standard cuts were used. The indicated polar cap curve was generated according to [10] and the outer gap model curve taken from [7]. Note that the southern location of H.E.S.S. allows only observations at rather high zenith angles for Crab, prohibiting a deep exposure especially at low energy thresholds.

nificantly in their predictions of the exact shape and energy of the turnover, the search for pulsed γ -ray emission from pulsars provides interesting prospects for future satellite-based and ground-based γ -ray instruments.

Acknowledgements

The support of the Namibian authorities and of the University of Namibia in facilitating the construction and operation of H.E.S.S. is gratefully acknowledged, as is the support by the German Ministry for Education and Research (BMBF), the Max Planck Society, the French Ministry for Research, the CNRS-IN2P3 and the Astroparticle Interdisciplinary Programme of the CNRS, the U.K. Particle Physics and Astronomy Research Council (PPARC), the IPNP of the Charles University, the South African Department of Science and Technology and National Research Foundation, and by the University of Namibia. We appreciate the excellent work of the technical support staff in Berlin, Durham,

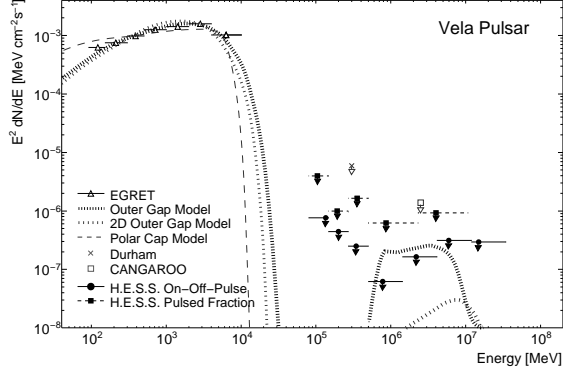


Figure 4: H.E.S.S. energy flux limits (99% c.l.) for pulsed emission of the Vela pulsar (see Fig. 3 for point descriptions). The polar cap (black dotted) and outer gap (dashed) model curves are generated according to the model of [10] and [6], respectively. The dotted grey outer gap model curve is taken from [11].

Hamburg, Heidelberg, Palaiseau, Paris, Saclay, and in Namibia in the construction and operation of the equipment.

References

- [1] Aharonian et al. (H.E.S.S. collaboration). *A&A*, 457:899–915, October 2006.
- [2] Aharonian et al. (H.E.S.S. collaboration). *A&A*, 466:543–554, May 2007.
- [3] K. S. Cheng, R. E. Taam, and W. Wang. *ApJ*, 617:480–489, December 2004.
- [4] C. D. Dermer and S. J. Sturmer. *ApJ*, 420:L75–L78, January 1994.
- [5] J. M. Fierro, P. F. Michelson, P. L. Nolan, and D. J. Thompson. *ApJ*, 494:734, February 1998.
- [6] K. Hirotani, A. K. Harding, and S. Shibata. *ApJ*, 591:334–353, July 2003.
- [7] K. Hirotani and S. Shibata. *ApJ*, 558:216–227, September 2001.
- [8] W. Hofmann. In *International Cosmic Ray Conference*, page 2811, July 2003.
- [9] R. N. Manchester, G. B. Hobbs, A. Teoh, and M. Hobbs. <http://www.atnf.csiro.au/research/pulsar/psrcat/>, *AJ*, 129:1993–2006, April 2005.
- [10] B. Rudak and J. Dyks. *MNRAS*, 303:477–482, March 1999.
- [11] J. Takata, S. Shibata, K. Hirotani, and H.-K. Chang. *MNRAS*, 366:1310–1328, March 2006.
- [12] D. J. Thompson, M. Bailes, and D. L. Bertsch, et al. *ApJ*, 516:297–306, May 1999.

Observation of orbital modulation of the VHE emission from the binary system LS 5039 with H.E.S.S.

MATHIEU DE NAUROS¹, GAVIN ROWELL² FOR THE H.E.S.S. COLLABORATION

¹LPNHE IN2P3 - CNRS - Universités Paris VI et Paris VII, France

²School of Chemistry & Physics, University of Adelaide, Adelaide 5005, Australia

denauroi@in2p3.fr

Abstract: The binary system LS 5039 was serendipitously discovered with the High Energy Stereoscopic system (H.E.S.S.) during the scan of the inner galactic plane in 2004. Deeper observations were carried out in 2005, and brought clear evidence for TeV emission periodicity. This is the highest energy periodic source known so far. The observed flux modulation is attributed to a modulated absorption of the VHE gamma-ray emission of the compact object through pair creation on the stellar photosphere. Spectral modulation is also observed in this system; this might have several origins such as modulation of particle acceleration or reprocessing of high energy photons towards lower energy through cascading.

We will present detailed studies of the source variability (flux and spectral shape), the timescales compared to other wavelengths, and briefly review the implications for existing emission models.

Introduction

In the commonly accepted paradigm, microquasars consist of a compact object (black hole or neutron star) fed by a massive star. They can exhibit superluminal radio jets[11], and emission from the accretion disk. LS 5039, identified in 1997[12] as a massive X-ray binary system with faint radio emission[10], was resolved by Paredes et al.[14] into a bipolar radio outflow emanating from a central core, thus possibly placing it into the *microquasar class*. The detection of radio and variable X-ray emission[5] and its possible association with the EGRET source 3EG J1824-1514 suggested the presence of multi-GeV particles accelerated in jets. This binary system (Fig 1) consists of a massive O6.5V star in a ~ 3.9 day mildly eccentric orbit ($e = 0.35$)[6] around a compact object whose exact nature (black hole or neutron star) is still under debate.

H.E.S.S. Observations

The High Energy Stereoscopic System (H.E.S.S.) is an array of four Atmospheric Cherenkov Tele-

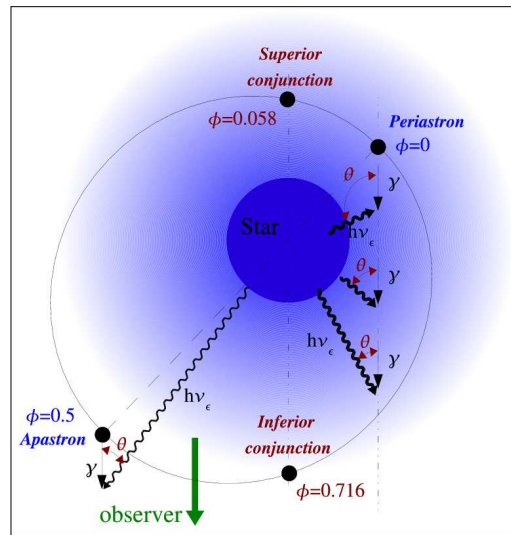


Figure 1: Orbital geometry of the binary system LS 5039 viewed from above and using the orbital parameters derived by Casares et al.[6]. Shown are: phases (ϕ) of minimum (*periastron*) and maximum (*apastron*) binary separation; epoch of superior and inferior conjunctions occurring when the compact object and the star are aligned along the observer's light-of-sight.

scopes (ACT)[3] located in the Southern Hemisphere (Namibia, 1800 m a.s.l.) and sensitive to γ rays above 100 GeV. LS 5039 was serendipitously detected in 2004 during the H.E.S.S. galactic scan[1]. The 2004 observations have been followed up by a deeper observation campaign[2] in 2005, leading to a total dataset of 69.2 hours of observation after data quality selection.

After selection cuts, a total of 1969 γ -ray events were found within 0.1° of the VLBA radio position of LS 5039 (statistical significance of 40σ). The best fit position, $l = 16.879^\circ$, $b = -1.285^\circ$ is compatible with the VLBA position within uncertainties $\pm 12''$ (stat.) and $\pm 20''$ (syst.). We obtain an upper limit of $28''$ (at 1σ) on the source size.

Timing Analysis

The runwise VHE γ -ray flux at energies ≥ 1 TeV was decomposed into its frequency components using the Lomb-Scargle periodogram[15] (Fig. 2). A very significant peak (chance probability of $\sim 10^{-20}$ before trials) occurs in the Lomb-Scargle periodogram at the period 3.9078 ± 0.0015 days, consistent with the most recent optical orbital period[6] (3.90603 ± 0.00017 days). After sub-

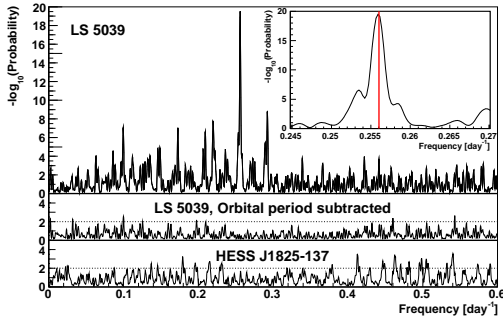


Figure 2: Lomb-Scargle (LS) periodogram of the VHE runwise flux of LS 5039 above 1 TeV (Chance probability to obtain the LS power vs. frequency). From [2]. Zoom: inset around the highest peak, which corresponds to a period of 3.9078 ± 0.0015 days, compatible with the optical orbital period[6] denoted as a red line. Middle: LS periodogram of the same data after subtraction of a pure sinusoidal component (see text). Bottom: LS periodogram obtained on HESS J1825-137 observed in the same field of view.

traction of a pure sinusoid at the orbital period, the orbital peak disappears as expected (Fig. 2, middle), but also the numerous satellite peaks which correspond to beat periods of the orbital period with observation gaps (day-night cycle, moon period, annual period). The bottom panel of the same figure shows the result obtained on the neighbouring source HESS J1825-137 observed in the same field of view as LS 5039. The absence of any significant peak demonstrates that the observed periodicity is genuinely associated with LS 5039.

Flux Modulation

The runwise Phasogram (Fig 3) of integral flux at energies ≥ 1 TeV vs. orbital phase (ϕ) shows an almost sinusoidal behaviour, with the bulk of the emission largely confined in a phase interval $\phi \sim 0.45$ to 0.9 , covering about half of the orbital period. The emission maximum ($\phi \sim 0.7$) appears to lag behind the apastron epoch and to align better with the *inferior conjunction* ($\phi = 0.716$), when the compact object lies in front of the massive star (see Fig. 1). The VHE flux minimum occurs at phase ($\phi \sim 0.2$), slightly further along the orbit

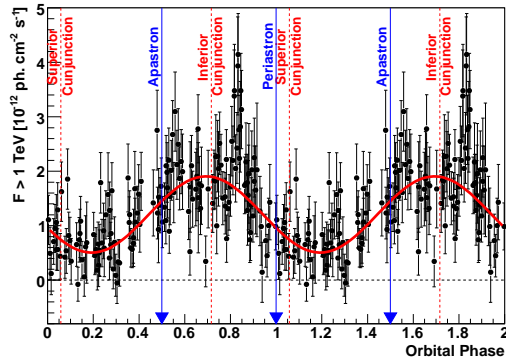


Figure 3: Phasogram (Integral run-by-run γ -ray flux above 1 TeV as function of orbital phase) of LS 5039 from H.E.S.S. data from 2004 to 2005. Each run is ~ 28 minutes. Two full phase periods are shown for clarity. The vertical blue arrows depict the respective phases of minimum (*periastron*) and maximum (*apastron*) binary separation. The vertical dashed red lines show the respective phases of inferior and superior conjunction, when the star and the compact object are aligned along the observer's line of sight. From [2].

than *superior conjunction* ($\phi = 0.058$). Neither evidence for long-term secular variations nor any other modulation period are found in the presented H.E.S.S. data.

Spectral Modulation

Due to the changing environment with orbital phase (magnetic field strength, stellar photon field, relative position of compact object and star with respect to observer, ...), the VHE γ -ray emission spectrum is expected to vary along the orbit.

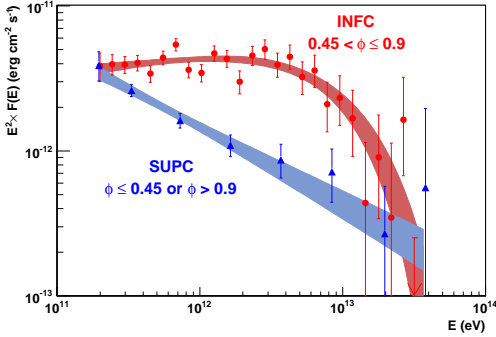


Figure 4: Very high energy spectral energy distribution of LS 5039 for the two broad orbital phase intervals defined in the text, **INFC** (red circles) and **SUPC** (blue triangles). The shaded regions represent the 1σ confidence bands on the fitted functions. A clear spectral hardening is occurring in the 200 GeV to a few TeV range during the **INFC** phase interval. From [2].

We first define two broad phase intervals: **INFC** centered on the inferior conjunction ($0.45 < \phi \leq 0.9$) and its complementary **SUPC** centered on the superior conjunction, corresponding respectively to high and low flux states. The high state VHE spectral energy distribution (Fig 3) is consistent with a hard power law with index $\Gamma = 1.85 \pm 0.06_{\text{stat}} \pm 0.1_{\text{syst}}$ and exponential cutoff at $E_0 = 8.7 \pm 2.0$ TeV. In contrast, the spectrum for low state is compatible with a relatively steep ($\Gamma = 2.53 \pm 0.06_{\text{stat}} \pm 0.1_{\text{syst}}$) pure power law extending from 200 GeV to ~ 20 TeV. Interestingly, the flux appears to be almost unmodulated at 200 GeV as well as around 20 TeV, whereas the modulation is maximum around a few (~ 5) TeV.

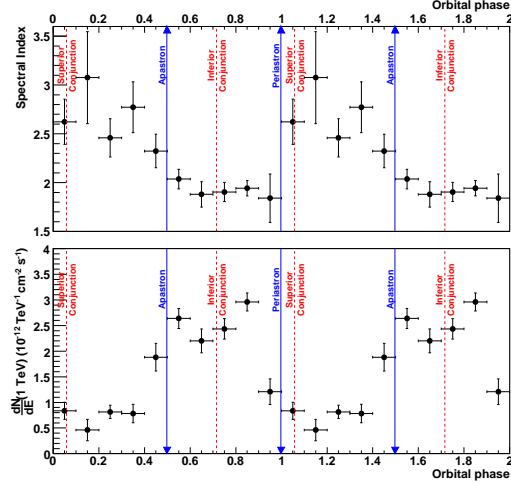


Figure 5: Top: Fitted pure power-law photon index vs. phase interval of width $\Delta\phi = 0.1$. Bottom: Differential flux at 1 TeV for the same phase interval. From [2].

Looking at smaller phase intervals, Fig 5 shows the results of a pure power-law fit of the high energy spectra in 0.1 orbital phase bins (restricted to energies below 5 TeV to avoid systematic effect introduced by the high state cutoff). The flux normalisation at 1 TeV (bottom) and photon index (top) are strongly correlated, the flux being higher when the spectrum is harder and vice-versa.

Interpretation and Conclusion

The basic paradigm of VHE γ -ray production requires the presence of particles accelerated to multi-TeV energies and a target comprising photons (for γ -ray production through the Inverse Compton effect) and/or matter of sufficient density (for γ -ray production through pion decay in hadronic processes). Several model classes are available to explain VHE emission from gamma-ray binaries, differentiating one from the other by the nature of accelerated particles and/or the location of the acceleration region. In jet-based models, particle acceleration could take place directly inside and along the jet, e.g. [4, and references therein], and also in the jet termination shock regions[8]. Non-jet scenarios are also available, e.g. [9, 7], where the emission arises from the in-

teraction of a pulsar wind with the stellar companion equatorial wind.

New observations by HESS have established orbital modulation of the VHE γ -ray flux and energy spectrum from the XRB LS 5039. The observed VHE modulation indicates that the emission most probably takes place close (within ~ 1 AU) to the massive stellar companion, where modulated γ -ray absorption via pair production (e^+e^-) on the intense stellar photon field is unavoidable (e.g. [7]). The observed spectral modulation is however incompatible with a pure absorption scenario, which in particular predicts a maximum variability around 300 GeV and a VHE spectral hardening in the low flux state, inconsistent with observations.

Modulation could also arise from a modulation of the acceleration and cooling timescales along the orbit due to varying magnetic field and photon field densities (e.g. [2, and references therein]) which could modify the maximum electron energy and therefore induce a phase-dependent energy break in the γ -ray spectrum. Modulation of the accretion rate due to interaction of the stellar wind with the compact object in the microquasar scenario (e.g. [13]) could be another ingredient of the observed modulation.

A detailed study is now required to fully explain these new observations and understand the complex relationship between γ -ray absorption and production processes within these binary systems.

Acknowledgements

The support of the Namibian authorities and of the University of Namibia in facilitating the construction and operation of H.E.S.S. is gratefully acknowledged, as is the support by the German Ministry for Education and Research (BMBF), the Max Planck Society, the French Ministry for Research, the CNRS-IN2P3 and the Astroparticle Interdisciplinary Programme of the CNRS, the U.K. Particle Physics and Astronomy Research Council (PPARC), the IPNP of the Charles University, the South African Department of Science and Technology and National Research Foundation, and by the University of Namibia. We appreciate the excellent work of the technical support staff in Berlin, Durham, Hamburg, Heidelberg, Palaiseau, Paris, Saclay, and in Namibia in the construction and operation of the equipment.

References

- [1] F. Aharonian (HESS Collaboration). Discovery of very high-energy gamma rays associated with an X-ray binary. *Science*, 309:746, 2005.
- [2] F. Aharonian (HESS Collaboration). 3.9 day orbital modulation in the TeV gamma-ray flux and spectrum from the X-ray binary LS 5039. *A&A*, 460:743–749, 2006.
- [3] F. Aharonian (HESS Collaboration). Observations of the Crab Nebula with H.E.S.S. *A&A*, 457:899–915, 2006.
- [4] F. Bosch-Ramon and J.M. Paredes. A numerical model for the γ -ray emission of the microquasar LS 5039 Orbital X-Ray Variability of the Microquasar LS 5039. *A&A*, 417:1075, 2004.
- [5] F. Bosch-Ramon, J.M. Paredes, and M. Ribó. Orbital X-Ray Variability of the Microquasar LS 5039. *ApJ*, 628:388, 2005.
- [6] J. Casares, M. Ribó, I. Ribas, J.M. Paredes, et al. A possible black hole in the γ -ray microquasar LS 5039. *MNRAS*, 364:899, 2005.
- [7] G. Dubus. Gamma-ray binaries: pulsars in disguise? *A&A*, 456:801, 2006.
- [8] S. Heinz and R. Sunyaev. Cosmic rays from microquasars : A narrow component to the CR spectrum? *A&A*, 390:751–766, 2002.
- [9] L. Maraschi and A. Treves. A model for LSI 61°303. *MNRAS*, 194:1, 1981.
- [10] J. Martí, J. M. Paredes, and M. Ribó. The system LS 5039: a new massive radio emitting X-ray binary. *A&A*, 338:L71–L74, 1998.
- [11] I.F. Mirabel and L.F. Rodríguez. A Superluminal Source in the Galaxy. *Nature*, 371:46, 1994.
- [12] C. Motch, F. Haberl, K. Dennerl, et al. New massive X-ray binary candidates from the ROSAT Galactic Plane Survey. I. Results from a cross-correlation with OB star catalogues. *A&A*, 323:853–875, July 1997.
- [13] J. M. Paredes, V. Bosch-Ramon, and G. E. Romero. Spectral energy distribution of the γ -ray microquasar LS 5039. *A&A*, 451:259–266, May 2006.
- [14] J. M. Paredes, J. Martí, M. Ribó, et al. Discovery of a High-Energy Gamma-Ray-Emitting Persistent Microquasar. *Science*, 288:2340–2342, June 2000.
- [15] J. D. Scargle. Studies in astronomical time series analysis. II - Statistical aspects of spectral analysis of unevenly spaced data. *ApJ*, 263:835–853, December 1982.



Report on TeV γ -Ray Observations of PSR B1259–63/SS2883 near the 2007 Periastron with the H.E.S.S. Stereoscopic System of Cherenkov Telescopes

M. KERSCHHAGGL¹, F. AHARONIAN², M. FUESSLING¹, U. SCHWANKE¹
FOR THE H.E.S.S. COLLABORATION

¹*Institut für Physik, Humboldt-Universität zu Berlin, Newtonstr. 15, D 12489 Berlin, Germany*

²*Dublin Institute for Advanced Studies, 5 Merrion Square, Dublin 2, Ireland*

mkersch@physik.hu-berlin.de

Abstract: PSR B1259–63 / SS 2883 is a binary system consisting of a 48 ms radio pulsar orbiting a Be star with a period of 3.4 y in a highly eccentric orbit ($e = 0.87$). The system was first detected in TeV γ -rays by H.E.S.S. around the last periastron passage in March 2004. These observations established PSR B1259–63 / SS 2883 as the first variable galactic source in the very high energy (VHE) regime. A lightcurve for the system, covering mainly the post periastron part, could be deduced, clearly showing a variable flux in VHE photons. New data have been taken this year from April to June with the system approaching its next periastron (July 27, 2007). The status and outcome so far of the corresponding campaign will be discussed.

Introduction

The binary system PSR B1259–63 / SS 2883 was first observed in TeV γ -rays during its periastron passage between February and June 2004 [1], establishing it as the first variable galactic TeV γ -ray source (see Fig. 1). The corresponding data showed a clear pointlike signal with a statistical significance of 13 standard deviations at the position of PSR B1259–63. A time averaged spectrum as well as a lightcurve for the integrated flux above 380 GeV from this object could be extracted (see Fig. 2 & 3). Moreover, it was the first time in the history of TeV γ -ray astronomy where two sources have been discovered within the same field of view as this campaign lead to the serendipitous discovery of HESS J1303-631 [2] (see Fig. 1).

The peculiar shape of the PSR B1259–63 lightcurve has been object of various model descriptions trying to explain the underlying physical processes causing the VHE emission. Mechanisms like Inverse Compton (IC) scattering of ultrarelativistic electrons on the stellar photons or hadronic scenarios (e.g. $pp \rightarrow \pi^0 \rightarrow \gamma\gamma$)

have been suggested as possible origins of TeV photons in the interactions of the pulsar wind with the stellar outflow and radiation field of the companion Be star (e.g. [3]). Some of them take into account the influence of the dense stellar disc that might play a crucial role in the generation mechanism of VHE γ -rays (see [5]). In order to constrain the various parameters used in the model predictions as well as to be able to discriminate between the models in question, data for the up to now unknown pre-periastron (lightcurve) part of PSR B1259–63 are needed.

As the next periastron takes place on July 27, 2007, a campaign of 60 h of intended exposure during the pre-periastron phase from April to July 2007 has been started.

The H.E.S.S. PSR B1259–63 2007 Campaign

Figure 4 shows the H.E.S.S. visibility windows of PSR B1259–63 in 2007 for zenith angles below 45° together with data from 2004 with respect to periastron. The numbers underneath each observa-

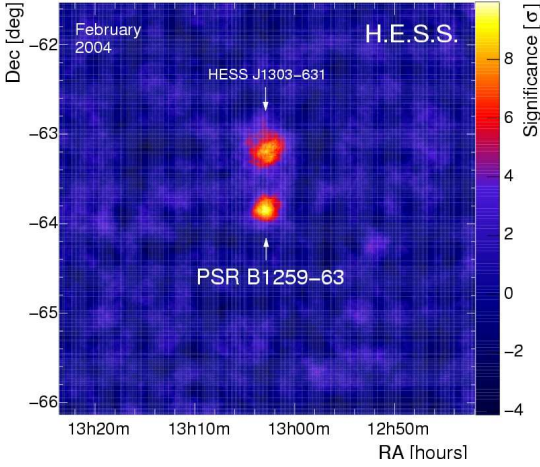


Figure 1: Significance skymap of the PSR B1259-63 field of view as seen in February 2004. The unidentified γ -ray source HESS J1303-631 is located 0.6° to the north of the source.

tion slot indicate the amount of intended exposure time for this month. Observations will cover the pre-periastron orbital phase until 14 days prior to the periastron passage. Green boxes refer to time windows where data taking already has been accomplished. The overall exposure time of roughly 60 h was chosen to match the dataset from 2004, in terms of good quality data, in order to have a comparable amount of data for the pre-periastron part of the lightcurve.

So far, data from April to June with an overall live-time of 33 h have been taken (see Tab. 1). The livetime for the overall 2004 dataset was ~ 45 h.

Period	τ [h]	S [σ]	Calibration Status
2007			
April	5.3	1.0	final
May	14.6	3.2	final
June	13.2	6.4	preliminary

Table 1: PSR B1259-63 April-June 2007: Live-time τ , Significance S for a preliminary point source analysis. The June data has been calibrated preliminarily on site in Namibia.

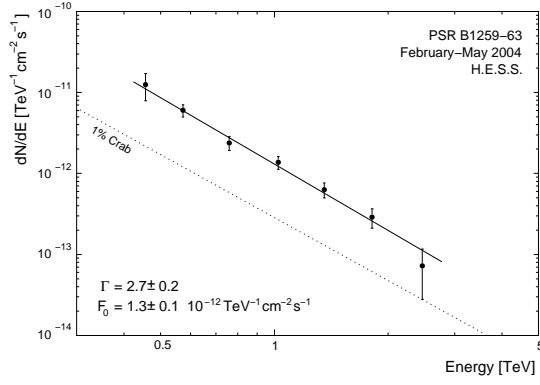


Figure 2: Energy spectrum dN/dE of γ -rays from PSR B1259-63 determined from the H.E.S.S. 2004 data. The solid line indicates the power-law fit $F(E) = F_0 E^{-\Gamma}$.

A preliminary standard point source analysis of these data has been carried out (for details on the H.E.S.S. analysis chain see [1]). The significance for a γ -ray excess from the source in April and May is 1.0 and 3.2 standard deviations respectively, showing no strong detection for these months. However, when analyzing data from June on site, using a preliminary on site calibration, a clear signal with a significance of 6.4σ can be seen from PSR B1259-63 (see Tab. 1).

Multi Wavelength Coverage

In order to also have Multi Wavelength (MWL) data available coincident with the TeV data provided by H.E.S.S. a cooperation with the *SUZAKU* [4] satellite project has been established. Corresponding observation schedules have been optimized for a maximum MWL coverage. *SUZAKU* will observe PSR B1259-63 from July to September 2007 in eight pointings of 20 ks duration each. Four pointings will take place in July coincident with the H.E.S.S. observations covering the assumed first entrance of the pulsar into the dense circumstellar disc. This interesting phase of the system's orbit is therefore covered in the keV and TeV energy bands.

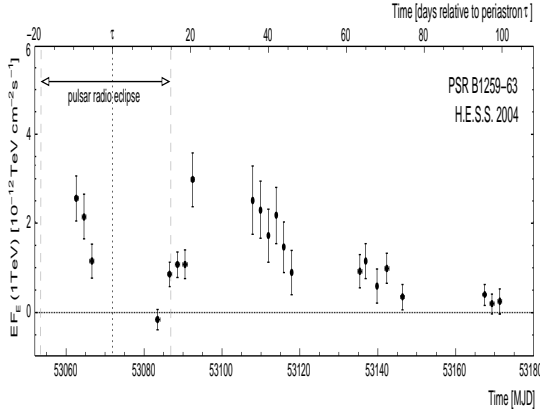


Figure 3: The PSR B1259–63 lightcurve around periastron in 2004. The vertical dashed black line indicates the position of the periastron. The data clearly indicate a variable flux.

Summary & Outlook

PSR B1259–63 is currently re-observed by the H.E.S.S. Cherenkov Telescope System in Namibia in a 60 h exposure campaign lasting from April to July 2007. 33 h of livetime data have already been taken during the April to June period. A preliminary point source analysis yields no significant excess from the system for April and May. The preliminarily calibrated June data (on site calibration) however shows a clear signal at 6.4σ .

The campaign is carried on in July with a planned exposure of 14.5 h coinciding with 4 pointings on the target done by the X-ray satellite *SUZAKU* covering the crucial first disc crossing of the pulsar. Further isolated post-periastron H.E.S.S. observations are planned during August when *SUZAKU* as well as *Chandra* will observe this unique HE & VHE accelerator.

References

- [1] Aharonian F. et al. *Discovery of the Binary Pulsar PSR B1259–63 in Very-High-Energy Gamma Rays around Periastron with H.E.S.S.* A&A 442 1 (2005) 1-10, 2005.
- [2] Aharonian F. et al. *Serendipitous discovery of the unidentified extended TeV γ -ray source*

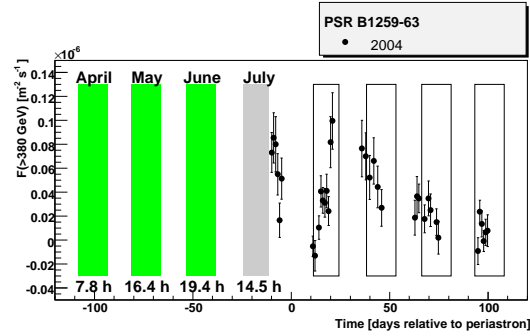


Figure 4: The PSR B1259–63 observation windows in 2007 for zenith angles $< 45^\circ$ with respect to the system's time relative to periastron. Green boxes indicate that data taking has already been accomplished during the corresponding month. The empty boxes are the 2007 observation windows mirrored with respect to periastron, overlaid with the 2004 data for comparison.

HESS J1303-631 with the H.E.S.S. Cherenkov telescopes. A&A 439 3 (2005) 1013-1021, 2005.

- [3] Khangulyan D. et al. *TeV lightcurve of PSR B1259–63/ SS 2883.* astro-ph/0601241, 2006.
- [4] Mitsuda K. et al. *The X-Ray Observatory Suzaku.* PASJ 58, 2006.
- [5] Neronov A. et al. *Radio-to-TeV γ -ray emission from PSR B1259–63.* astro-ph/0610139, 2006.



A search for VHE γ -ray binaries in the H.E.S.S. Galactic Plane Scan

HUGH DICKINSON¹, IAN LATHAM¹, PAULA CHADWICK¹ FOR THE H.E.S.S. COLLABORATION

¹ *Physics Department, University of Durham, South Road, Durham, County Durham, DH1 3LE, United Kingdom*

h.j.dickinson@dur.ac.uk

Abstract: Utilising the unprecedented TeV sky coverage of the H.E.S.S. galactic plane scan, we present the results of a search for Very High Energy gamma-ray sources coincident with the positions of known X-ray binaries. Although no significant detections were obtained, upper limits to the TeV flux from 18 X-ray binaries were derived.

Introduction

The H.E.S.S. galactic plane scan [4] is an extensive survey of the inner part of the galaxy in TeV γ -rays. It consists of 230 hours of observation comprising 500 pointings between $\pm 30^\circ$ in galactic longitude and $\pm 3^\circ$ in galactic latitude. The average flux sensitivity of the scan is $\sim 2\%$ of the Crab nebula flux at photon energies above 200 GeV.

X-ray binaries are galactic systems containing a normal donor star which is in the process of transferring mass onto a compact object, such as a neutron star or black hole, to which it is gravitationally bound. A significant fraction of the gravitational potential liberated by this mass transfer is emitted as X-radiation, hence the nomenclature.

Some X-ray binaries are observed to eject a proportion of the accreted matter in collimated and often highly relativistic jets (See e.g. [21, 17]). These ‘microquasars’ are named for their structural similarities with Active Galactic Nuclei (AGN), several of which are known VHE γ -ray sources (See e.g. [5, 1]). Indeed, the extremes of temperature, pressure and radiation density likely to be generated close to the compact object in X-ray binary systems provide excellent conditions for the acceleration of charged particles to multi-TeV energies. Such acceleration, although not synonymous with VHE γ -ray emission, has nonetheless been identified as an apparent prerequisite for the production of photons with energies $E_\gamma > 200$ GeV.

Several plausible mechanisms exist which permit the generation of VHE γ -rays in X-ray binary systems. Indeed, both the necessary particle acceleration and the actual photon production can proceed via a number of potential avenues. In general, particle acceleration is thought to be accomplished at shock fronts either at the interface between the in-falling matter and an outflow or jet, or within the outflow itself.

In systems where the companion is a low-mass star, the mass transfer proceeds mainly via Roche lobe overflow. In such systems particle acceleration can occur across internal shocks within the jet structures. In systems containing high-mass donor, accretion is often wind-fed, with high energy particles from the stellar wind being accreted onto the compact primary. If the primary is a pulsar, shocks can occur at the pulsar standoff distance, where the ram pressures due to the stellar and pulsar winds equilibrate [12].

Given a population of energetic charged particles, the mechanisms of γ -ray production may be broadly segregated into two categories: Those in which the emitting particles are hadronic, and those where they are leptons. Leptonic models closely resemble those used to explain the continuum spectra of AGN, relying as they do on the Synchrotron Self-Compton (SSC) and External Compton (EC) processes [12, 12, 10]. The SSC process involves the up-scattering of low energy synchrotron photons by the high energy electrons

which generated them, while in the EC process, the target photons are generated elsewhere. In relativistic jets aligned close to the observer line-of-sight, the Comptonised radiation is both beamed and Doppler boosted, producing a measurable flux of photons in the TeV band.

While protonic SSC and EC processes are possible [1, 11], most hadronic emission models rely on the production and subsequent decay of neutral pions.

$$pp \rightarrow pp\pi^0 \rightarrow e^+e^-\gamma$$

For example, [24] and [22] show that pions and consequently TeV photons can be produced via the interaction of stellar wind protons with those in a microquasar jet.

Only three X-ray binary systems are known to emit VHE γ -rays. LS 5039 [3] and PSR B1259-63 [1] were detected by the H.E.S.S. Telescope array while in the northern hemisphere LS I +61°303 [1] has been observed by the MAGIC collaboration. While their detections by the MAGIC and H.E.S.S. collaborations confirm the existence of γ -ray binaries, the catalogue of such objects remains rather small. In terms of morphology, PSR B1259-63 is a Be star-pulsar binary with a 3.4 yr orbital period and while both LS 5039 and LS I +61°303 are high-mass X-ray binaries with donor masses of 23 and 12 M_\odot and orbital periods of 3.9 and 26.5 days respectively. The nature of the compact primaries in both systems is uncertain, although the LS I +61°303 system seems likely to contain a pulsar [10]. [12] argues that despite observed millisecond radio structure [22, 20], the observed TeV emission of both LS I +61°303 and LS 5039 is rotationally derived from pulsars.

The aim of this work was to expand the catalogue of known γ -ray binaries and identify candidates for further observation. As galactic objects, X-ray binaries are concentrated in the plane of the galaxy. Consequently, the H.E.S.S. galactic plane scan is an excellent dataset for our purposes. We make no selections on the basis of target morphology and test the positions of all known X-ray binaries with sufficient exposure.

The Sample

As a source of targets for the search we utilise the catalogues of [18] for high-mass X-ray binaries and [17] for low-mass systems. The selection criteria required only that the target object was within 1.5° of the H.E.S.S. camera centre in at least one good observation run in the galactic plane scan. Run quality selection was carried out as discussed in [2] in an effort to minimise the systematic uncertainties introduced inherently by the telescope system itself and also by the atmosphere which, in effect, forms the scintillating medium of the detector.

The resulting sample consists of 29 X-ray binaries comprising 8 high-mass systems with the remaining 21 having low-mass donors.

Analysis and Results

Data reduction and analysis were carried out using the standard H.E.S.S. analysis procedure outlined in [2]. The event selection cuts placed on image size, θ^2 and the mean reduced scaled parameters are identical to those described as standard in [2], and are consistent with the expected point-like nature of the target objects. The γ -ray background was estimated using a ‘reflected’ background model with several run dependent *off* regions defined the same distance from the camera camera as the *on* region. Areas of the sky containing known TeV γ -ray sources are precluded from being chosen as *off* regions to ensure that the background estimate remains as uncontaminated as possible. Nonetheless, contamination can occur when the *on* region coincides with a known γ -ray source. Despite having excellent angular resolution for an instrument of its type, the H.E.S.S. point spread function is somewhat extended, with a 68% containment radius of $\sim 0.1^\circ$. For this reason it can be impossible to disentangle the signals from nearby objects. This is particularly difficult when the expected target spectrum and flux are unknown.

As reported in [4] the region exposed by the galactic plane scan is somewhat crowded with VHE γ -ray sources, and it is therefore unsurprising that some contamination of our targets did indeed occur. Table 2 outlines the results of the search. Up-

Target Name	Significance [σ]	Excess [counts]	Livetime [hours]	Mass	Flux Upper Limit ($E_\gamma > 1 \text{ TeV}$) [$\text{ph cm}^{-2}\text{s}^{-1}$]
RX J1744.7-2713	1.367	114.874	7.71613	H	5.472×10^{-12}
AX J1749.2-2725	3.021	320.949	13.46	H	6.3659×10^{-12} (HESS J1747-281)
GRO J1750-27	1.521	94.006	4.715	H	1.050×10^{-11}
AX J1820.5-1434	-1.582	-22.290	4.339	H	1.507×10^{-12}
H 1833-076	1.074	23.038	8.075	H	1.882×10^{-12} (HESS J1837-069)
GS 1839-04	0.178	2.059	1.701	H	2.530×10^{-12}
AX 1845.0-0433	0.639	6.574	1.711	H	5.142×10^{-12}
2S 1845-024	0.805	7.111	1.711	H	5.142×10^{-12}
J1744-28	4.652	461.619	10.874	L	1.569×10^{-11} (HESS J1745-290)
1742.8-2853	11.202	1060.91	10.0287	L	2.564×10^{-11} (HESS J1745-290)
1742.9-2852	7.397	214.67	11.309	L	4.700×10^{-12} (HESS J1745-290)
1743.1-2852	6.064	177.667	11.741	L	4.013×10^{-12} (HESS J1745-290)
1742.9-2849	5.553	162.729	11.741	L	3.637×10^{-12} (HESS J1745-290)
1742.5-2845	2.364	67.242	11.966	L	2.253×10^{-12} (HESS J1745-290)
1743-288	3.521	101.948	11.7405	L	2.910×10^{-12} (HESS J1745-290)
1743.1-2843	3.102	93.775	12.594	L	2.918×10^{-12} (HESS J1745-290)
J1750.8-2900	0.346	10.159	12.392	L	1.479×10^{-12}
1739-278	2.563	65.670	5.068	L	2.556×10^{-11}
J1748-288	3.100	260.002	13.656	L	1.254×10^{-11} (HESS J1747-281)
1735-269	-0.661	-5.023	1.288	L	2.755×10^{-12}
1749-285	-1.570	-117.739	9.444	L	6.684×10^{-12}
1744-265	-0.238	-4.268	5.148	L	1.964×10^{-12}
1745-248	-1.736	-36	0.435	L	1.372×10^{-11}
1758-258	-1.124	-36.520	1.727	L	4.395×10^{-12}
1758-250	-0.270	-14.736	3.013	L	6.083×10^{-12}
J1806-246	-0.079	-1.921	5.491	L	9.490×10^{-12}
1758-205	-0.501	-8.545	3.890	L	1.534×10^{-12}
1811-171	1.777	50.112	10.626	L	1.609×10^{-12}
1813-140	-1.088	-7.373	0.855	L	2.451×10^{-12}

Table 1: The results of the X-ray binary search. Where obtainable, upper limits to the γ -ray flux at energies $> 1 \text{ TeV}$ are given. Where the target region is contaminated by the flux from a known TeV source, the derivation of an upper limit is not possible, but there is no way to safely associate the observed flux with the X-ray binary system. In this case the contaminating object is indicated in the *Flux Upper Limit* column. Negative excesses and significances result purely from fluctuations in the γ -ray background and should not be interpreted as a genuine deficit in the photon flux. In the *Mass* column, ‘H’ indicates a high-mass system and ‘L’ a low mass system.

per limits to the photon flux above 1 TeV have been derived for 18 of the 29 targets. These upper limits represent 99% confidence intervals derived using the unified Feldman-Cousins method [14]. The remaining 11 targets were too close to known TeV emitters for a reliable upper limit or flux estimate to be obtained. In particular, those lying along a line of sight to the galactic centre are subject to heavy contamination from HESS J1745-290.

Conclusions

99% confidence upper limits have been derived for 18 X-ray binaries. The absence of a conclusive detection by H.E.S.S. could be explained in a number of ways. The flux from all three known γ -ray binaries is highly variable, and their detection would be somewhat dependent upon the timing of observations. Additional variability can occur due to $\gamma\gamma \rightarrow e^+e^-$ interactions with near infra-red photons absorbing the intrinsic γ -ray flux. [14] shows that the angular dependence of this process leads to an orbital modulation of the γ -ray flux similar to that observed in LS 5039 [4]. In some cases the intrinsic flux may be low enough, or the near IR radiation density high enough that no γ -rays are detected. Finally it may be the case that highly specific conditions are required for the emission of VHE γ -rays to occur.

Nonetheless, with the increasing sensitivity of ground based Cherenkov telescopes and the advent of experiments such as *GLAST* and H.E.S.S. Phase II to bridge the gap between soft and VHE γ -rays, it seems unlikely that the γ -ray binary catalogue of three will remain so small for long.

References

- [1] F. Aharonian et al. (*H.E.S.S. Collaboration*). *A&A*, 406:L9, 2003.
- [2] F. Aharonian et al. (*H.E.S.S. Collaboration*). *ApJ*, 636:777, 2006.
- [3] F. Aharonian et al. (*H.E.S.S. Collaboration*). *Science*, 309:746, 2005.
- [4] F. Aharonian et al. (*H.E.S.S. Collaboration*). *A&A*, 442:1, 2005.
- [5] F. Aharonian et al. (*H.E.S.S. Collaboration*). *A&A*, 430:865, 2005.
- [6] F. Aharonian et al. (*H.E.S.S. Collaboration*). *A&A*, 457:899, 2006.
- [7] F. Aharonian et al. (*H.E.S.S. Collaboration*). *A&A*, 460:743, 2006.
- [8] F. Aharonian et al. (*H.E.S.S. Collaboration*). *MNRAS*, 332:215, 2002.
- [9] J. Albert et al. (*MAGIC Collaboration*). *Science*, 312:1771, 2006.
- [10] A. M. Atoyan and F. Aharonian. *MNRAS*, 302:253, 1999.
- [11] V. Bosch-Ramon, F. A. Aharonian and J. M. Paredes. *A&A*, 432:609, 2005.
- [12] V. Bosch-Ramon, J. M. Paredes, G. E. Romero and D. F. Torres. *A&A*, 446:1081, 2006.
- [13] V. Dhawan, A. Mioduszewski and M. Rupen. *VI Microquasar Workshop: Microquasars and Beyond*, 2006.
- [14] G. Dubus. *A&A*, 451:9, 2006.
- [15] G. Dubus. *A&A*, 456:801, 2006.
- [16] G. J. Feldman and R. D. Cousins. *Phys. Rev. D*, 57:3837, 1998.
- [17] R. Fender, K. Wu, H. Johnston et al. *Nature*, 427:222, 2004.
- [18] Q. Z. Liu, J. van Paradijs and E. P. J. van den Heuvel. *A&A*, 368:1021, 2001.
- [19] Q. Z. Liu, J. van Paradijs and E. P. J. van den Heuvel. *A&A*, 455:1165, 2006.
- [20] M. Massi, M. Ribó, J. M. Paredes et al. *A&A*, 414:L1, 2004.
- [21] I. F. Mirabel and L. F. Rodriguez. *Nature*, 371:46, 1994.
- [22] M. Orellana, G. E. Romero and H. R. Christiansen. *Boletín de la Asociación Argentina de Astronomía La Plata Argentina*, 48:334, 2005.
- [23] J. M. Paredes, M. Ribó, E. Ros, J. Martí and M. Massi. *A&A*, 393:L99, 2002.
- [24] G. E. Romero, D. F. Torres, M. M. Kaufman Bernadó, and I. F. Mirabel. *A&A*, 410:L1, 2003.



A Very High Energy γ -ray Survey of X-ray Binaries with H.E.S.S.

HUGH DICKINSON¹, IAN LATHAM¹, PAULA CHADWICK¹ FOR THE H.E.S.S. COLLABORATION

¹ *Physics Department, University of Durham, South Road, Durham, County Durham, DH1 3LE, United Kingdom*

h.j.dickinson@dur.ac.uk

Abstract: Since the discovery of TeV emission from the LS 5039/RX J1826.2-1450 binary system, microquasars are an established class of Very High Energy γ -ray sources. Nonetheless, the current catalogue of γ -ray binaries remains somewhat limited, with only four examples known. We present the results of a systematic search for TeV emission from known X-ray binaries with similar properties to LS 5039/RX J1826.2-1450 using the H.E.S.S. atmospheric Cherenkov telescope array.

Introduction

Galactic binary systems were established as a new class of TeV γ -ray sources when the pulsar-Be star binary PSR B1259-63 was detected by the H.E.S.S. Collaboration [1]. In this system very high energy γ -rays are likely generated as a result of the interaction of a strong pulsar wind with the dense equatorial wind of the Be star companion.

Subsequent H.E.S.S. observations of the microquasar LS 5039/RX J1826.2-1450 provided the first known example of an orbitally modulated TeV γ -ray signal [4]. Furthermore, the association of bipolar millisecond radio structures with the LS 5039 system [22] permits consideration of jet-powered scenarios of VHE γ -ray emission [6] suggesting possible parallels with the supermassive cousins of microquasars - the Active Galactic Nuclei (AGNs) (See however [12]). The companion star in the LS 5039 system has been spectroscopically identified as a massive O6.5V((f)) star [9]. The nature of the compact primary is somewhat ambiguous, with the recent ephemeris of [8] indicative of a black hole, but only when combined with the assumption of pseudo-synchronicity of the companion star. Neglecting this assumption, the derived lower mass limit of $\approx 1.5M_{\odot}$ is consistent with a neutron star primary. [8] also derive an somewhat short orbital period for the system of 3.9 days, combined with a rather low eccentricity of 0.35. In the X-ray band, LS 5039 is an unremarkable source albeit with a

somewhat hard spectrum [19]. The system was also associated with the soft γ -ray EGRET source 3EG J1824-1514 [21].

The most recently discovered γ -ray binary is the northern hemisphere object LS I +61°303, detected by the MAGIC collaboration [1]. Like LS 5039, this system exhibits a variable VHE γ -ray flux, although the existence of any orbital modulation is yet to be established. The orbital period of ≈ 26.5 days [14, 7] is somewhat longer than that of LS 5039 but a higher eccentricity of 0.72 gives a similar periastron distance of ~ 0.1 AU. [16] identified the optical counterpart of LS I +61°303 as a B0 V star with an equatorial disk. At radio frequencies LS I 61°+303 also exhibits jet-like structure on millisecond scales [20], although recent observations by [10] suggest that these “jets” may in fact result from interactions of a pulsar wind with the stellar wind of the companion. The X-ray characteristics of LS I 61°+303 are remarkably similar to those of LS 5039 [15], and also reminiscent is the tentative association with the EGRET source 2CG 135+01 [23].

These three systems constitute the entire VHE γ -ray binary catalogue. [11] performed a search for TeV signals coincident with the positions of known X-ray binaries using a sample containing a wide range of donor masses, compact primary types, radio, X-ray and soft γ -ray behaviours. Nonetheless no significant detections were obtained.

Instead of this blind search approach, a more sensible methodology might be to use the characteristics of the known γ -ray binaries as selection criteria for a more targeted survey. Indeed it is apparent that the objects in the existing catalogue share several physical and observational characteristics, some or all of which may be prerequisites for detectable TeV emission. In deriving our selection criteria we focus on the shared characteristics of LS 5039 and LS I 61°+303, since PSR B1259-63 is only detectable during a very small fraction of its 1237 day orbit and the probability of detecting a similar long period system is consequently rather low. We then use the generated criteria to construct a sample of likely VHE γ -ray binaries.

Source Selection

The final sample of 11 X-ray binaries is shown in Table 1, together with an outline of the selection criteria employed, and the degree to which each object in the sample fulfils these criteria. Five characteristics common to both LS 5039 and LS I 61°+303 were chosen as selection criteria. Based upon the observed similarities we should select short period ($P \sim 3 - 20$ days) systems with high mass donors, feeding neutron star or pulsar primaries, displaying extended millisecond radio structure and carrying associations with known soft γ -ray sources.

Unfortunately, there are only two known systems which fulfil all of these criteria, and these are LS 5039 and LS I 61°+303. In fact, choosing targets which do not precisely match the γ -ray binary template gives a useful diagnostic of which system properties or combinations thereof are important for the generation of a detectable TeV flux. Suitable targets were identified using the X-ray binary catalogues of [18] and [17] together with references therein. Ultimately, seven of the targets in our sample were chosen because they share at least some of the characteristics of our idealised γ -ray binary. The remaining four systems, GRS 1915+105, Circinus X-1, GX 339-4 and V4641 Sgr are known superluminal sources. The possibility of observing a transient VHE γ -ray flare during a superluminal outburst event was seen as sufficient justification for their inclusion in the survey.

Analysis and Results

Data reduction and analysis were carried out using the standard H.E.S.S. analysis procedure outlined in [2]. The event selection cuts placed on image size, θ^2 and the mean reduced scaled parameters are identical to those described as standard in [2], and are consistent with the expected point-like nature of the target objects. The γ -ray background was estimated using a ‘reflected’ background model with several run dependent *off* regions defined the same distance from the camera centre as the *on* region. Areas of the sky containing known TeV γ -ray sources are precluded from being chosen as *off* regions to ensure that the background estimate remains as uncontaminated as possible. Nonetheless, contamination can occur when the *on* region coincides with a known γ -ray source. Despite having excellent angular resolution for an instrument of its type, the H.E.S.S. point spread function is somewhat extended, with a 68% containment radius of $\sim 0.1^\circ$. For this reason it can be impossible to disentangle the signals from nearby objects. This is particularly difficult when the expected target spectrum and flux are unknown.

As reported in [4] the region exposed by the galactic plane scan is somewhat crowded with VHE γ -ray sources, and it is therefore unsurprising that some contamination of our targets did indeed occur.

Table 2 outlines the results of the survey. Upper limits to the photon flux above 1 TeV have been derived for 10 of the 11 targets. These upper limits represent 99% confidence intervals derived using the unified Feldman-Cousins method [14]. The remaining target OAO 1657-415, was too close to the known TeV emitter HESS J1702-420 for a reliable upper limit or flux estimate to be obtained.

Conclusions

99% confidence upper limits to the VHE γ -ray flux above 1 TeV have been derived for seven X-ray binaries with properties similar to LS 5039 and four superluminal microquasars. No significant detections were obtained. For the LS5039-like systems this could be due to orbital modulation of the TeV flux and observations contemporaneous with a low

Name	Companion Type	Compact Object	Radio Structure	Orbital Period (d)	γ -ray Emission
Vela X-1	OB	NS	No	8.96	TeV?
Cen X-3	OB	NS	No	2.09	GeV/TeV?
GX339-4	LM	BH	Yes	?	No
Cir X-1	LM	NS	Yes	16.6	No
GRO J1665-40	LM	BH	Yes	2.62	GeV
OA0 1657-415	B0-B6 Supergiant	NS	No	10.4	No
4U 1700-37	O6.5Iaf ⁺	NS?	No	3.96	No
4U 1538-52	B0I	NS	No	4	GeV?
V4641 Sgr	LM	BH	Yes	2.81	No
4U 1907+097	OB/Be	NS	No	8.38	No
GRS 1915+105	LM	BH	Yes	35	No

Table 1: The targets for our X-ray binary survey are shown in the table below. In the Companion Type column the spectral type of the donor is listed unless LM is specified, indicating a low-mass companion. The compact object type is either a black hole (BH) or neutron star (NS). Question marks indicate ambiguity in the quoted values or an absence of data.

Target Name	Significance [σ]	Excess [counts]	Livetime [hours]	Flux Upper Limit ($E_\gamma > 1 \text{ TeV}$) [$\text{ph cm}^{-2}\text{s}^{-1}$]
Vela X-1	-1.407	-73.000	4.360	3.550×10^{-12}
Cen X-3	0.778	21.589	5.283	5.845×10^{-12}
GX339-4	1.349	106.640	8.495	6.657×10^{-12}
Cir X-1	-0.942	-106.704	27.906	1.406×10^{-13}
GRO J1665-40	0.939	46.390	9.536	1.625×10^{-11}
OA0 1657-415	7.197	604.597	26.744	1.440×10^{-11}
4U 1700-37	2.929	289.137	38.708	(Contaminated by HESS J1702-420) 1.058×10^{-11}
4U 1538-52	-0.4256	-22.339	7.524	
V4641 Sgr	1.215	62.175	2.554	
4U 1907+097	-0.567	-13.490	14.997	
GRS 1915+105	0.156	4.566	19.692	

Table 2: The preliminary results of the survey are shown below. The region exposed by the galactic plane scan is crowded with VHE γ -ray sources, and it is therefore unsurprising that some contamination of our targets occurred due to overlap with known VHE sources. Where the target region is contaminated by the flux from a known TeV source, the derivation of an upper limit is not possible, but there is no way to safely associate the observed flux with the X-ray binary system. In this case the contaminating object is indicated in the Flux Upper Limit column. Negative excesses and significances result purely from fluctuations in the γ -ray background and should not be interpreted as a genuine deficit in the photon flux.

flux state. In some cases a rather short exposure time might also explain the lack of a detection. However, it may be that all the specific conditions found in the LS 5039 and LS I 61°+303 are required to produce a detectable VHE γ -ray signal. For the superluminal sources, failure to observe during a flaring event is the most likely explanation for a non-detection.

In the absence of a significant detection, it seems conspicuous, given that nearly 300 X-ray binaries are known, that only three should be detectable in the VHE γ -rayband. It may be that LS 5039, LS I 61°+303 and PSR B1259-63 are unique systems in our galaxy, or perhaps with the advent of more sensitive instruments such as H.E.S.S.II combined with the high energy γ -raycoverage of *GLAST* will reveal a much larger population of faint γ -raybinaries.

Acknowledgements The support of the Namibian authorities and of the University of Namibia in facilitating the construction and operation of H.E.S.S. is gratefully acknowledged, as is the support by the German Ministry for Education and Research (BMBF), the Max Planck Society, the French Ministry for Research, the CNRS-IN2P3 and the Astroparticle Interdisciplinary Programme of the CNRS, the U.K. Science and Technology Facilities Council (STFC), the IPNP of the Charles University, the Polish Ministry of Science and Higher Education, the South African Department of Science and Technology and National Research Foundation, and by the University of Namibia. We appreciate the excellent work of the technical support staff in Berlin, Durham, Hamburg, Heidelberg, Palaiseau, Paris, Saclay, and in Namibia in the construction and operation of the equipment.

References

- [1] F. Aharonian et al. (*H.E.S.S. Collaboration*). *A&A*, 442:1, 2005.
- [2] F. Aharonian et al. (*H.E.S.S. Collaboration*). *A&A*, 457:899, 2006.
- [3] F. Aharonian et al. (*H.E.S.S. Collaboration*). *ApJ*, 636:777, 2006.
- [4] F. Aharonian et al. (*H.E.S.S. Collaboration*). *A&A*, 460:743, 2006.
- [5] J. Albert et al. (*MAGIC Collaboration*). *Science*, 312:1771, 2006.
- [6] V. Bosch-Ramon and J. M. Paredes. *Chinese Journal of Astronomy and Astrophysics Supplement*, 5:133, 2005.
- [7] J. Casares, I. Ribas, J. M. Paredes, J. Martí and C. Allende Prieto. *MNRAS*, 360:1105, 2005.
- [8] J. Casares, M. Ribó, I. Ribas, et al. *MNRAS*, 364:899, 2005.
- [9] J. S. Clark, P. Reig, S. P. Goodwin, et al. *A&A*, 376:476, 2001.
- [10] V. Dhawan, A. Mioduszewski and M. Rupen. *VI Microquasar Workshop: Microquasars and Beyond*, 2006.
- [11] H. J. Dickinson. *International Cosmic Ray Conference, These Proceedings*, 2007.
- [12] G. Dubus. *A&A*, 456:801, 2006.
- [13] G. J. Feldman and R. D. Cousins. *Phys. Rev. D*, 57:3837, 1998.
- [14] P. C. Gregory. *ApJ*, 575:427, 2002.
- [15] F. A. Harrison, P. S. Ray, D. A. Leahy, E. B. Waltman and G. G. Pooley. *ApJ*, 528:454, 2000.
- [16] J. B. Hutchings and D. Crampton. *PASP*, 93:486, 1981.
- [17] Q. Z. Liu, J. van Paradijs and E. P. J. van den Heuvel. *A&A*, 368:1021, 2001.
- [18] Q. Z. Liu, J. van Paradijs and E. P. J. van den Heuvel. *A&A*, 455:1165, 2006.
- [19] A. Martocchia, C. Motch and I. Negueruela. *A&A*, 430:245, 2005.
- [20] M. Massi, J. M. Paredes, R. Estalella and M. Felli. *A&A*, 269:249, 1993.
- [21] J. M. Paredes, J. Martí, M. Ribó and M. Massi. *Science*, 288:2340, 2000.
- [22] J. M. Paredes, M. Ribó, E. Ros, J. Martí and M. Massi. *A&A*, 393:L99, 2002.
- [23] M. Tavani, D. Kniffen, J. R. Mattox, J. M. Paredes and R. Foster. *ApJ*, 497:L89, 1998.



Localising the H.E.S.S. Galactic Center point source

C. VAN ELDIK¹, O. BOLZ¹, I. BRAUN¹, G. HERMANN¹, J. HINTON², W. HOFMANN¹.

¹*Max-Planck-Institut für Kernphysik, Saupfercheckweg 1, 69117 Heidelberg, Germany*

²*School of Physics & Astronomy, University of Leeds, Leeds LS2 9JT, UK*

Christopher.van.Eldik@mpi-hd.mpg.de

Abstract: Observations by the H.E.S.S. system of imaging atmospheric Cherenkov telescopes provide the most sensitive measurements of the Galactic Centre region in the energy range 150 GeV - 30 TeV. The vicinity of the kinetic centre of our galaxy harbours numerous objects which could potentially accelerate particles to very high energies (VHE, > 100 GeV) and thus produce the γ -ray flux observed. Within statistical and systematic errors, the centroid of the point-like emission measured by H.E.S.S. was found [3] to be in good agreement with the position of the supermassive black hole Sgr A* and the recently discovered PWN candidate G359.95-0.04 [22]. Given a systematic pointing error of about $30''$, a possible association with the SNR Sgr A East could not be ruled out with the 2004 H.E.S.S. data. In this contribution an update is given on the position of the H.E.S.S. Galactic Centre source using 2005/2006 data. The systematic pointing error is reduced to $6''$ per axis using guiding telescopes for pointing corrections, making it possible to exclude with high significance Sgr A East as the source of the VHE γ -rays.

Introduction

The centre of the Milky-Way is the most violent and active region in our galaxy. Dust along the line of sight prevents observations of the Galactic Centre (GC) by optical telescopes, but precise data from this region have been obtained at radio, infrared, X-ray, and hard X-ray/soft γ -ray (< 200 keV) energies. These data have established the existence of a $2.6 \times 10^6 M_{\odot}$ black hole at the kinematic centre of our galaxy, commonly identified with the bright compact radio source Sgr A*, surrounded by a massive star cluster, a bright supernova remnant shell, and giant molecular clouds (see, e.g., [18, 11] for recent reviews).

VHE γ -ray emission from the direction of the Galactic Centre was reported by several ground-based γ -ray observatories [15, 20, 1, 8]. A recent deep exposure by H.E.S.S. [4] revealed the existence of two discrete VHE γ -ray sources, on top of diffuse emission along the inner 300 pc of the Galactic Centre ridge. One of the sources, HESS J1747-281 [2], is identified with the pulsar wind nebula (PWN) associated with the supernova remnant (SNR) G0.9+0.1. However, no unique identification is possible for HESS J1745-290, the

position of which is within errors coincident with the kinematic centre of our galaxy.

A firm identification of HESS J1745-290 is difficult because the GC region is densely packed with sources of non-thermal radiation – possibly emitting at VHE energies. In direct vicinity of the H.E.S.S. source, at least three different objects are discussed as possible counterparts of HESS J1745-290. First, various models predict VHE γ -ray production near the super-massive black hole itself (see, e.g., [7]). Sgr A* is partially surrounded by the bright, shell-like radio emission of the SNR Sgr A East [17], which is the second favoured candidate counterpart of the VHE γ -ray emission. Finally, in a deep Chandra survey, G359.95-0.04, a candidate pulsar wind nebula, was recently discovered [22] only $8.7''$ away from Sgr A*. Despite its faint X-ray flux, models [14] predict a TeV γ -ray flux that is compatible with H.E.S.S. observations.

A precise localisation of HESS J1745-290 is essential for shedding light onto this source confusion. In this paper preliminary results concerning a refined position measurement of HESS J1745-290 are reported using an improved telescope pointing strategy, for which the systematic error on the ob-

servation position is reduced by a factor of three compared to previous results.

H.E.S.S. observations of the Galactic Centre region

The most precise published results on the position of HESS J1745-290 are based on a 50 h exposure carried out with the H.E.S.S. array in 2004. Within a statistical error of $14''$ the best-fit position of HESS J1745-290 was found [3] to coincide with the position of Sgr A*. The systematic pointing error of the H.E.S.S. telescope system for this data set is about $28''$, already the most precise pointing in the field of ground-based γ -ray astronomy.

The results reported here are based on data recorded between May 14th and July 27th, 2005, and between April 4th and September 24th, 2006. The total good-quality exposure of the dataset is 73.2 h (live time). Most of the data (66.1 h) were taken in “wobble mode” around Sgr A*, i.e. the observation direction was offset from the source direction by typically $0.5^\circ - 0.7^\circ$ in either right ascension or declination. The remaining data were taken at various offsets, within 1.4° from Sgr A*. The zenith angle distribution ranges from $6^\circ - 60^\circ$, and the mean zenith angle of observation is 21.6° .

Data were analysed with the standard H.E.S.S. calibration and reconstruction chain [5]. *Hard cuts* [9] were used for γ -ray selection, resulting in a sample of well-reconstructed showers with an average angular resolution of 0.07° (68% containment radius). The data show a strong excess of γ -rays from the direction of the GC source HESS J1745-290, accompanied by diffuse γ -ray emission along the Galactic Plane. An excess of 1300 γ events is found within 0.1° from the GC, corresponding to a statistical significance of 44.3 standard deviations above background. The integral γ -ray flux above 1 TeV is in agreement with published results based on 2004 data [3].

Precision pointing

For an exact localisation of the centroid of the VHE γ -ray emission, precise knowledge of the telescope pointing direction is mandatory. The pointing de-

viation of individual telescopes is typically of the order of $2-3'$. Various causes have been identified, with the most important ones being small misalignments of azimuth and altitude axes during construction, sagging of telescope foundations over time, (mostly) elastic deformations of the masts connecting the camera body to the mirror dish, gravitational bending of the mirror dish, and inelastic deformations of the whole structure leading to hysteresis effects. The amount these effects contribute to the mispointing strongly depends on the observation direction. It should however be noted that - due to the rigidity of the steel construction - the overall pointing deviation is very small given the size and weight of the H.E.S.S. telescopes.

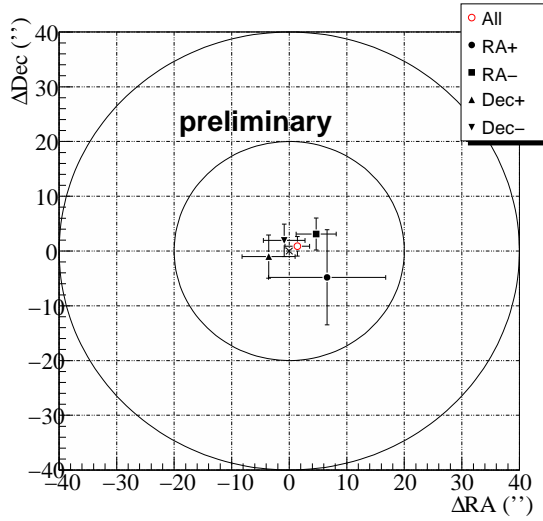


Figure 1: Position of the centroid of VHE γ -ray emission from PKS 2155-304 relative to its nominal position. Data were taken in 2006 during an exceptional VHE γ -ray flare of this source [6]. The γ -ray excess was fit by a two-dimensional multi-gaussian profile representing the point spread function of the H.E.S.S. instrument. The red data point shows the position derived from the full data set. When subdividing the data into the four wobble offsets, the positions shown by the black symbols are obtained. Note that for most of the RA+ wobble data, no bright stars were found in the field of view of the guiding telescopes, reducing the available live time for this analysis.

Most pointing deviations can be corrected for by taking calibration data at regular intervals. Each

telescope is pointed at typically 50 bright stars uniformly distributed in the sky. The star is imaged by the telescope mirror onto a screen in front of the Cherenkov camera, and an image of the spot is recorded by a central CCD camera mounted at the centre of the mirror dish. The position of each spot is then compared to the nominal centre of the Cherenkov camera as determined from eight positioning LEDs mounted on the camera body. The data are fit with a 17 parameter model which accounts for elastic deformations of the telescope structure. In the analysis of γ -ray data, this model is then used to correct the position of the shower images in the focal plane of the Cherenkov cameras. The precision achieved on the observation direction of the H.E.S.S. array is about $20''$ per axis [12].

For the 2005-2006 data set presented here, the systematic error is reduced further using guiding cameras mounted at each telescope. During γ -ray observations, stars in the field of view ($0.3^\circ \times 0.5^\circ$) of these cameras are recorded at a typical rate of 1 min^{-1} , and their reconstructed positions matched to the Hipparcos and Tycho star catalogues. From this information position-dependent corrections in right ascension and declination are calculated for the individual H.E.S.S. telescopes. Additionally, the position of the Cherenkov camera is monitored by the central CCD camera. With this method, the systematic error on the telescope orientation is reduced to $6''$ per axis for observations with the full H.E.S.S. array ([10], details will be published elsewhere).

The procedure was extensively tested on VHE γ -ray point sources of known position. Fig. 1 shows a representative study on the position of the high-frequency peaked BL Lac PKS 2155-304. Excellent agreement with the nominal position of the source is found even when splitting the data into different wobble offsets.

Position of HESS J1745-290

The position of HESS J1745-290 is determined by fitting, in a window of $\pm 0.2^\circ$ around the maximum excess, the acceptance corrected and background subtracted γ -ray count map. Diffuse γ -ray emission is subtracted prior to the fit using the model

presented in [4]. The width of the 2-dimensional gaussian fit to these data is composed of a fixed term describing the mean angular resolution of the data set, and a parameter left free to fit the intrinsic size of the source. The count map is divided into sky bins of $0.04^\circ \times 0.04^\circ$, and the fit function is integrated over the bin area for best accuracy. χ^2 -minimisation is used to obtain the best-fit position.

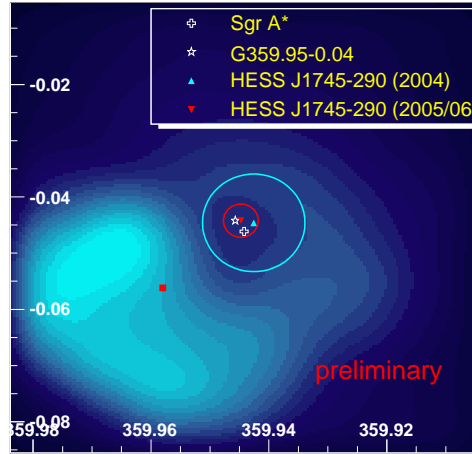


Figure 2: Smoothed 90 cm VLA radio image (reproduced from [16]) of the SNR Sgr A East in Galactic coordinates. The position of Sgr A* and G359.95-0.04 are marked with a cross and a star, respectively. The blue triangle and circle mark the best fit position and total error (68% CL) from the 2004 data set [3]. The best fit result of this analysis is shown by the red triangle and red circle. The red square marks the expected position of the centroid of the VHE γ -ray emission if it followed the observed radio flux of Sgr A East.

The best-fit position of HESS J1745-290 in Galactic coordinates is $l = 359^\circ 56' 41.1'' \pm 6.4''$ (stat.), $b = -0^\circ 2' 39.2'' \pm 5.9''$ (stat.). These results are preliminary and subject to final checks. Fig. 2 shows the new H.E.S.S. position measurement on top of a 90 cm VLA radio image of the inner 10 pc region of the GC. The shell-like structure of the SNR Sgr A East is clearly visible. The position of HESS J1745-290 is coincident within $7.3'' \pm 8.7''$ (stat.) $\pm 8.5''$ (syst.) with the radio

position of Sgr A* [19], and is also consistent with the position reported from the 2004 data set [3]. While the latter was marginally consistent with the radio emission from Sgr A East, the result obtained in this analysis does rule out Sgr A East as the counterpart of HESS J1745-290 with high significance. Due to the improved pointing accuracy of the H.E.S.S. array, the probability that the observed γ -ray flux is produced near the radio maximum of Sgr A East is about 10^{-11} . Assuming that the VHE γ -ray flux follows the radio morphology of Sgr A East (corresponding to the red square in Fig. 2), the chance probability of finding the centroid of the emission at the reported position is 10^{-7} .

The position of HESS J1745-290 agrees well with the location of the other two counterpart candidates, Sgr A* and G359.95-0.04, which are separated by only $8.7''$. Since the pointing precision obtained in this work is at the limit of what can be achieved with an instrument such as H.E.S.S., other measures have to be taken to disentangle the remaining source confusion. The most promising method is to search for variability in the VHE γ -ray flux, which would hint at a connection between the VHE flux and Sgr A*. The most convincing signature would be the detection of correlated flaring in X-rays and VHE γ -rays. Such searches have been presented at this conference [21, 22].

Acknowledgements

The support of the Namibian authorities and of the University of Namibia in facilitating the construction and operation of H.E.S.S. is gratefully acknowledged, as is the support by the German Ministry for Education and Research (BMBF), the Max Planck Society, the French Ministry for Research, the CNRS-IN2P3 and the Astroparticle Interdisciplinary Programme of the CNRS, the U.K. Science and Technology Facilities Council (STFC), the IPNP of the Charles University, the Polish Ministry of Science and Higher Education, the South African Department of Science and Technology and National Research Foundation, and by the University of Namibia. We appreciate the excellent work of the technical support staff in Berlin, Durham, Hamburg, Heidelberg, Palaiseau, Paris, Saclay, and in Namibia in the construction and operation of the equipment.

References

- [1] F. Aharonian et al. *Astron. Astrophys.*, 425:L13–L17, 2004.
- [2] F. Aharonian et al. *Astron. Astrophys.*, 432:L25–L29, 2005.
- [3] F. Aharonian et al. *Phys. Rev. Lett.*, 97:221102, 2006.
- [4] F. Aharonian et al. *Nature*, 439:695–698, 2006.
- [5] F. Aharonian et al. *Astron. Astrophys.*, 457:899–915, 2006.
- [6] F.A. Aharonian et al. *arxiv:0706.0797*, 2007.
- [7] Felix Aharonian and Andrii Neronov. 2005.
- [8] J. Albert et al. *Astrophys. J.*, 638:L101–L104, 2006.
- [9] W. Benbow. *Proc. Towards a Network of Atmospheric Cherenkov Detectors*, 2005.
- [10] I. Braun. *PhD thesis, University of Heidelberg*, 2007.
- [11] R. Genzel and V. Karas. *arXiv:0704.1281, to appear in Proc. "Black Holes: from Stars to Galaxies"*, 2007.
- [12] S. Gillessen. *PhD thesis, University of Heidelberg*, 2004.
- [13] J. Hinton et al. Simultaneous H.E.S.S. and Chandra observations of Sgr A* during and X-ray flare. These proceedings.
- [14] J. A. Hinton and F. A. Aharonian. *Astrophys. J.*, 657:302–307, 2007.
- [15] K. Kosack et al. *Astrophys. J.*, 608:L97–L100, 2004.
- [16] T.N. LaRosa et al. *Astron. Journal*, 119:207–240, 2000.
- [17] Y. Maeada et al. *Astrophys. J.*, 570:671–687, 2002.
- [18] F. Melia. *The Galactic Supermassive Black Hole. Princeton University Press*, 2007.
- [19] M.J. Reid et al. *Astrophys. Journal*, 524:816–823, 1999.
- [20] Ken'ichi Tsuchiya et al. *Astrophys. J.*, 606:L115–L118, 2004.
- [21] M. Vivier et al. Search for variability and QPO activity from Sgr A*. These proceedings.
- [22] Q. Daniel Wang, F. J. Lu, and E. V. Gotthelf. *Mon. Not. Roy. Astron. Soc.*, 367:937–944, 2006.



Simultaneous H.E.S.S. and Chandra observations of Sgr A* during an X-ray flare

JIM HINTON¹, MATTHIEU VIVIER², ROLF BÜHLER³, GERD PÜHLHOFFER⁴, STEFAN WAGNER⁴

FOR THE H.E.S.S. COLLABORATION

¹*School of Physics & Astronomy, University of Leeds, Leeds LS2 9JT, UK*

²*DAPNIA/DSM/CEA, CE Saclay, F-91191 Gif-sur-Yvette, Cedex, France*

³*Max-Planck-Institut für Kernphysik, P.O. Box 103980, D 69029 Heidelberg, Germany*

⁴*Landessternwarte, Universität Heidelberg, Königstuhl, D 69117 Heidelberg, Germany*

j.a.hinton@leeds.ac.uk

Abstract: The rapidly varying non-thermal X-ray emission observed from Sgr A* points to particle acceleration taking place close to the supermassive black hole. The TeV γ -ray source HESS J1745–290 is coincident with Sgr A* and may be closely related to the X-ray emission. Simultaneous X-ray and TeV observations are required to elucidate the relationship between these two objects. Here we report on joint H.E.S.S./Chandra observations in July 2005, during which an X-ray flare was detected. Despite a factor > 10 increase in the X-ray flux of Sgr A*, no evidence is found for an increase in the TeV γ -ray flux. We find that an increase of the γ -ray flux of a factor 2 or greater can be excluded at a confidence level of 99%. This finding disfavors scenarios in which the bulk of the γ -ray emission observed is produced close to Sgr A*.

Introduction

The existence of a supermassive ($3.6 \pm 0.3 \times 10^6$ solar mass) black hole at the centre of our galaxy has been inferred using measurements of stellar orbits in the central parsec (see e.g. [1]). The supermassive black hole (SMBH) is coincident with the faint radio source: Sgr A*. The compact nature of Sgr A* has been demonstrated both by direct VLBI measurements [2] and by the observation of X-ray and near IR flares with timescales as short as a few minutes (see for example [3, 4]). Variability on such short timescales limits the emission region (via causality arguments) to within < 10 Schwarzschild radii of the black hole. X-ray flares from Sgr A* have reached fluxes of $4 \times 10^{35} \text{ erg s}^{-1}$, two orders of magnitude brighter than the quiescent flux [4, 5], and exhibit a range of spectral shapes [4]. Several models exist for the origin of this variable emission, all of which invoke non-thermal processes close to the event horizon of the central black hole to produce a population of relativistic particles.

Model independent evidence for the existence of ultra-relativistic particles close to Sgr A* can be provided by the observation of TeV γ -rays from this source. Indeed, TeV γ -ray emission has been detected from the Sgr A region by several ground-based instruments [6, 7, 8, 9]. The most precise measurement of this source, HESS J1745–290, are those made using the H.E.S.S. telescope array. The centroid of the source is located $7'' \pm 14''_{\text{stat}} \pm 28''_{\text{sys}}$ from Sgr A*, and has an rms extension of $< 1.2'$ [10].

TeV emission from Sgr A* is expected in several models of particle acceleration in the environment of the black hole. In some of these scenarios [11, 12] TeV emission is produced in the immediate vicinity of the SMBH and variability is expected. In alternative scenarios particles are accelerated at Sgr A* but radiate in within the central ~ 10 parsec region [13], or are accelerated at the termination shock of a wind driven by the SMBH [14]. However, several additional candidate objects exist for the origin of the observed γ -ray emission. The radio centroid of the supernova remnant (SNR) Sgr A East lies $\sim 1'$ from Sgr A*,

only marginally inconsistent with the position of the TeV source given in [10]. Shell-type SNR are now well established TeV γ -ray sources [15, 16] and several authors have suggested Sgr A East as the origin of the TeV emission (see for example [17]). However, recent improvements in the statistical and systematic uncertainties of the centroid of HESS J1745–290 effectively exclude Sgr A East as the dominant γ -ray source in the region [8]. The recently discovered pulsar wind nebula candidate G 359.95-0.04 [19] lies only 9 arcseconds from Sgr A* and can plausibly explain the TeV emission [20]. Particle acceleration at stellar wind collision shocks within the central young stellar cluster has also been hypothesised to explain the γ -ray source [21]. Finally, an origin of this source in the annihilation of WIMPs in a central dark matter cusp has been extensively discussed [22, 23, 10].

Given the limited angular resolution of current VHE γ -ray telescopes, the most promising tool for identification of the TeV source is the detection of *correlated variability* between the γ -ray and X-ray and/or NIR regimes. A significant increase of the flux of HESS J1745–290 simultaneous with a flare in wavebands with sufficient angular resolution to isolate Sgr A*, would provide an unambiguous identification of the γ -ray source. Therefore, whilst not all models for TeV emission from Sgr A* predict variability of the VHE source, co-ordinated IR/keV/TeV observations can be seen as a key aspect of the ongoing program to understand the nature of this enigmatic source.

Observations & Results

A coordinated multi-wavelength campaign on Sgr A* took place during July/August 2005. As part of this campaign observations with H.E.S.S. occurred for 4-5 hours each night from the 27th of July to the 1st of August (MJD 53578-53584). Four Chandra observations with IDs 5950-5954 took place between the 24th of July and the 2nd of August. A search for flaring events in the X-ray data yielded two significant events during the Chandra campaign, both during observation ID 5953 on the 30th of July. The second of these flares occurred during a period of H.E.S.S. coverage, at MJD 53581.94.

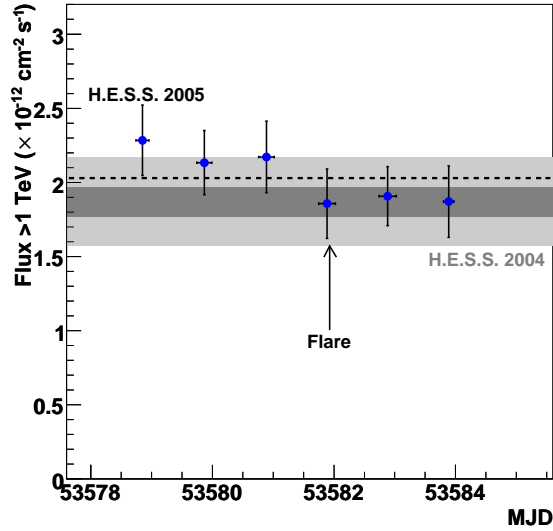


Figure 1: Nightly γ -ray flux light-curve of HESS J1745–290 from the 27th of July to the 1st of August 2005. The H.E.S.S. data have typical thresholds of 150-300 GeV. The grey band shows the mean flux from 2004 observations as published in [10]. Statistical (dark grey) and systematic (light grey) errors are shown. The dashed line is a fit to the MJD 53578-53584 data.

The γ -ray data consist of 72 twenty-eight minute runs, 66 of which pass all the quality selection cuts described by [2]. All runs on the night of the X-ray flare pass these cuts and in addition we find no evidence for cloud cover in the simultaneous sky temperature (radiometer) measurements (see [2, 25]). These data were analysed using the H.E.S.S. standard *Hillas parameter* based method described in [2]. An independent analysis based on the *Model Analysis* method described in [26] produced consistent results. Figure 1 shows a night-by-night TeV flux light-curve for this period. There is no evidence for variations of the flux on day timescales and the mean > 1 TeV γ -ray flux for this week of observations was $2.03 \pm 0.09_{\text{stat}} \times 10^{-12} \text{ cm}^{-2} \text{ s}^{-1}$, consistent with the average value for H.E.S.S. observations in 2004, $1.87 \pm 0.1_{\text{stat}} \pm 0.3_{\text{sys}} \times 10^{-12} \text{ cm}^{-2} \text{ s}^{-1}$ [10].

Figure 1 shows the X-ray and γ -ray light curves for the night MJD 53581-2. There is a clear in-

crease in the X-ray flux of Sgr A* with an excess of 103 ± 10 events with respect to the quiescent level. The time-profile of this excess is consistent with a Gaussian of rms 13.1 ± 2.5 minutes. The time window for the γ -ray analysis is defined as the region within $\pm 1.3\sigma$ of the X-ray flare (containing 80% of the signal). The lower panel of Figure 1 shows the mean TeV flux within this time window (grey shaded region) of $2.05 \pm 0.76 \times 10^{-12} \text{ cm}^{-2} \text{ s}^{-1}$ as a short dashed line. This flux level is almost identical to the mean flux level for this week of observations. There is therefore no evidence for an increase in γ -ray flux of HESS J1745-290 during the flare and a limit on the relative flux increase of < 2 is derived at the 99% confidence level. In principle a (positive or negative) time lag might be expected between the X-ray and any associated γ -ray flare. The existence of a counterpart γ -flare with a flux increase $\gg 2$ requires a lag of at least 100 minutes.

Summary

For the first time simultaneous TeV γ -ray observations have been presented for a period of X-ray activity of Sgr A*. The non-detection of an increase in the TeV flux provides an important constraint on scenarios in which the source HESS J1745-290 is associated with the supermassive black hole.

References

- [1] Eisenhauer, F. et al. 2005, *Astrophys. J.* 628, 246.
- [2] Shen, Z.-Q. et al. 2005, *Nature* 438, 62.
- [3] Eckart, A. et al. 2006, *Astron. & Astrophys.* 450, 535.
- [4] Porquet, D. et al. 2003, *Astron. & Astrophys.* 407, L17.
- [5] Baganoff, F.K. et al. 2003, *Astrophys. J.* 591, 891.
- [6] Kosack, K. et al. 2004, *Astrophys. J. Letters* 608, L97.
- [7] Tsuchiya, K. et al. 2004, *Astrophys. J. Letters* 606, L115.
- [8] Aharonian, F. et al. 2004, *Astron. & Astrophys.* 425, L13.
- [9] Albert, J. et al. 2006, *Astrophys. J. Letters* 638, L101.
- [10] Aharonian, F. et al. 2006, *Physical Review Letters* 97, 221102.
- [11] Levinson, A., Boldt, E. 2002, *Astroparticle Physics* 16, 265.
- [12] Aharonian F.A., Neronov A. 2005, *Astrophys. J.* 619, 306.
- [13] Aharonian F.A., Neronov A. 2005, *Space Sci. Rev.* 300, 255.
- [14] Atoyan A.M., Dermer C.D. 2004, *Astrophys. J. Letters* 617, L123.
- [15] Aharonian, F. et al. 2006, *Astron. & Astrophys.* 449, 223.
- [16] Aharonian, F. et al. 2007, *Astrophys. J.* 661, 236.
- [17] Crocker R.M. et al. 2005, *Astrophys. J.*, 622, 892.
- [18] Van Eldik, C. (for the H.E.S.S. Collaboration) 2007, *These Proceedings*.
- [19] Wang, Q.D., Lu, F.J., Gotthelf, E. V. 2006, *MNRAS* 367, 937.
- [20] Hinton, J.A., Aharonian, F.A. 2007, *Astrophys. J.* 657, 302.
- [21] Quataert, E. and Loeb, A. 2005, *Astrophys. J. Letters* 635, L45.
- [22] Hooper, D. et al. 2004, *Journal of Cosmology and Astro-Particle Physics* 9, 2.
- [23] Profumo, S. 2005, *Phys. Rev. D* 72, 103521.
- [24] Aharonian, F. et al. 2006, *Astron. & Astrophys.* 457, 899.
- [25] Le Gallou, R. et al. 2003, *Proc. International Cosmic Ray Conference*, 2879.
- [26] de Naurois, M. 2005, *Proc. Conf. Towards a Network of Atmospheric Cherenkov Detectors VII*, Palaiseau, France, 2005, p. 149

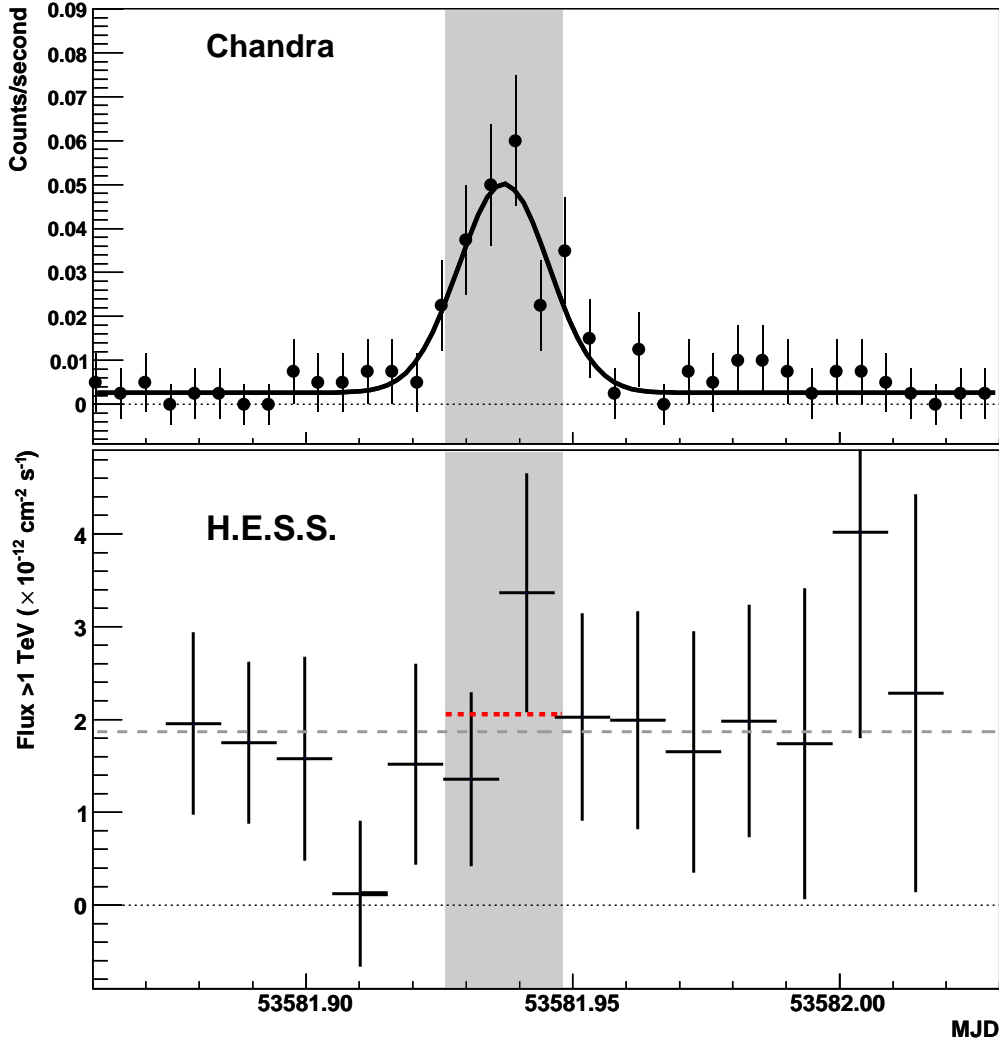


Figure 2: X-ray and γ -ray light curves for the Galactic Centre on MJD 53581. Top: Chandra 1-10 keV count rate in 400 second bins. The X-ray flare is well described by Gaussian (solid curve), the shaded region shows $\pm 1.3\sigma$ of the flare position. Bottom: Very High Energy γ -ray light curve from H.E.S.S. in 15 minute bins. The long dashed line shows the historical flux level [10]. The short dashed line indicates the mean TeV flux during the X-ray flare.

Search for variability and QPO activity from SgrA* from H.E.S.S observations

M. VIVIER¹, O. DE JAGER², J. HINTON³ FOR THE H.E.S.S. COLLABORATION

¹DAPNIA/DSM/CEA, CE Saclay, F-91191 Gif-sur-Yvette, Cedex France

²Unit for Space Physics, North-West University, Potchefstroom 2520, South Africa

³School of Physics and Astronomy, University of Leeds, Leeds LS2 9JT, UK

matthieu.vivier@cea.fr

Abstract: One interesting possibility is that the galactic center (GC) source HESS J1745-290 is associated with the galactic center source Sgr A*, the galactic center black hole, in which case we may expect variability as seen in IR and X-rays, with QPO frequencies predicted by Aschenbach et al. (2006). We will present the results of a search for such variable signatures using HESS observations of this source.

Introduction

H.E.S.S. (High Energy Stereoscopic System) [1] consists of four imaging atmospheric-Cherenkov telescopes (IACT's) located in Namibia. The Cherenkov light emitted by γ -induced air showers is detected by a camera of 960 photomultiplier tubes, located at the focus of the four 12 m diameter telescopes. The field of view of a camera is 5° in diameter. A description of the H.E.S.S. instrument and operation can be found in [2, 3].

A strong signal was detected by H.E.S.S. toward the GC [4, 5]. A refined analysis of the HESS J1745-290 source position is presented in [8]. Given the HESS J1745-290 source position uncertainties, several sources are plausible candidates. Among them, the black hole SgrA* located at the center of our galaxy [6, 7] is one of the most popular candidate. The dark matter origin of the H.E.S.S. signal has also been strongly constrained in [5]. Thus, it is important to study the flux variability of the source to constrain the emission mechanisms of the detected TeV signal. X-ray flares of SgrA* were detected with periods ranging from 100 s to 2250 s [9]. Here we report a search for similar variabilities in the TeV energy range using H.E.S.S. GC data.

The observations presented here were obtained during the 2004, 2005 and 2006 observing seasons of the GC. Photons were selected and

reconstructed with the so-called "model analysis" [10, 11]. Spectra are presented elsewhere [12]. Results were checked with a different reconstruction method based on Hillas statistical moment of the images [13]. The total live time of the whole data set is 97 h. The total significance corresponds to a 59.8σ deviation above the background using a point-like source analysis (i.e. using a cut on the angular distance θ between the reconstructed direction of the γ -rays and the pointed direction: $\theta < 0.14^\circ$).

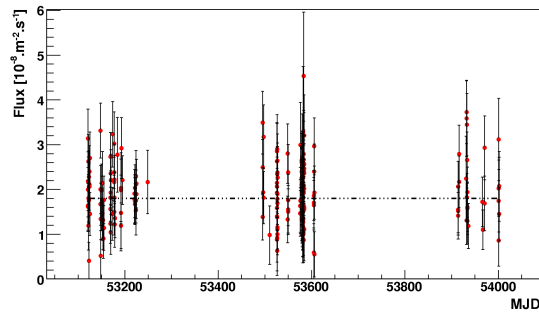


Figure 1: Run by run light curve of HESS J1745-290. Data cover the 2004-2006 time period.

The run by run integral flux of γ -rays above 1 TeV is shown on Fig.1. A run corresponds to a 28 min observation time. The χ^2 of a constant fit to data is 228/211 d.o.f. This is consistent with a constant

flux of:

$$\Phi(> 1 \text{ TeV}) = 2.14 \cdot 10^{-12} \text{ cm}^{-2} \text{ s}^{-1}$$

No significant variations are detected on timescales longer than 28 min.

Flare sensitivity

As mentioned in the introduction, the flaring of SgrA* has been detected in various passbands such as IR or X-rays. Simultaneous H.E.S.S./Chandra observations were carried out during an X-ray flare. No flare was detected by H.E.S.S. as reported in [14]. Because of the large error bars implied by low statistics, the H.E.S.S. signal is sensitive to relatively larger amplitude flares. The flare sensitivity was estimated by adding a fake gaussian with variable duration σ_t and maximum amplification time t_0 to the H.E.S.S. light curve (LC). The modified LC is thus represented by:

$$\text{LC}_{\text{mod}}(t) = \text{LC}(t) \times \left(1 + A \times e^{\frac{(t-t_0)^2}{\sigma_t^2}} \right) \quad (1)$$

Fig.2 shows the maximum amplification factor A compatible with no flare detection at the $3\text{-}\sigma$ confidence level as function of the flare duration. Typical numbers for A are of order unity. A decreases with the flare duration as expected.

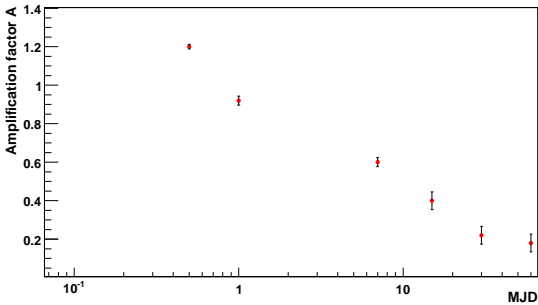


Figure 2: Mean sensitivity to a $3\text{-}\sigma$ flare detection as a function of the flare duration. The mean sensitivity decreases with the flare duration.

Search for QPO's at the X-ray periods

Four oscillation frequencies ranging from 100 s to 2250 s have been observed in the X-ray light curve of SgrA* [9]. These frequencies are likely to correspond to gravitational cyclic modes associated with the accretion disk of SgrA*. We searched for the occurrence of these frequencies in our data. First, we assume that the coherence time of oscillations is less than 28 min. We then perform a Rayleigh test [16] on photon time arrival distributions for continuous observations of 28 min. The Rayleigh power averaged over 2004-2006 data is shown on Fig.3 as a function of the frequency. The probed frequencies range from $1/28 \text{ min}^{-1}$ to the inverse of the average time spacing between two consecutive events of 1.2 min^{-1} . The Rayleigh power is compatible with a flat function of frequency. No significant peaks are seen at the 100 s, 219 s, 700 s and 1150 s periods observed in X-rays.

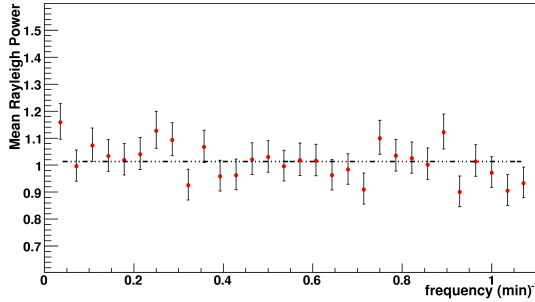


Figure 3: Rayleigh power plotted as a function of the frequency. A fit to a constant power gives a χ^2 of 35/29 d.o.f. compatible with a flat distribution.

Next, we assume that the coherence time of oscillations is of the order of a few hours. We then construct the Fourier power distribution using a Lomb-Scargle periodogram [15] for each night of our dataset. Data are binned into 5 min points. The Fourier power averaged over 2004-2006 data is displayed on Fig.4 as a function of the frequency. Frequencies tested range from 10^{-2} min^{-1} to 0.1 min^{-1} . No significant oscillation frequencies are detected, as shown on Fig.5.

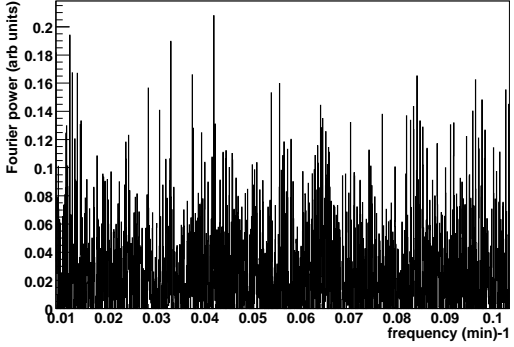


Figure 4: $[10^{-2} \text{ min}^{-1} - 0.1 \text{ min}^{-1}]$ Lomb-Scargle periodogram of the H.E.S.S. SgrA* light curve averaged over the 2004-2006 nights of observation. No significant peak is visible.

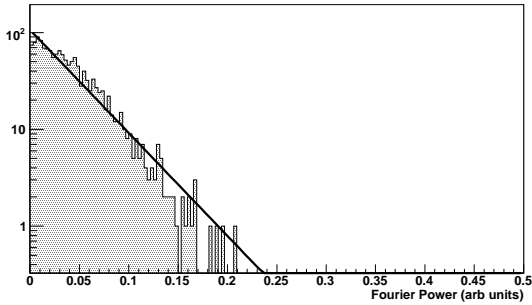


Figure 5: Fourier power distribution derived from the average Lomb-Scargle periodogram. The χ^2 of the exponential fit to data is 72/55 d.o.f.

Conclusions

The light curve of the very high energy source HESS J1745-290 observed towards the GC is compatible with a constant integrated flux above 1 TeV of $\Phi(> 1 \text{ TeV}) = 2.14 \cdot 10^{-12} \text{ cm}^{-2} \text{ s}^{-1}$. The source appears to be steady in time for timescales from a year down to 1 min. The flare sensitivity study shows that H.E.S.S. was sensitive to flux increases with amplification factor of order of the unity. As the flare duration increases, lower amplification factors are needed for a $3\text{-}\sigma$ detection. Searches for QPO's in the H.E.S.S. GC signal did not uncover any periodicities, in particular none of those observed by [9]. The constraints on the variability of HESS J1745-290 will be improved by new observations taken in 2007.

Acknowledgments

The support of the Namibian authorities and of the University of Namibia in facilitating the construction and operation of H.E.S.S. is gratefully acknowledged, as is the support by the German Ministry for Education and Research (BMBF), the Max Planck Society, the French Ministry for Research, the CNRS-IN2P3 and the Astroparticle Interdisciplinary Programme of the CNRS, the U.K. Particle Physics and Astronomy Research Council (PPARC), the IPNP of the Charles University, the Polish Ministry of Science and Higher Education, the South African Department of Science and Technology and National Research Foundation, and by the University of Namibia. We appreciate the excellent work of the technical support staff in Berlin, Durham, Hamburg, Heidelberg, Palaiseau, Paris, Saclay, and in Namibia in the construction and operation of the equipment.

References

- [1] Hofmann, W. (for the H.E.S.S. collaboration), Proc.of the 28th ICRC (Tsubuka),(2003).
- [2] Aharonian, F.A., et al. (H.E.S.S. collaboration), *Astropart.Phys.*22, 109 (2004)
- [3] Funk, S., et al. *Astropart.Phys.*22, 285 (2004)
- [4] Aharonian, F.A., et al. (H.E.S.S. collaboration), *A&A* 425, L13 (2004)
- [5] Aharonian, F.A., et al. (H.E.S.S. collaboration), *Phys.Review Letter* (2006)
- [6] Aharonian, F.A.& Neronov, A., *ApJ* 619, 306 (2005)
- [7] Atoyan, A. & Dermer, C.D., *ApJ* 617, L123 (2004)
- [8] van Eldik, C., these proceedings, (2007)
- [9] Aschenbach, B., et al., *A&A*, (2006)
- [10] de Naurois, M., et al., Proc.of the 28th ICRC (Tsubuka), (2003)
- [11] de Naurois, M., et al., In *Towards a Network of Atmospheric Cherenkov Dectectors* (2005)
- [12] Ripken, J., these proceedings, (2007)
- [13] Aharonian, F.A., et al., *A&A* 430, 865 (2005)
- [14] Hinton, J., et al., these proceedings, (2007)
- [15] Scargle, J.D., *ApJ* 263, 835 (1982)
- [16] de Jager, O.C., Swanepoel, J.W.H. & Raubenheimer, B.C.,(1989)



The H.E.S.S. survey of the inner Galactic plane

S. HOPPE¹, FOR THE H.E.S.S. COLLABORATION

¹Max-Planck-Institut für Kernphysik, P.O. Box 103980, D 69029 Heidelberg, Germany

stefan.hoppe@mpi-hd.mpg.de

Abstract: The High Energy Stereoscopic System (H.E.S.S.), located in the Khomas Highlands of Namibia, is an array of four imaging atmospheric-Cherenkov telescopes designed to detect γ -rays in the very high energy (VHE; > 100 GeV) domain. Its high sensitivity and large field-of-view (5°) make it an ideal instrument to perform a survey within the Galactic plane for new VHE sources. Previous observations in 2004/2005 resulted in numerous detections of VHE gamma-ray emitters in the region $l = 330^\circ - 30^\circ$ Galactic longitude. Recently the survey was extended, covering the regions $l = 280^\circ - 330^\circ$ and $l = 30^\circ - 60^\circ$, leading to the discovery of several previously unknown sources with high statistical significance. The current status of the survey will be presented.

Introduction

The majority of the newly discovered sources of very high energy (VHE; > 100 GeV) γ -rays are related to late phases of stellar evolution, either directly to massive stars or to the compact objects they form after their collapse. The possible associations include pulsar wind nebulae (PWN) of high spin-down luminosity pulsars such as G 18.0–0.7 [5], supernova remnants like RX J1713.7–3946 [8], and open star clusters like Westerlund 2 [9]. As these objects cluster closely along the Galactic plane, a survey of this region is an effective approach to discover new sources and source classes of VHE γ -ray emission.

The H.E.S.S. experiment and its Galactic plane survey

The High Energy Stereoscopic System (H.E.S.S.) is an array of four imaging atmospheric-Cherenkov telescopes located 1800 m above sea level in the Khomas Highlands in Namibia [3]. Each of the telescopes is equipped with a camera comprising 960 photomultipliers and a tessellated mirror with an area of 107 m^2 , resulting in a comparatively large field-of-view of 5° in diameter. The H.E.S.S. array can detect point sources at flux levels of

about 1% of the Crab nebula flux near zenith with a statistical significance of 5σ in 25 hours of observation. This high sensitivity and the large field-of-view enable H.E.S.S. to survey large celestial areas – such as the Galactic plane – within a reasonable time.

The H.E.S.S. Galactic plane survey began 2004 and has been a major part of the observation program since. In the years 2004/2005 the survey was conducted in the Galactic longitude band $\pm 30^\circ$ around $l = 0^\circ$, covering most of the inner part of the Galactic plane from the tangent of the Norma arm to the tangent of the Scutum arm. Observations of 28 minutes duration each were taken at pointings with a spacing of 0.7° in longitude in three strips in Galactic latitude, covering an approximately 6° wide region along the Galactic plane. 95 h of data were taken in pure survey mode. Promising source candidates were re-observed in dedicated observations, comprising 30 h of data. In addition, dedicated observations in this region were taken on known or assumed VHE γ -ray sources. The total amount of good quality data in this region was 230 hours, Fig. 1 (blue). This first stage of the H.E.S.S. Galactic plane survey resulted in the discovery of eight previously unknown sources of VHE γ -rays at a significance level greater than 6σ after accounting for all trials involved in the search (post-trials) [4]. Additionally, six likely sources were

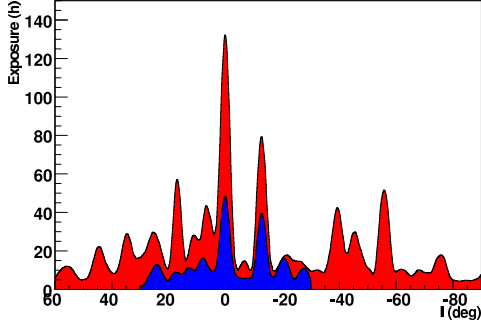


Figure 1: Acceptance corrected livetime (equivalent time spent at an offset of 0.5°) along the Galactic plane. All observations passing quality selection are considered, including survey-mode observations, re-observations of promising source candidates, and dedicated observations of known or expected VHE γ -ray sources. *Blue*: Observations taken in 2004/2005, published in [7]. *Red*: Present status of data taking near the Galactic plane.

found with significances above 4σ [7].

In the years 2005-2007, the survey region was extended further along the Galactic Plane. The scan region now covers $-85^\circ < l < 60^\circ$, $-3^\circ < b < 3^\circ$, containing the Carina-Sagittarius arm and part of the Perseus arm. In total, ~ 325 h of data were taken in survey mode within this region, together with 625 h of pointed observations, which include re-observations of source candidates and dedicated observations of known or assumed VHE γ -ray emitters. Figure 1 shows the present (red) and past (blue) exposure of the H.E.S.S. Galactic plane scan.

New sources of VHE γ -rays

In the continuation of the H.E.S.S. Galactic plane survey, >14 new VHE γ -ray sources were discovered so far at statistical significances larger than 5σ post-trials. The possible associations range from young pulsars such as PSR J1846-258 (Kes 75), over middle-aged pulsars (PSR J1913+1011) to a source first discovered at TeV energies by the Milagro collaboration (MGRO J1908+06). A non-negligible fraction of the sources, however, have no obvious counterparts.

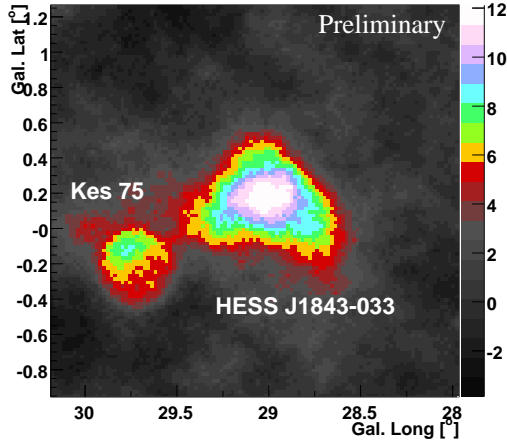


Figure 2: γ -ray significance map of the region containing Kes 75, obtained by counting γ -rays within 0.22° from a given location. The integration radius is part of the standard survey analysis, chosen a-priori and therefore not adjusted to the individual source sizes. Significance values shown do not take the statistical trials involved in the survey into account.

PSR J1846-0258 and Kes 75

The young shell-type supernova remnant (SNR) Kes 75 is in many ways similar to the well-studied Crab SNR. It contains the central pulsar PSR J1846-0258, which powers an extended radio and X-ray core, and is therefore another example of a centre-filled SNR, or plerion. Its distance is estimated as ~ 19 kpc [14]. PSR J1846-0258 has a rotation period of 325 ms and a spin-down age of 728 yrs [15], which apparently makes it the youngest rotation-powered pulsar yet discovered [10]. The extensions of the core and the shell are $30''$ and $3.5'$, respectively [14]. Like from the Crab nebula, a point-like source of VHE γ -ray emission is detected, coincident with the position of Kes 75, at a significance level of more than 8σ post-trials. For details concerning the H.E.S.S. detection of this object see [1]. In the same field of view, an extended source HESS J1843-303 was discovered with a statistical significance of more than 11σ post-trials. In contrast to Kes 75, no obvious counterpart for this source was found yet, but a detailed archival search is still ongoing.

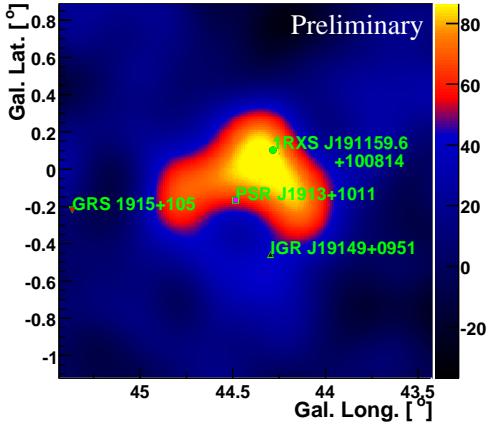


Figure 3: Image of the VHE γ -ray excess from HESS J1912+101, smoothed with a Gaussian profile of width 0.13° . The positions of the pulsar PSR J1913+1011, the ROSAT source 1RXS J191159.6+100814, the INTEGRAL source IGR J19149+0951 and the microquasar GRS 1915+105 are marked.

HESS J1912+101

Another possible example of VHE γ -ray emission from a PWN of a high spin-down luminosity pulsar is HESS J1912+101, located at $l = 44.4^\circ$ and $b = -0.1^\circ$, detected at a post-trials significance of more than 5σ . The corresponding pulsar, PSR J1913+1011, is rather old, with a spin-down age of $t_c = 1.7 \times 10^5$ yrs, and nearby, at a distance of ~ 4.5 kpc [15]. In contrast to PSR J1846–0258 mentioned earlier, no PWN was detected during a dedicated Chandra observation of the pulsar. The H.E.S.S. source is offset from the position of PSR J1913+1011, which can be explained by either the proper motion of the pulsar, or by an expansion of the PWN in an inhomogeneous medium [12]. The latter explanation seems plausible as clumpy molecular material was found close to the pulsar position in $^{13}\text{CO}(J=1\rightarrow 0)$ line measurements [11]. The scenario of an asymmetric PWN would make HESS J1912+101 similar to HESS J1825–137 [5].

MGRO J1908+06

The Milagro collaboration, operating a ground-based air shower detector near Los Alamos, announced the detection of several new candidate emitters of TeV γ -rays in the Galactic plane [3]. Compared to the H.E.S.S. array, Milagro has a higher energy threshold - the median energy of detected events is about 20 TeV - and a reduced angular resolution of about 1° . The Milagro coverage of the Galactic plane extends from about 30° longitude towards higher longitudes. Four sources are detected at sufficient significance, the Crab Nebula and the new sources MGRO 2019+37, MGRO 1908+06 and MGRO 2031+41. Of these, only MGRO 1908+06, with a flux of 80% of the Crab flux and a diameter of up to 2.6° , located at around 40° longitude is also contained within the H.E.S.S. Galactic plane survey. Confirming the Milagro result, a γ -ray source is detected with a significance of more than 5σ post-trials. The H.E.S.S. source is located at $l = 40.45^\circ$ and $b = -0.80^\circ$, consistent with the Milagro position of $l = 40.4^\circ$ and $b = -1.0^\circ$, with an error radius on the Milagro position of 0.24° . The rms size of the H.E.S.S. source is about 0.2° . For more details on the H.E.S.S. result see [2].

Unidentified sources

A significant fraction of the recently discovered sources of VHE γ -rays within the Galactic plane lack obvious counterparts. For seven of these sources extensive archival searches in multi-wavelength data and standard catalogues were performed to search for associated objects in the radio, X-ray and GeV γ -ray domains. While some of them are partially coincident with known or unidentified X-ray sources, none provide a clear counterpart which matches all of the observed characteristics of the VHE emission. The lack of a lower-energy counterpart challenges VHE emission scenarios, both leptonic and hadronic. More details are given in a separate contribution to this conference [13].

Summary

The H.E.S.S. Galactic plane survey, which started in the year 2004, now reaches from -85° longitude to 60° longitude, and covers an approximately 6° broad band around latitude $b = 0^\circ$. In total, more than 950 hours of data were taken in this region, including survey mode observations, re-observations of source candidates and dedicated observations of known or suspected γ -ray sources. The first stage of the survey, covering the inner 60° of the Galactic plane, has increased the number of known VHE γ -sources within this region from three at the beginning of 2004 to seventeen. Further follow-up observations within this region and the extension of the survey along the Galactic plane resulted in the discovery of even more additional VHE γ -ray emitters. Most of them were presented during this conference. Multi-wavelength follow-up observations and archival searches have already begun, and will be crucial for understanding the underlying processes at work in these astrophysical objects.

Acknowledgments

The support of the Namibian authorities and of the University of Namibia in facilitating the construction and operation of H.E.S.S. is gratefully acknowledged, as is the support by the German Ministry for Education and Research (BMBF), the Max Planck Society, the French Ministry for Research, the CNRS-IN2P3 and the Astroparticle Interdisciplinary Programme of the CNRS, the U.K. Science and Technology Facilities Council (STFC), the IPNP of the Charles University, the Polish Ministry of Science and Higher Education, the South African Department of Science and Technology and National Research Foundation, and by the University of Namibia. We appreciate the excellent work of the technical support staff in Berlin, Durham, Hamburg, Heidelberg, Palaiseau, Paris, Saclay, and in Namibia in the construction and operation of the equipment.

References

- [1] A. Djannati-Ataï et al. for the H.E.S.S. collaboration. *In 30th ICRC, Merida, Mexico*, 2007.
- [2] A. Djannati-Ataï et al. for the H.E.S.S. collaboration. *In 30th ICRC, Merida, Mexico*, 2007.
- [3] A. A. Abdo. *ApJL*, 664:L91–L94, 2007.
- [4] Aharonian F. A. et al. (H.E.S.S. collaboration). *Science*, 307:1938–1942, 2005.
- [5] Aharonian F. A. et al. (H.E.S.S. collaboration). *A&A*, 460:365–374, 2006.
- [6] Aharonian F. A. et al. (H.E.S.S. collaboration). *A&A*, 457:899–915, 2006.
- [7] Aharonian F. A. et al. (H.E.S.S. collaboration). *ApJ*, 636:777–797, 2006.
- [8] Aharonian F. A. et al. (H.E.S.S. collaboration). *A&A*, 464:235–243, 2007.
- [9] Aharonian F. A. et al. (H.E.S.S. collaboration). *A&A*, 467:1075–1080, 2007.
- [10] E. V. Gotthelf et al. *ApJL*, 542:L37–L40, 2000.
- [11] J. A. Jackson et al. *ApJ Supplement*, 163:145–159, 2006.
- [12] J. M. Blondin et al. *ApJ*, 563:806–815, 2001.
- [13] K. Kosack et al. for the H.E.S.S. collaboration. *In 30th ICRC, Merida, Mexico*, 2007.
- [14] R. H. Becker et al. *ApJ*, 283:154–157, 1984.
- [15] R. N. Manchester et al. *AJ*, 129:1993–2006, April 2005.



Establishing a connection between high-power pulsars and very-high-energy gamma-ray sources

S. CARRIGAN¹, J.A. HINTON^{1,2}, W. HOFMANN¹, K. KOSACK¹, T. LOHSE³ AND O. REIMER⁴ FOR THE H.E.S.S. COLLABORATION

¹Max-Planck-Institut für Kernphysik, P.O. Box 103980, D 69029 Heidelberg, Germany

²Landessternwarte, Universität Heidelberg, Königstuhl, D 69117 Heidelberg, Germany

³Institut für Physik, Humboldt-Universität zu Berlin, Newtonstr. 15, D 12489 Berlin, Germany

⁴Stanford University, HEPL & KIPAC, Stanford, CA 94305-4085, USA

svenja.carrigan@mpi-hd.mpg.de

Abstract: In the very-high-energy (VHE) gamma-ray wave band, pulsar wind nebulae (PWNe) represent to date the most populous class of Galactic sources. Nevertheless, the details of the energy conversion mechanisms in the vicinity of pulsars are not well understood, nor is it known which pulsars are able to drive PWNe and emit high-energy radiation. In this paper we present a systematic study of a connection between pulsars and VHE γ -ray sources based on a deep survey of the inner Galactic plane conducted with the High Energy Stereoscopic System (H.E.S.S.). We find clear evidence that pulsars with large spin-down energy flux are associated with VHE γ -ray sources. This implies that these pulsars emit on the order of 1% of their spin-down energy as TeV γ -rays.

In 1989, the Crab Nebula was discovered as the first celestial source of VHE γ -radiation [15]. The pulsar inside the nebula drives a powerful wind of highly relativistic particles that ends in a termination shock from which high-energy particles with a wide spectrum of energies emerge [8]. High-energy electrons¹ among these particles can give rise to two components of electromagnetic radiation: a low-energy component from synchrotron radiation and a high-energy component from inverse Compton (IC) up-scattering of ambient photons.

Recently, advances in VHE instrumentation have made the discovery of many new, predominantly Galactic, sources possible. Of these, a significant number can be identified as PWNe. Prominent examples are the PWN of the energetic pulsar PSR B1509–58 in the supernova remnant MSH 15–52 [2], and HESS J0835–455 [3], associated with Vela X, the nebula of the Vela pulsar. These γ -ray PWNe are extended objects with an angular size of a fraction of a degree, translating into a size of some 10 pc for typical distances of a few kpc. In addition to the open puzzle of pulsar

spin-down power conversion, a surprising observation is that the centroids of these γ -ray PWNe are often displaced from their pulsars by distances similar to the nebular size. Such displacements, although usually at smaller scales, are also seen in some X-ray PWNe. The origin of the displacement remains unknown. It might be attributed to pulsar motion (e.g. [14]), causing the pulsar to leave its nebula behind, or to a density gradient in the ambient medium [6].

The aforementioned examples of coincidences between VHE γ -ray sources and radio pulsars motivated a systematic search for VHE counterparts of energetic pulsars using the H.E.S.S. system of imaging Cherenkov telescopes located in Namibia [9]. To be detectable by H.E.S.S., a source at distance d has to provide a γ -ray luminosity in the 1 TeV to 10 TeV range of $L_\gamma \sim 10^{32} d^2 \text{ erg s}^{-1} \text{ kpc}^{-2}$. Assuming a conversion efficiency of 1% of pulsar spin-down energy loss \dot{E} into TeV γ -rays (where \dot{E} is determined from the measurement of the rotation period Ω and the rate

1. here and in the following, ‘electrons’ refers to both electrons and positrons

at which the rotation slows down $\dot{\Omega}$), PWNe of pulsars with \dot{E} around $10^{34} \text{ erg s}^{-1} \text{ kpc}^{-2}$ might be detectable. We note that for typical electron spectra, only a small fraction of the total energy in electrons is carried by the multi-TeV electrons, that are responsible for TeV γ -rays by IC scattering off ambient photons (including those from the cosmic microwave background) and for keV γ -rays by synchrotron radiation. Even a 1% energy output in TeV γ -rays already implies a large fraction of spin-down energy loss going into relativistic electrons.

Here we investigate how the probability to detect in VHE γ -rays PWNe surrounding known pulsars varies with the spin-down energy loss of the pulsar, testing the plausible assumption that the γ -ray output of a PWN correlates in some fashion with the power of the pulsar feeding it.

The VHE γ -ray data set used to search for γ -ray emission near the location of known radio pulsars comprises all data used in the H.E.S.S. Galactic plane survey [4, 5], including an extension of the survey to Galactic longitudes $-60^\circ < l < -30^\circ$, dedicated observations of Galactic targets and re-observations of H.E.S.S. survey sources. The search covers a range in Galactic longitude from -60° to 30° while the range in Galactic latitude is restricted to $\pm 2^\circ$, a region well covered in the survey. A total of 435 pulsar locations are tested, taken from the Parkes Multibeam Pulsar Survey (PMPS, [10] and references therein), as recorded in the ATNF pulsar catalogue. Pulsars without measured period derivatives are ignored. Over the range of the H.E.S.S. survey, the PMPS provides reasonably uniform sensitivity [16], enabling a reliable estimate of the frequency of chance coincidences between a γ -ray source and a pulsar. The analysis of the γ -ray data follows the standard H.E.S.S. analysis [4]. Initially, a sky map is generated providing the significance of a γ -ray excess for a given position. Taking into account the properties of known γ -ray PWNe, the search is optimised for slightly extended sources – on the scale of the angular resolution ($\approx 0.1^\circ$) of the H.E.S.S. telescopes – and allows for small offsets from the pulsar positions. Each excess is determined by counting γ -ray candidate events within $\theta \leq 0.22^\circ$ ($\theta^2 \leq 0.05^\circ^2$) of a given position and subtracting a background estimated from areas in the same field of view. The sky map is used to

look up the significance of a γ -ray excess at the position of the radio pulsars, as well as for randomly generated test positions used to evaluate the statistical significance of the association (details are given below). We require an excess significance of at least 5 standard deviations above the background as a signature of a VHE γ -ray signal. Given the modest number of trials – the 435 pulsar locations – the number of false detections is negligible with this requirement and in any case small compared to the probability for chance coincidences between radio pulsars and VHE γ -ray sources.

Of the 435 pulsars, 30 are found with significant γ -ray emission at the pulsar location (Fig. 1, top left panel). The lower left panel of Fig. 1 displays the fraction of pulsars with such γ -ray emission for different intervals in spin-down flux \dot{E}/d^2 . The fraction is about 5% for pulsars with spin-down flux below $10^{33} \text{ erg s}^{-1} \text{ kpc}^{-2}$ and increases to about 70% for pulsars with \dot{E}/d^2 above $10^{35} \text{ erg s}^{-1} \text{ kpc}^{-2}$. Not all of these associations are necessarily genuine. The rate of chance coincidences is estimated by generating 10^6 realisations of random pulsar samples (each consisting on average of 435 “pulsars”) following the distribution in longitude and latitude of the PMPS pulsars and taking into account the narrowing of the distribution in latitude with increasing spin-down flux. The expected fraction of chance coincidences is shown as dark shaded areas in Fig. 1 and varies between 4% to 12%. All associations with pulsars with $\dot{E}/d^2 < 10^{33} \text{ erg s}^{-1} \text{ kpc}^{-2}$ are within statistical errors consistent with chance coincidences. Indeed for plausible values of the ratio between the γ -ray luminosity and the pulsar spin-down energy loss, L_γ/\dot{E} , no detectable emission would be expected from such pulsars. On the other hand, the detection of emission from high-power pulsars is statistically significant. The probability that the detection of VHE sources coincident with 9 or more of the total of 23 pulsars above $\dot{E}/d^2 > 10^{34} \text{ erg s}^{-1} \text{ kpc}^{-2}$ results from a statistical fluctuation is $\sim 3.4 \times 10^{-4}$. For detection of 5 or more of the total of 7 pulsars above $10^{35} \text{ erg s}^{-1} \text{ kpc}^{-2}$, the chance probability is $\sim 4.2 \times 10^{-4}$.

Given the high density of pulsars, a single γ -ray source may even coincide with more than a single pulsar, and thus appear more than once amongst the “detections” in the upper left panel of Fig. 1.

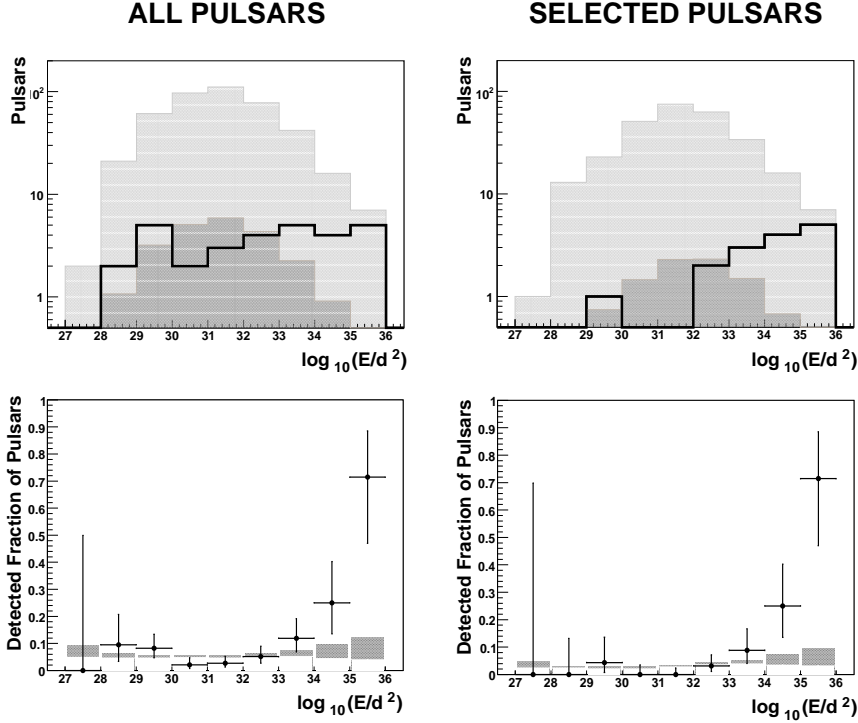


Figure 1: **Top row:** Distribution in $\log_{10}(\dot{E}/d^2)$ of all PMPS pulsars in the H.E.S.S. scan range (shaded in light grey), of chance coincidences (shaded in dark grey) and of detected pulsars (black line). Here, \dot{E}/d^2 is measured in $\text{erg s}^{-1} \text{kpc}^{-2}$. **Bottom row:** The points show the fraction of pulsars with significant γ -ray excess at the pulsar position, as a function of $\log_{10}(\dot{E}/d^2)$. The shaded band represents the probability for a chance coincidence. The width of the band accounts for the uncertainty in the width of the latitude distribution of pulsars. **Left:** all pulsars; **right:** double occurrences of gamma-ray sources removed by omitting pulsars which overlap with stronger pulsars or known non-pulsar sources.

Removal of such double occurrences (Right panels of Fig. 1) does not change the conclusion, and none of the high-luminosity pulsars is affected. Details will be given elsewhere.

The results shown in Fig. 1 demonstrate that a large fraction of high-luminosity pulsars correlate with sources of VHE γ -rays, emitting with a γ -ray luminosity of order 1% of the pulsar spin-down power. The positive correlation does not necessarily imply that the pulsar or PWN itself is responsible for the γ -ray flux. It could also result from some other mechanism correlated with the pulsar or its creation, such as a supernova shock wave. The correlation found between γ -ray detectability and spin-down flux \dot{E}/d^2 argues in favour of a pulsar-related origin of the γ -ray signal. On the other hand, for the PMPS pulsar sample, \dot{E}/d^2 also cor-

relates closely with the spin-down age T of the pulsar, $\dot{E}/d^2 \sim T^{-3/2}$, and obviously with distance d , both parameters relevant for determining the γ -ray flux from shock-wave driven supernova remnants.

The exact relation between pulsar parameters and γ -ray luminosity is an interesting issue. Variations in exposure and hence in detection threshold over the survey range, as well as the uncertainty in pulsar distance will smear out the turn-on curve of detectability versus \dot{E}/d^2 shown in Fig. 1, but cannot fully account for the rather slow turn-on over a range of more than one order of magnitude in \dot{E}/d^2 , combined with a detection probability below unity for even the highest-power pulsars. This indicates that \dot{E}/d^2 cannot be the only parameter relevant for the γ -ray flux. The same conclusion is obtained from the observed variation of L_γ/\dot{E}

of about an order of magnitude among the detected pulsars. However, this present pulsar sample is too small to investigate the dependence of L_γ on multiple pulsar parameters, e.g. including pulsar age.

A constant L_γ/\dot{E} is also not necessarily expected. For a given age, the integral energy fed by the pulsar into the PWN increases with \dot{E} . Apart from expansion losses, pulsar spin-down power is shared between particle energy and magnetic field energy. If equipartition between the two energy densities is assumed [13, 12], the magnetic field in the PWN will increase with \dot{E} and hence the energy loss by synchrotron radiation will increase relative to and at the expense of inverse Compton γ -ray production. Indeed, un-pulsed X-ray luminosity of pulsars is observed to increase faster than \dot{E} , $L_X \propto \dot{E}^{1.4 \pm 0.1}$ [7]. In such scenarios, magnetic field values and therefore the balance between X-ray and γ -ray emission will also depend on volume, i.e. on the expansion speed of the nebula and hence on the ambient medium. In addition, the current spin-down luminosity \dot{E} may not be the only relevant scale; if the pulsar age is shorter than or comparable to the electron cooling time, relic electrons injected in early epochs with higher spin-down power will still contribute and may enhance L_γ significantly compared to the quasi-steady state achieved for old pulsars.

Acknowledgements

The support of the Namibian authorities and of the University of Namibia in facilitating the construction and operation of H.E.S.S. is gratefully acknowledged, as is the support by the German Ministry for Education and Research (BMBF), the Max Planck Society, the French Ministry for Research, the CNRS-IN2P3 and the Astroparticle Interdisciplinary Programme of the CNRS, the U.K. Science and Technology Facilities Council (STFC), the IPNP of the Charles University, the Polish Ministry of Science and Higher Education, the South African Department of Science and Technology and National Research Foundation, and by the University of Namibia. We appreciate the excellent work of the technical support staff in Berlin, Durham, Hamburg, Heidelberg, Palaiseau, Paris, Saclay, and in Namibia in the construction and operation of the equipment.

References

- [1] F. Aharonian et al. A New Population of Very High Energy Gamma-Ray Sources in the Milky Way. *Science*, 307:1938–1942, March 2005.
- [2] F. Aharonian et al. Discovery of extended VHE gamma-ray emission from the asymmetric pulsar wind nebula in MSH 15-52 with HESS. *A&A*, 435:L17–L20, May 2005.
- [3] F. Aharonian et al. First detection of a VHE gamma-ray spectral maximum from a cosmic source: HESS discovery of the Vela X nebula. *A&A*, 448:L43–L47, March 2006.
- [4] F. Aharonian et al. Observations of the Crab nebula with HESS. *A&A*, 457:899–915, October 2006.
- [5] F. Aharonian et al. The H.E.S.S. Survey of the Inner Galaxy in Very High Energy Gamma Rays. *ApJ*, 636:777–797, January 2006.
- [6] J. M. Blondin, R. A. Chevalier, and D. M. Frieson. Pulsar Wind Nebulae in Evolved Supernova Remnants. *ApJ*, 563:806–815, December 2001.
- [7] K. S. Cheng, R. E. Taam, and W. Wang. Pulsar Wind Nebulae and the X-Ray Emission of Nonaccreting Neutron Stars. *ApJ*, 617:480–489, December 2004.
- [8] Bryan M. Gaensler and Patrick O. Slane. The evolution and structure of pulsar wind nebulae. *Annual Review of Astronomy and Astrophysics*, 44:17, 2006.
- [9] J. A. Hinton. The status of the HESS project. *New Astronomy Review*, 48:331–337, April 2004.
- [10] G. Hobbs et al. The Parkes multibeam pulsar survey - IV. Discovery of 180 pulsars and parameters for 281 previously known pulsars. *MNRAS*, 352:1439–1472, August 2004.
- [11] R. N. Manchester, G. B. Hobbs, A. Teoh, and M. Hobbs. The Australia Telescope National Facility Pulsar Catalogue. *AJ*, 129:1993–2006, April 2005.
- [12] M. J. Rees and J. E. Gunn. The origin of the magnetic field and relativistic particles in the Crab Nebula. *MNRAS*, 167:1–12, April 1974.
- [13] S. P. Reynolds and R. A. Chevalier. Evolution of pulsar-driven supernova remnants. *ApJ*, 278:630–648, March 1984.
- [14] E. van der Swaluw, T. P. Downes, and R. Keegan. An evolutionary model for pulsar-driven supernova remnants. A hydrodynamical model. *A&A*, 420:937–944, June 2004.
- [15] T. C. Weekes, M. F. Cawley, D. J. Fegan, K. G. Gibbs, A. M. Hillas, P. W. Kowk, R. C. Lamb, D. A. Lewis, D. Macomb, N. A. Porter, P. T. Reynolds, and G. Vacanti. Observation of TeV gamma rays from the Crab nebula using the atmospheric Cerenkov imaging technique. *ApJ*, 342:379–395, July 1989.



H.E.S.S. VHE Gamma-ray sources without identified counterparts

K. KOSACK¹, A. DJANNATI-ATAI², A. LEMIERE², E. MOULIN³, G. PÜHLHOFER⁴, E. DE OÑA WILHELMI² FOR THE H.E.S.S. COLLABORATION

¹Max-Planck-Institut für Kernphysik, P.O. Box 103980, D 69029 Heidelberg, Germany, ²APC, 11 Place Marcelin Berthelot, F-75231 Paris Cedex 05, France, ³Laboratoire de Physique Théorique et Astroparticules, IN2P3/CNRS, Université Montpellier II, CC 70, Place Eugène Bataillon, F-34095 Montpellier Cedex 5, France. ⁴Landessternwarte, Universität Heidelberg, Königstuhl, D 69117 Heidelberg, Germany
Karl.Kosack@mpi-hd.mpg.de

Abstract: Scan-based observations of the Galactic plane and continuing re-observations of known very-high-energy (VHE) gamma-ray sources with the H.E.S.S. system of imaging atmospheric Cherenkov telescopes have revealed a wide variety of new VHE objects. While in many cases these objects can be associated with known sources in the X-ray, radio, or optical wavebands, a subset of them currently have no obvious cataloged lower-energy counterpart. An analysis of 8 such unidentified sources is presented here.

Introduction

The current generation of Imaging Atmospheric Cherenkov Telescopes (IACTs) have provided an unprecedented level of sensitivity to the field of VHE ($E = 100$ GeV–100 TeV) astronomy. In particular, the H.E.S.S. instrument and the ongoing H.E.S.S. Galactic Plane Survey of the inner Galaxy [3], has increased the number of known VHE sources by nearly an order of magnitude. While many of the new VHE sources discovered in the survey can be associated through multi-wavelength data with previously identified objects (e.g. shell-type supernova remnants, pulsar-wind nebulae, or X-ray binaries), a growing population of VHE sources have yet to be identified. Since at least weak X-ray and radio emission is predicted by most common VHE emission models, the lack of lower-energy detections may provide substantial model constraints and may even point to a new class of objects which emit primarily in the VHE energy range.

The results presented here should be considered preliminary; further details (sky maps and spectra) and final results will be available shortly in a refereed article.

Technique

H.E.S.S. (the High Energy Stereoscopic System) is an array of four atmospheric Cherenkov telescopes located in the Khomas highland of Namibia at an altitude of 1800 m above sea-level. Each telescope consists of a 107m² optical reflector made up of segmented mirrors that focus light into a camera of 960 photo-multiplier tube pixels [10]. The telescopes image the UV/blue flashes of Cherenkov light emitted by the secondary particles produced in gamma-ray-induced air-showers. Stereoscopic shower observations using the *imaging atmospheric Cherenkov technique* (e.g. [13, 20, 9]) allow for accurate reconstruction of the direction and energy of the primary gamma rays as well as for the rejection of background events from air showers of cosmic ray origin. H.E.S.S. is sensitive to gamma rays above a post-cuts threshold energy of approximately 150 GeV and has an average energy resolution of $\sim 16\%$ [2].

The data discussed here were taken as part of the H.E.S.S. Galactic Plane Survey, which covers the band $-50^\circ < l < 60^\circ$ in galactic longitude and $-3^\circ < b < 3^\circ$ in latitude. Data are taken as a series of 28-minute “runs”, each centered on regular grid points along the survey region, or in case

of re-observed sources, in *wobble-mode*, where the runs are taken at alternating offsets from the source position (typically 0.7°). The data are analyzed using the standard H.E.S.S. analysis and calibration techniques described in [2]. The predefined *hard* gamma-ray selection cuts were applied to the data, which provide better gamma-hadron separation (and are thus better for source detection) at the expense of a higher analysis energy threshold. For source detection and morphology studies, the *ring-background* technique [6] was used for background subtraction with an on-source integration radius of 0.22° and an off-source annulus with typical radius 0.7° (standard for H.E.S.S. scan sources).

Source Selection

The VHE sources discussed here include all new sources discovered (with post-trials significances over 6σ) in the H.E.S.S. Galactic Plane Survey for which there is no obvious cataloged counterpart at lower wavelengths, according to the criteria cited below. Additionally, two sources meeting these criteria that were previously published in [3] are included due to a substantial increase in exposure time. A search for counterparts to the VHE emission was made by first looking in source catalogs for objects which are of a type known to produce VHE photons, including the ATNF pulsar catalog [16], the Green’s supernova remnant catalog [12], and the High-Mass X-ray binary (HMXB) catalog by [14]. We also checked the Low-Mass X-ray binary (LMXB) catalog by [15], the INTEGRAL source catalog [7], and the SIMBAD database. Additionally, publicly available images for lower-wavelength survey data in the radio and X-ray wavebands, from the Molonglo [11, 17], NRAO VLA [8], ROSAT [19], ASCA [18] Galactic plane surveys, were compared with the H.E.S.S. excess maps.

To reduce the possibility of chance coincidences, some minimal selection criteria were applied to the possible candidates. For pulsar wind nebulae, only pulsars with spin-down fluxes $\dot{E}/D^2 > 10^{33} \text{ erg sec}^{-1} \text{ kpc}^{-2}$ (e.g. ones which would require $< 100\%$ spin-down power to gamma ray conversion efficiency) were considered. For shell-type SNRs, only those that reasonably match the

Source	R.A.	Dec
HESS J1303-631 \ddagger	13 ^h 03 ^m 00 ^s	−63°11′55″
HESS J1614-518 \ddagger	16 ^h 14 ^m 19 ^s	−51°49′12″
HESS J1632-478	16 ^h 32 ^m 09 ^s	−47°49′12″
HESS J1634-472	16 ^h 34 ^m 58 ^s	−47°16′12″
HESS J1745-303	17 ^h 45 ^m 02 ^s	30°22′12″
HESS J1837-069	18 ^h 37 ^m 38 ^s	−6°57′00″
TeV J2032+4130 \ddagger	20 ^h 32 ^m 57 ^s	41°29′57″

Table 2: Previously published unidentified VHE sources, not discussed here. Coordinates are in J2000 epoch. Sources with \ddagger have no obvious lower-wavelength counterpart. For other sources, possible counterparts exist, which are however unidentified themselves or did not yet permit an identification of the VHE source. Results are from [5], [3], and [1].

morphology (size and position) of the VHE emission, and for XRBs (which have so far not been observed to produce extended emission), only those with small offsets from the VHE source were considered plausible candidates.

Results

The details of the six new and two updated unidentified H.E.S.S. VHE sources are presented in Table 1, while previously published unidentified VHE sources are listed in 2 for reference. The results of a simple two-dimensional Gaussian function convolved with the H.E.S.S. point-spread function to the uncorrelated excess event maps is given in Table 3. This gives a rough impression of the size of each object, however as the emission is in most cases not Gaussian.

Discussion

Though the general characteristics (size, location, flux) of the eight unidentified sources described here are similar to previously identified galactic VHE sources (e.g. PWNe), they have so far no clear counterpart in lower wavebands and further multi-wavelength study is required to understand the emission mechanisms powering them.

Source	R. A.	Dec	$l(^{\circ})$	$b(^{\circ})$	T (hrs)	$S(\sigma)$	Counts
HESS J1427–608	14 ^h 27 ^m 2 ^s	–60°51′00″	314.409	–0.145	21	7.3	197
HESS J1626–490	16 ^h 26 ^m 04 ^s	–49°05′13″	334.772	0.045	12	7.5	153
HESS J1702–420†	17 ^h 02 ^m 44 ^s	–42°00′57″	344.304	–0.184	9	12.8	412
HESS J1708–410†	17 ^h 08 ^m 24 ^s	–41°05′24″	345.683	–0.469	39	10.7	513
HESS J1731–347	17 ^h 31 ^m 55 ^s	–34°42′36″	353.565	–0.622	14	8.1	218
HESS J1841–055	18 ^h 40 ^m 55 ^s	–05°33′00″	26.795	–0.197	26	10.6	346
HESS J1857+026	18 ^h 57 ^m 11 ^s	02°40′00″	35.972	–0.056	21	8.7	223
HESS J1858+020	18 ^h 58 ^m 20 ^s	02°05′24″	35.578	–0.581	25	7.0	168

Table 1: Positions in equatorial (J2000 epoch) and Galactic (l, b) coordinates along with the detection significances of unidentified sources in the H.E.S.S. Galactic Plane scan discussed in this proceeding. S is the significance (number of standard deviations above the background level) of the source using a fixed integration radius of 0.22° , which was used for selecting the sources from the scan data. The position of each source is based on a model fit to the background-subtracted gamma-ray maps. The fit positions have an average statistical error of 0.05 degrees. Sources marked with a † are previously published in [3] and have been updated with new data. The exposure time is corrected for the off-axis sensitivity of the telescope system and accounts for instrumental readout dead-time.

Source	$\sigma_1(^{\circ})$	$\sigma_2(^{\circ})$	$\phi(^{\circ})$
HESS J1427–608	0.04 ± 0.02	0.08 ± 0.03	80 ± 17
HESS J1626–490	0.07 ± 0.02	0.10 ± 0.05	3 ± 40
HESS J1702–420	0.30 ± 0.02	0.15 ± 0.01	68 ± 7
HESS J1708–410	0.06 ± 0.01	0.08 ± 0.01	-20 ± 23
HESS J1731–347	0.18 ± 0.07	0.11 ± 0.03	-89 ± 21
HESS J1841–055	0.41 ± 0.04	0.25 ± 0.02	39 ± 6
HESS J1857+026	0.11 ± 0.08	0.08 ± 0.03	-3 ± 49
HESS J1858+020	0.08 ± 0.02	0.02 ± 0.04	4 ± 17

Table 3: Results from an elongated 2-D Gaussian model fit to the gamma-ray excess for each source. σ_1 and σ_2 are the intrinsic semi-major and semi-minor axes (in degrees on the sky), with the effect of the point-spread function removed. The errors are statistical. The position angle (ϕ) is measured counter-clockwise in degrees relative to the RA axis.

Therefore, follow-up observations with higher-sensitivity X-ray and GeV gamma-ray telescopes will be beneficial. Since most VHE sources are predicted to emit X-ray and radio emission, a non-detection of lower-wavelength emission with current-generation experiments for some of these objects may indicate a new VHE source class (as suggested in [4]), and may provide new insight into high-energy processes within our Galaxy.

Acknowledgements

The support of the Namibian authorities and of the University of Namibia in facilitating the construction and operation of H.E.S.S. is gratefully acknowledged, as is the support by the German Ministry for Education and Research (BMBF), the Max Planck Society, the French Ministry for Research, the CNRS-IN2P3 and the Astroparticle Interdisciplinary Programme of the CNRS, the U.K. Science and Technology Facilities Council (STFC), the IPNP of the Charles University, the Polish Ministry of Science and Higher Education, the South African Department of Science and Technology and National Research Foundation, and by the University of Namibia. We appreciate the excellent work of the technical support staff in Berlin, Durham, Hamburg, Heidelberg, Palaiseau, Paris, Saclay, and in Namibia in the construction and operation of the equipment.

This research has made use of the SIMBAD database, operated at CDS, Strasbourg, France and the ROSAT

Data Archive of the Max-Planck-Institut für extraterrestrische Physik (MPE) at Garching, Germany.

References

- [1] F. A. Aharonian et al. (HEGRA Collaboration). The unidentified TeV source (TeV J2032+4130) and surrounding field: Final HEGRA IACT-System results. *A&A*, 431:197–202, February 2005.
- [2] F. A. Aharonian et al. (HEGRA Collaboration). Observations of the Crab nebula with HESS. *A&A*, 457:899–915, October 2006.
- [3] F. A. Aharonian et al. (HEGRA Collaboration). The H.E.S.S. Survey of the Inner Galaxy in Very High Energy Gamma Rays. *ApJ*, 636:777–797, January 2006.
- [4] F. A. Aharonian et al. (H.E.S.S. Collaboration). A New Population of Very High Energy Gamma-Ray Sources in the Milky Way. *Science*, 307:1938–1942, March 2005.
- [5] F. A. Aharonian et al. (H.E.S.S. Collaboration). Serendipitous discovery of the unidentified extended TeV γ -ray source HESS J1303-631. *A&A*, 439:1013–1021, September 2005.
- [6] D. Berge, S. Funk, and J. Hinton. Background modelling in very-high-energy gamma-ray astronomy. *A&A*, 466:1219–1229, May 2007.
- [7] A. J. Bird, A. Malizia, A. Bazzano, E. J. Barlow, L. Bassani, A. B. Hill, G. Bélanger, F. Capitanio, D. J. Clark, A. J. Dean, M. Fiocchi, D. Götz, F. Lebrun, M. Molina, N. Produit, M. Renaud, V. Sguera, J. B. Stephen, R. Terrier, P. Ubertini, R. Walter, C. Winkler, and J. Zurita. The Third IBIS/ISGRI Soft Gamma-Ray Survey Catalog. *ApJS*, 170:175–186, May 2007.
- [8] J. J. Condon, W. D. Cotton, E. W. Greisen, Q. F. Yin, R. A. Perley, G. B. Taylor, and J. J. Broderick. The NRAO VLA Sky Survey. *AJ*, 115:1693–1716, May 1998.
- [9] A. Daum et al. First results on the performance of the HEGRA IACT array. *Astroparticle Physics*, 8:1–2, December 1997.
- [10] Bernlöhr et al. The optical system of the H.E.S.S. imaging atmospheric Cherenkov telescopes. Part I: layout and components of the system. *Astroparticle Physics*, 20:111–128, November 2003.
- [11] A. J. Green, L. E. Cram, M. I. Large, and T. Ye. The Molonglo Galactic Plane Survey. I. Overview and Images. *ApJS*, 122:207–219, May 1999.
- [12] D. A. Green. Galactic supernova remnants: an updated catalogue and some statistics. *Bulletin of the Astronomical Society of India*, 32:335–370, December 2004.
- [13] A. M. Hillas. Differences between Gamma-Ray and Hadronic Showers. *Space Science Reviews*, 75:17–30, January 1996.
- [14] Q. Z. Liu, J. van Paradijs, and E. P. J. van den Heuvel. Catalogue of high-mass X-ray binaries in the Galaxy (4th edition). *A&A*, 455:1165–1168, September 2006.
- [15] Q. Z. Liu, J. van Paradijs, and E. P. J. van den Heuvel. A catalogue of low-mass X-ray binaries in the Galaxy, LMC, and SMC (Fourth edition). *A&A*, 469:807–810, July 2007.
- [16] R. N. Manchester, G. B. Hobbs, A. Teoh, and M. Hobbs. The Australia Telescope National Facility Pulsar Catalogue. *AJ*, 129:1993–2006, April 2005.
- [17] T. Mauch, T. Murphy, H. J. Buttery, J. Curran, R. W. Hunstead, B. Piestrzynski, J. G. Robertson, and E. M. Sadler. SUMSS: a wide-field radio imaging survey of the southern sky - II. The source catalogue. *MNRAS*, 342:1117–1130, July 2003.
- [18] Y. Tanaka, H. Inoue, and S. S. Holt. The X-ray astronomy satellite ASCA. *PASJ*, 46:L37–L41, June 1994.
- [19] W. Voges, B. Aschenbach, T. Boller, H. Brauning, U. Briel, W. Burkert, K. Dennerl, J. Englhauser, R. Gruber, F. Haberl, G. Hartner, G. Hasinger, E. Pfeffermann, W. Pietsch, P. Predehl, J. Schmitt, J. Trümper, and U. Zimmermann. Rosat All-Sky Survey Faint Source Catalogue. *IAU Circ.*, 7432:3–+, May 2000.
- [20] T. C. Weekes. The Atmospheric Cherenkov Technique in Very High Energy Gamma-Ray Astronomy. *Space Science Reviews*, 75:1–15, January 1996.



HESS J1023–575: Non-thermal particle acceleration associated with the young stellar cluster Westerlund 2

O. REIMER¹, J. HINTON², W. HOFMANN³, S. HOPPE³, C. MASTERSON⁴, M. RAUE⁵,
FOR THE H.E.S.S. COLLABORATION⁶.

¹ *Stanford University, HEPL & KIPAC, Stanford, CA 94305-4085, USA*

² *School of Physics & Astronomy, University of Leeds, Leeds LS2 9JT, UK*

³ *Max-Planck-Institut für Kernphysik, P.O. Box 103980, 69029 Heidelberg, Germany*

⁴ *Dublin Institute for Advanced Studies, 5 Merrion Square, Dublin 2, Ireland*

⁵ *Universität Hamburg, Institut für Experimentalphysik, Luruper Chaussee 149, 22761 Hamburg, Germany*

⁶ http://www.mpi-hd.mpg.de/hfm/HESS/public/hn_hesscollab.html

olr@stanford.edu; martin.raue@desy.de

Abstract: The results from H.E.S.S. observations towards Westerlund 2 are presented. The detection of very-high-energy gamma-ray emission towards the young stellar cluster Westerlund 2 in the HII complex RCW49 by H.E.S.S. provides ample evidence that particle acceleration to extreme energies is associated with this region. A variety of possible emission scenarios is mentioned, ranging from high-energy gamma-ray production in the colliding wind zone of the massive Wolf-Rayet binary WR 20a, collective wind scenarios, diffusive shock acceleration at the boundaries of wind-blown bubbles in the stellar cluster, and outbreak phenomena from hot stellar winds into the interstellar medium. These scenarios are briefly compared to the characteristics of the associated new VHE gamma-ray source HESS J1023–575, and conclusions on the validity of the respective emission scenarios for high-energy gamma-ray production in the Westerlund 2 system are drawn.

The young stellar cluster Westerlund 2 in the HII region RCW 49

The prominent giant HII region RCW 49, and its ionizing young stellar cluster Westerlund 2, are located towards the outer edge of the Carina arm of our Milky Way. RCW 49 is a luminous, massive star formation region, and has been extensively studied at various wavelengths. Recent mid-infrared measurements with SPITZER revealed still ongoing massive star formation [5]. The regions surrounding Westerlund 2 appear evacuated by stellar winds and radiation, and dust is distributed in fine filaments, knots, pillars, bubbles, and bow shocks throughout the rest of the HII complex [6, 2]. Radio continuum observations revealed two wind-blown shells in the core of RCW 49 [1], surrounding the central region of Westerlund 2, and the prominent Wolf-Rayet star WR 20b. A long-standing distance ambiguity has

been recently [4] revised in a determination of the distance to Westerlund 2 by spectro-photometric measurements of 12 cluster member O-type stars of (8.3 ± 1.6) kpc. This value is in good agreement with the measurements from the light curve of the eclipsing binary WR 20a [7], associating WR 20a as a cluster member of Westerlund 2 (Note, however the 2.8 kpc as of [20]). The stellar cluster contains an extraordinary ensemble of hot and massive stars, presumably at least a dozen early-type O-stars, and two remarkable WR stars. Only recently WR20a was established to be a binary [3, 8] by presenting a solutions for a circular orbit with a period of 3.675, and 3.686 days, respectively. Based on the orbital period, the minimum masses have been found to be $(83 \pm 5) M_{\odot}$ and $(82 \pm 5) M_{\odot}$ for the binary components [7]. At that time, it classified the WR binary WR 20a as the most massive of all confidently measured binary systems in our Galaxy. The supersonic stellar winds of both WR stars collide, and a wind-wind interaction zone forms at the

stagnation point with a reverse and forward shock. In a detached binary system like WR 20a, the colliding wind zone lies between the two stars, and is heavily skewed by Coriolis forces. The winds of WR 20a can only be accelerated to a fraction of their expected wind speed $v_\infty \sim 2800$ km/s, and a comparatively low pre-shock wind velocity of ~ 500 km/s follows. Synchrotron emission has not yet been detected from the WR 20a system, presumably because of free-free-absorption in the optically thick stellar winds along the line of sight. WR 20a has been detected in X-rays [9], but non-thermal and thermal components of the X-ray emission remain currently indistinguishable. Detectable VHE gamma-radiation from the WR 20a binary system was only predicted in a pair cascade model [10], although detailed modeling of the WR 20a system in other scenarios (e.g. as of [19] when produced either by optically-thin inverse Compton scattering of relativistic electrons with the dense photospheric stellar radiation fields in the wind-wind collision zone or in neutral pion decays, with the mesons produced by inelastic interactions of relativistic nucleons with the wind material) is still pending. At VHE gamma-rays, photon-photon absorption will diminish the observable flux from a close binary system such as WR 20a [11].

H.E.S.S. observations of Westerlund 2

The H.E.S.S. (High Energy Stereoscopic System) collaboration observed the Westerlund 2 region between March and July 2006, and obtained 14 h (12.9 h live time) of data, either on the nominal source location of WR 20a or overlapping data from the ongoing Galactic plane survey. Standard quality selections were imposed on the data. The data have been obtained in wobble-mode observations to allow for simultaneous background estimation. The wobble offsets for these observations range from 0.5° to 2° , with the majority of data taken with wobble offset less than 0.8° . The zenith angles range between 36° and 53° , resulting in an energy threshold of 380 GeV for the analysis. The data have been analyzed using the H.E.S.S. standard Hillas analysis with standard cuts (> 80 p.e.). A point source analysis on the nominal position of WR 20a resulted in a clear signal with a significance of 6.8σ . Further investigations revealed

an extended excess with a peak significance exceeding 9σ (Fig.3 left). The center of the excess was derived by fitting the two-dimensional point spread function (PSF) of the instrument folded with a Gaussian to the uncorrelated excess map: $\alpha_{2000} = 10^h 23^m 18^s \pm 12^s$, $\delta_{2000} = -57^\circ 45' 50'' \pm 1' 30''$. The systematic error in the source location is $20''$ in both coordinates. The source is clearly extended beyond the nominal extension of the PSF (Fig. 1). A fit of a Gaussian folded with the PSF of the H.E.S.S. instruments gives an extension of $0.18^\circ \pm 0.02^\circ$.

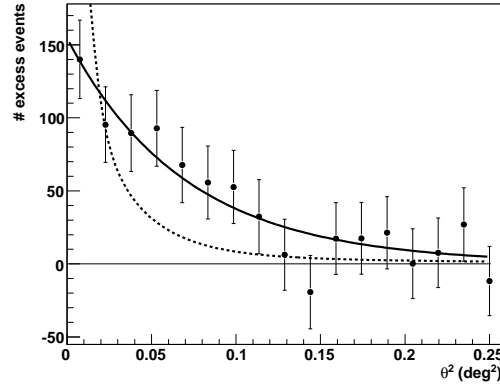


Figure 1: Number of excess events versus the squared angular distance from the best fit position of the excess. The dashed line shows the expectation for a point source derived from Monte Carlo data. The solid line is a fit of the PSF folded with a Gaussian ($\sigma = 0.18^\circ \pm 0.02^\circ$).

The differential energy spectrum for photons inside the corresponding 85% containment radius of 0.39° is shown in Fig. 2. It can be described by a power law ($dN/dE = \Phi_0 \cdot (E/1 \text{ TeV})^{-\Gamma}$) with a photon index of $\Gamma = 2.53 \pm 0.16_{\text{stat}} \pm 0.1_{\text{syst}}$ and a normalization at 1 TeV of $\Phi_0 = (4.50 \pm 0.56_{\text{stat}} \pm 0.90_{\text{syst}}) \times 10^{-12} \text{ TeV}^{-1} \text{ cm}^{-2} \text{ s}^{-1}$. The integral flux for the whole excess above the energy threshold of 380 GeV is $(1.3 \pm 0.3) \times 10^{-11} \text{ cm}^{-2} \text{ s}^{-1}$. No significant flux variability could be detected in the data set. The fit of a constant function to the lightcurve binned in data segments of 28 minutes has a chance probability of 0.14. The results were checked with independent analyses and found to be in good agreement.

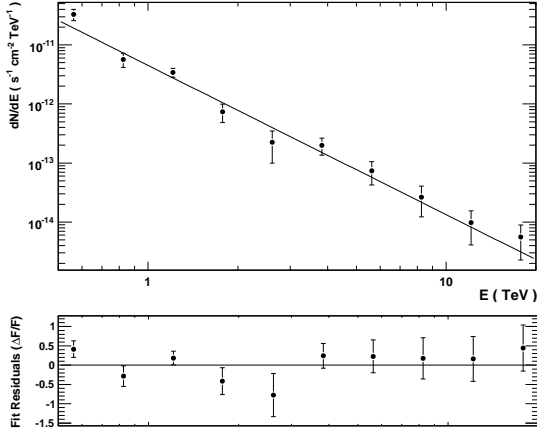


Figure 2: Differential energy spectrum and residuals to a single power-law fit of HESS J1023–575 from photons inside the 85% containment radius (0.39°) around the best fit position. The background is estimated with background regions of the same size and distance from the camera center as the signal region.

HESS J1023–575 in the context of γ -ray emission scenarios

The detection of VHE gamma-ray emission from the Westerlund 2 region [12] is proof for extreme high-energy particle acceleration associated with this young star forming region. With a projected angular size of submilliarcsecond scale, the WR 20a binary system, including its colliding wind zone, would appear as a point source for observations with the H.E.S.S. telescope array. Unless there are extreme differences in the spatial extent of the particle distributions producing radio, X-ray, and VHE gamma-ray emission, a *colliding stellar wind scenario* for the WR 20a binary faces the severe problem of accounting for the observed VHE source extension. At a nominal distance of 8.0 kpc, this source extension is equivalent to a diameter of 28 pc for the emission region, consistent in size with theoretical predictions of bubbles blown from massive stars into the ISM [13]. The spatial extension found for HESS J1023–575 contradicts emission scenarios where the bulk of the gamma-rays are produced close to the massive stars. Alternatively, the emis-

sion could arise from *collective effects of stellar winds* in the Westerlund 2 stellar cluster. Diffusive shock acceleration in cases where energetic particles experience multiple shocks can be considered for Westerlund 2. The stellar winds may provide a sufficiently dense target for high-energy particles, allowing the production of π^0 -decay γ -rays via inelastic pp-interactions. Collective wind scenarios [14, 15] suggest that the spatial extent of the gamma-ray emission corresponds to the volume filled by the hot, shocked stellar winds, but HESS J1023–575 substantially supersedes the boundary of Westerlund 2. Supershells, molecular clouds, and inhomogeneities embedded in the dense hot medium may serve as the targets for gamma-ray production in Cosmic Ray interactions. Such environments have been studied in the non-linear theory of particle acceleration by large-scale MHD turbulence [16]. *Shocks and MHD turbulent motion inside a stellar bubble or superbubble* can efficiently transfer energy to cosmic rays if the particle acceleration time inside the hot bubble is much shorter than the bubble’s expansion time.

Finally, shock acceleration at the boundaries of the “blister” (Fig. 3 right) may enable particles to diffusively re-enter into the dense medium, thereby interacting in hadronic collisions and producing gamma-rays. A scenario as outlined in [17] for a Supernova-driven expansion of particles into a low density medium may be applicable to the expanding stellar winds into the ambient medium. If one accepts such a scenario here, it might give the first observational support of gamma-ray emission due to diffusive shock acceleration from supersonic winds in a wind-blown bubble around WR 20a, or the ensemble of hot and massive OB stars from a superbubble in Westerlund 2, breaking out beyond the edge of a molecular cloud. Accordingly, one has to consider that such acceleration sites will also contribute to the observed flux of cosmic rays in our Galaxy [18].

Further observations with the H.E.S.S. telescope array will help to discriminate among the alternatives in the interpretation of HESS J1023–575. However, the convincing association with a new type of astronomical object a massive HII region and its ionizing young stellar cluster profoundly distinguishes this new detection by the H.E.S.S. telescope array already from other source findings

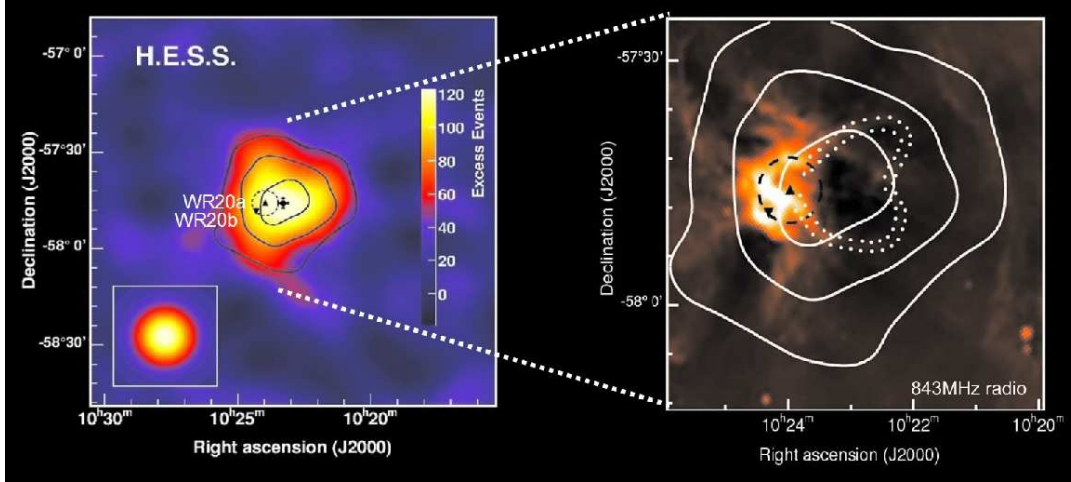


Figure 3: Left: H.E.S.S. γ -ray sky map of the Westerlund 2 region, smoothed to reduce the effect of statistical fluctuations. The inset in the lower left corner shows how a point-like source would have been seen by H.E.S.S. WR 20a and WR 20b are marked as filled triangles, and the stellar cluster Westerlund 2 is represented by a dashed circle. Right: Significance contours of the γ -ray source HESS J1023–575 (corresponding 5, 7 and 9 σ), overlaid on a MOST radio image. The wind-blown bubble around WR 20a, and the blister to the west of it can be seen as depressions in the radio continuum. The blister is indicated by white dots as in [1], and appears to be compatible in direction and location with HESS J1023–575.

made during earlier Galactic Plane Scan observations.

Acknowledgements

The support of the Namibian authorities and of the University of Namibia in facilitating the construction and operation of H.E.S.S. is gratefully acknowledged, as is the support by the German Ministry for Education and Research (BMBF), the Max Planck Society, the French Ministry for Research, the CNRS-IN2P3 and the Astroparticle Interdisciplinary Programme of the CNRS, the U.K. Science and Technology Facilities Council (STFC), the IPNP of the Charles University, the Polish Ministry of Science and Higher Education, the South African Department of Science and Technology and National Research Foundation, and by the University of Namibia. We appreciate the excellent work of the technical support staff in Berlin, Durham, Hamburg, Heidelberg, Palaiseau, Paris, Saclay, and in Namibia in the construction and operation of the equipment.

References

- [1] Whitney, B. A. et al. 2004, *ApJS* 154, 315
- [2] Churchwell, E., et al. 2004, *ApJS* 154, 322
- [3] Conti, P. S. & Crowther, P. A. 2004, *MNRAS* 255, 899
- [4] Whiteoak, J. B. Z., & Uchida, K. I. 1997, *A&A* 317, 563
- [5] Rauw, G. et al. 2007, *A&A* 463, 981
- [6] Rauw, G. et al. 2005, *A&A* 432, 985
- [7] Rauw, G. et al. 2004, *A&A* 420, L9
- [8] Bonanos, A. Z. et al. 2004, *ApJ* 611, L33
- [9] Belloni, T., & Mereghetti, S. 1994, *A&A* 286, 935
- [10] Bednarek, W. 2005, *MNRAS* 363, L46
- [11] Reimer, A., Pohl, M. K., & Reimer, O. 2006, *ApJ* 644, 1118
- [12] Dubus, G. 2006, *A&A* 451, 9
- [13] Aharonian, F. et al. (*H.E.S.S. Collaboration*) 2007, *A&A* 467, 1075
- [14] Castor, J., McCray, R., & Weaver, R. 1975, *ApJ* 200, L107
- [15] Klepach, E. G., Ptuskin, V. S., & Zirakashvili, V. N. 2000, *Aph* 13, 161
- [16] Domingo-Santamaria, E. & Torres, D. F. 2006, *A&A* 448, 613
- [17] Bykov, A. M. & Toptygin, I. N. 1987, *Ap&SS* Vol.138, No.2, 341
- [18] Völk, H. J. 1983, *Space Sci. Rev.* 36, 3
- [19] Cassé, M. & Paul, J. A. 1980, *ApJ*, 237, 236
- [20] Ascenso, J. et al. 2007, *A&A* 466, 137



HESS sources possibly associated with massive star clusters

A. MARCOWITH¹, N. KOMIN¹, Y.A. GALLANT¹, D. HORNS², G. PÜHLHOFER³, S. SCHWEMMER³, O. REIMER⁴ FOR THE H.E.S.S. COLLABORATION

¹*Laboratoire de Physique théorique et astroparticules, université Montpellier II, CNRS/IN2P3, Montpellier, France*

²*Landessternwarte Universität Heidelberg, Germany*

³*Institut für Theoretische Physik, Lehrstuhl IV: Weltraum und Astrophysik, Ruhr-Universität Bochum, Germany*

⁴*Stanford University, HEPL & KIPAC, CA 94305-4085, USA*

Alexandre.Marcowith@lpta.in2p3.fr

Abstract: In view of the discovery of HESS J1023-575 (discussed in a separate presentation), we examine another very high energy (VHE) gamma-ray source possibly associated with massive star clusters. Particle acceleration in massive star forming regions can proceed at the interface of two interacting winds or result from a collective process; e.g. multiple shock acceleration or MHD turbulence. The gamma-ray emission can also take place at the edge of the superbubble blown by the winds and multiple supernova explosions. Non-thermal radiation from the shell structure then traces the interaction of energetic particles (ions and/or electrons) with the surrounding interstellar matter. In particular, HESS J1837-069 is spatially coincident with a recently discovered very massive star cluster. We discuss the VHE gamma-ray data resulting from H.E.S.S. observations on this or other possible such associations. We consider data in other wavelength domains, in particular in X-rays, and examine the available evidence that the VHE emission could originate in particles accelerated by the above-mentioned mechanisms in massive star clusters.

Introduction

High energy radiative processes are strongly connected with very energetic events as only a fraction of the free energy of the source is necessary to be injected into a small amount of relativistic particles. The Galactic cosmic-rays (GCRs) are probably connected with the explosion of supernovæ (see [5]). A majority of the supernova (SN) progenitors are associated with massive stars (the so-called core collapse supernova) and a majority of massive stars are born, live and die in groups: in massive star clusters and/or OB associations (both hereafter together called massive star forming regions or MSFR); see [6], [2], [1]. The question of the production of energetic particles (EP), the non-thermal signatures and the contribution of MSFR to the GCR population then arises naturally. The acceleration and the propagation of EP in MSFR as well as their interaction with the ambient medium

have been widely debated in the literature ([4], [7], [3], [8], [6]). Observational probes of energetic events in MSFR have concentrated on the search of radiative signatures of supernova remnants in superbubbles (SB); e.g. the low density high temperature region blown up by the collective interaction of stellar winds and supernova explosions (see [9]). Usually a firm detection have been proven to be difficult unless the shock is currently interacting with a molecular cloud (as it is probably the case of IC443 discussed by [10] and recently by [11]), or with the shell produced by the multiple wind system. The termination shock or wind-wind interaction shocks in massive star systems have been explored as sites of non-thermal radiation ([12] and references therein). With its improved sensitivity (able to detect at 5σ level a source at 1% of the Crab in 25h), a large field of view (5°) and a good angular resolution (about 0.1°) the H.E.S.S. (High Energy Stereoscopic System) telescope has

the technical capacities to explore the faint and diffuse VHE gamma-ray emission that may be produced in MSFR. In this work, we examine different acceleration and radiation scenarios that should contribute to the high energy emission in MSFR (section). We discuss the possible association of the source HESS J1837-069 with a MSFR (section).

Particle acceleration and non-thermal radiation

Several acceleration processes and radiation mechanisms could give rise to the TeV γ -ray emission detected from HESS J1023-575 (Reimer et al, these proceedings and [13]), as well as in the source TeV J2032+4130 detected by HEGRA in the Cygnus OB2 SB [14]. We discuss briefly here the most relevant acceleration and gamma-ray radiative mechanisms.

Scenario 1: Massive star termination shock: Several authors have considered the possibility of accelerating EP at the terminal shock of massive stars ([15], [16]). The shock particle acceleration efficiency appears to be highly reduced by the magnetic field configuration; the toroidal component dominates at the termination shock radius R_t and is perpendicular to the shock normal. Unless a turbulent component randomizes the magnetic field orientation over a rotational period, the acceleration process is inoperant. Even in the case of a stronger stellar magnetic field, the maximum energy EP can reach would hardly be above the threshold for neutral pion production. The result is also relatively insensitive to the modelling of the wind modulation which uses mean free path estimates strictly valid for protons with energies \sim GeV in the solar wind. The re-acceleration of an ambient CR population has also been proven to be inefficient [16]. It appears that the modulation factor (the ratio of advective and diffusive lengths) in the downstream region is probably so large that the shock region is shielded from the outer medium. Flare particles accelerated in the star atmosphere cool adiabatically in the strongly diverging wind flow and do not contribute to the EP at the shock front. Several issues seem however interesting to be investigated. Firstly, only proton or ion acceleration and radiation have been considered. A leptonic scenario

(non-thermal bremsstrahlung or Inverse Compton) may contribute to a gamma-ray emission. Secondly, other turbulence regimes can lead to smaller and/or anisotropic mean free paths that are possibly more convenient for the particle transport.

Scenario 2: Wind-wind interaction in massive binary systems: As discussed above, non-thermal radio synchrotron emission from several massive star binaries supports the scenario of particle acceleration at the interface of two colliding winds. Eichler & Usov (1993) [17] demonstrated the possibility of an efficient particle acceleration at strong shocks created by the wind-wind collision. A more precise treatment of both acceleration and loss effects lead generally to a gamma-ray spectrum with a cut-off in the sub-TeV regime [18]. Good knowledge of the viewing angle and the system parameters are also necessary to evaluate the $\gamma - \gamma$ absorption properly. Alternatively, VHE radiation could be produced by the interaction of a SNR shock wave and a stellar wind [19]. The result is the production of two reflected shocks, one propagating inside the SNR, the second one inside the wind bubble and a converging flow which develops between the two shocks where particle acceleration can take place.

Scenario 3: Collective wind scenario: Gamma-rays produced by neutral pion decay can also result from collective interaction of winds, where the interaction region could serve both as accelerating region and target for the high energy hadrons, or just provide the target material alone. The former has been partly discussed above, the sources of radiation being in that case the termination shock of massive stars or the colliding winds. The second case requires an accelerator relatively close to the star cluster and has been considered by [20]. There are several issues to the gamma-ray observability of these sources. Firstly, the opacity from $\gamma - \gamma$ pair production in the stellar photon field should be low enough. Secondly, if the CR source is outside the star cluster where the interaction takes place, as discussed above, the wind modulation can prevent low energy particles to enter the wind regions. The threshold energy E_{lim} is very sensitive to the structure of the magnetic field, both to normalisation and energy dependence of the spatial diffusion coefficient and to the dominance of the parallel to the perpendicular diffusion coefficient. Depending on the strengths of these effects, E_{lim} can range from

GeV to TeV energies. The modulation is treated similarly to the modelling in [15].

Scenario 4: MHD turbulence and collective particle acceleration processes: The SB turbulent model ([3] and references therein) predicts a peak in the acceleration efficiency after a few times 10^5 years after the ignition of the turbulence (a network of MHD fluctuations and weak reflected shocks). The peak is reached at the maximum of turbulence conversion into non-thermal particles. The particles accelerated by the last or the aforementioned scenarii can interact with dense surrounding shells [4]. In that case gamma-rays are expected to be produced not only from neutral pion decay but also by non-thermal Bremsstrahlung in dense surroundings shells or in molecular clouds. An accurate spectral measurement at lower energies by AGILE and GLAST would offer better constraints to the emitting process.

A new possible association with a MSFR: HESS 1837-069

HESS 1837-069 is an extended source discovered during the galactic plane scan survey [21]. It shows a flux characterised by a power-law $I_0(E/TeV)^{-\Gamma}$ with $I_0 \simeq 5 \times 10^{-12} \text{ TeV}^{-1} \text{ cm}^{-2} \text{ s}^{-1}$ and $\Gamma = 2.27(\pm 0.06)$. The source has still no clear counterpart. At the edge (towards the north-east) of the peak flux, [22] reported on a cluster composed of 14 red super-giants (RSGs) using 2MASS data. The cluster is located at an estimated distance of 5.8 kpc with an age of ~ 10 Myrs. In X-rays, a bright source AX J1838.0-0655 (with a photon index of $\Gamma = 0.65$) was previously reported [23] located at the south-East of the star cluster and close to the peak of the HESS source. Our Chandra observations (see figure 1) reveal a large number of previously unknown X-ray sources. Although diffuse X-ray emission is often associated with MSFRs, we find no evidence for extended emission coincident with the RSG star cluster. AX J1837.8-0653 appears as a point source coincident with a radio source (GPSR5 25.252-0139) itself at the center of elongated radio emission [22]. Structure is resolved in the X-rays source AX J1838.10648 (coincident with the HII region W42) but this source appears too distant to power the H.E.S.S. source. Diffuse emission is apparent surrounding

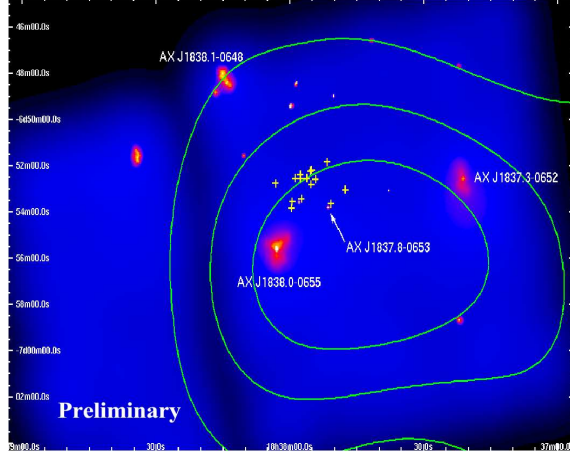


Figure 1: Adaptively smoothed Chandra map (0.3-7 keV band - ObsId 6719 - 20 ks exposure) background-subtracted and exposure corrected. H.E.S.S. excess contours are in green, RSG cluster stars as yellow crosses. Coordinates are J2000

the hard X-ray source AX J1838.0-0655 (also detected by INTEGRAL [24]).

Several possible scenarios can produce the gamma-ray radiation. The RSG stage is short compared to the main sequence phase (about one order of magnitude less). In this stage a massive star is known to have slow winds ($v_w \sim 10 - 15 \text{ km/s}$) and mass losses a few times $10^{-6} M_\odot/\text{yr}$. This aspect does not favor scenarios relying on the wind activity (scenarios 1 to 3 above). Another important issue is that SN have probably already exploded (contrary to Westerlund 2) in the RSG cluster as suggested by [22]. In the framework of an association between HESS J1837-069 and the RSG cluster, the scenarios of type 4 offer an interesting alternative. Further multiwavelength observations are necessary to confirm or reject them.

Perspectives and conclusions

The high energy gamma-ray H.E.S.S. observations (as well as well multi-wavelength survey) are of prime importance to directly probe the occurrence of efficient particle acceleration processes in MSFR in connection with the origin of galactic

cosmic rays. Unfortunately, these regions are complex and associated with diverse environments (extended ionised regions, multiple shell structures, molecular clouds), all in themselves potential sites of particle acceleration and non-thermal radiation. Several scenarios of particle acceleration and radiation mechanisms in MSFR have been examined. They differ by the extension of the cluster and the acceleration / radiation zone, the massive star content, the impact of SN explosion over the cluster or the amount of dense material in the environment. The production of TeV gamma-rays is not systematic and requires favorable conditions: efficient conversion of free energy into turbulence or supersonic flows, sufficiently weak radiation losses, optically thin media. We discuss in some details the source HESS J1837-069. This VHE source is still unidentified and close to an exceptional cluster of RSG stars in the Galactic ridge. Among the scenarios we considered, an extended source associated with dense shells or a molecular cloud seems to be possible but further multi-wavelength observations are necessary to support this conclusion.

Acknowledgements

The support of the Namibian authorities and the University of Namibia in facilitating the construction and the operation of H.E.S.S. is gratefully acknowledged, as is the support by the German Ministry for Education and Research (BMBF), the Max Planck Society, the French Ministry of Research, the CNRS-IN2P3 and the Astroparticle Interdisciplinary Programme of the CNRS, the U.K. Particle Physics and Astronomy Research Council (PPARC), the IPNP of the Charles University, the Polish Ministry of Science and Higher Education, the South African Department of Science and Technology and National Research Foundation, and by the University of Namibia. We appreciate the excellent work of the technical support staff in Berlin, Durham, Hamburg, Heidelberg, Palaiseau, Paris, Saclay, and in Namibia in the construction and operation of the equipment.

References

[1] Drury L. C. et al. *SSR*, 99:329–352, 2001.

- [2] Higdon J. C. and Lingenfelter R. E. *ApJ*, 628:738–749, 2005.
- [3] Higdon J. C., Lingenfelter R. E., and Ramaty R. *ApJ*, 509:L33–36, 1998.
- [4] Parizot E., Marcowith A., van der Swaluw E., Bykov A., and Tatischeff V. *A&A*, 424:747–760, 2004.
- [5] Bykov A. and Fleishmann G.D. *A&A*, 280:L27–L29, 1993.
- [6] Klepach E.G., Ptuskin V.S., and Zirakashvili V.N. *Astr.Phys.*, 13:161–172, 2000.
- [7] Bykov A. *SSR*, 99, 317–326, 2001.
- [8] Parizot E. and Drury L.C. *A&A*, 349, 673–684, 1999.
- [9] Chu Y.-H. and Kennicutt R.C. *Astr. & Sp.Sc.*, 216, 253–262, 1994.
- [10] Esposito J.A., Hunter S.D., Kanbach G., Sreekumar, P.Y.-H. *ApJ*, 421, 820–827, 1996.
- [11] Albert J. et al. (MAGIC collaboration) arXiv:0705.3119
- [12] Dougherty S. M. et al. *ApJ*, 623, 447–459, 2005.
- [13] Aharonian F.A. et al. (H.E.S.S. collaboration) *A&A*, 467, 1075–1080 2007.
- [14] Aharonian F.A. et al. (HEGRA. collaboration) *A&A*, 431, 197–202 2005.
- [15] Völk H.J. and Forman M.A. *ApJ*, 253, 188–198, 1982.
- [16] Webb G.M., Axford W.L., Forman M.A. *ApJ*, 298, 684–709, 1985.
- [17] Eichler D. and Usov V. *ApJ*, 402, 271–279, 1993.
- [18] Reimer A., Pohl M., Reimer O. *ApJ*, 644, 1118–1144, 2006.
- [19] Velázquez P.F., Koenigsberger G., Raga A.C. *ApJ*, 584, 284–292, 2003.
- [20] Domingo-Santamaría E. and Torres D.F. *A&A*, 444, 403–415, 2005.
- [21] Aharonian F.A. et al. *ApJ*, 636, 777–797, 2006.
- [22] Figer D.F. et al. *ApJ*, 643, 1166–1179., 2006.
- [23] Bamba A., Ueno M., Koyama K., Yamauchi S. *ApJ* 589, 253–260, 2003.
- [24] Malizia A. et al. *ApJ*, 630, L157-L160, 2005.



H.E.S.S. Galactic Plane Survey unveils a Milagro Hotspot

A. DJANNATI-ATAI¹, E. OÑA-WILHELMI¹, M. RENAUD² & S. HOPPE² FOR THE H.E.S.S. COLLABORATION³

¹*APC, 11 Place Marcelin Berthelot, F-75231 Paris Cedex 05, France*

²*Max-Planck-Institute für Kernphysik, P.O. Box 103980, D 69029 Heidelberg, Germany*

³ www.mpi-hd.mpg.de/HESS

djannati@apc.univ-paris7.fr; emma@apc.univ-paris7.fr

Abstract: We report here on a new VHE source, HESS J1908+063, discovered during the extended H.E.S.S. survey of the Galactic plane and which coincides with the recently reported MILAGRO unidentified source MGRO J1908+06. The position, extension and spectrum measurements of the HESS source are presented and compared to those of MGRO J1908+06. Possible counterparts at other wavelengths are discussed. For the first time one of the low-latitude MILAGRO sources is confirmed.

Introduction

H.E.S.S. observations of the inner Galactic plane in the $[270^\circ, 30^\circ]$ longitude range have revealed more than two dozens of new VHE sources, consisting of shell-type SNRs, pulsar wind nebulae, X-ray binary systems, a putative young star cluster, etc, and yet unidentified objects (see e.g. [3] and [10] in these proceedings for a summary).

The extended H.E.S.S. survey in the $[30^\circ\text{--}60^\circ]$ longitude range performed between 2005 and 2007 overlaps with regions covered by the MILAGRO sky survey at longitudes greater than 30° . The latter experiment has recently reported [1] three low-latitude sources including, MGRO J1908+06, detected after seven years of operation (2358 days of data) at 8.3σ (pre-trials) confidence level. MGRO J1908+06, of which the extension remains unknown but bounded to a maximum diameter of 2.6° , is located near the galactic longitude $\sim 40^\circ$ and hence is covered by the H.E.S.S. galactic plane survey.

A new H.E.S.S. source, HESS J1908+063, which coincides with MGRO J1908+06, is presented here. Its position, size and spectrum are measured and compared to the MILAGRO source. Possible counterparts at other wavelengths are discussed in the light of the H.E.S.S. measurements.

Observations, Analysis & Results

Results presented in this section should be considered as preliminary.

Observations around HESS J1908+063 were first performed during June 2005 and then from May to September 2006 as part of the extension of the Galactic plane survey in the range of galactic longitude and latitude of $30^\circ < l < 60^\circ$ and $-3^\circ < b < 3^\circ$, respectively. Followup observations were made during May and June 2007. In the available data-set the source is offset from the field of view center, at different angular distances with an average offset of 1.4° . Observations for which the source is offset by more than 2.5° were not considered for the analysis. The total dead-time corrected and quality selected data-set amounts to 14.9 hours with the zenith angle ranging from 30 to 46° and with a mean energy threshold of ~ 300 GeV.

After calibration, the standard H.E.S.S. event reconstruction scheme was applied to the data [4]. In order to reject the background of cosmic-ray showers, γ -ray like events were selected using cuts on image shape scaled with their expected values obtained from Monte Carlo simulations. As described in [5], two different sets of cuts, depending on the image size, were applied. Cuts optimized for a hard spectrum and a weak source with a rather

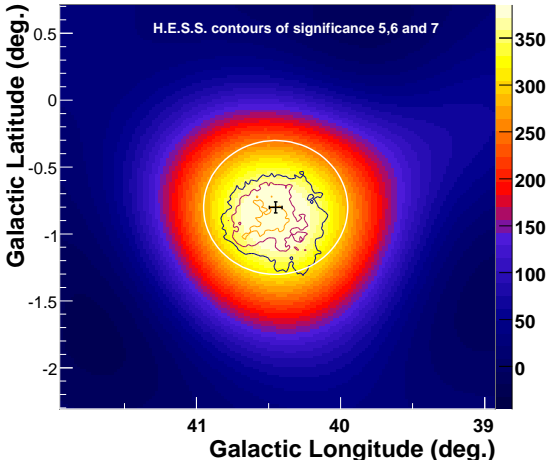


Figure 1: Smoothed excess map ($\sigma = 0.5^\circ$) of the $1.5^\circ \times 1.5^\circ$ field of view around the position of HESS J1908+063. The contours show the pre-trials significance levels for 5, 6 and 7σ , while the white circle shows the 0.5° integration radius used for the spectrum derivation.

tight cut on the image size of 200 p.e. (photoelectrons), which achieve a maximum signal-to-noise ratio, were applied to study the morphology of the source, while for the spectral analysis, the image size cut is loosened to 80 p.e. in order to cover the maximum energy range. The background estimation (described in [8]) for each position in the two-dimensional sky map is computed from a ring with an (apriori) increased radius of 1.0° , as compared to the standard radius of 0.5° , in order to deal with the large source diameter. This radius yields four times a larger area for the background estimation than the considered on-source region. Also events coming from known sources were excluded to avoid contamination of the background. For the spectrum analysis, the background is evaluated from positions in the field of view with the same radius and same offset from the pointing direction as the source region.

Fig. 1 shows the Gaussian-smoothed excess map for a size cut on the images above 200 p.e. The colored contours indicate the H.E.S.S. pre-trials significance contour levels for 5, 6 and 7σ . HESS J1908+063 was discovered first as a hot-spot

within the standard survey analysis scheme [3] and was subsequently confirmed at 7.7σ (pre-trials). A conservative estimate of the trials yields a post-trials significance of 5.7σ .

To evaluate the extension and the position of the source, the sky-map was fitted to a simple symmetrical two-dimensional Gaussian function, convolved with the instrument PSF (point spread function). The best-fit position lies at $l = 40.45^\circ \pm 0.06^\circ_{\text{stat}} \pm 0.06^\circ_{\text{sys}}$ and $b = -0.80^\circ \pm 0.05^\circ_{\text{sta}} \pm 0.06^\circ_{\text{sys}}$, while the intrinsic extension derived is $\sigma_{\text{src}} = (0.21^\circ + 0.07^\circ_{\text{sta}} - 0.05^\circ_{\text{sta}})$. As the shape of the source seems to depart from a symmetrical Gaussian, these values should be taken as first approximations.

The differential energy spectrum was computed within an integration radius of 0.5° (corresponding to the FWHM of the source size and shown as a white circle in Fig. 1) centred on the best-fit position by means of a forward-folding maximum likelihood fit [12]. The spectrum is well fitted with a simple power-law function (Fig. 2) with a hard photon index of $2.08 \pm 0.10_{\text{stat}} \pm 0.2_{\text{sys}}$ and a differential flux at 1 TeV of $(3.23 \pm 0.45_{\text{stat}} \pm$

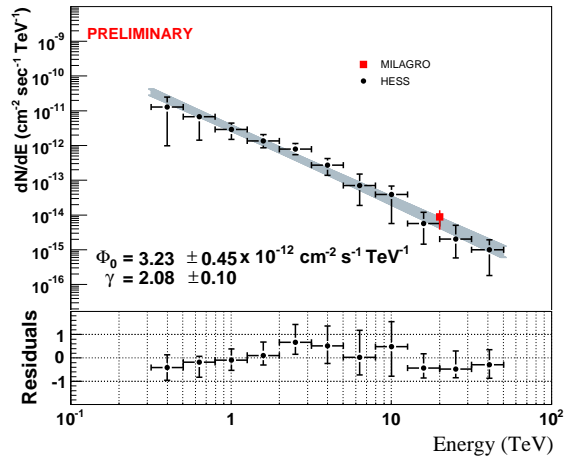


Figure 2: Differential energy spectrum measured above 300 GeV for HESS J1908+063. The shaded area shows the 1σ confidence region for the fit parameters. The differential flux of MGRO J1908+06 at 20 TeV is shown in red. Fit residuals are given in the bottom panel.

$0.65_{\text{sys}}) \times 10^{-12} \text{ cm}^{-2} \text{ s}^{-1}$. The integrated flux above 1 TeV corresponds to 14% of the Crab Nebula flux above that energy.

Comparison with MGRO1908+06 & Search for Counterparts

Fig. 3 shows the $1.5^\circ \times 1.5^\circ$ field of view around the position of HESS J1908+063 together with sources at other wavelengths including MGRO J1908+06. The latter source was discovered by the MILAGRO collaboration [1] after seven years of operation (2358 days of data) at the galactic longitude and latitude of $l = (40.4^\circ \pm 0.1^\circ_{\text{stat}} \pm 0.3^\circ_{\text{sys}})$ and $b = (-1.0^\circ \pm 0.1^\circ_{\text{stat}} \pm 0.3^\circ_{\text{sys}})$, respectively. The differential flux, at the median energy of 20 TeV, and assuming a spectral index of -2.3, is at a level of $(8.8 \pm 2.4_{\text{stat}} \pm 2.6_{\text{sys}}) \times 10^{-15} \text{ TeV}^{-1} \text{ cm}^{-1} \text{ s}^{-1}$. MGRO J1908+06 is reported to be both compatible with a point or extended source up to a diameter of 2.6° .

As clearly seen on Fig. 3, the positions of the two VHE sources are fully compatible within errors. There is also a quite good agreement between the differential flux at 20 TeV of MGRO J1908+06 and the spectrum measured by HESS as shown on Fig. 2. Given the larger integration radius of 1.3° for the MILAGRO source as compared to the 0.5° radius for HESS J1908+063, the flux agreement implies the absence of any other significant emission to the MILAGRO flux: the two sources can consequently be identified to each other.

The better determination of the position of HESS J1908+063 and the measurement of its size and spectrum allow to search for counterparts with stronger constraints.

At radio wavelengths, SNR G40.5-0.5 [7] at an estimated distance of 5.3 kpc overlaps with HESS J1908+063. At EGRET energies, 3EG J1903+0550, shown in green contours, lies close to the SNR and has been suggested as possibly associated with it [14]. However G40.5-0.5 is not in exact coincidence with HESS J1908+063 position and 3EG J1903+0550 is only marginally overlapping with the latter. HEGRA observations of this region of the sky [6] yielded an upper limit at 0.7 TeV at the SNR position of 4.8% of the Crab

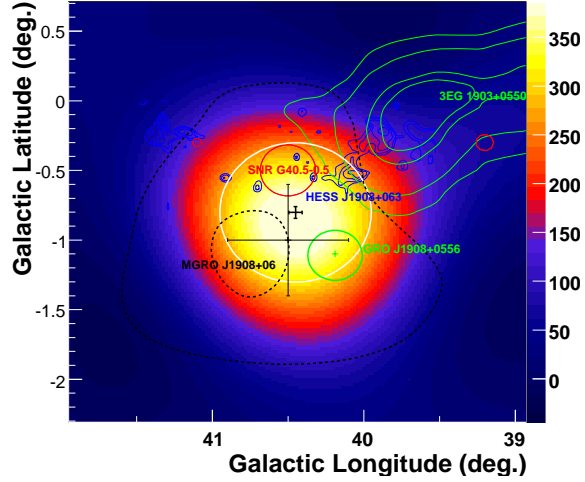


Figure 3: Multi-wavelength view of the $1.5^\circ \times 1.5^\circ$ field of view around the position of HESS J1908+063. The dotted black line shows the MILAGRO significance contours for 5 (inner) and 8σ (outer) contour. The position of the EGRET GeV source GRO J1908+0556 is marked with a green cross as well as the 1σ error in the position. The 3EG 1903+0550 contours corresponding to 99, 95, 68 and 50% confidence levels are shown in green. The red circle marks the size and position of the radio-bright SNR G40.5-00.5. Contours in blue show the ^{13}CO molecular cloud in the velocity range between (45,65) km/s.

Nebula flux. As this limit only applies for a point-like source it is not in contradiction with the measurements reported here.

If the SNR is associated with the VHE source, the fact that the 22 arc-min size of the shell is smaller than the FWHM of HESS J1908+063 would contrast to previously discovered HESS sources identified with shell-type VHE emitters, such as RX J1713.7-3946 [2] or RCW 86 reported at this conference [9]. The contribution of nearby unresolved sources or interactions of accelerated cosmic rays with molecular matter in the vicinity of the source could explain a larger size. However, for the latter case, the position of the nearby ^{12}CO cloud [15] or alternatively the ^{13}CO con-

tours (shown in blue on Fig. 3) do not favour this scenario.

An analysis of the highest energy photons (>1 GeV) observed by EGRET [13, 11] from this region shows a nearby and yet unidentified source, GRO J1908+0556/GEV J1907+0557. The positions of the two GeV derivations are compatible within errors. GRO J1908+0556, shown as a green circle on Fig. 3, lies within a distance of less than two times the EGRET 68% position measurement error to HESS J1908+063. A simple extrapolation of the H.E.S.S. spectrum to lower energies leads to a lower flux than that reported for the EGRET source ($6.33 \times 10^{-8} \text{ cm}^{-1}\text{s}^{-1}$). However given the large PSF of EGRET even at GeV energies, other unresolved sources can contribute to the flux measurement of GRO J1908+0556. The association of the HESS and MILAGRO sources to the GeV source is then likely, although a coincidence by chance is not excluded.

*

Summary In summary, a new source, HESS J1908+063 is reported above 300 GeV at the level of 14% of the Crab Nebula flux and a post-trials significance of 5.7σ . The H.E.S.S. source is extended, with a FWHM size of 0.5° , and shows a hard spectrum with an index of 2.08 ± 0.10 . This detection confirms for the first time one of the low-latitude sources reported by the MILAGRO collaboration, MGRO 1908+062. A connection to the EGRET GeV source GRO J1908+0556/GEV J1907+0557 at lower energies remains possible. The association with SNR G40.5-0.5 is not excluded but the larger size of the TeV emission should then find an explanation in terms of either contribution of unresolved sources or interactions of ultra-relativistic particles with molecular matter in the vicinity of the SNR. Deeper observations of this region with Cherenkov telescopes and GLAST data would help the interpretation of the detected VHE emission.

*

Acknowledgments The support of the Namibia authorities and of the University of Namibia in facil-

itating the construction and operation of H.E.S.S. is gratefully acknowledged, as is the support by the German Ministry for Education and Research (BMBF), the Max Planck Society, the French Ministry for Research, the CNRS-IN2P3 and the Astroparticle Interdisciplinary Programme of the CNRS, the U.K. Particle Physics and Astronomy Research Council (PPARC), the IPNP of the Charles University, the Polish Ministry of Science and Higher Education, the South African Department of Science and Technology and National Research Foundation, and by the University of Namibia. We appreciate the excellent work of the technical support staff in Berlin, Durham, Hamburg, Heidelberg, Palaiseau, Paris, Saclay, and in Namibia in the construction and operation of the equipment.

References

- [1] A.A. Abdo et al. *astro-ph/0611691*, 2006.
- [2] F.A. Aharonian et al. (H.E.S.S. Collaboration). *Nature*, 432:75–77, November 2004.
- [3] F.A. Aharonian et al. (H.E.S.S. Collaboration). *ApJ*, 636:777–797, January 2006.
- [4] F.A. Aharonian et al. (H.E.S.S. Collaboration). *A&A*, 457:899–915, 2006.
- [5] F.A. Aharonian et al. (H.E.S.S. Collaboration). *A&A*, 456:245–251, 2006.
- [6] F.A. Aharonian et al. (HEGRA Collaboration). *A&A*, 439:635, 2005.
- [7] D.A. Green et al. *A Catalogue of Galactic Supernova Remnants*, 2006.
- [8] J.A.. Hinton et al. In *Cherenkov 2005, Palaiseau*, 2005.
- [9] S. Hoppe & M. Lemoine-Goumard for the H.E.S.S. Collaboration. In *30th ICRC, Merida, Mexico*, 2007.
- [10] S. Hoppe for the H.E.S.S. Collaboration. In *30th ICRC, Merida, Mexico*, 2007.
- [11] R. C. Lamb and D. J. Macomb. *ApJ*, 488:872, 1997.
- [12] F. Piron et al. *A&A*, 374:895, 2001.
- [13] O.. Reimer et al. In *25th ICRC, Durban, South Africa*, page 97, 1997.
- [14] S. J. Sturmer and C. D. Dermer. *A&A*, 293:L17–L20, January 1995.
- [15] J. Yang et al. *A&A*, 6:210, 2006.



Search for very high energy gamma-ray emission from parts of the Gould belt with the H.E.S.S. ground based Cherenkov telescopes

D. HORNS¹, G.P. ROWELL², F. AHARONIAN^{3,4}, S. GABICI⁴, A. SANTANGELO¹, S. SCHWARZBURG¹
FOR THE H.E.S.S. COLLABORATION.

¹ *Institute for Astronomy and Astrophysics, University Tuebingen*

² *School of Chemistry and Physics, Adelaide, Australia*

³ *Dublin Institute for Advanced Science, Dublin, Ireland*

⁴ *Max-Planck Institute for nuclear physics, Heidelberg, Germany*

horns@astro.uni-tuebingen.de

Abstract: The Gould belt, a well-known region of enhanced star formation in the solar neighbourhood, is observed to be an expanding disk with a diameter of about 1 kpc and a width of a few 100 pc. Most of the nearby OB stellar associations and molecular clouds are found to be aligned with the Gould belt. With the high star formation rate along the Gould belt, the local supernova rate during the last few million years is believed to be three to four times larger than the Galactic average. Under the assumption that supernova remnants are efficient accelerators of cosmic rays, the Gould belt and its environment should show an increased cosmic ray density with respect to the Galactic average. The cosmic rays are expected to interact with the dense molecular gas which results mainly in pi-meson production with subsequent decay in gamma-rays and neutrinos. We have searched for gamma-ray emission from various parts of the Gould belt with the HESS Cherenkov telescopes. Results will be presented at the conference.

Introduction

The Gould belt is a local region with enhanced stellar formation and molecular clouds within 0.5 kpc of the solar system (for a review see [6]). A large fraction of young (spectral type O and B) massive stars in the solar vicinity are aligned with the Gould belt. However, late type stars have been associated to the Gould belt as well [4]. The age of the stars (≈ 50 Myrs) tracing the Gould belt and the dynamical timescale derived from the expansion velocity of the belt like structure (≈ 25 Myrs, [2, 5]) constrains the age of the Gould belt within roughly a factor of 2 to be 25–50 Myrs.

The nature of the event which triggered the star formation in the Gould belt is unclear, but various suggestions have been made including a cascade of supernova explosions or the impact of a high velocity cloud to the Galactic plane. An initial kinetic energy of 10^{52} ergs (equivalent to 10 supernova explosions) is required to drive the Gould belt expansion [5].

The supernova explosion rate of 75 to 95

$\text{Myr}^{-1} \text{ kpc}^{-2}$ implied by the age and stellar present population in the Gould belt is a factor of 3–5 larger than the expected local value of $20 \text{ Myr}^{-1} \text{ kpc}^{-2}$ [3]. The more massive molecular cloud complexes associated with the Gould belt (e.g. Taurus, ρ -Oph, Lupus, Orion A, Orion B) are therefore good targets to search for gamma-ray emission from the interaction of cosmic rays with the dense molecular clouds (see e.g. [1]).

Observations of regions in the Gould belt with the H.E.S.S. telescopes

The H.E.S.S. system of four imaging air Cherenkov telescopes is located at an altitude of 1 800 m in the Khomas Highlands of Namibia. The telescope system is sensitive to Gamma-rays above 100 GeV. Parts of the Gould belt have been observed during dedicated observation runs as well as part of observations taken on dedicated targets which coincide with the Gould belt region.

Results and Discussion

The final results of the analysis will be presented at the conference.

Darkness to Light: Origin and Evolution of Young Stellar Clusters, volume 243 of *Astrophysical Society of the Pacific Conference Series*, pages 667–+, 2001.

Acknowledgements

The support of the Namibian authorities and of the University of Namibia in facilitating the construction and operation of H.E.S.S. is gratefully acknowledged, as is the support by the German Ministry for Education and Research (BMBF), the Max Planck Society, the French Ministry for Research, the CNRS-IN2P3 and the Astroparticle Interdisciplinary Programme of the CNRS, the U.K. Science and Technology Facilities Council (STFC), the IPNP of the Charles University, the Polish Ministry of Science and Higher Education, the South African Department of Science and Technology and National Research Foundation, and by the University of Namibia. We appreciate the excellent work of the technical support staff in Berlin, Durham, Hamburg, Heidelberg, Palaiseau, Paris, Saclay, and in Namibia in the construction and operation of the equipment.

References

- [1] F. A. Aharonian. Very high and ultra-high-energy gamma-rays from giant molecular clouds. *Astrophysics & Space Science*, 180:305–320, June 1991.
- [2] F. Comerón. Vertical motion and expansion of the Gould belt. *A&A*, 351:506–518, November 1999.
- [3] I. A. Grenier. Gamma-ray sources as relics of recent supernovae in the nearby Gould belt. *A&A*, 364:L93–L96, December 2000.
- [4] P. Guillout, M. F. Sterzik, J. H. M. M. Schmitt, C. Motch, and R. Neuhauser. Discovery of a late-type stellar population associated with the Gould belt. *A&A*, 337:113–124, September 1998.
- [5] C. A. Perrot and I. A. Grenier. 3d dynamical evolution of the interstellar gas in the Gould belt. *A&A*, 404:519–531, June 2003.
- [6] W. G. L. Pöppel. The Gould belt system. In T. Montmerle and P. André, editors, *From*



Long-Term VHE Gamma-Ray Monitoring of PKS 2155–304 with H.E.S.S. and Multiwavelength measurements, 2002-2005

M. PUNCH¹, FOR THE H.E.S.S. COLLABORATION².

¹ *Astroparticule et Cosmologie (APC), UMR 7164 (CNRS, Université Paris VII, CEA, Observatoire de Paris), Paris, France* ² www.mpi-hd.mpg.de/HESS
punch@in2p3.fr

Abstract: The high-frequency peaked BL Lac PKS 2155–304, the lighthouse of the Southern hemisphere sky at VHE gamma-ray energies, has been followed by the H.E.S.S. array of atmospheric Cherenkov telescopes since the first light of the project, first with a single telescope in 2002, then with two & three telescopes in 2003, and since 2004 with the full-sensitivity four-telescope array. In this mode, a number of multi-wavelength campaigns have been performed with observations from the Rossi X-ray Timing Explorer (RXTE), Rotse (Optical), Spitzer (IR), James Clark Maxwell Telescope (JCMT, sub-mm) and others in both quiescent and active states, based on both fixed campaigns and triggers from H.E.S.S. Here we present the results of this series of observations up to 2005 inclusive, together with the implications for source models of the spectral measurements and search for correlated variability with X-rays, Optical, and IR measurements. The exceptional flare activity of 2006 is covered in a separate paper at this conference.

Introduction

The H.E.S.S. experiment (High Energy Stereoscopic System, [1]) has been in operation since 2002, though reaching full sensitivity in 2004 with the installation of the final element in the four-telescope array. During all this time, a prime target of H.E.S.S. has been the high-frequency peaked BL Lac PKS 2155–304, which is one of the brightest blazars in the Southern sky in the very-high-energy (VHE) γ -ray domain. These observations have been coupled with multi-wavelength campaigns, both planned and resulting from Target of Opportunity (ToO) triggers by H.E.S.S. in the case of exceptional activity of this source, working with such instruments as the Rossi X-ray Timing Explorer (RXTE), the Chandra X-ray satellite, the X-ray telescope (XRT) and UV-optical telescope (UVOT) on board the SWIFT satellite, Spitzer (IR), James Clark Maxwell Telescope (JCMT, sub-mm), the Rapid Optical Transient Search Explorer (ROTSE-III), and the Nançay Radio Telescope (NRT).

The source PKS 2155–304, at a red-shift of $z = 0.116$, is an X-ray selected object of the BL Lac

class, and has been the focus of studies in many wavelength ranges (see e.g. [2]) over the past 20 years. It was first seen at VHE energies by the Durham Mark 6 telescope [3], and this detection was confirmed by H.E.S.S. in the observations referred to here. The multi-wavelength observations of this source have shown broad-band variability on timescales from years to minutes, as also seen in the VHE range with H.E.S.S. This variability is presumed to be associated with a relativistic jet aligned close to the line of sight to the observer, allowing the processes in the jet to be probed by such studies.

Observations with H.E.S.S.

PKS 2155–304 has been observed by H.E.S.S. since its inception, first with a single telescope in 2002, then with two & three telescopes in 2003, and since 2004 with the full-sensitivity four-telescope array. Figure 2 shows a summary of the observations taken on this source, where in each case the average integral flux above 1 TeV is shown for each observation period, together with

the significance of the detection above the threshold of the instrument in the given configuration. All data here are analysed using the H.E.S.S. standard analysis procedures, for data passing run quality selection criteria, some previously reported in [4]. The data for 2005/2006 are still undergoing analysis, and these preliminary results are shown for comparison, including the excess number of γ -rays above threshold for both standard and loose cuts. The 2006 data are not detailed on a month-by-month basis here.

The most striking conclusions which can be drawn from this series of observations is that the source is clearly variable on year-by-year and month-by-month timescales, and that it is detected in all months where a hour or more observation time was taken. It can also be seen that the activity of the source was very high in 2002, though it was observed with a low-sensitivity single-telescope configuration; this activity was greater on average than that in 2006. However, as described in [6] at this conference & published in [7], the large data-set in 2006 contains nights with exceptional activity, in one of which ~ 3 minute time-variability is seen.

Multi-wavelength campaign in 2003

On October 18th 2003, the highly-significant detections of this source with H.E.S.S. (in its 3-telescope stereo configuration) prompted the triggering of an RXTE ToO proposal, with a number of quasi-simultaneous observations being taken in conjunction with RXTE/PCA, ROTSE, and NRT. From October 19th to November 26th, 2003, This campaign provided the first wide-band simultaneous spectrum on PKS 2155–304, although the source appeared to be in a low state during these observations. The Spectral Energy Distribution measured by the instruments in this campaign is shown in Figure 1. The average spectral index measured with H.E.S.S. was $3.37 \pm 0.07_{\text{stat}}$, similar to that measured at other epochs. The simultaneous data-points are fitted by several models. Due to the relatively distant red-shift of this source, the models must include absorption on the Extragalactic Background Light (EBL) in the μ metre range. Two leptonic models were fitted: single-zone Synchrotron Self-Compton (SSC) models in which the

Obs. Period [mth-year]	Live- time [hrs]	Avg flux @ 1 TeV \pm Error $10^{-11} \text{ cm}^{-2} \text{ s}^{-1} \text{ TeV}^{-1}$	Standard cuts Excess ($>$ thr.)	Signif. [σ]	System status	
07-02	~ 4	15.6 ± 2.1		13	Single dish, 1-telescope	
10-02	~ 10	6.4 ± 1.8		8		
06-03	~ 10	2.4 ± 0.3		21	Four stereo, 2-telescope	
07-03		1.8 ± 0.2		22		
08-03	~ 50	1.8 ± 0.2		28	Stereo, 2-telescope	
09-03		2.4 ± 0.3		15		
10:11-03		2.7 ± 0.2		34	Stereo, 3-telescope	
					Stereo, 4-telescope	
07:10-04	~ 96	2.2 ± 0.1		96	Loose cuts	
8-05	0.9	1.4 ± 0.3	84	9		158 5
9-05	1.7	1.4 ± 0.2	155	13		357 10
10-05	3.4	2.0 ± 0.2	314	19		809 15
11-05	0.4	~ 0	-5	-1		2 0
2005	6.5	1.6 ± 0.2	548	18		1326 18
2006	61.1	6.9 ± 0.1	32216	268		71729 264

Figure 2: Long-term monitoring of PKS 2155–304 with H.E.S.S., showing where available for each observation period, the observation time, average flux above 1 TeV in units of $10^{-12} \text{ cm}^{-2} \text{ s}^{-1} \text{ TeV}^{-1}$, γ -ray excess above threshold, and significance.

optical emission is either from the same population of electrons as the X-ray, or produced by an extra VLBI component, probably from the compact core, along with the radio. These models imply values of EBL in the low range for reasonable values of fitted magnetic field and Doppler factor. One hadronic model was tested, the Synchrotron Proton Blazar (SPB) model, which also could fit the data for a range of EBL values. Note that subsequent observations of more distant blazars with H.E.S.S., IES 1101–232 and H 2356–309, favour the low range of EBL values also [10].

In this campaign, no correlation was seen between the VHE γ -rays and the X-rays or the optical flux, or indeed between X-rays and optical. However, within the X-ray band a correlation was seen between the hardness ratio (defined as ratio of the flux from 4–11 keV to that from 1–4 keV) and the rate, with a correlation of $r = 0.76 \pm 0.12$ (see Figure 3), implying that the spectrum becomes harder as the source brightens in X-rays.

This campaign is reported in greater detail in [9].

Multi-wavelength campaign in 2004

In 2004, a planned monitoring programme on PKS 2155–304, proposed by H.E.S.S., was carried out from July 14th to September 11th. Ob-

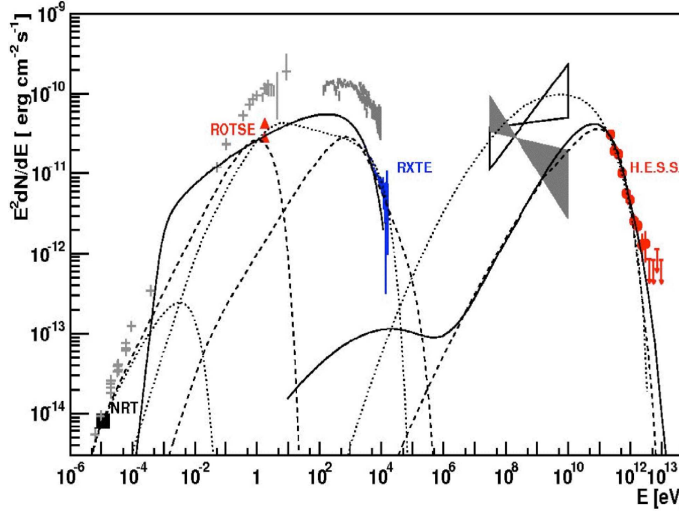


Figure 1: SED of PKS 2155–304 as measured in 2003. Only simultaneous data are labelled; non-contemporaneous data are shown in grey. The H.E.S.S. spectrum is from Oct. and Nov. 2003 data (filled circles) as is the RXTE spectrum. The NRT radio point (filled square) is the average value for the observation during this period. The two triangles are the highest and lowest ROTSE measurements for the Oct.-Nov. observations. Archival SAX data show the high state observed in 1997 [12]. Archival EGRET data are from the third EGRET catalogue (shaded bowtie) and from a very high γ -state reported in [11] (open bowtie). The solid line is the hadronic blazar model described in the text, while the dotted and dashed lines are the leptonic models

servations were performed simultaneously with RXTE/PCA, ROTSE, and NRT. The source in this case had become more active than in the previous year as seen by the X-ray data, and a preliminary analysis of the VHE data passing strict quality criteria show a strong positive correlation ($r = 0.71 \pm 0.05$) between the VHE γ -rays and the X-rays [5]. Compared to the previous campaign in 2003, then, it would appear that the correlation became apparent for the larger variability range seen in this years' data.

A number of nights of H.E.S.S. data from this campaign were affected by large-scale smokey haze; the correction of these data for loss of Cherenkov photons is covered in [8] at this conference. This should provide further data to be included for the VHE γ -ray / X-ray correlation.

Multi-wavelength campaign in 2006

The exceptional activity in 2006 previously referred to prompted the publication of an Astronomers Telegram by H.E.S.S., and the obser-

vation of the source with RXTE, CHANDRA, SWIFT, and optical telescopes. This campaign is still under analysis, but the much wider variability range shown (up to 15 Crab-level at peak) should provide ample testing-ground for multi-band correlations.

Conclusions

The observations of PKS 2155–304 with H.E.S.S. since the inception of the telescope has provided a relatively long baseline over which the activity of this brightest blazar in the Southern sky can be evaluated, and giving an estimate of its duty-cycle. In VHE γ -rays alone, the activity is seen to vary over orders of magnitude, on time-scales of years, months, days, down to minutes, and very high activity was seen both in the first year of observation, 2002, and last year, in 2006.

Several multi-wavelength campaigns have been carried out, either planned or as target of opportunity. In these campaigns, it has been seen that the X-ray spectrum became harder as the source

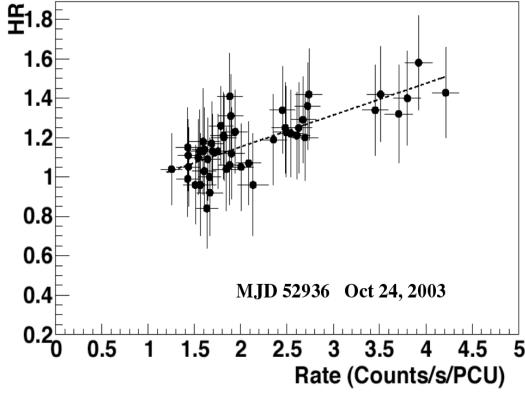


Figure 3: Correlation within the RXTE measurements taken during the H.E.S.S. multi-wavelength campaign in 2003, where a clear correlation is seen with between the X-ray activity and the hardness ratio as defined in the text, with a correlation factor $r = 0.76 \pm 0.12$.

increased in brightness (2003 campaign), and that inter-band (VHE γ -ray / X-ray) correlations became apparent only with a larger variability range (2004 campaign). From the 2003 campaign, a multi-waveband SED has been produced which can be fitted by either leptonic or hadronic models, in the former case favouring a low range of Extragalactic Background Light. The 2006 multi-wavelength campaign triggered by H.E.S.S. due to spectacular activity of the source is still under analysis but should yield further insights into the processes at work in this category of source.

This source, given its highly active and variable states and soft spectrum, should be a prime candidate for future GLAST/H.E.S.S. multi-wavelength campaigns.

Acknowledgements

The support of the Namibian authorities and of the University of Namibia in facilitating the construction and operation of HESS is gratefully acknowledged, as is the support by the German Ministry for Education and Research (BMBF), the Max Planck Society, the French Ministry for Research, the CNRS-IN2P3 and the Astroparticle Interdisciplinary Programme of the CNRS, the U.K. Science and Technology Facilities Council (STFC), the IPNP of the Charles University, the Polish Ministry of Science and Higher Education, the South African Department of Science and Technology and Na-

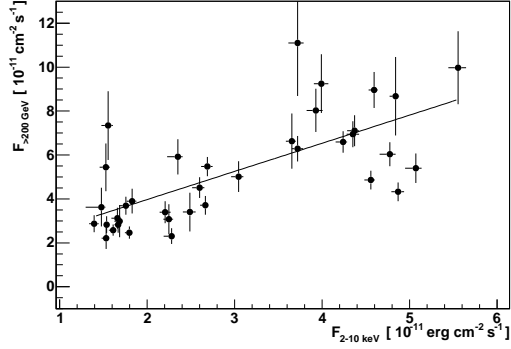


Figure 4: Correlation between H.E.S.S. and RXTE for coincident measurements, in quality selected runs during the X-ray flares of Aug. 2004 (44 data segments within 2 weeks); a close correlation is seen with a correlation factor $r = 0.71 \pm 0.05$.

tional Research Foundation, and by the University of Namibia. We appreciate the excellent work of the technical support staff in Berlin, Durham, Hamburg, Heidelberg, Palaiseau, Paris, Saclay, and in Namibia in the construction and operation of the equipment.

References

- [1] Hinton, J. *et al.* (H.E.S.S. coll.), 2004, *New Astron. Rev.* **48**, 331
- [2] Urry, C.M. *et al.*, 2004, *ApJ* **411**, 614
- [3] Chadwick, P.M. *et al.*, *ApJ* 1999, **513**, 161
- [4] Fontaine, G. *et al.* (H.E.S.S. coll.), *Proc 29th ICRC*, Pune, 2005, **4**, 279
- [5] Giebels, B. *et al.* (H.E.S.S. coll.), *Proc. SF2A-2005: Semaine de l'Astrophysique Française*, 2005, 527
- [6] Benbow, W. *et al.* (H.E.S.S. coll.), *These proceedings*, 2007
- [7] Aharonian, F. *et al.* (H.E.S.S. coll.), *ApJ*, **664**, L71, 2007
- [8] Nolan, S. *et al.* (H.E.S.S. coll.), *These proceedings*, 2007
- [9] Aharonian, F. *et al.* (H.E.S.S. coll.), *A&A*, 2005, **455**, 895
- [10] Aharonian, F. *et al.* (H.E.S.S. coll.), *Nature*, 2006, **440**, 1018
- [11] Vestrand, W.T. *et al.*, *ApJ*, 1995, **454**, L93
- [12] Chiappetti, L. *et al.*, *ApJ*, 1999, **521**, 552



A Spectacular VHE Gamma-Ray Outburst from PKS 2155-304 in 2006

W. BENBOW¹, C. BOISSON², L. COSTAMANTE¹, O. DE JAGER³, G. DUBUS⁴,
D. EMMANOULOPOULOS⁵, B. GIEBELS⁶, S. PITA⁷, M. PUNCH⁷, C. RAUBENHEIMER³, M. RAUE⁸,
H. SOL², AND S. WAGNER⁵ FOR THE HESS COLLABORATION

¹ Max-Planck-Institut für Kernphysik, Heidelberg, Germany; ² LUTH, UMR 8102 du CNRS, Observatoire de Paris, Section de Meudon, France; ³ Unit for Space Physics, North-West University, Potchefstroom, South Africa; ⁴ Laboratoire d'Astrophysique de Grenoble, INSU/CNRS, Université Joseph Fourier, France; ⁵ Landessternwarte, Heidelberg, Germany; ⁶ LLR, CNRS/IN2P3, Ecole Polytechnique, Palaiseau, France; ⁷ Astrophysique et Cosmologie (APC), Paris, France; ⁸ Universität Hamburg, Institut fuer Experimentalphysik, Germany

Wystan.Benbow@mpi-hd.mpg.de

Abstract:

Since 2002 the VHE (>100 GeV) γ -ray flux of the high-frequency peaked BL Lac PKS 2155–304 has been monitored with the High Energy Stereoscopic System (HESS). An extreme γ -ray outburst was detected in the early hours of July 28, 2006 (MJD 53944). The average flux above 200 GeV observed during this outburst is ~ 7 times the flux observed from the Crab Nebula above the same threshold. Peak fluxes are measured with one-minute time scale resolution at more than twice this average value. Variability is seen up to ~ 600 s in the Fourier power spectrum, and well-resolved bursts varying on time scales of ~ 200 seconds are observed. There are no strong indications for spectral variability within the data. Assuming the emission region has a size comparable to the Schwarzschild radius of a $\sim 10^9 M_\odot$ black hole, Doppler factors greater than 100 are required to accommodate the observed variability time scales.

Introduction

In the Southern Hemisphere, PKS 2155–304 (redshift $z = 0.116$) is generally the brightest blazar at VHE energies, and is probably the best-studied at all wavelengths. The VHE flux observed [1] from PKS 2155–304 is typically of the order $\sim 15\%$ of the Crab Nebula flux above 200 GeV. The highest flux previously measured in one night is approximately four times this value and clear VHE-flux variability has been observed on daily time scales. The most rapid flux variability measured for this source is 25 min [2], occurring at X-ray energies. The fastest variation published from any blazar, at any wavelength, is an event lasting ~ 800 s where the X-ray flux from Mkn 501 varied by 30% [16]¹, while at VHE energies doubling time scales as fast as ~ 15 minutes have been observed from Mkn 421 [9].

As part of the normal HESS observation program the flux from known VHE AGN is monitored regularly to search for bright flares. During the July 2006 dark period, the average VHE flux observed by HESS from PKS 2155–304 was more than ten times its typical value. In particular, an extremely bright flare of PKS 2155–304 was observed in the early hours of July 28, 2006 (MJD 53944). This contribution focuses solely on this particular flare, which is described in more detail in [4].

Results from MJD 53944

A total of three observation runs (~ 28 min each) were taken on PKS 2155–304 in the early hours of MJD 53944. These data entirely pass the stan-

1. Xue & Cui [16] also demonstrate that a 60% X-ray flux increase in ~ 200 s observed [8] from Mkn 501 is likely an artifact.

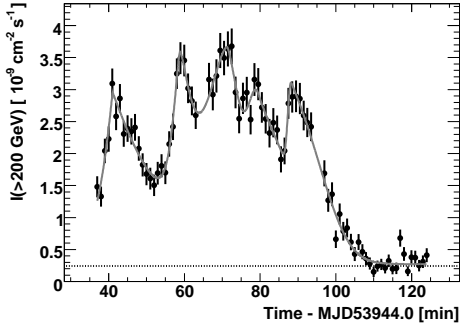


Figure 1: $I(>200 \text{ GeV})$ observed from PKS 2155–304 binned in 1-minute intervals. The horizontal line represents $I(>200 \text{ GeV})$ observed [3] from the Crab Nebula. The curve is the fit to these data of the superposition of five bursts (see text) and a constant flux.

standard HESS data-quality selection criteria, yielding an exposure of 1.32 h live time at a mean zenith angle of 13° . The analysis method is described in [4]. The observed excess is 11771 events (168σ), corresponding to a rate of $\sim 2.5 \text{ Hz}$. This is the first time the detected VHE γ -ray rate has exceeded 1 Hz.

Flux Variability

The average integral flux above 200 GeV observed from PKS 2155–304 is $I(>200 \text{ GeV}) = (1.72 \pm 0.05_{\text{stat}} \pm 0.34_{\text{syst}}) \times 10^{-9} \text{ cm}^{-2} \text{ s}^{-1}$, equivalent to ~ 7 times the $I(>200 \text{ GeV})$ observed from the Crab Nebula (I_{Crab} , [3]). Figure 1 shows $I(>200 \text{ GeV})$, binned in one-minute intervals, versus time. The fluxes in this light curve range from $0.65 I_{\text{Crab}}$ to $15.1 I_{\text{Crab}}$, and their fractional root mean square (rms) variability amplitude [15] is $F_{\text{var}} = 0.58 \pm 0.03$. This is ~ 2 times higher than archival X-ray variability [18, 19]. The Fourier power spectrum calculated from Figure 1 is shown in Figure 2. There is power significantly above the measurement noise level up to $1.6 \times 10^{-3} \text{ Hz}$ (600 s). The power spectrum derived from the data is compatible with a light curve generated by a stochastic process with a power-law Fourier spectrum of index -2. An index of -1 produces too much power at high frequencies and is rejected.

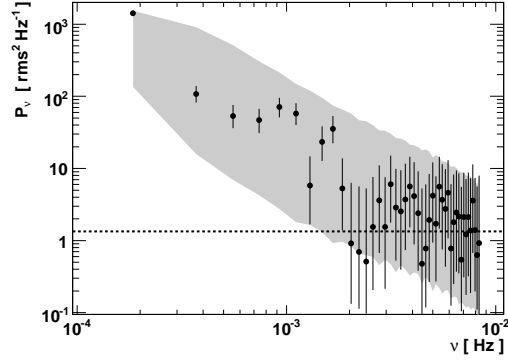


Figure 2: The Fourier power spectrum of the light curve and associated measurement error. The grey shaded area corresponds to the 90% confidence interval for a light curve with a power-law Fourier spectrum $P_\nu \propto \nu^{-2}$. The horizontal line is the average noise level.

These power spectra are remarkably similar to those derived in X-rays [18] from the same source.

Figure 1 clearly contains substructures with even shorter rise and decay time scales than found in the Fourier analysis. Therefore, the light curve is considered as consisting of a series of bursts, which is common for AGN and γ -ray bursts (GRBs). To characterize these bursts, the “generalized Gaussian” shape from Norris et al. [13] is used, where the burst intensity is described by: $I(t) = A \exp[-(|t - t_{\text{max}}|/\sigma_{r,d})^\kappa]$, where t_{max} is the time of the burst’s maximum intensity (A); σ_r and σ_d are the rise ($t < t_{\text{max}}$) and decay ($t > t_{\text{max}}$) time constants, respectively; and κ is a measure of the burst’s sharpness. The rise and decay times, from half to maximum amplitude, are $\tau_{r,d} = [\ln 2]^{1/\kappa} \sigma_{r,d}$. Five significant bursts were found with a peak finding tool based on a Markov chain algorithm [12]. The data are well fit² by a function consisting of a superposition of an identical number of bursts plus a constant signal. The best fit has a χ^2 probability of 20% and the fit parameters are shown in Table 1. Interestingly, there is a marginal trend for κ to increase with subsequent bursts, making them less sharp, as the flare progresses, which could imply the bursts are not stochastic. The κ values are close to the bulk of

2. All parameters are left free in the fit.

Table 1: The results of the best χ^2 fit of the superposition of five bursts and a constant to the data shown in Figure 1.

t_{\max} [min]	τ_r [s]	τ_d [s]	κ
41.0	173 ± 28	610 ± 129	1.07 ± 0.20
58.8	116 ± 53	178 ± 146	1.43 ± 0.83
71.3	404 ± 219	269 ± 158	1.59 ± 0.42
79.5	178 ± 55	657 ± 268	2.01 ± 0.87
88.3	67 ± 44	620 ± 75	2.44 ± 0.41

those found by Norris et al. [13], but the time scales measured here are two orders of magnitude larger. During both the first two bursts there is clear doubling of the flux within τ_r . Such doubling is sometimes used as a characteristic time scale of flux variability. For compatibility with such estimators, the definition of doubling time, $T_2 = |I_{ij}\Delta T/\Delta I|$, from [18] is also used³. Here, $\Delta T = T_j - T_i$, $\Delta I = I_j - I_i$, $I_{ij} = (I_j + I_i)/2$, with T and I being the time and flux, respectively, of any pair of points in the light curve. The fastest $T_2 = 224 \pm 60$ s is compatible with the fastest significant time scale found by the Fourier transform. Averaging the five lowest T_2 values yields 330 ± 40 s.

Spectral Analysis

Figure 3 shows the time-averaged photon spectrum for these data. The data are well fit, $\chi^2 = 17.1$ for 13 degrees of freedom (d.o.f.), by a broken power-law function with $E_B = 430 \pm 22 \pm 80$ GeV, $\Gamma_1 = 2.71 \pm 0.06 \pm 0.10$, and $\Gamma_2 = 3.53 \pm 0.05 \pm 0.10$. For each parameter, the two uncertainties are the statistical and systematic values, respectively. The time-averaged spectrum ($\Gamma = 3.32$) of PKS 2155–304 measured in 2003 [1], multiplied by the ratio (48.7) of $I(>200 \text{ GeV})$ from the respective data sets, is also shown in Figure 3. Despite a factor of ~ 50 change in flux there is qualitatively little difference between the two spectra which is surprising. The lack of any strong ($\Delta\Gamma > 0.2$) temporal variability in the VHE spectrum within these data (tested on time scales of 5, 10 and 28 minutes) is also surprising.

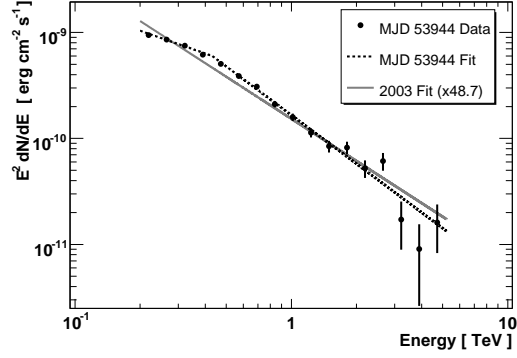


Figure 3: The time-averaged spectrum observed from PKS 2155–304 on MJD 53944. The dashed line is the best χ^2 fit of a broken power law to the data. The solid line represents the fit to the time-averaged spectrum of PKS 2155–304 from 2003 [1] scaled by 48.7.

Discussion

It is very likely that the electromagnetic emission in blazars is generated in jets that are beamed and Doppler-boosted toward the observer. Superluminal expansions observed with VLBI [14] provide evidence for moderate Doppler boosting in PKS 2155–304. Causality implies that γ -ray variability on a time scale t_{var} , with a Doppler factor⁴ (δ), is related to the radius (R) of the emission zone by $R \leq ct_{\text{var}}\delta/(1+z)$. Conservatively using the best-determined rise time (i.e. τ_r with the smallest error) from Table 1 for $t_{\text{var}} = 173 \pm 28$ s limits the size of the emission region to $R\delta^{-1} \leq 4.65 \times 10^{12} \text{ cm} \leq 0.31 \text{ AU}$.

The jets of blazars are believed to be powered by accretion onto a supermassive black hole (SMBH). Thus accretion/ejection properties are usually presumed to scale with the Schwarzschild radius R_S of the SMBH, where $R_S = 2GM/c^2$, which is the smallest, most-natural size of the system (see, e.g., [7]). Expressing the size R of the γ -ray emitting region in terms of R_S , the variability time

3. Only values of T_2 with less than 30% uncertainty are considered.

4. With δ defined in the standard way as $[\Gamma(1 - \beta \cos \theta)]^{-1}$, where Γ is the bulk Lorentz factor of the plasma in the jet, $\beta = v/c$, and θ is the angle to the line of sight.

scale limits its mass by $M \leq (c^3 t_{\text{var}} \delta / 2G(1+z)) R_S / R \sim 1.6 \times 10^7 M_\odot \delta R_S / R$. The reported host galaxy luminosity $M_R = -24.4$ (Table 3 in [11]) would imply a SMBH mass of order $1-2 \times 10^9 M_\odot$ [6], and therefore, $\delta \geq 60 - 120 R/R_S$. Emission regions of only a few R_S would require values of δ much greater than those typically derived for blazars ($\delta \sim 10$) and come close to those used for GRBs, which would be a challenge to understand.

Although the choice of a ~ 3 minute variability time scale in this article is conservative, it is still the fastest ever seen in a blazar, at any wavelength, and is almost an order of magnitude smaller than previously observed from this object. The variability is a factor of five times faster than VHE variability previously measured from Mkn 421 [9] and comparable to that reported from Mkn 501 [5]. However, in terms of the light-crossing time of the Schwarzschild radius, R_S/c , the variability of PKS 2155–304 is more constraining by another factor⁵ of $\approx 6 - 12$ for Mkn 421, and a factor of $\approx 2.5 - 5$ for Mkn 501.

The light curve presented here is strongly over-sampled, allowing for the first time in the VHE regime a detailed statistical analysis of a flare, which shows remarkable similarity to other longer duration events at X-ray energies. More detailed discussion of this outburst can be found in [4], and the event continues to be investigated with other statistical techniques. As the sensitivity of VHE instruments continues to improve, it is likely that similar extreme flaring episodes will be more commonly detected in the future. Similar flares will only strengthen the conclusion that either very large Doppler factors can be present in AGN jets, or that the observed variability is not connected to the central black hole.

Acknowledgements

The support of the Namibian authorities and of the University of Namibia in facilitating the construction and operation of HESS is gratefully acknowledged, as is the support by the German Ministry for Education and Research (BMBF), the Max Planck Society, the French Ministry for Research, the CNRS-IN2P3 and the Astroparticle Interdisci-

plinary Programme of the CNRS, the U.K. Science and Technology Facilities Council (STFC), the IPNP of the Charles University, the Polish Ministry of Science and Higher Education, the South African Department of Science and Technology and National Research Foundation, and by the University of Namibia. We appreciate the excellent work of the technical support staff in Berlin, Durham, Hamburg, Heidelberg, Palaiseau, Paris, Saclay, and in Namibia in the construction and operation of the equipment.

References

- [1] Aharonian, F., et al. (HESS Collaboration) 2005, A&A, 430, 865
- [2] Aharonian, F., et al. (HESS Collaboration) 2005, A&A, 442, 895
- [3] Aharonian, F., et al. (HESS Collaboration) 2006, A&A, 457, 899
- [4] Aharonian, F., et al. (HESS Collaboration) 2007, ApJ, 664, L71
- [5] Albert, J., et al. 2007, ApJ, in press [arXiv:astro-ph/0702008]
- [6] Bettoni, D., Falomo, R., Fasano, G. & Govoni, F. 2003, A&A, 399, 869
- [7] Blandford, R.D. & Payne, D.G. 1982, MNRAS, 199, 883
- [8] Catanese, M. & Sambruna, R.M. 2000, ApJ, 534, L39
- [9] Gaidos, J.A., et al. 1996, Nature, 383, 319
- [10] Hinton, J. 2004, New Astron Rev, 48, 331
- [11] Kotilainen, J.K., Falomo, R., & Scarpa, R. 1998, A&A, 336, 479
- [12] Morhac, M., et al. 2000, Nucl. Instrum. and Methods Phys. Res. A, 443, 108
- [13] Norris, J.P., et al. 1996, ApJ, 459, 393
- [14] Piner, B.G. & Edwards, P.G. 2004, ApJ, 600, 115
- [15] Vaughan, S., Edelson, R., Warwick, R.S. & Uttley, P. 2003, MNRAS, 345, 1271
- [16] Xue, Y. & Cui, W. 2005, ApJ, 622, 160
- [17] Woo, J.-H., et al. 2005, ApJ, 631, 762
- [18] Zhang, Y.H., et al. 1999, ApJ, 527, 719
- [19] Zhang, Y.H., et al. 2005, ApJ, 629, 686

5. These factors assume black hole masses of $10^{8.22} M_\odot$ and $10^{8.62} M_\odot$ for Mkn 421 and Mkn 501, respectively [17].



Active Atmospheric Calibration for H.E.S.S. Applied to PKS 2155-304

NOLAN, S.J.¹, PÜHLHOFER G.², & CHADWICK, P.M.¹ FOR THE H.E.S.S. COLLABORATION

¹ *Physics Department, Durham University, South Road, Durham, County Durham, DH1 3LE, United Kingdom*

² *Landessternwarte, Universität Heidelberg, Königstuhl, D 69117 Heidelberg, Germany*

Email : s.j.nolan@dur.ac.uk

Abstract: Using data derived from the H.E.S.S. telescope system and the LIDAR facility on site, a method of correcting for changing atmospheric quality based on reconstructed shower parameters is presented. The method was applied to data from the active galactic nucleus PKS 2155-304, taken during August and September 2004 when the quality of the atmosphere at the site was highly variable. Corrected and uncorrected fluxes are shown, and the method is discussed as a first step towards a more complete atmospheric calibration.

Introduction

Imaging Atmospheric Cherenkov Telescopes (IACTs) rely heavily on the atmosphere as their detecting medium. Although the atmosphere gives the telescope systems huge effective areas, daily variations in atmospheric quality can affect the system performance and lead, in the worst cases, to systematic bias in the estimated energy of a given event. Significant effort has been made in the past to take account of this problem by using the cosmic-ray background seen by the telescope on a given night to normalise the data [5]. However, given a better understanding of the location of atmospheric aerosol populations from LIDAR measurements and via modelling of these populations, it is possible to determine an active atmospheric correction to the data. Herein, recent work on such a technique is discussed as applied to observations with the H.E.S.S. telescope array of the active galactic nucleus (AGN) PKS 2155-304, this work continues from that presented in an earlier proceedings [6].

Technique

The LIDAR system at the H.E.S.S. site works at a wavelength of 905 nm, and has an active range

of 7.5 km. It is mounted on an alt-azimuth drive allowing on-source pointing during observations. During August and September 2004, a large population of aerosols was seen by the LIDAR below 2 km above the site, concurrent with a significant drop in the H.E.S.S. array trigger-rate for cosmic-rays. This population was seen to vary on a night to night basis, but not within a given night. In order to simulate its effects, the atmospheric simulation code MODTRAN was used to generate optical depth tables for wavelengths in the range 200 to 750 nm and for successive heights above the site (which is 1.8 km above sea level). The aerosol desert model within MODTRAN introduces a layer of aerosols into the first 2 km above ground level, whose density is then increased as the wind speed parameter is increased. Thus optical depth tables were produced for the range of wind speeds from 0 m/s to 30 m/s. The wind speed therefore acts as a tuning parameter to match simultaneously cosmic-ray trigger-rate and image parameter distributions, and is not a reflection of the measured wind speed at the site. These tables were then applied to a set of CORSIKA cosmic-ray simulations at various zenith angles between 0 and 60 degrees and with a southern pointing, to best match the data taken on PKS 2155-304, and a cosmic-ray trigger-rate for each atmosphere was derived for the H.E.S.S. array based upon the spectra given

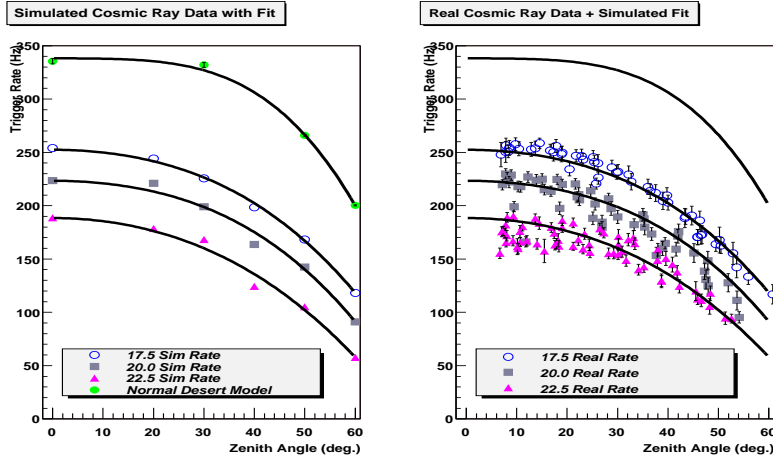


Figure 1: Simulated array trigger-rate for a spectrum of cosmic-rays [2] for various atmospheric models with function fit in left panel, versus measured cosmic-ray trigger rates for the PKS 2155-304 2004 dataset in right hand panel.

in [2]. By matching the trigger-rate from simulations and real data, taking into account zenith angle dependence effects and gain changes over the experiment lifetime, an atmospheric model can be selected, as discussed in [6]. The real cosmic-ray trigger rate and that due to simulation for the PKS 2155-304 dataset discussed later are shown in figure 1 for comparison. The figure clearly shows that the data can be separated into 3 classes corresponding to MODTRAN model wind speeds of 17.5, 20.0 and 22.5 m/s.

In addition, as the LIDAR has a limited range and sensitivity, and to further confirm the choice of atmospheric models, a set of atmospheric models with aerosol densities at higher altitudes was simulated using MODTRAN. These simulated atmospheres represent conditions which could in principle also have occurred during data-taking, as they result in similar cosmic-ray trigger rates as the low-level aerosol models. As shown in figure 2, by comparing the reconstructed shower depth for gamma-rays between real-data and simulations, these models are shown to be considerably less favoured than the simple low-level aerosol models of 17.5, 20.0 and 22.5 m/s wind speed, which trigger-rate, image parameters, mean shower-depth and LIDAR data validate.

The atmospheric model is then applied to a full

set of CORSIKA gamma-ray simulations within a telescope simulation code. The simulations cover the zenith angle range of the observations, and produce lookup tables for image parameter cuts, energy and effective area, and these in turn are applied to the data using the standard H.E.S.S. analysis procedure [1].

PKS 2155-304

PKS 2155-304 is an AGN of the blazar class at a redshift of $z = 0.116$. It was first detected in TeV gamma-rays by the Durham Mark 6 telescope [4], and has been observed from the earliest days of the H.E.S.S. experiment [7]. The data set from August and September 2004 is formed from 86 hours of four telescope observations. By combining flux data into atmospheric correction groups, figure 3 shows the results for corrected and non-corrected data in the form of a plot of the flux distribution derived on a run by run basis. It appears that in the data set considered here, as no run was taken under normal, clear atmospheric conditions, all runs are subject to systematically lowered detection rates, which if uncorrected may lead to significantly different results. In addition, figure 4 shows the spectra derived from this data. Without correction, sig-

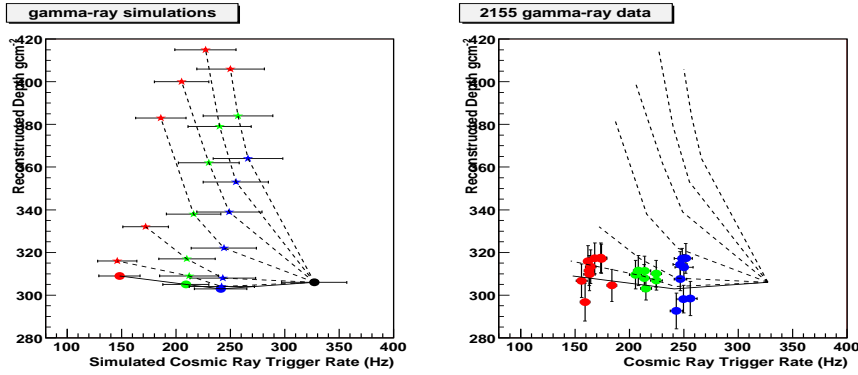


Figure 2: The left panel shows the mean of reconstructed depth (for a Gaussian fit) for gamma-ray shower simulations at 20 degrees zenith-angle versus telescope trigger-rate. The lower points (solid circles) show the results for the 17.5, 20.0 and 22.5 m/s wind speed models, with the other points showing the result for atmospheres with increasing altitude of the aerosol contaminant layer, with lines connecting similar altitudes. These lines are reproduced on the right hand plot, which shows the preliminary real mean reconstructed depth for gamma-ray data on PKS 2155-304 taken during 2004 at zenith angles between 15 and 25 degrees, slightly scaled to match the results at 20 degrees. The data shown no indication of high level aerosols, independently confirming the LIDAR results.

nificantly differing results are arrived at, with spectral index for a power-law fit differing by (at worst) $\Delta = 0.7$, which is within errors marginally incompatible with a constant index. With correction all fit spectral indices agree well within errors.

Conclusion

A new method for correcting for changes in low-level atmospheric quality is applied to the variable source PKS 2155-304. The method, based on cosmic-ray trigger-rate, and LIDAR input, has allowed a corrected set of fluxes for PKS 2155-304 to be produced from data that would otherwise be unusable. This is particularly important as this data set forms part of a large multi-wavelength campaign so removing atmospheric biases is vital. To the lowest order, the effect on integral gamma-ray flux is seen to be proportional to the zenith- and time-corrected cosmic-ray trigger-rate.

The current LIDAR system operates at a wavelength somewhat removed from typical Cherenkov photon wavelengths, and has a range which doesn't quite cover the maximum of shower development. Two new LIDARs recently installed at the H.E.S.S.

site operate at wavelengths closer to Cherenkov light and have a greater range, and will hopefully allow more straight forward correction. As has been shown, though, the comparison of real and simulated reconstructed shower depth under the application of different atmospheric models allows a coarse appreciation of atmospheric conditions, which is a useful check for the more accurate LIDAR dataset expected to be obtained soon.

References

- [1] F. Aharonian et al. *Ap. J.*, 430:865–875, February 2005.
- [2] F. Aharonian et al. *A. & A.*, 457:899–915, October 2006.
- [3] A. M. Brown et al. volume 4 of *International Cosmic Ray Conference*, pages 411–+, 2005.
- [4] P. M. Chadwick et al. *Ap. J.*, 513:161–167, March 1999.
- [5] A. Karle et al. *Astroparticle Physics*, 4:1–13, October 1995.
- [6] S. Lebohec and J. Holder. *Astroparticle Physics*, 19:221–233, May 2003.

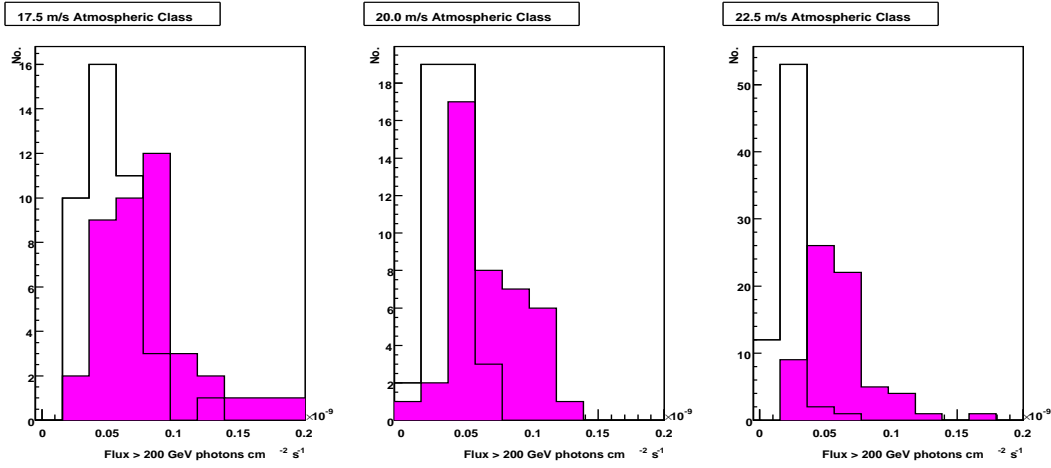


Figure 3: The preliminary distribution of muon corrected integral flux for PKS 2155-304 above 200 GeV derived from 28 minute runs is plotted before (open histograms) and after (filled histograms) the application of corrections for low-level dust. As noted each panel shows a subset of the data of differing atmospheric class.

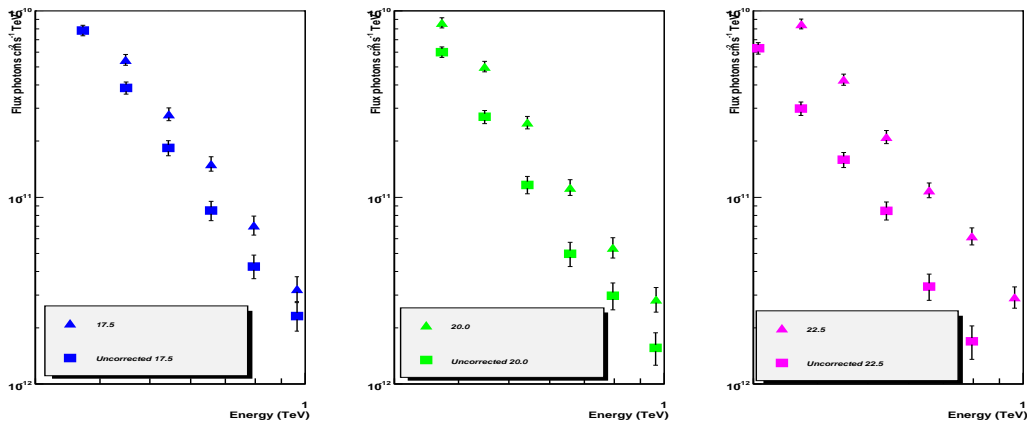


Figure 4: The preliminary uncorrected and corrected differential spectral for the 3 subsets of data is shown between 300 GeV and 1 TeV. Above 1 TeV differences are negligible compared to statistical errors.



Discovery of fast variability of the TeV γ -ray flux from the radio galaxy M 87 with H.E.S.S.

M. BEILICKE¹, F. AHARONIAN², W. BENBOW², G. HEINZELMANN¹, D. HORNS³, O. MARTINEAU-HUYNH⁴, M. RAUE¹, J. RIPKEN¹, G. ROWELL⁵, H. SOL⁶ FOR THE H.E.S.S. COLLABORATION

¹ *Institut für Experimentalphysik, Univ. of Hamburg, Luruper Chaussee 149, D-22761 Hamburg, Germany*

² *MPI-K Heidelberg, P.O. Box 103980, D-69029 Heidelberg, Germany*

³ *Institut für Astronomie und Astrophysik, Universität Tübingen, Sand 1, D-72076 Tübingen, Germany*

⁴ *Laboratoire de Physique Nucleaire et de Hautes Energies, IN2P3/CNRS, Universites Paris VI & VII, 4 Place Jussieu, F-75252 Paris Cedex 5, France*

⁵ *School of Chemistry & Physics, University of Adelaide 5005, Australia*

⁶ *LUTH, UMR 8102 du CNRS, Observatoire de Paris, Section de Meudon, F-92195 Meudon Cedex, France*
matthias.beilicke@desy.de

Abstract: The giant radio galaxy M 87 was observed at GeV/TeV γ -ray energies with the H.E.S.S. (High Energy Stereoscopic System) Cherenkov telescopes in the years 2003–2006. The observations confirm M 87 as the first extragalactic TeV γ -ray source not of the blazar type (first indications of a signal were reported by the HEGRA collaboration earlier). The TeV γ -ray flux from M 87 as measured with H.E.S.S. was found to be variable on time-scales of years and surprisingly also of days which strongly constrains the size of the emission region. The results (position, energy spectrum and light curve) as well as theoretical interpretations will be presented.

Introduction

Observations of extragalactic objects at GeV/TeV γ -ray energies play a key role in the understanding of non-thermal processes and emission models of relativistic plasma jets. Meanwhile, more than 15 extragalactic TeV γ -ray sources are established, whereas only the giant FRI radio galaxy M 87 [1, 2, 3] is not a blazar¹, making it an important object for the understanding of jet formation and VHE γ -ray emission processes in AGN. M 87 is well studied in various wavelengths – allowing to constrain different system parameters, as for example the black hole mass, the accretion rate, etc.

The H.E.S.S. collaboration operates an array of four Cherenkov telescopes [4, 5] situated in Namibia. The telescopes measure cosmic γ -rays in the energy range between 100 GeV and several 10 TeV by recording the Cherenkov light which is emitted from an air shower which develops when a very high energy (VHE) particle (hadron or photon) enters the Earth's atmosphere. The stereo-

scopic observation together with a corresponding hardware trigger assures that an air shower is recorded by at least two of the four telescopes, allowing for an angular and energy resolution per event of $\delta\Theta < 0.1^\circ$ and $\Delta E/E \leq 15\%$, respectively, as well as an improved cosmic ray (CR) background suppression.

Variable TeV γ -ray emission from M 87

Radio-loud galaxies contain AGN with jets, but in contrast to blazars the emission is not (strongly) Doppler boosted due to larger viewing angles between the jet and the observer's line of sight. The radio-loud galaxy M 87 is located in the Virgo cluster of galaxies at a distance of ~ 16 Mpc ($z = 0.0043$) and hosts a central black hole of

1. Blazars are active galactic nuclei (AGN) with their plasma jet pointing closely towards the observer's line of sight (the energy and flux of the emitted photons are boosted due to relativistic effects, making blazars detectable at TeV energies).

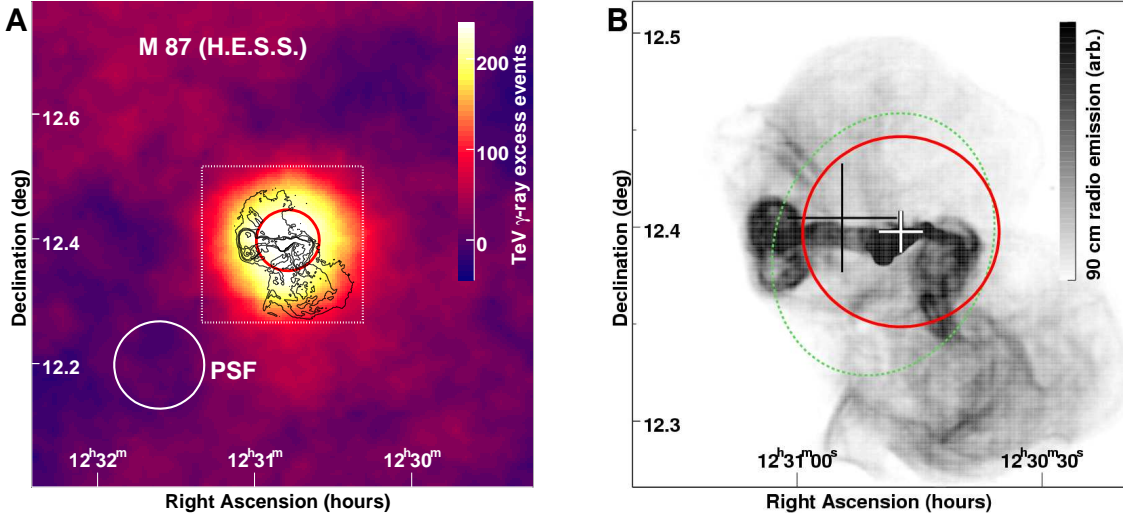


Figure 1: **Left:** Smoothed TeV γ -ray excess map and the upper limit on the intrinsic source extension (99.9% c.l., red circle) together with the 90 cm radio contours adopted from [13] as well as the H.E.S.S. point spread function (PSF, r_{68}). The white box indicates the cut-out of the right image. **Right:** The 90 cm radio image [13] showing the large scale structure (~ 80 kpc in diameter) of M87 together with the TeV position (white cross, including the statistical as well as the $20''$ pointing uncertainty error) and again the extension limit (circle). The black cross indicates the position of the excess reported by HEGRA [1]. The green ellipse shows the extension of the M87 galaxy in the optical band.

$(3.2 \pm 0.9) \cdot 10^9 M_{\odot}$ [6]. Due to its proximity M87 is discussed as a possible source of the highest energy (10^{20} eV) CRs [7]. The 2 kpc scale plasma jet (inclination angle of 30° [8]) is spatially resolved in different wavelengths, ranging from radio, optical to X-rays. Previously, evidence ($> 4\sigma$) for $E > 730$ GeV γ -ray emission from M87 in 1998/1999 was reported by HEGRA [1, 2] and no significant emission above 400 GeV was observed by Whipple [9] in 2000-2003.

M87 was observed by H.E.S.S. between 2003 and 2006 for a total of 89 h after data quality selection. Using hard event selection cuts [5] an excess of 243 γ -ray events (13σ) was found in the whole data set. The position of the excess is compatible with the nominal position of the nucleus of M87. With the given angular resolution of H.E.S.S., the extension is consistent with a point-like object with an upper limit for a Gaussian surface brightness profile of $3'$ (99.9% c.l.), corresponding to a radial distance of 14 kpc in M87, see Fig. 1.

The energy spectra for the 2004 and 2005 data sets are shown in Fig. 2 (left) and are well fit by a power-law function $dN/dE = I_0(E/1 \text{ TeV})^{-\Gamma}$ with photon indices of $\Gamma = 2.62 \pm 0.35$ (2004) and $\Gamma = 2.22 \pm 0.15$ (2005). The systematic error on the photon index and flux normalisation are estimated to be $\Delta\Gamma = 0.1$, and $\Delta I_0/I_0 = 0.2$, respectively. The hard spectrum measured in 2005 (reaching beyond an energy of 10 TeV) challenges hadronic as well as leptonic VHE γ -ray emission models discussed for M87 in the literature, see [10] and references therein.

The integral γ -ray flux above 730 GeV is shown in Fig. 3 (right) for the years 2003–2006 with a statistical significance for variability on a yearly basis of 3.2σ . This is confirmed by a Kolmogorov test comparing the distribution of photon arrival times to the distribution of background arrival times yielding a significance for burst-like behaviour above 4σ . Surprisingly, variability on time-scales of days (flux doubling) was found in the high state data of 2005 (Fig. 3, upper right

panel) with a statistical significance of more than 4σ . This is the fastest variability observed in any waveband from M 87 and strongly constrains the size of the emission region of the TeV γ -rays to $R \leq c \cdot \Delta t \cdot \delta \approx 5 \times \delta R_s$, where δ is the relativistic Doppler factor of the source of γ radiation and $R_s \approx 10^{15}$ cm is the Schwarzschild radius of the supermassive black hole in M 87. This very compact emission region excludes a variety of models for the emission of the TeV γ radiation, i.e. CR interaction with matter in M 87, radiation due to annihilation of dark matter particles, the kpc plasma jet or even individual knots of the jet, and leaves only a region very close to the central black hole as a reasonable production site of the TeV γ -rays with possibly novel mechanisms involved, see [10] for a more detailed discussion. For instance, the observed γ -ray flux may be explained by inverse Compton emission of ultrarelativistic electron-positron pairs which are produced in an electromagnetic cascade in the black hole magnetosphere [11].

M 87 was monitored during the past years by the Chandra X-ray satellite, see Fig. 3 (right). The X-ray flux of the knot HST-1 (located very close to the nucleus) increased by a factor of ~ 50 between 2003 and 2005 [12], whereas the emission of the nucleus itself remained rather constant. However, no unique correlation between the X-ray and TeV γ -ray fluxes can be stated, since the measurements were not performed simultaneously.

Summary and Conclusion

H.E.S.S. confirmed the giant radio galaxy M 87 as the first extragalactic TeV γ -ray source which does not belong to the class of blazars. The hard energy spectrum in 2005 challenges hadronic as well as leptonic models. The surprisingly discovered variability of the TeV γ -ray emission on short time-scales of days strongly constrains the size of the emission region and excludes several models discussed for M 87, leaving a location close to the central black hole as reasonable production site of the TeV γ -ray emission. Simultaneous multi-wavelengths observations and observations in the MeV/GeV energy range with GLAST are of special importance to estimate the position of the max-

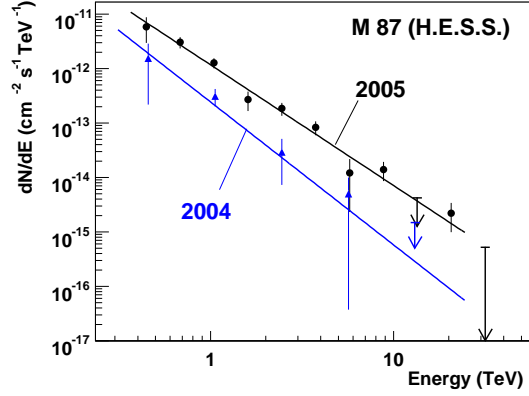


Figure 2: Energy spectra of M 87 (2004/05 data, using standard event selection cuts [5]) covering a range of ~ 400 GeV to ~ 10 TeV. Spectra for the 2003 and 2006 data sets could not be derived due to limited event statistics. The lines show the fits of a power-law function.

imum of the VHE peak in the SED and further constrain model parameters. Taken M 87 as an established TeV γ -ray emitting radio galaxy, one should also mention the FRI radio galaxy Centaurus A (Cen A), which is located at an even closer distance of 3.4 Mpc ($z = 0.0018$) and shows a jet angle of $\theta > 50^\circ$. Cen A is the only AGN not belonging to the class of blazars which was detected in the GeV energy regime by EGRET [14, 15], making a detection with GLAST promising. So far, no excess was found in the ~ 5 h of H.E.S.S. data taken in 2004 and 2005 [16].

Acknowledgements

The support of the Namibian authorities and of the University of Namibia in facilitating the construction and operation of H.E.S.S. is gratefully acknowledged, as is the support by the German Ministry for Education and Research (BMBF), the Max Planck Society, the French Ministry for Research, the CNRS-IN2P3 and the Astroparticle Interdisciplinary Programme of the CNRS, the U.K. Particle Physics and Astronomy Research Council (PPARC), the IPNP of the Charles University, the South African Department of Science and Technol-

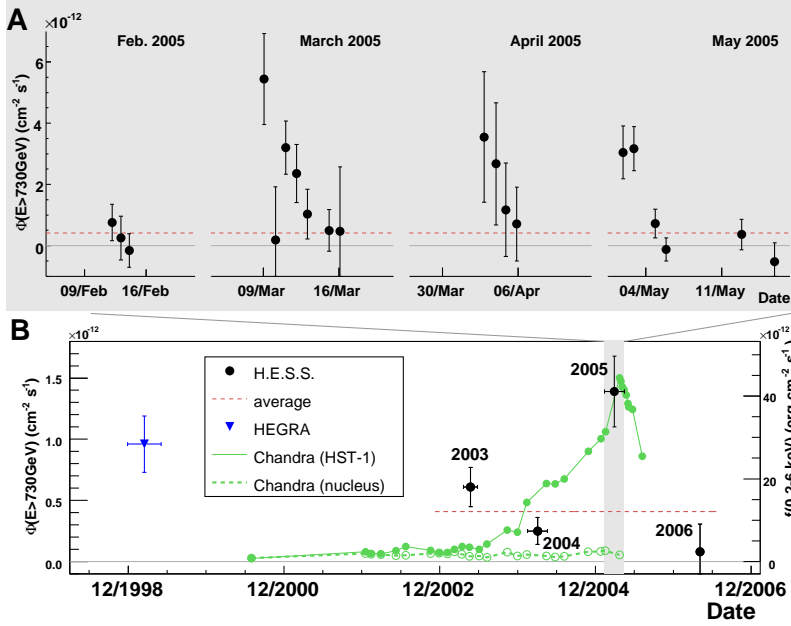


Figure 3: Gamma-ray flux above 730 GeV. (B) The average flux values for the years 2003 to 2006 as measured with H.E.S.S. together with a fit of a constant function (red line). The flux reported by HEGRA is also drawn. (A) The night-by-night fluxes for the four individual months (February to May) of the high-state measurements in 2005 with significant variability on (flux doubling) time-scales of days. The green points in (B) correspond to the 0.2 – 6 keV X-ray flux of the knot HST-1 (solid, [12]) and the nucleus (dashed, D. Harris, priv. comm.) as measured by Chandra; the lines are linear interpolations of the flux points.

ogy and National Research Foundation, and by the University of Namibia. We thank D. Harris for providing the Chandra X-ray light curve of the M 87 nucleus.

References

- [1] F.A. Aharonian, et al. (HEGRA collaboration), *A&A* **403**, L1-L5 (2003).
- [2] N. Götting, et al., "Recent Results from HEGRA" in *European Physical Journal C*, **33**, 932-934 (2004), see also: astro-ph/0310308.
- [3] M. Beilicke, W. Benbow, R. Cornils, et al., *Proc. of the 29th ICRC (Pune)* **4**, 299-302 (2005).
- [4] W. Hofmann, *Proc. of the 29th ICRC* **10**, 97-114 (2005).
- [5] W. Benbow, *Proc. 'Towards a network of atmospheric Cherenkov detectors VII (Palaiseau)*, p.163 (2005).
- [6] F. Macchetto, et al., *ApJ*, **489**, 579-600 (1997).
- [7] P.L. Biermann, et al., *NuPhS*, **87**, 417-419 (2000).
- [8] G.V. Bicknell, and M.C. Begelman, *ApJ*, **467**, 597-621 (1996).
- [9] S. Le Bohec, et al., *ApJ*, **610**, 156-160 (2004).
- [10] F. Aharonian, et al. (H.E.S.S. collaboration), *Science*, **314**, 1424-1427 (2006).
- [11] A. Neronov & F. Aharonian, *submitted*, see arXiv:0704.3282v1.
- [12] D.E. Harris, et al., *ApJ*, **640**, 211-218 (2006).
- [13] F.N. Owen, J.A. Eilek, and J.A. Kassim, *ApJ*, **543**, 611-619 (2000).
- [14] P. Sreekumar, et al., *Aph*, **11**, 221-223 (1999).
- [15] R.C. Hartman et al., *ApJS* **123:79**, 202 (1999).
- [16] F.A. Aharonian, et al. (H.E.S.S. collaboration), *A&A*, **441**, 465-472 (2005).



Multiwavelength observations of PKS 2005-489 and H 2356-309 with HESS

LUIGI COSTAMANTE¹, WYSTAN BENBOW¹, CATHERINE BOISSON², SANTIAGO PITA³, HELENE SOL²,
FOR THE H.E.S.S. COLLABORATION

¹ *Max-Planck-Institut für Kernphysik, PO box 103980, D69029 Heidelberg, Germany*

² *LUTH, UMR 8102 du CNRS, Observatoire de Paris, Section de Meudon, F-92195 Meudon Cedex, France*

³ *APC, CNRS, Université Paris 7 Denis Diderot, F-75205 Paris Cedex 13, France*

Luigi.Costamante@mpi-hd.mpg.de

Abstract: Very-high-energy (VHE; >100 GeV) γ -ray observations of PKS 2005-489 and H 2356-309 were made with the High Energy Stereoscopic System (HESS) in 2005 and 2006. Previous 2004 data have been reanalysed to correct for the degradation of the optical efficiency of the HESS system. Both sources have been detected during all 3 years, at a level of 1-3% of the Crab flux. A total excess of $\sim 16\sigma$ and $\sim 12\sigma$, respectively, is accumulated. Significant flux variations are seen on a monthly basis for H 2356-309, and in 2006 for PKS 2005-489. The spectra confirm the previously reported values, in particular the hard spectrum of H 2356-309. Multiwavelength observations performed with XMM and RXTE in 2004 and 2005 reveal remarkable flux (10x) and spectral ($\Delta\Gamma=0.7$) variations for PKS 2005-489. Despite a $\sim 10\times$ flux increase above 1 keV, no flux variation is seen at VHE, implying in an SSC scenario a corresponding decrease of the energy density of the seed photons for inverse Compton (IC) scattering, not observed in the SED. A possible explanation is that a new component is emerging in the jet, whose electrons do not see the photons of the observed synchrotron peak. The SED of both objects shows the potential for significantly higher VHE fluxes.

Introduction

The blazars PKS 2005-489 ($z=0.071$) and H 2356-309 ($z=0.165$) are two high-frequency-peaked BL Lac objects (HBL). PKS 2005-489 is one of the brightest HBL in the southern hemisphere, and is characterized by very large variability in the X-ray band [1, 2]. H 2356-309 is an *extreme* BL Lac [3], characterized by the synchrotron peak of the spectral energy distribution (SED) at energies above a few keV. Both objects have been discovered by HESS as VHE sources in 2004 [4, 5], though at a rather faint flux (~ 2 -3% Crab). Coordinated X-ray observations performed in the same epoch with XMM and RXTE revealed historically low fluxes, for both objects. Since in HBLs the X-ray band usually samples the synchrotron emission of TeV electrons, which produce VHE photons by inverse Compton (IC) scattering of low energy photons, significantly higher VHE fluxes can be expected. Monitoring observations in 2005 and 2006 were thus performed, both to increase the event statistics and to catch flaring events. Further multi-

wavelength observations were also performed with XMM (as pre-planned pointings due to the narrow overlap between HESS and XMM visibility windows) and RXTE (as ToO). The main preliminary results on the average data are here reported.

HESS Results

All data have been analyzed with the HESS standard analysis [6, 8]. For the spectral and flux determination the energy of each event is corrected [6] for the absolute optical efficiency of the system using efficiencies determined from simulated and observed muons. This correction eliminates any potential long-term variations in the absolute energy scale of the HESS analysis due to a changing optical throughput. The systematic error is $\sim 20\%$ on flux and ~ 0.1 for the photon index.

On PKS 2005-489, a total of 135.4 hours of observations were taken from 2004 through 2006. After data-quality selection, an exposure of 78.3 h livetime is obtained, at a mean zenith angle 36° .

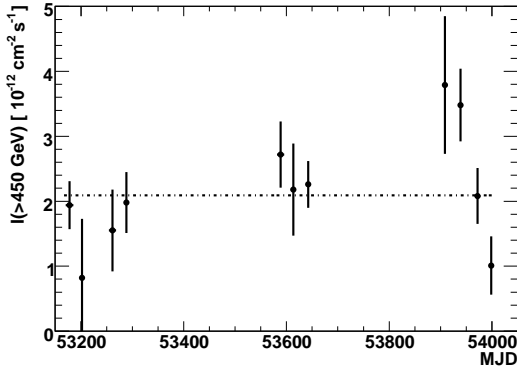


Figure 1: The integral flux (>450 GeV) measured by HESS from PKS 2005-489 in monthly bins. The 2004 values are ~ 3 times higher than previously published[4] as all fluxes are corrected[6] for degradation in the optical efficiency of the HESS system. Only the statistical errors are shown. The fluxes are calculated assuming the time-average spectrum measured in the respective year (Table 1). Simultaneous X-ray observations were performed on MJD 53282, 53608-53622 (RXTE) and 53641 (Table 2, respectively).

A point-like VHE γ -ray excess from PKS 2005-489 is detected each year, with an average flux of $\sim 2.8\%$ Crab. On a monthly basis (Fig. 1), there is indication of $\sim 3\times$ flux variability in 2006. At shorter timescales, no significant variability is detected, though comparable variations cannot be excluded. The annual VHE spectra measured are shown in Fig. 2 and Table 1. Among years, the flux below 1 TeV remains basically constant. There is only a slight ($\sim 1.8\sigma$) indication of hardening between 2004 and 2006 spectra.

H 2356-309 has been observed by HESS for a total of 164 hours from 2004 through 2006. After data-quality selection, an exposure of 109.8 h is obtained, at mean zenith angle 19° . Significant VHE emission is detected during each year, with clear indications of variability on an annual and monthly timescale (probability of constant flux $< 0.4\%$). At shorter timescales no significant variability is detected, though comparable variations cannot be excluded given the low statistics. Despite the variability, no significant spectral changes are observed (Table 1).

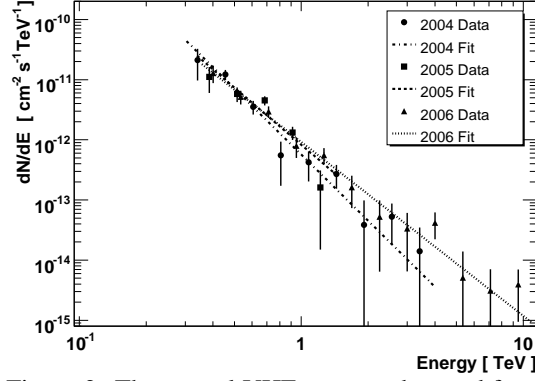


Figure 2: The annual VHE spectra observed from PKS 2005-489. The lines represent the best fit of a power-law model to the observed data, with photon index Γ reported in Table 1.

Table 1: Results of the HESS observations. Shown are the epoch, exposure time, significance of the excess, integral flux (in units of $10^{-13} \text{ cm}^{-2} \text{ s}^{-1}$) and photon index for a single power-law fit. Only the statistical errors are shown.

Epoch	Time [h]	Sign. [σ]	Int. Flux [f.u.]	Γ
PKS 2005-489			(>450 GeV)	
2004	24.2	7.7	1.81 ± 0.26	3.65 ± 0.39
2005	32.6	11.0	2.38 ± 0.27	3.15 ± 0.30
2006	21.5	8.8	2.20 ± 0.26	2.89 ± 0.20
Total	78.3	15.9	2.08 ± 0.15	3.18 ± 0.16
H 2356-309			(>200 GeV)	
2004	39.9	9.6	5.97 ± 0.61	2.97 ± 0.19
2005	46.7	5.9	3.28 ± 0.65	2.99 ± 0.39
2006	23.2	5.1	3.49 ± 0.82	3.43 ± 0.41
Total	109.8	12.1	4.47 ± 0.39	3.09 ± 0.16

For the discussion of the SED properties of these two HBL, all the HESS spectra have been corrected for γ - γ absorption on the diffuse Extragalactic Background Light (EBL) with the P0.45 shape in [7] (close to the level from galaxy counts).

SED Changes in PKS 2005–489

Simultaneous X-ray observations were performed with XMM in Oct. 2004 and Sept. 2005, and with RXTE in Aug-Sept 2005. No significant variability

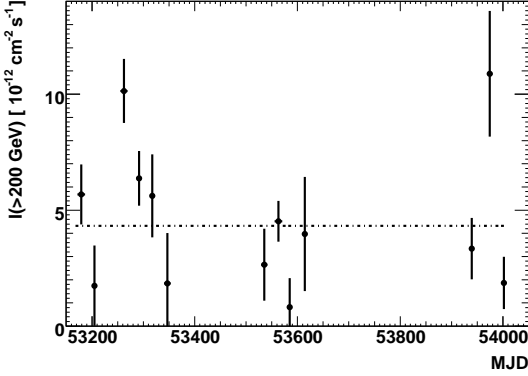


Figure 3: The integral flux (>200 GeV) measured by HESS from H 2356-309, in monthly bins. All fluxes are corrected for the degradation of the HESS optical efficiency [6]. Statistical errors only. The fluxes are calculated assuming the time-average spectrum measured in the respective year (Table 1). There is clear indication of variability (probability of constant flux $<0.4\%$). Simultaneous X-ray observations were performed on MJD 53320 (RXTE), 53534 and 53536 (Table 2, respectively).

Table 2: Best-fit parameters of the X-ray data. Single and broken power-law models (XMM: MOS+PN data). Column density N_H fixed to galactic values, and modelled with Tbags using Wilms abundances. The errors are quoted at the 90% confidence level. Unabsorbed flux in units of $\text{erg cm}^{-2} \text{s}^{-1}$ in the 2-10 KeV band.

Instr.	Γ_1	E_{br} [keV]	Γ_2	Flux [f.u.]
PKS 2005-489				
XMM	-	-	3.04 ± 0.05	$1.2\text{E-}12$
RXTE	-	-	2.9 ± 0.2	$7.6\text{E-}12$
XMM	3.0 ± 0.1	0.5	2.27 ± 0.03	$2.0\text{E-}11$
H 2356-309				
RXTE	-	-	2.43 ± 0.25	$9.7\text{E-}12$
XMM	2.00 ± 0.05	1.0	2.34 ± 0.03	$7.2\text{E-}12$
XMM	1.92 ± 0.06	0.9	2.23 ± 0.03	$8.7\text{E-}12$

is observed within each data set, on any timescale. From 2004 to 2005, the spectrum above 1 keV hardens strongly ($\Delta\Gamma=0.7$), yielding a $\sim 10\times$ flux increase. The UV fluxes (close to the synchrotron peak) show a $\sim 30\%$ increase as well. In contrast,

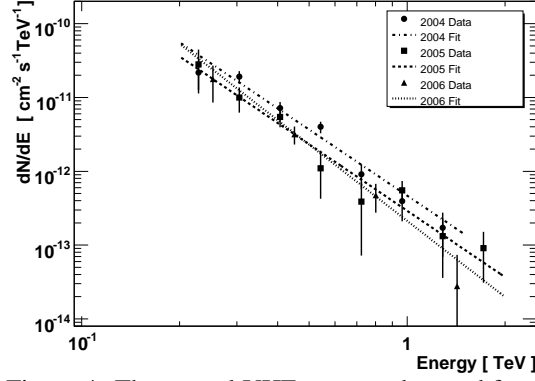


Figure 4: The annual VHE spectra observed from H 2356-309. The lines represent the best fit of a power-law model to the observed data, with photon index Γ reported in Table 2. No significant spectral variation is observed. An analysis of combined data for different flux levels is on-going.

the VHE emission remains almost constant, with a spectrum that suggests it can be produced by the same electrons emitting by synchrotron in the hard X-ray band. However, the VHE flux should have increased at least linearly with the X-ray flux between the two epochs, if these electrons could up-scatter by IC the observed synchrotron peak photons. For the VHE flux to remain constant, a corresponding decrease of the seed-photons energy density is required. This suggests that a new jet component is emerging, physically separated from the main emitting blob, and whose synchrotron peak emission remains at present hidden below the observed SED.

SED Changes in H 2356–309

The X-ray flux and spectral properties appear to be almost constant among these three epochs, at a flux level $\sim 3\times$ lower than the *BeppoSAX* values (June 1998[3]). The XMM spectra confirm the location of the synchrotron peak in the X-ray band (at 1-2 KeV), as derived from the *BeppoSAX* data. The hard VHE spectra, now measured with better statistics, confirm the constraints on the EBL previously obtained from the 2004 dataset[7]. Once corrected for intergalactic $\gamma - \gamma$ absorption, the hard VHE spectrum locates the IC peak of the SED above 1 TeV.

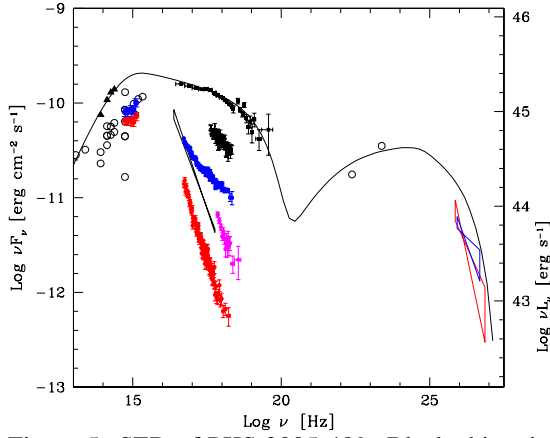


Figure 5: SED of PKS 2005-489. Black: historical data and modelling of the strong 1998 flare [2]. Corrected for EBL absorption (P0.45 curve in [7]), the intrinsic VHE slopes obtained are $\Gamma_{int}=3.1 \pm 0.4$ (red, year 2004) and $\Gamma_{int}=2.6 \pm 0.3$ (blue, year 2005). The Opt-UV fluxes from the Optical Monitor (OM) onboard XMM are corrected for galactic extinction using the Cardelli et al. (1998) curve. XMM data processed with SAS7.0. The hard ($\Gamma < 2$) UV spectrum indicated by the OM photometry locates the synchrotron peak between the Far-UV and Soft X-ray range.

Conclusion

Observations performed by HESS from 2004 through 2006 have confirmed PKS 2005-489 and H 2356-309 as VHE gamma-ray sources, at an average annual level of 1-3% Crab. The VHE spectra confirm the very different SED properties of these two HBL, with very soft and hard intrinsic spectra respectively. Simultaneous observations with RXTE and XMM have confirmed the correlation between SED peak energies, with the higher synchrotron peak frequency observed in the object with the higher IC peak energy. X-ray observations have also shown the objects to be in historically low states. For PKS 2005-489, the overall SED evolution suggests that a new jet component is emerging, with harder properties. Since PKS 2005-489 has historically demonstrated a $100\times$ dynamical range in the X-ray band, dramatically higher VHE fluxes ($10^2 - 10^4\times$) can be expected in a leptonic scenario, unless counterbalanced by a strong ($>10\times$) and simultaneous increase of the magnetic field. These results confirm the strong

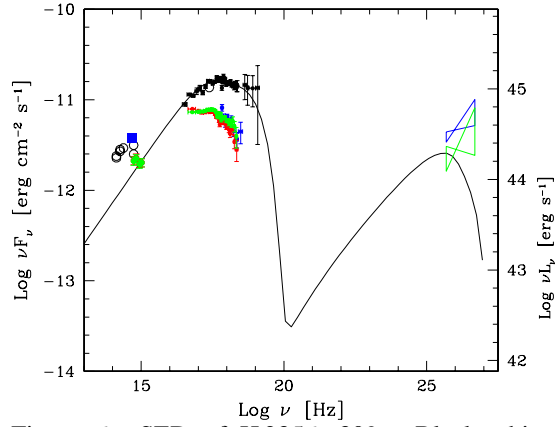


Figure 6: SED of H 2356-309. Black: historical data and modelling[3]. After correction for EBL absorption, the intrinsic VHE slopes are $\Gamma_{int}=1.7\pm0.2$ (blue, year 2004) and $\Gamma_{int}=1.7\pm0.4$ (green, year 2005). Blue symbols: data discussed in [5]. Optical fluxes from ROTSE and XMM-OM

diagnostic potential of coordinated Optical-X-ray-VHE observations. Further monitoring of these objects is highly encouraged.

Acknowledgements

The support of the Namibian authorities and of the University of Namibia in facilitating the construction and operation of HESS is gratefully acknowledged, as is the support by the German Ministry for Education and Research (BMBF), the Max Planck Society, the French Ministry for Research, the CNRS-IN2P3 and the Astroparticle Interdisciplinary Programme of the CNRS, the U.K. Science and Technology Facilities Council (STFC), the IPNP of the Charles University, the Polish Ministry of Science and Higher Education, the South African Department of Science and Technology and National Research Foundation, and by the University of Namibia. We appreciate the excellent work of the technical support staff in Berlin, Durham, Hamburg, Heidelberg, Palaiseau, Paris, Saclay, and in Namibia in the construction and operation of the equipment.

References

- [1] Perlman E. et al., 1999, ApJ 523L, 11
- [2] Tagliaferri G. et al., 2001, A&A 368, 38
- [3] Costamante L. et al., 2001, A&A 371, 512
- [4] Aharonian F. et al., 2005, A&A 436L, 17
- [5] Aharonian F. et al., 2006, A&A 455, 461
- [6] Aharonian F. et al., 2006, A&A, 457, 899
- [7] Aharonian F. et al., 2006, Nature, 440, 1018
- [8] W. Benbow, 2005, Proc. of "Towards a Network of Atmospheric Cherenkov Detectors VII", p163



Multi-wavelength Observations of PG 1553+113 with HESS

W. BENBOW¹, C. BOISSON², R. BÜHLER¹, AND H. SOL² FOR THE HESS COLLABORATION

¹ *Max-Planck-Institut für Kernphysik, Heidelberg, Germany*

² *LUTH, UMR 8102 du CNRS, Observatoire de Paris, Section de Meudon, France*

Wystan.Benbow@mpi-hd.mpg.de

Abstract: Very high energy (VHE; >100 GeV) γ -ray observations of PG 1553+113 were made with the High Energy Stereoscopic System (HESS) in 2005 and 2006. A strong signal, ~ 10 standard deviations, is detected by HESS during the 2 years of observations (24.8 hours live time). The time-averaged energy spectrum, measured between 225 GeV to ~ 1.3 TeV, is characterized by a very steep power law (photon index of $\Gamma = 4.5 \pm 0.3_{\text{stat}} \pm 0.1_{\text{syst}}$). The integral flux above 300 GeV is $\sim 3.4\%$ of the Crab Nebula flux and shows no evidence for any variations, on any time scale. H+K ($1.45\text{--}2.45\mu\text{m}$) spectroscopy of PG 1553+113 was performed in March 2006 with SINFONI, an integral field spectrometer of the ESO Very Large Telescope (VLT) in Chile. The redshift of PG 1553+113 is still unknown, as no absorption or emission lines were found.

Introduction

Evidence for VHE (>100 GeV) γ -ray emission from the high-frequency-peaked BL Lac object PG 1553+113 was first reported by the HESS collaboration [3] based on observations made in 2005. This detection was later confirmed [6] with MAGIC observations in 2005 and 2006. The measured VHE spectra are unusually soft (photon index $\Gamma=4.0\pm 0.6$ and $\Gamma=4.2\pm 0.3$ for the HESS and MAGIC experiments, respectively) but the errors are large, clearly requiring improved measurements before detailed interpretation of the complete SED is possible. Further complicating any SED interpretation is the absorption of VHE photons [10, 11] by pair-production on the Extragalactic Background Light (EBL). This absorption, which is energy dependent and increases strongly with redshift, distorts the VHE energy spectra observed from distant objects. For a given redshift, the effects of the EBL on the observed spectrum can be reasonably accounted for during SED modeling. Unfortunately, the redshift of PG 1553+113 is unknown, despite many attempts to measure it (see, e.g., [8, 16]).

In 2005 and 2006, a total of 30.3 hours of HESS observations were taken on PG 1553+113. The 2005 HESS observations are exactly the same as reported in [3]. The good-quality exposure is 24.8 hours live time. The data are processed using the standard HESS calibration [2] and analysis tools [6]. *Soft cuts* [3] are applied to select candidate γ -ray events, resulting in an average post-analysis energy threshold of 300 GeV at the mean zenith angle of the observations, 37° .

HESS Results

A significant VHE γ -ray signal is detected in each year of HESS data taking. The total observed excess is 785 events, corresponding to a statistical significance of 10.2 standard deviations (σ). Table 1 shows the results of the HESS observations of PG 1553+113. Figure 1 shows the on-source and normalized off-source distributions of the square of the angular difference between the reconstructed shower position and the source position (θ^2) for all observations. The background is approximately flat in θ^2 as expected, and there is a clear point-like excess of on-source events at small values of θ^2 , corresponding to the observed signal. The peak

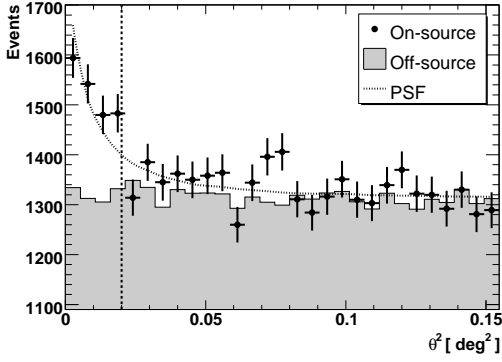


Figure 1: The distribution of θ^2 for on-source events (points) and normalized off-source events (shaded) from observations of PG 1553+113. The dashed curve represents the θ^2 distribution expected for a point source of VHE γ -rays at 40° zenith angle with a photon index $\Gamma = 4.5$. The vertical line represents the cut on θ^2 applied to the data.

of a two-dimensional Gaussian fit to a sky map of the observed excess is coincident with the position of PG 1553+113.

The photon spectrum for the entire data set is shown in Figure 2. These data are well fit (χ^2 of 8.4 for 5 degrees of freedom) by a power-law function, $dN/dE \sim E^{-\Gamma}$, with a photon index $\Gamma = 4.5 \pm 0.3_{\text{stat}} \pm 0.1_{\text{syst}}$. Fits of either a power law with an exponential cut-off or a broken power law do not yield significantly better χ^2 values.

The observed integral flux above 300 GeV for the entire data set is $I(>300 \text{ GeV}) = (4.6 \pm 0.6_{\text{stat}} \pm$

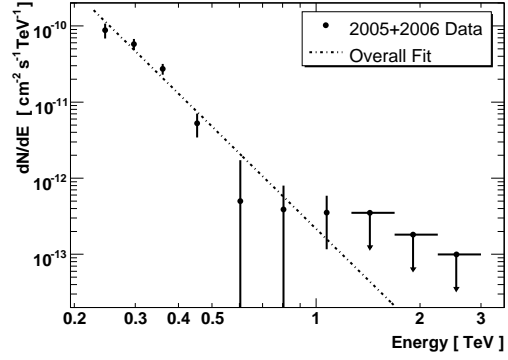


Figure 2: The overall VHE energy spectrum observed from PG 1553+113. The dashed line represents the best χ^2 fit of a power law to the observed data. The upper limits are at the 99% confidence level [7]. Only the statistical errors are shown.

$0.9_{\text{syst}}) \times 10^{-12} \text{ cm}^{-2} \text{ s}^{-1}$. This corresponds to $\sim 3.4\%$ of $I(>300 \text{ GeV})$ determined from the HESS Crab Nebula spectrum [3]. The integral flux, $I(>300 \text{ GeV})$, is shown in Table 1 for each year of observations. Figure 3 shows the flux measured for each dark period. There are no indications for flux variability on any time scale within the HESS data. The data previously published [3] for HESS observations of PG 1553+113 in 2005 were not corrected for long-term changes in the optical sensitivity of the instrument. Relative to a virgin telescope, the total optical throughput was decreased by 29% in 2005 and 33% in 2006. Correcting [3] for this decrease, using efficiencies determined from simulated and observed muon events, increases the flux measured from the object. The effect of this correction is larger for soft spectrum sources than it is for hard spectrum sources. Due to the correction, the flux measured in 2005 is three times higher than previously published.

On July 24 and 25, 2006, PG 1553+113 was observed by the Suzaku X-ray satellite ([13], Suzaku Observation Log: <http://www.astro.isas.ac.jp/suzaku/index.html.en>). On these two dates HESS observed PG 1553+113 for 3.1 hours live time, resulting in a marginally significant excess of 101 events (3.9σ). The average flux measured on these two nights is $I(>300 \text{ GeV}) = (5.8 \pm 1.7_{\text{stat}} \pm 1.2_{\text{syst}}) \times 10^{-12} \text{ cm}^{-2} \text{ s}^{-1}$.

Table 1: Shown are the excess, the significance of the excess, and the integral flux above 300 GeV, from HESS observations of PG 1553+113. The flux units are $10^{-12} \text{ cm}^{-2} \text{ s}^{-1}$. The systematic error on the flux is 20% and is not shown.

Epoch	Time [h]	Excess	Sig [σ]	$I(>300 \text{ GeV})$ [f.u.]
2005	7.6	249	6.0	5.44 ± 1.23
2006	17.2	536	8.3	4.22 ± 0.72
Total	24.8	785	10.2	4.56 ± 0.62

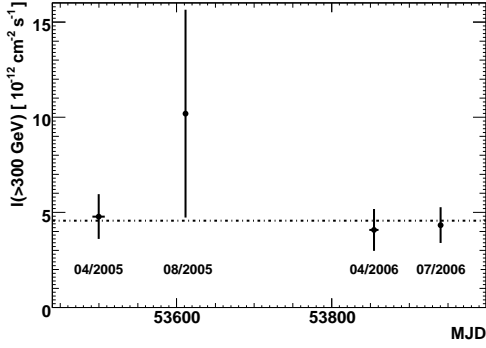


Figure 3: The integral flux, $I(>300 \text{ GeV})$, measured by HESS from PG 1553+113 during each dark period of observations. The horizontal line represents the average flux for all the HESS observations. Only the statistical errors are shown.

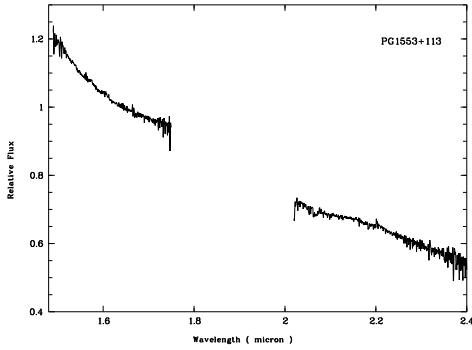


Figure 4: The measured H+K-band spectrum of PG 1553+113 in relative flux units. The gap is due to the highly reduced atmospheric transmission between H and K bands.

SINFONI Near-IR Spectroscopy

The determination of the redshift of an AGN is generally based upon the detection of emission or absorption lines in its spectrum. In an attempt to detect absorption features from the host galaxy or emission lines from the AGN, H+K ($1.50\text{--}2.40\mu\text{m}$) spectroscopy of PG 1553+113 was performed with SINFONI, an integral field spectrometer mounted at Yepun, Unit Telescope 4 of the ESO Very Large Telescope in Chile. The source was observed on March 9, 2006 and March 15, 2006. The resulting images are spatially unresolved and no underlying host galaxy is detected.

The H+K-band spectrum of PG 1553+113 measured here is shown in Figure 4. The signal-to-noise reach is ~ 250 in the H-band and ~ 70 in the K-band. The observed near-IR spectrum is featureless apart from some residuals from the atmospheric corrections. Thus in neither the broad-band images nor in the spectrum are the influences of the gas of a host galaxy or the AGN detected, even though PG 1553+113 is bright in the IR. As a result, a redshift determination from these observations is not possible.

Discussion

As the redshift of PG 1553+113 is likely $z > 0.2$, the observed VHE spectrum should be strongly affected by VHE γ -ray absorption on the EBL. If the redshift were known the spectrum intrinsic to the source could be reconstructed assuming a model of the EBL density. However, the EBL SED is not well-determined. Using a *Maximal* EBL model at the level of the upper limits from [2] or a *Minimal* model near the EBL lower limits from galaxy counts [12] can yield a significantly different intrinsic spectrum. Figure 5 shows the intrinsic spectrum versus redshift for both the *Maximal* and *Minimal* EBL parameterizations. Here, scaled models of [13] are used, exactly as described in [3]. The redshift of the AGN can be limited using assumptions for the intrinsic spectrum. Assuming the intrinsic photon index is not harder than $\Gamma_{\text{int}} = 1.5$, a limit of $z < 0.69$ is thus determined from the *Minimal* EBL model.

Conclusion

With a $\sim 25 \text{ h}$ data set, ~ 3 times larger than previously published [3], the HESS signal from PG 1553+113 is now highly significant ($\sim 10\sigma$). Thus the evidence for VHE emission from PG 1553+113 previously reported is now clearly verified. However, the flux observed in 2005 is now ~ 3 times higher than initially reported due to an improved calibration of the absolute energy scale of HESS, and agrees well with the flux measured in 2005 by MAGIC [6]. The statistical error on the VHE photon index is still rather large (~ 0.3), primarily due to the extreme softness of

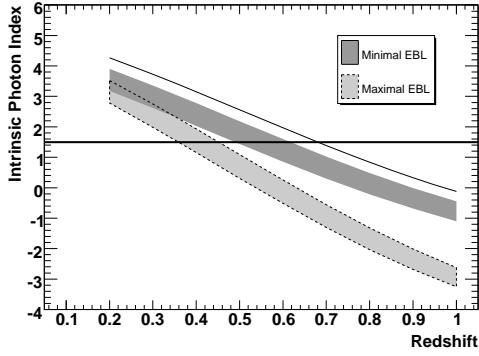


Figure 5: The photon index Γ_{int} determined from a power-law fit to the intrinsic spectrum of PG 1553+113 (i.e. the H.E.S.S. data de-absorbed with an EBL model) for a range of redshifts. The contours reflect the 1σ statistical uncertainty of the fits. The upper curve is the sum of Γ_{int} for the “Minimal” model and twice its statistical error.

the observed spectrum ($\Gamma = 4.5$). The total HESS exposure on PG 1553+113 is ~ 25 hours. Barring a flaring episode, not yet seen in two years of observations, a considerably larger total exposure (~ 100 hours) would be required to significantly improve the spectral measurement. However, the VHE flux from other AGN is known to vary dramatically and even a factor of a few would reduce the observation requirement considerably. Should such a VHE flare occur, not only will the error on the measured VHE spectrum be smaller, but the measured photon index may also be harder (see, e.g., [1]). Both effects would dramatically improve the redshift constraints and correspondingly the accuracy of the source modeling. Therefore, the VHE flux from PG 1553+113 will continue to be monitored by HESS. In addition, the soft VHE spectrum makes it an ideal target for the lower-threshold HESS Phase-II [15] which should make its first observations in 2009.

Acknowledgements

The support of the Namibian authorities and of the University of Namibia in facilitating the construction and operation of H.E.S.S. is gratefully acknowledged, as is the support by the German Ministry for Education and Research (BMBF), the Max

Planck Society, the French Ministry for Research, the CNRS-IN2P3 and the Astroparticle Interdisciplinary Programme of the CNRS, the U.K. Science and Technology Facilities Council (STFC), the IPNP of the Charles University, the Polish Ministry of Science and Higher Education, the South African Department of Science and Technology and National Research Foundation, and by the University of Namibia. We appreciate the excellent work of the technical support staff in Berlin, Durham, Hamburg, Heidelberg, Palaiseau, Paris, Saclay, and in Namibia in the construction and operation of the equipment. Based on ESO-VLT SIN-FONI program 276.B-5036 observations.

References

- [1] Aharonian, F., et al. (HEGRA Collaboration) 2002, *A&A*, 393, 89
- [2] Aharonian, F., et al. (HESS Collaboration) 2004, *Astroparticle Physics*, 22, 109
- [3] Aharonian, F., et al. (HESS Collaboration) 2006, *A&A*, 448, L19
- [4] Aharonian, F., et al. (HESS Collaboration) 2006, *Nature*, 440, 1018
- [5] Aharonian, F., et al. (HESS Collaboration) 2006, *A&A*, 457, 899
- [6] Albert, J., et al. 2007, *ApJ*, 654, L119
- [7] Benbow, W. 2005, *Proceedings of Towards a Network of Atmospheric Cherenkov Detectors VII* (Palaiseau), 163
- [8] Carangelo, N., et al. 2003, *ASP Conference Series*, 299, 299
- [9] Feldman, G.J. & Cousins, R.D. 1998, *Phys Rev D*, 57, 3873
- [10] Gould, R.J., & Schröder, G.P. 1967, *Phys Rev*, 155, 1408
- [11] Hauser, M.G. & Dwek, E. 2001, *ARA&A*, 39, 249
- [12] Madau, P. & Pozzetti, L. 2000, *MNRAS*, 312, L9
- [13] Primack, J.R., et al. 2001, *AIP Conference Proceedings*, 558, 463
- [14] Mitsuda, K., et al. 2007, *PASJ*, 59, 1
- [15] Punch, M. 2005, *Proceedings of Towards a Network of Atmospheric Cherenkov Detectors VII* (Palaiseau), 509
- [16] Sbarufatti, B., et al. 2006, *Astronomical Journal*, 132, 1



Observations of 1ES 1101–232 with H.E.S.S. and at lower frequencies: A hard spectrum blazar and constraints on the extragalactic background light

GERD PÜHLHOFER¹, WYSTAN BENBOW², LUIGI COSTAMANTE², HELENE SOL³, CATHERINE BOISSON³, DIMITRIOS EMMANOULOPOULOS¹, STEFAN WAGNER¹, DIETER HORNS⁴, BERRIE GIEBELS⁵, FOR THE H.E.S.S. COLLABORATION.

¹ *Landessternwarte, Universität Heidelberg, Königstuhl, D 69117 Heidelberg, Germany*

² *Max-Planck-Institut für Kernphysik, P.O. Box 103980, D 69029 Heidelberg, Germany*

³ *LUTH, UMR 8102 du CNRS, Observatoire de Paris, Section de Meudon, F-92195 Meudon Cedex, France*

⁴ *Institut für Astronomie und Astrophysik, Universität Tübingen, Sand 1, D 72076 Tübingen, Germany*

⁵ *Laboratoire Leprince-Ringuet, IN2P3/CNRS, Ecole Polytechnique, F-91128 Palaiseau, France*

G.Puehlhofer@lsw.uni-heidelberg.de

Abstract: VHE observations of the distant ($z=0.186$) blazar 1ES 1101–232 with H.E.S.S. are used to constrain the extragalactic background light (EBL) in the optical to near infrared band. As the EBL traces the galaxy formation history of the universe, galaxy evolution models can be tested with the data. In order to measure the EBL absorption effect on a blazar spectrum, we assume that usual constraints on the hardness of the intrinsic blazar spectrum are not violated. We present an update of the VHE spectrum obtained with H.E.S.S. and the multifrequency data that were taken simultaneously with the H.E.S.S. measurements. The data verify that the broadband characteristics of 1ES 1101–232 are similar to those of other, more nearby blazars, and strengthen the assumptions that were used to derive the EBL upper limit.

Introduction

The detection of VHE emission from 1ES 1101–232 with the H.E.S.S. Cherenkov telescopes has attracted particular attention for two reasons: The object has been the farthest detected VHE blazar with confirmed redshift ($z=0.186$), and at the same time it has exhibited a hard spectrum, with a photon index of $\Gamma \approx 2.9$ between 0.2 and 4 TeV. Both facts taken together allowed to place a limit on the density of the extragalactic background light (EBL) in the near-infrared band: under the assumption of a normal-behaved intrinsic emission spectrum of 1ES 1101–232, the energy density of the EBL at $1.5 \mu\text{m}$ has to be at or below $\nu F_\nu = 14 \text{ nWm}^{-2}\text{sr}^{-1}$ [1].

Here we present an update of the VHE spectrum and broadband data that were taken simultaneously to the H.E.S.S. data. We show that the hard γ -ray spectrum of 1ES 1101–232 is close to the borderline of what is possible to model using standard

one-zone blazar emission scenarios. On the other hand, from the broadband data there is no evidence that the emission characteristics of 1ES 1101–232 are not in agreement with those of the remaining class of VHE blazars. A detailed description of the results can also be found in [2].

H.E.S.S. data and EBL limit

Fig. 1 shows the spectrum of 1ES 1101–232, derived from the total H.E.S.S. data set of the years 2004 and 2005. Compared to the analysis results used in [1], an improved energy calibration of the telescope system was applied to the data [5]. For the given total data sample, this energy scale recalibration yields a safe energy threshold of 225 GeV (compared to 165 GeV used in [1]) and a flux normalisation increase of 27% at 1 TeV. After this correction, the systematic flux uncertainty is now estimated as 20% [5]. Reconstructed spectral indices were not affected significantly by these calibration

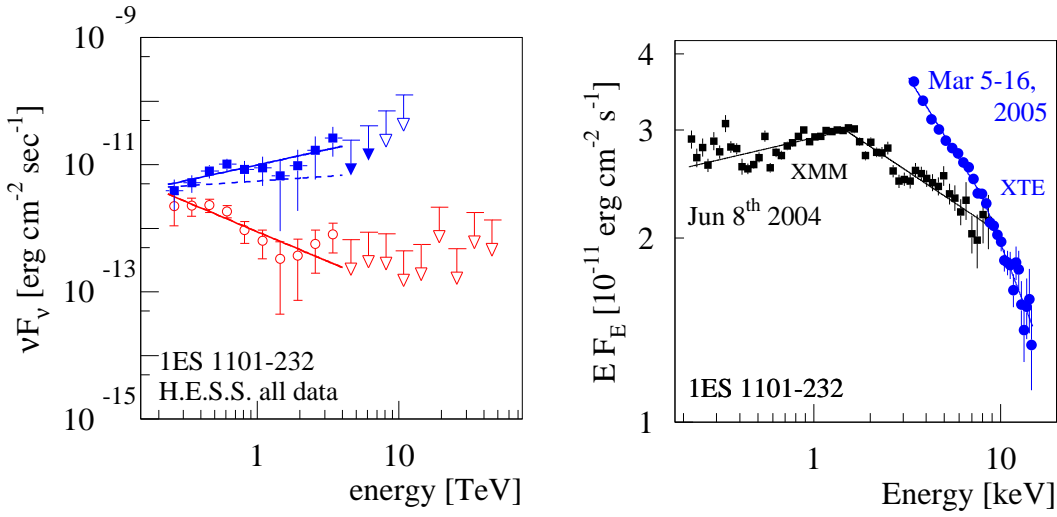


Figure 1: **Left panel:** VHE γ -ray spectrum of 1ES 1101–232, from the total H.E.S.S. data set of the years 2004 and 2005, in νF_ν -representation. The red, open circles denote the reconstructed flux as measured with H.E.S.S. The spectrum after correction for *maximum* EBL absorption with $14 \text{ nWm}^{-2}\text{sr}^{-1}$ at $1.5 \mu\text{m}$ is shown with blue, filled circles. Upper limits in the deabsorbed spectrum above 7 TeV are shown as open symbols only, because of strong EBL uncertainties at these high energies. The solid lines denote power-law fits between 0.2 and 4 TeV to the measured and deabsorbed spectra. The dashed line indicates the effect if the EBL level used for deabsorption would be lowered to $10 \text{ nWm}^{-2}\text{sr}^{-1}$ at $1.5 \mu\text{m}$. **Right panel:** X-ray spectra from observations taken simultaneously with the H.E.S.S. June 2004 (XMM-Newton) and March 2005 (RXTE) data.

	livetime	Γ_{abs}	$\Gamma_{\text{deabs,max}}$	$\Gamma_{\text{deabs,min}}$
EBL shape used for deabsorption			$P0.45$	$P0.34$
present day EBL shape			$P0.55$	$P0.40$
present day $\nu F_\nu(1.5 \mu\text{m})$			$14 \text{ nWm}^{-2}\text{sr}^{-1}$	$10 \text{ nWm}^{-2}\text{sr}^{-1}$
fit energy range		0.23–4.0 TeV	0.23–4.0 TeV	0.23–4.0 TeV
All Data	42.7 hrs	$2.94^{+0.20}_{-0.21}$	$1.51^{+0.17}_{-0.19}$	$1.85^{+0.18}_{-0.19}$
March 2005	31.6 hrs	$2.94^{+0.21}_{-0.23}$	$1.49^{+0.19}_{-0.20}$	$1.84^{+0.20}_{-0.21}$
June 2004	8.4 hrs	$3.16^{+0.48}_{-0.61}$	$1.70^{+0.47}_{-0.61}$	$2.05^{+0.47}_{-0.61}$

Table 1: Photon indices from power-law fits to the VHE spectra of 1ES 1101–232. Γ_{abs} are from fits to the measured spectra. $\Gamma_{\text{deabs,max}}$ are from fits to the deabsorbed spectra using the EBL shape $P0.45$, corresponding to the *maximum* EBL level with the present day shape $P0.55$ ($\nu F_\nu(1.5 \mu\text{m}) = 14 \text{ nWm}^{-2}\text{sr}^{-1}$) after scaling down by 15% to take galaxy evolution effects into account. $\Gamma_{\text{deabs,min}}$ represents the result if the EBL level is lowered to $\nu F_\nu(1.5 \mu\text{m}) = 10 \text{ nWm}^{-2}\text{sr}^{-1}$, at the level of the EBL lower limit from galaxy counts. Γ_{abs} and $\Gamma_{\text{deabs,max}}$ correspond to the fits shown as solid lines in Fig. 1, the fit corresponding to $\Gamma_{\text{deabs,min}}$ is shown as dashed line.

updates, the systematic error estimate for reconstructed photon indices is $\Delta\Gamma_{\text{sys}} \sim 0.1$ [1, 5]. Lacking the intrinsic blazar spectrum, one can assume a power-law type intrinsic spectrum with Γ_{deabs} and a typical EBL model around $1.5\,\mu\text{m}$. Then EBL absorption simply leads to a softening of the VHE spectrum above $\sim 100\,\text{GeV}$ of $\Delta\Gamma = \Gamma_{\text{abs}} - \Gamma_{\text{deabs}}$, where Γ_{abs} is the photon index of the measured spectrum. Using a template EBL spectrum “P” and scaling it with a factor p results in the relation $\Delta p = 0.34\Delta\Gamma$ [1].

The EBL has a *lower limit* from galaxy counts [3], with about $10\,\text{nWm}^{-2}\text{sr}^{-1}$ at $1.5\,\mu\text{m}$, corresponding to $P0.40$ using the scaled EBL scheme. Already with this smallest possible deabsorption, the VHE spectrum of 1ES 1101–232 is harder than $\Gamma_{\text{deabs}} = 2$ (see dashed line in Fig. 1), i.e. the intrinsic VHE power output peak of the source is above $\sim 3\,\text{TeV}$ for any EBL level.

The intrinsic spectrum of VHE blazars is expected to be not harder than 1.5, i.e. $\Gamma_{\text{deabs}} \geq 1.5$, taking the present observational and theoretical knowledge of VHE blazar spectra into account [1]. This translates into an *upper limit* of the EBL of $P0.55$. This *maximum* EBL has $14\,\text{nWm}^{-2}\text{sr}^{-1}$ at $1.5\,\mu\text{m}$. This limit is identical (within 1%) using either the spectrum used in [1], with $\Gamma_{\text{abs}} = 2.88$ between 0.16 - 3.3 TeV, or the recalibrated spectrum with $\Gamma_{\text{abs}} = 2.94$ between 0.23 - 4.0 TeV. We note that the limit at $1.5\,\mu\text{m}$ is quite insensitive to the choice of the EBL parametrisation, see [1], [4].

This EBL upper limit is in conflict with models such as the “fast evolution” model by [6] and the “best fit” model by [7], with an EBL density of about $\nu F_{\nu}(1.5\,\mu\text{m}) \simeq 20\,\text{nWm}^{-2}\text{sr}^{-1}$. Such high EBL levels would lead to an intrinsic spectrum of 1ES 1101–232 with $\Gamma_{\text{deabs}} \sim 1$. Such a Γ would isolate 1ES 1101–232 in the class of VHE blazars.

Broadband data and SED

Here we present truly simultaneous SEDs of 1ES 1101–232. The data show no indication for a $\Gamma \sim 1$ type spectrum in the synchrotron branch. 2004 H.E.S.S. observations were made in April and June (4 nights each). On June 8, 2004, XMM-Newton X-ray and optical monitor data were obtained. In March 2005, H.E.S.S., RXTE X-ray, and

ROTSE 3c optical data were taken simultaneously during 11 nights. The H.E.S.S. data did not reveal variability on any time scale. Also, the XMM-Newton data showed a constant flux. The nightly averaged light curve of the RXTE data showed mild variations of 15% (min-max), optical variations were below 10%. We note that the two X-ray spectra obtained in the two different years are quite different, see right panel of Fig. 1.

We therefore constructed two simultaneous SEDs, one for March 2005 and one for June 2004, see Fig. 2. The SED was modeled using a time-independent SSC model [8], with a one-zone homogeneous, spherical emitting region and a homogeneous magnetic field which propagates towards the observer. The high-energy electron distribution was modeled with a broken power law, with particle energy index p_1 between Lorentz factors γ_{min} and γ_{b} , and p_2 between γ_{b} and γ_{max} . Thin lines correspond to models with $p_1 = 2$ as expected from an uncooled, shock-accelerated particle distribution. Thick lines are models with $p_1 \simeq 1.5$, for instance from particle acceleration at strong shocks in a relativistic gas.

The $p_1=2$ models nicely reproduce the X-ray and optical data, but fail to fit the 2005 H.E.S.S. data. The $p_1=1.5$ model can marginally fit the 2005 H.E.S.S. data. An improved fit could be obtained if the EBL was below $\nu F_{\nu} = 14\,\text{nWm}^{-2}\text{sr}^{-1}$. Adopting the $p_1 \simeq 1.5$ models, one has to attribute the optical emission to a different emission zone (not modeled in Fig. 2), which is viable because of the lack of correlated variability arguments.

Conclusions

The VHE SED of 1ES 1101–232 peaks above 3 TeV. Nevertheless, a standard emission scenario can be used to essentially explain the broadband data of 1ES 1101–232, if the EBL used to deabsorb the VHE data is at or below $\nu F_{\nu}(1.5\,\mu\text{m}) = 14\,\text{nWm}^{-2}\text{sr}^{-1}$. H.E.S.S. observations of other distant VHE blazars (H 2356–309, 1ES 0347–121) confirm the low EBL level as deduced from the 1ES 1101–232 H.E.S.S. spectrum. The general “hardness” of the spectra of distant VHE blazars might be explained through the better VHE detectability of hard-spectrum sources.

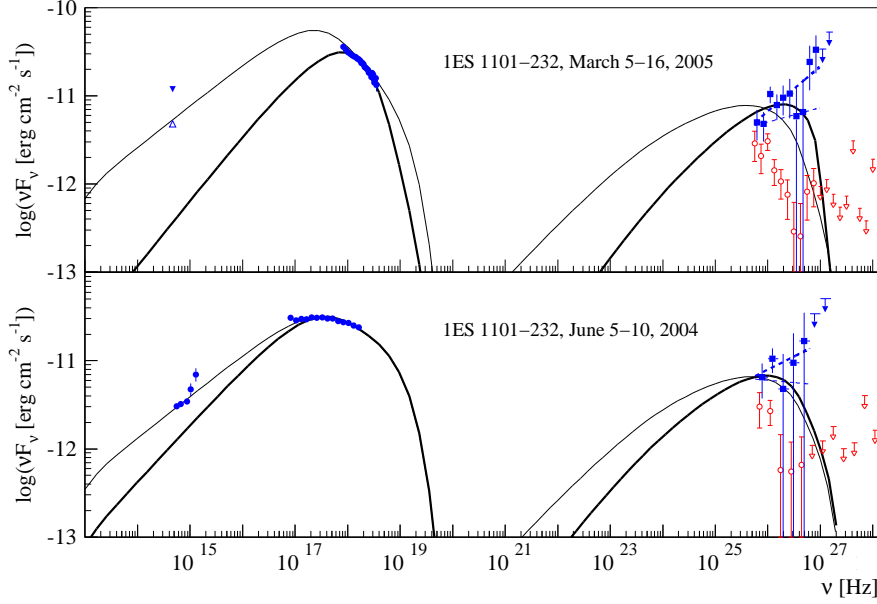


Figure 2: Spectral energy distribution of 1ES 1101–232. **Upper panel:** Data from March 5–16, 2005. In the VHE band, the measured H.E.S.S. spectrum (red, open symbols) and the deabsorbed spectrum using a maximum EBL level of $14 \text{ nWm}^{-2}\text{sr}^{-1}$ at $1.5 \mu\text{m}$ are shown. The thick dashed line is a power-law fit to the deabsorbed data as plotted, while the thin dashed line indicates the effect if the EBL is lowered to the minimum level of $10 \text{ nWm}^{-2}\text{sr}^{-1}$. X-ray data are from RXTE. In the optical band, an upper limit (filled triangle) and a tentative lower limit (open triangle) from ROTSE 3c data are shown. **Lower panel:** Data from June 2004. In the VHE band, H.E.S.S. data taken between June 5–10, 2004, are shown. X-ray and optical data were derived from an XMM-Newton pointing on June 8, 2004.

Acknowledgements

The support of the Namibian authorities and of the University of Namibia in facilitating the construction and operation of H.E.S.S. is gratefully acknowledged, as is the support by the German Ministry for Education and Research (BMBF), the Max Planck Society, the French Ministry for Research, the CNRS-IN2P3 and the Astroparticle Interdisciplinary Programme of the CNRS, the U.K. Particle Physics and Astronomy Research Council (PPARC), the IPNP of the Charles University, the South African Department of Science and Technology and National Research Foundation, and by the University of Namibia. We appreciate the excellent work of the technical support staff in Berlin, Durham, Hamburg, Heidelberg, Palaiseau, Paris, Saclay, and in Namibia in the construction and operation of the equipment. We thank the ROTSE collaboration for providing the ROTSE 3c optical data, and L. Ostorero for help with the optical data analysis.

References

- [1] Aharonian, F. A., et al. (H.E.S.S. Collaboration), *Nature*, 2006a, 440, 1018
- [2] Aharonian, F. A., et al. (H.E.S.S. Collaboration), *A&A*, 2007, 470, 475
- [3] Madau, P., & Pozzetti, L., *MNRAS*, 2000, 312, L9
- [4] Mazin, D., & Raue, M., *A&A*, 2007, 471, 439
- [5] Aharonian, F. A., et al. (H.E.S.S. Collaboration), *A&A*, 2006c, 457, 899
- [6] Stecker, F. W., Malkan, M. A., & Scully, S. T., *ApJ*, 2006, 648, 774
- [7] Kneiske, T. M., Bretz, T., Mannheim, K., Hartmann, D. H., *A&A*, 2004, 413, 807
- [8] Katarzyński, K., Sol, H., & Kus, A., *A&A*, 2001, 367, 809



Discovery of Two New TeV Blazars with the H.E.S.S. Cherenkov Telescope System

MARTIN RAUE¹, WYSTAN BENBOW², LUIGI COSTAMANTE², AND DIETER HORNS³

FOR THE H.E.S.S. COLLABORATION

¹*Institut für Experimentalphysik, Universität Hamburg, Luruper Chaussee 149, D-22761 Hamburg,* ²*MPI-K Heidelberg, P.O. Box 103980, D 69029 Heidelberg, Germany,* ³*Institut f. Astronomie und Astrophysik, Universität Tübingen, Sand 1, D 72076 Tübingen, Germany*

martin.raue@desy.de

Abstract: Since the new generation of imaging atmospheric-Cherenkov telescopes came online with the commissioning of the four telescopes of the H.E.S.S. experiment in 2004, the number of known extragalactic γ -ray emitters in the very high energy (VHE) domain has more than doubled. All of the sources detected so far are active galactic nuclei and all but one belong to the class of BL Lac objects. The emission process for VHE γ -rays in this class of objects is not fully understood and a large sample of sources and multi-wavelength data is needed to discriminate between different models. Furthermore, VHE photons from these distant sources are attenuated via pair production with the extragalactic photon field in the optical to infrared wavelength band (extragalactic background light, EBL), which contains cosmological information on the star and galaxy formation history. With assumptions about the source physics, limits on this photon field can be derived. We report the detection of VHE gamma-rays from the BL Lac 1ES 0229+200 ($z = 0.14$) and 1ES 0347-121 ($z = 0.1880$) with the H.E.S.S. Cherenkov telescope system. 1ES 0347-121 is among the most distant source detected in VHE gamma-rays to date.

Introduction

The H.E.S.S. collaboration operates an array of four large imaging atmospheric-Cherenkov telescopes (107 m² mirror area per telescope; $\sim 5^\circ$ field of view) located in the Southern hemisphere in Namibia (1800 m a.s.l.) [21]. H.E.S.S. observes very high energy (VHE; >100 GeV) γ -rays from many types of astrophysical objects. About one third of the H.E.S.S. observation time (~ 300 hours) is dedicated to study active galactic nuclei (AGN). In the following the detection of VHE γ -rays from two AGNs of the BL Lac class 1ES 0347-121 and 1ES 0229+200 is reported. Details on the discoveries and the implication for the extragalactic background light (EBL) are discussed in [3] and [6]

Methods

H.E.S.S. takes data during dark moonless nights. The data are calibrated [2] and an image analy-

sis provides properties of the primary particle like arrival direction, energy and particle type. The telescopes operate in coincidence mode to allow a stereoscopic event reconstruction [13]. Usually the data is recorded in *wobble mode* where the telescope point with and offset of 0.5° to the nominal source position to allow a simultaneous estimation of the background. The data presented here has been analyzed with a standard Hillas-type analysis as described in [4]. The signal is extracted from a circular region around the source position, the background (off-source data) is estimated using the *Reflected-Region* method [13]

1ES 0347-121

1ES 0347-121 was discovered in the Einstein Slew Survey and was later classified as an BL Lac object [11, 17]. Located at a redshift of $z = 0.1880$ it harbours a super massive black hole of mass $\log(M_{\text{BH}}/M_{\text{Sun}}) = 8.02 \pm 0.11$ [20]. [18] used simple physical considerations about the

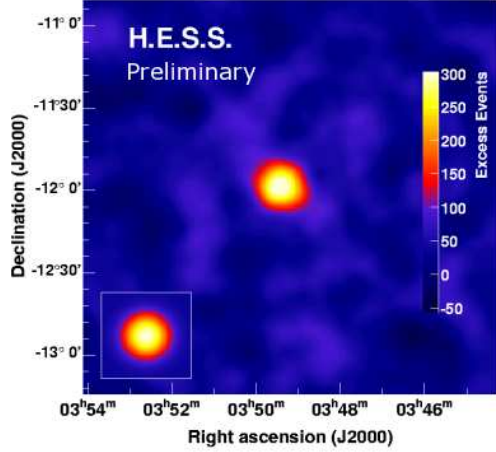


Figure 1: Smoothed sky-map of excess events centered on the position of 1ES 0347-121 (ring background). An excess of 327 γ -ray candidates is detected corresponding to a statistical significance of 10.1 standard deviations.

synchrotron and inverse Compton component of the spectrum to predict the flux above 0.3 TeV of $3.8 \times 10^{-12} \text{ cm}^{-2} \text{ s}^{-1}$, which should easily be detectable with H.E.S.S. An upper limit on the integral flux above an energy threshold of 1.46 TeV of $5.14 \times 10^{-12} \text{ cm}^{-2} \text{ s}^{-1}$ (0.56 Crab) has been reported by the HEGRA collaboration [2], considerably higher than the flux estimate from [18].

The H.E.S.S. observations of 1ES 0347-121 were carried out between August and December 2006. 25.4 h (corrected for the detector downtime) of good-quality data was recorded. The zenith angles of the observations ranged from 12 to 40° , with a mean zenith angle of $\sim 19^\circ$. The analysis energy threshold for the observation is ~ 250 GeV.

An excess of 327 γ -ray candidates was found corresponding to a statistical significance of 10.1 standard deviations (Fig. 1). The extension of the excess is compatible with a point-source whose position coincides with that of 1ES 0347-121. The VHE flux is constant during the H.E.S.S. observation period (Fig. 2).

The VHE energy spectrum, ranging from ~ 250 GeV to >3 TeV, is well described by a power law with a photon index of $\Gamma \sim 3.1$. The integral flux above 250 GeV corresponds to $\sim 2\%$

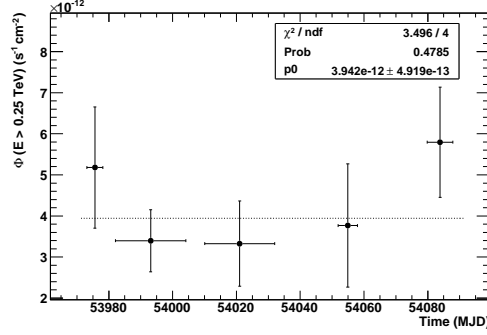


Figure 2: Monthly averaged light-curve of 1ES 0347-121. No significant variability is detected in the H.E.S.S. data-set. The dashed line is the fit of a constant function to the light-curve (parameters are given in the figure).

of the flux of the Crab Nebula above the same threshold.

1ES 0229+200

The active galactic nucleus (AGN) 1ES 0229+200 was initially discovered in the *Einstein* IPC Slew Survey [11] and later identified as a BL Lac object [17]. It is now classified as a high-frequency peaked BL Lac (HBL) due to its X-ray-to-radio flux ratio [14]. The HBL is hosted [12] by an elliptical galaxy $M_R = -24.53$ located at a redshift of $z = 0.14$ [17]. Based on its spectral energy distribution (SED) and its relative proximity, 1ES 0229+200 was suggested [9, 18] as a potential source of VHE γ -rays. However, despite several attempts, it has not been previously detected in the VHE regime. The HEGRA [2], Whipple [10, 16], and Milagro [19] collaborations have each reported upper limits on the flux from 1ES 0229+200 during various epochs. The most constraining upper limit (99.9% confidence level) on the flux is $I(>410 \text{ GeV}) < 2.76 \times 10^{-12} \text{ cm}^{-2} \text{ s}^{-1}$, based on ~ 1 hour of HESS observations made in 2004 [3].

1ES 0229+200 was observed with the H.E.S.S. array for a total of 70.3 h (161 runs of ~ 28 min each) in 2005 and 2006 [6]. After applying the standard HESS data-quality selection, 98 runs remain yielding an exposure of 41.8 h live time at a mean zenith angle $Z_{\text{mean}} = 46^\circ$. The event-selection criteria

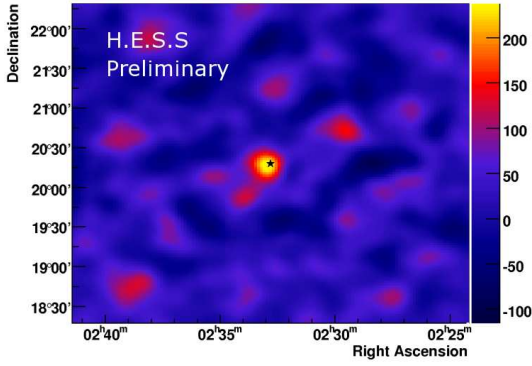


Figure 3: Smoothed sky-map of excess events centered on the position of 1ES 0229+200 (ring background). An excess of 261 γ -ray candidates is detected corresponding to a statistical significance of 6.6 standard deviations.

are performed using the *standard cuts* [6] resulting in a post-analysis energy threshold of 580 GeV at Z_{mean} . Results consistent with those presented below are also found using independent calibration and/or analysis chains.

A significant excess of 261 events (6.6σ) from the direction of 1ES 0229+200 is detected in the total data set (Fig. 3). The VHE flux is constant during the H.E.S.S. observation period (Fig. 4) and the integral flux above 580 GeV corresponds to $\sim 2\%$ of the flux of the Crab Nebula above the same threshold. The VHE energy spectrum, ranging from ~ 500 GeV to ~ 10 TeV, is well described by a hard power law with a photon index of $\Gamma \sim 2.5$.

Discussion & Conclusion

BL Lac objects show highly variable emission in many wavelength bands. To understand and model the VHE emission processes in these objects contemporaneous multi-wavelength observations are necessary.

1ES 0347-121 has been observed by the SWIFT satellite at X-rays and UV/optical wavelengths and by the ATOM optical telescope during the H.E.S.S. observation periods [3]. The resulting broadband spectral energy distribution (SED) can be described by a simple one-zone synchrotron-self-

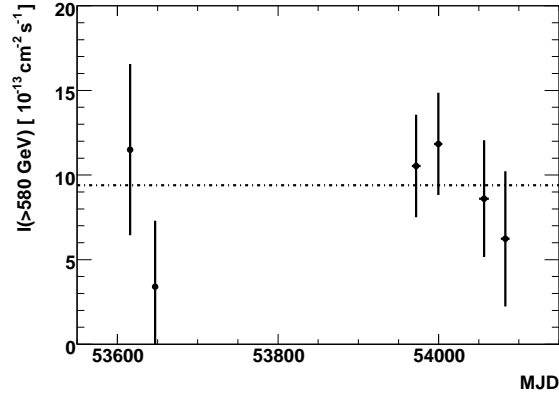


Figure 4: Monthly averaged light-curve of 1ES 0229+200. No significant variability is detected in the H.E.S.S. data-set. The dashed line corresponds to the average flux.

Compton model, though the data does not strongly constrain the model parameters. Due to the lack of contemporaneous X-ray data for 1ES 0229+200 an accurate modeling of the source is not possible.

The VHE spectra from both sources enable the determination of stringent upper limit on the extragalactic background light (EBL) in the ultraviolet to near-IR wavelength region. These limits are reported in [3] and [6].

Future VHE monitoring of 1ES 0347-121 and 1ES 0229+200, to search for high flux states (flares), is highly desirable. To derive stronger constraints on the emission models, further contemporaneous multiwavelength observations are also necessary.

Acknowledgements

The support of the Namibian authorities and of the University of Namibia in facilitating the construction and operation of H.E.S.S. is gratefully acknowledged, as is the support by the German Ministry for Education and Research (BMBF), the Max Planck Society, the French Ministry for Research, the CNRS-IN2P3 and the Astroparticle Interdisciplinary Programme of the CNRS, the U.K. Science and Technology Facilities Council (STFC), the IPNP of the Charles University, the Polish Ministry of Science and Higher Education, the South African Department of Science and Technology and Na-

tional Research Foundation, and by the University of Namibia. We appreciate the excellent work of the technical support staff in Berlin, Durham, Hamburg, Heidelberg, Palaiseau, Paris, Saclay, and in Namibia in the construction and operation of the equipment.

Ray Astronomy, ed. F. A. Aharonian, H. J. Völk, & D. Horns, 499–504, 2005.

[20] J.-H. Woo, C. M. Urry, R. P. van der Marel, P. Lira and J. Maza. *ApJ*, 631:762, 2005.

References

- [1] F. Aharonian et al. (*HEGRA Collaboration*). *A&A*, 421:529, 2004.
- [2] F. Aharonian et al. (*H.E.S.S. Collaboration*). *Astroparticle Physics*, 22:109, 2004.
- [3] F. Aharonian et al. (*H.E.S.S. Collaboration*). *A&A*, 441:465, 2005.
- [4] F. Aharonian et al. (*H.E.S.S. Collaboration*). *A&A*, 457:899, 2006.
- [5] F. Aharonian et al. (*H.E.S.S. Collaboration*). *A&A*, submitted, 2007.
- [6] F. Aharonian et al. (*H.E.S.S. Collaboration*). *A&A*, submitted, 2007.
- [7] W. Benbow. *Towards a Network of Atmospheric Cherenkov Detectors VII (Palaiseau)*, 163, 2005.
- [8] D. Berge, S. Funk and J. Hinton. *A&A*, 455:1219, 2007.
- [9] L. Costamante, G. Ghisellini, P. Giommi et al. *A&A*, 371:512, 2001.
- [10] I. de la Calle Pérez, I. H. Bond, P. J. Boyle et al. *ApJ*, 599:909, 2003.
- [11] M. Elvis, D. Plummer, J. Schachter and G. Fabbiano. *ApJS*, 80:257, 1992.
- [12] R. Falomo and J. K. Kotilainen. *A&A*, 352:85, 1999.
- [13] S. Funk, G. Hermann, J. Hinton et al. *Astroparticle Physics*, 22:285, 2004.
- [14] P. Giommi, S. G. Ansari and A. Micol. *A&AS*, 109:267, 1995.
- [15] J. A. Hinton. *New Astronomy Review*, 48:331, 2004.
- [16] D. Horan, H. M. Badran, I. H. Bond et al. *ApJ*, 603:51, 2004.
- [17] J. F. Schachter, J. T. Stocke, E. Perlman et al. *ApJ*, 412:541, 1993.
- [18] F. W. Stecker, O. C. de Jager and M. H. Salamon. *ApJL*, 473:L75, 1996.
- [19] D. A. Williams and MILAGRO Collaboration. *American Institute of Physics Conference Series*, Vol. 745, *High Energy Gamma-*

Discovery of VHE gamma-rays from the BL Lac object PKS 0548-322 with H.E.S.S.

G. SUPERINA¹, W. BENBOW², T. BOUTELIER³, G. DUBUS³, B. GIEBELS¹.

¹*LLR, Ecole Polytechnique, CNRS-IN2P3, 91128 Palaiseau, France*

²*Max-Planck-Institut für Kernphysik, P.O. 103980, Heidelberg, Germany*

³*LAOG, CNRS-INSU, 38400 Saint-Martin d'Hères, France*

superina@poly.in2p3.fr

Abstract: Observations and monitoring of active galactic nuclei (AGN) are a key part of the scientific observation programme of the High Energy Stereoscopic System (H.E.S.S.). The instrument was used to search for very high energy (VHE: > 100 GeV) gamma rays coming from PKS 0548-322, a BL Lac object visible from the Southern Hemisphere. An excess of VHE gamma rays ($\sim 6\sigma$) from the object is detected. The broad-band spectral energy distribution (SED), including the VHE spectrum ($\Gamma = 2.8 \pm 0.3_{\text{stat}}$) is presented.

Introduction

PKS 0548-322, at a redshift of $z = 0.069$ is among the closest blazars of the Southern sky. This extreme BL Lac is a promising source for VHE emission [5] so H.E.S.S. dedicated time (~ 45 hours) between 2004 and 2006 to its observation. The X-ray spectrum of this source has a rich history. The reported spectral indices show significant scatter (see [4] and [7]), with no well-defined correlation to the X-ray intensity. The X-ray fluxes and spectral indices of PKS 0548-322 show that the frequency of the synchrotron peak can vary from less than 1 keV to more than 20 keV, without any apparent correlation with the X-ray flux ([3]).

Analysis Technique and Results

A total of 21.3 hours of good-quality data remain after application of quality-selection criteria and dead-time correction. The data are analyzed with the 3D-model method [6], where a model is used to reconstruct a 3D picture of the detected shower. For each detected shower, the direction, energy and 3D-width (used for gamma-hadron separation) are reconstructed.

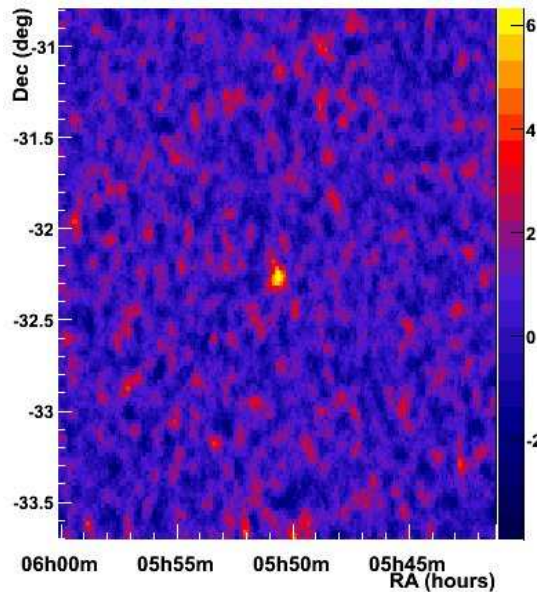


Figure 1: Preliminary significance map centred on the position of the point-like source PKS 0548-322.

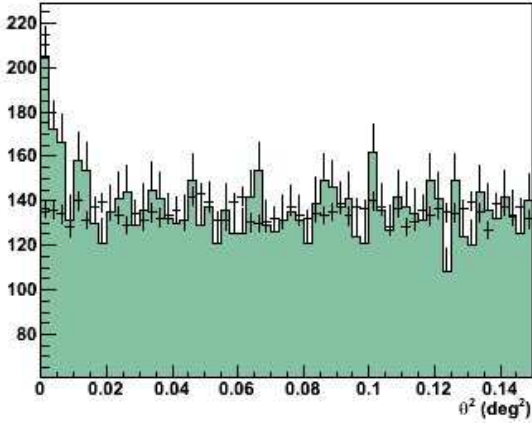


Figure 2: Distribution of θ^2 for on-source and normalized off-source events (preliminary). The excess is clearly visible in the region $\theta^2 \leq 0.01 \text{ deg}^2$ corresponding to a statistical significance of 5.8σ .

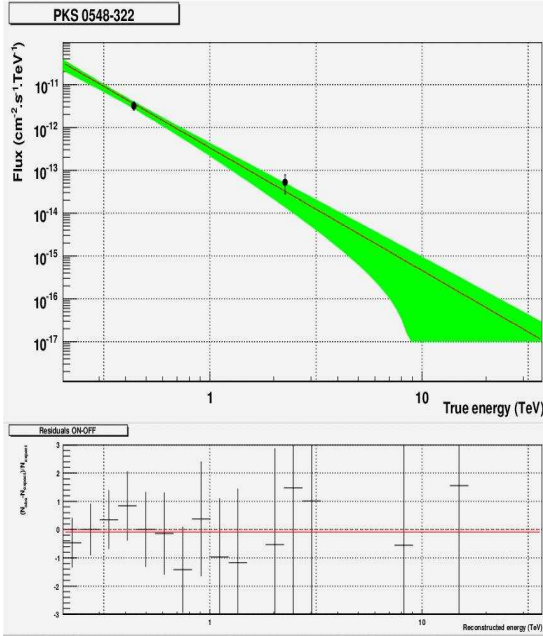


Figure 3: VHE spectrum of PKS0548-322 (preliminary). The shaded region represents the 1-sigma confidence bounds of the fitted spectrum (power-law hypothesis).

Gamma-ray-like events are selected using cuts on image size, 3D-width, and telescope multiplicity. For this analysis, only events that triggered at least three telescopes are kept, in order to have better gamma-hadron separation.

The significance map of PKS 0548-322 is shown in Figure 1. The distribution of squared angular distance from the source is given in Figure 2. The analysis yields an excess of 181 gamma rays, corresponding to a significance of 5.8 standard deviations. The differential energy spectrum is presented in Figure 3. For a simple power-law hypothesis, the likelihood maximization yields a spectral index of $2.8 \pm 0.3_{\text{stat}} \pm 0.1_{\text{sys}}$ and an integral flux above the energy threshold: $(I > 200 \text{ GeV}) = (3.3 \pm 0.7) 10^{-12} \text{ cm}^{-2} \text{ s}^{-1}$. This corresponds to $\sim 1.4\%$ of the HESS Crab Nebula flux [1] above the same threshold. No evidence for flux variability is seen in these data.

Spectral Energy Distribution

A simple homogeneous one-zone synchrotron self Compton (SSC) model (code from G.Dubus) is used to characterize the SED of PKS 0548-322 :

- the low-frequency emission, extending up to X-ray energies, is most likely due to synchrotron radiation of high-energy electrons.

- the VHE emission is believed to be produced through Compton upscattering of seed photons by the same population of relativistic electrons.

This model is adapted to the data of a soft state (X-ray data from BeppoSAX and RXTE) as well as of a hard state (BeppoSAX only). The HESS data derived from the spectrum (circles -opened: observed data, filled: intrinsic spectrum, i.e with the effects of EBL absorption removed using the upper limit of [2]) are well fitted, simultaneously, with either of these two sets of archival X-ray data.

Conclusions

Observations performed by H.E.S.S from 2004 up to 2006 have established PKS 0548-322 as a VHE gamma-ray source. It is among the closest TeV blazars discovered. Given its X-ray behaviour, the source is a very interesting object for understanding its VHE emission and discriminating between

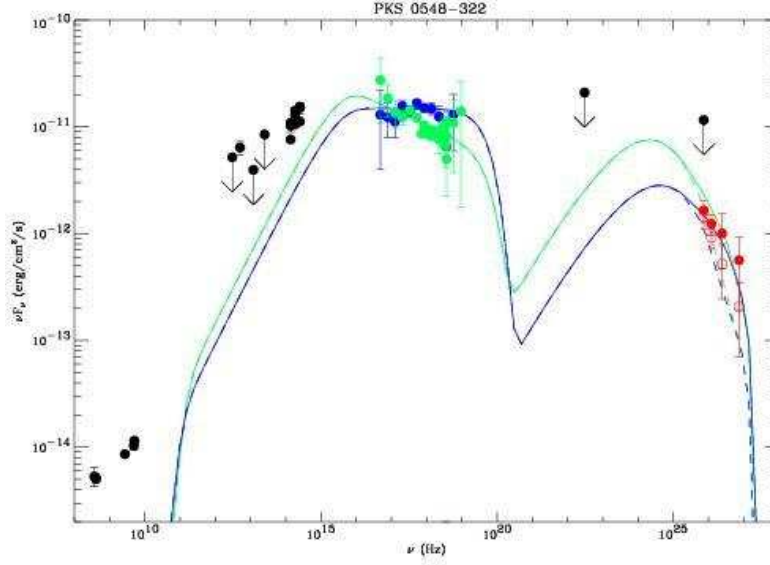


Figure 4: Preliminary spectral energy distribution of PKS 0548-322, modelled for both a soft and a hard X-ray state. Using a model with a reasonable set of parameters provides a satisfactory fits to the archival X-ray and VHE data. The emitting region is characterised by a Doppler factor $\delta = 20$, a magnetic field $B = 0.6$ G and a region blob size of $R \sim 2 \times 10^{15}$ cm.

different models. Quasi-simultaneous Swift data were taken during the 2006 H.E.S.S. observations and will later be used in a more detailed SED study.

Acknowledgements

The support of the Namibian authorities and of the University of Namibia in facilitating the construction and operation of H.E.S.S. is gratefully acknowledged, as is the support by the German Ministry for Education and Research (BMBF), the Max Planck Society, the French Ministry for Research, the CNRS-IN2P3 and the Astroparticle Interdisciplinary Programme of the CNRS, the U.K. Science and Technology Facilities Council (STFC), the IPNP of the Charles University, the Polish Ministry of Science and Higher Education, the South African Department of Science and Technology and National Research Foundation, and by the University of Namibia. We appreciate the excellent work of the technical support staff in Berlin, Durham, Hamburg, Heidelberg, Palaiseau, Paris,

Saclay, and in Namibia in the construction and operation of the equipment.

References

- [1] Aharonian et al. *Astron.Astrophys.*, 457:899–915, 2006.
- [2] Aharonian et al. *Nature*, 440:1018–1021, 2006.
- [3] Barr et al. *Astrophysical Journal*, 324:11–15, 1981.
- [4] Bradford et al. *Astrophysical Journal*, 233, 1979.
- [5] Costamante et al. *Astron.Astrophys.*, 371:512–526, 2001.
- [6] Lemoine et al. *Astropart. Phys.*, 25, 2006.
- [7] Worrall et al. *Astrophysical Journal*, 243:53–59, 1981.



Upper Limits from HESS Observations of AGN in 2005-2007

W. BENBOW¹ AND R. BÜHLER¹ FOR THE HESS COLLABORATION

¹ *Max-Planck-Institut für Kernphysik, Heidelberg, Germany*

Wystan.Benbow@mpi-hd.mpg.de

Abstract: Very high energy (VHE; >100 GeV) observations of a sample of selected active galactic nuclei (AGN) were performed between January 2005 and April 2007 with the High Energy Stereoscopic System (HESS), an array of imaging atmospheric-Cherenkov telescopes. Significant detections are reported elsewhere for many of these objects. Here, integral flux upper limits for twelve candidate very-high-energy (VHE; >100 GeV) gamma-ray emitters are presented. In addition, results from HESS observations of four known VHE-bright AGN are given although no significant signal is measured. For three of these AGN (1ES 1101–232, 1ES 1218+304, and Mkn 501) simultaneous data were taken with the Suzaku X-ray satellite.

Introduction

The HESS array [11] of four imaging atmospheric-Cherenkov telescopes located in Namibia is used to search for VHE γ -ray emission from various classes of astrophysical objects. Approximately 300 hours per year, $\sim 30\%$ of the total observation budget, are dedicated to HESS studies of AGN. These observations are divided between monitoring the flux of known VHE-bright AGN and searching for new VHE sources. For the monitoring observations, an AGN is typically observed for a few hours, distributed over several nights, a month for ~ 3 months, with the hopes of detecting a bright flaring episode (see, e.g., [5]). In the discovery part of the AGN program, a candidate from a large, diverse sample of relatively nearby AGN is typically observed for ~ 10 hours. If any of these observations show an indication for a signal (e.g., an excess with significance more than ~ 3 standard deviations), a deeper exposure is promptly scheduled to increase the overall significance of the detection and to allow for a spectral measurement.

The targets of HESS AGN observations are primarily blazars, a class which includes both BL Lac objects and Flat Spectrum Radio Quasars (FSRQ). The spectral energy distributions (SEDs) of these objects are generally characterized by two peaks: a lower-energy one in the optical to X-ray regime,

and another which potentially extends to γ -ray energies. Based on their SEDs, BL Lacs are generally categorized into groups that are either low (LBL), intermediate (IBL), or high-frequency-peaked (HBL). An overwhelming majority of VHE-emitting AGN are HBL, therefore these objects are the primary targets of HESS AGN observation program. However, prominent examples of different types of AGN are also observed with the hopes of detecting new AGN classes. These include radio-loud objects such as Fanaroff-Riley (FR) galaxies and narrow line Seyfert (NLS) galaxies, and radio-weak objects like typical Seyfert (Sy) galaxies, all of which come in several types (generally I or II).

For all the following results, the HESS standard analysis [6] is used. All upper limits are given at the 99% confidence level [7]. The flux quantities are calculated assuming a power-law spectrum with photon index $\Gamma=3.0$, with the exception of those for 1ES 1101–232 where $\Gamma=2.94$, as measured [4] in 2004-05, is chosen. The reported values change by less than $\sim 10\%$ when a different photon index (i.e. Γ between 2.5 and 3.5) is assumed. The effects of changes in the absolute optical efficiency of HESS are corrected for using efficiencies determined from simulated and observed muons [3]. The systematic error on all flux quantities is estimated to be $\sim 20\%$.

Table 1: The candidate AGN in groups of blazars and non-blazars. The asterisk denotes the four candidates detected by the EGRET satellite [9]. The redshift (z), total good-quality live time (T), mean zenith angle of observation (Z_{obs}), the observed excess and significance (S) are shown. Integral flux upper limits above the energy threshold of the observations (E_{th}), and the corresponding percentage of the HESS Crab Nebula flux [3] above the same threshold, are also shown. The flux units are $10^{-12} \text{ cm}^{-2} \text{ s}^{-1}$. The \dagger represents the six upper limits which are the most constraining ever reported for the object.

Object	z	Type	T [hrs]	Z_{obs} [$^{\circ}$]	Excess	S [σ]	E_{th} [GeV]	I(> E_{th}) [f.u.]	Crab %
<i>Blazar</i>									
III Zw 2	0.0893	FSRQ	1.7	37	12	1.4	420	5.36 †	6.4
BWE 0210+116*	0.250	LBL	6.0	43	-13	-0.9	530	0.72 †	1.2
1ES 0323+022	0.147	HBL	7.2	27	13	0.7	300	2.52	1.9
PKS 0521-365*	0.0553	LBL	3.1	26	11	0.8	310	5.40 †	4.2
3C 279*	0.536	FSRQ	2.0	26	5	0.5	300	3.98 †	2.9
RBS 1888	0.226	HBL	2.4	15	30	2.2	240	9.26	4.9
PKS 2316-423	0.055	IBL	4.1	20	29	1.6	270	4.74	3.0
1ES 2343-151	0.226	IBL	8.6	17	-16	-0.6	230	2.45 †	1.2
<i>Non-blazar</i>									
NGC 1068	0.00379	Sy II	1.8	29	9	1.1	330	5.76	4.9
Pictor A	0.0342	FR II	7.9	31	-23	-1.1	320	2.45	2.0
PKS 0558-504	0.137	NLS I	8.3	28	-14	-0.7	310	2.38 †	1.8
NGC 7469	0.0164	Sy I	3.4	34	-14	-1.3	330	1.38	1.2

Limits from Discovery Observations

Twenty-nine AGN were observed by HESS from January 2005 through April 2007. Some of these objects were previously shown by HESS to emit VHE γ -rays, and the discoveries of VHE emission from others are reported elsewhere. Of the remaining AGN with non-zero good-quality exposure, twelve show no indication of any VHE emission. As many of the HBL observed by HESS have been detected, the twelve candidates discussed in this section are largely not HBL. Table 1 shows these AGN, their redshift and AGN type, as well as details of their observations. The mean good-quality exposure for the candidates is 4.7 hours live time at a mean zenith angle of 28° . In 5 hours of observations, the sensitivity of HESS [6] enables a 5σ detection of an $\sim 2\%$ Crab Nebula flux source at 20° zenith angle.

As mentioned previously, no significant excess of VHE γ -rays is found from any of these twelve AGN in the given exposure time. Figure 1 shows

the distribution of the significance observed from the direction of each AGN. The measured excess, corresponding significance and resulting integral flux limits are given in Table 1 for each AGN. Six of the upper limits are the most constraining ever reported from these objects, and the other six limits are only surpassed by those from HESS observations in 2004 [1]. Combining the excess from all twelve candidates only yields a total of 29 events and a statistical significance of 1.1σ . No significant excess is found in a search for serendipitous source discoveries in the HESS field-of-view centered on each of the AGN. Further, as the nightly flux from each target is well-fit by a constant, no evidence for VHE flares is found from any of the twelve AGN.

Low Altitude HESS Observations

Three northern AGN, known to emit VHE γ -rays, were briefly (good-quality live time < 2.2 h) observed at low altitudes with HESS. At such al-

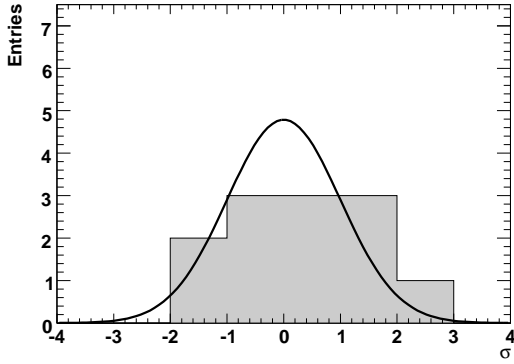


Figure 1: Distribution of the significance observed from the twelve candidate AGN. The curve represents a Gaussian distribution with zero mean and a standard deviation of one.

titudes the threshold of HESS is higher and the sensitivity is reduced. However, observations at low altitudes sample the VHE spectrum at much higher energies than the typical near-zenith observations made with Cherenkov-telescope arrays. Simultaneous measurements of the same northern target with HESS and a Northern Hemisphere instrument enable both the determination of the object's spectrum over several orders of magnitude in energy, as well as cross-calibration between the instruments (see, e.g., [12]). For two of these targets (1ES 1218+304 and Mkn 501) simultaneous observations were successfully performed by the MAGIC VHE telescope and the Suzaku X-ray satellite [13].

HESS observed Mkn 421 on April 12, 2005. The good-quality exposure is 0.9 h live time at a mean zenith angle of 63° . A marginally significant excess (28 events, 3.5σ) is found. The corresponding integral flux above the 2.1 TeV analysis threshold is $I(>2.1 \text{ TeV}) = (3.1 \pm 1.0_{\text{stat}}) \times 10^{-12} \text{ cm}^{-2} \text{ s}^{-1}$, or 45% of the HESS Crab Nebula flux above the same threshold.

The HESS observations of 1ES 1218+304 on May 19, 2006 yield a good-quality data set of 1.8 h live time at a mean zenith angle of 56° . The resulting excess is not significant (9 events, 1.2σ). The upper limit on the integral flux above the 1.0 TeV analysis threshold is $I(>1.0 \text{ TeV}) < 3.9 \times 10^{-12}$

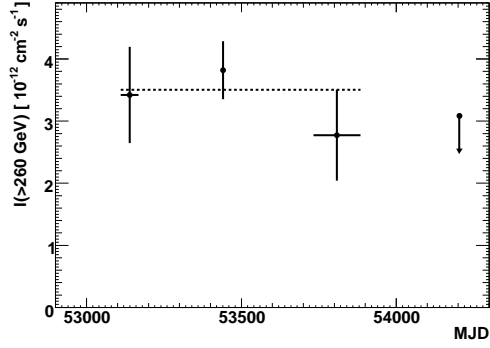


Figure 2: The annual light curve, $I(>260 \text{ GeV})$, from HESS measurements of 1ES 1101–232. The upper limit in 2007 is at the 99.9% confidence level. The 2004 and 2005 data are published elsewhere [4]. The actual observation dates are shown by the x-error bars. The dashed line is the average flux measured from 2004–2006.

$\text{cm}^{-2} \text{ s}^{-1}$. This corresponds to 17% of the HESS Crab Nebula flux above the same threshold.

HESS observations of Mkn 501 occurred on July 18, 2006. All data pass the standard quality-selection criteria, yielding an exposure of 2.2 h live time at a mean zenith angle of 64° . Mkn 501 is not detected by HESS as the resulting excess is -9 events (-0.8σ). The upper limit on the integral flux above the 2.5 TeV analysis threshold is $I(>2.5 \text{ TeV}) < 1.1 \times 10^{-12} \text{ cm}^{-2} \text{ s}^{-1}$, or 22% of the HESS Crab Nebula flux above the same threshold.

VHE Monitoring of 1ES 1101–232

1ES 1101–232 was discovered by HESS [2, 4] to emit VHE γ -rays during observations in 2004–2005. As part of a campaign to monitor its VHE flux, it was re-observed for a total (good-quality observations) of 18.3 h in 2006–07. A marginally significant excess (117 events, 3.6σ) is detected from 1ES 1101–232 in the 2006 observations (13.7 h), and the object is not detected (16 events, 0.9σ) in 2007. As can be seen from Figure 2 the upper limit from 2007 falls below the average flux measured by HESS from 2004–2006. Some of the 2006 HESS data (4.3 h) are simultane-

ous with Suzaku X-ray observations. In these data, the blazar is again marginally detected (51 events, 0.9σ) and the corresponding flux is $I(>260 \text{ GeV}) < (3.2 \pm 1.4_{\text{stat}}) \times 10^{-12} \text{ cm}^{-2} \text{ s}^{-1}$.

Discussion & Conclusions

One of the defining characteristics of AGN is their extreme variability. The VHE flux from any of these AGN may increase significantly during future flaring episodes (see, e.g., [5]) and could potentially exceed the limits presented here. In addition, accurate modeling of the SED requires that the state of the source is accounted for. Therefore, in the absence of contemporaneous observations at lower energies, it is recommended that these results be conservatively interpreted as limits on, or measurements of, the steady-component or quiescent flux from the AGN. Clearly, the simultaneous Suzaku X-ray data from Mkn 501, 1ES 1218+304, and 1ES 1101–232, make the HESS results from these objects particularly useful. Finally, interpretation of the SED of an AGN not only requires accounting for the state of the source, but also the redshift and energy dependent absorption [8] of VHE photons on the Extragalactic Background Light (EBL), which is potentially large [2, 10] for some of these sources.

With the detection of ten VHE AGN, including the discovery of seven, the HESS AGN observation program has been highly successful. However, despite more than five years of operations, the observation program is not complete as many proposed candidates have either not yet been observed or only have a fraction of their intended exposure. Therefore, the prospects of finding additional VHE-bright AGN with HESS are still excellent.

Acknowledgements

The support of the Namibian authorities and of the University of Namibia in facilitating the construction and operation of H.E.S.S. is gratefully acknowledged, as is the support by the German Ministry for Education and Research (BMBF), the Max Planck Society, the French Ministry for Research, the CNRS-IN2P3 and the Astroparticle Interdisci-

plinary Programme of the CNRS, the U.K. Science and Technology Facilities Council (STFC), the IPNP of the Charles University, the Polish Ministry of Science and Higher Education, the South African Department of Science and Technology and National Research Foundation, and by the University of Namibia. We appreciate the excellent work of the technical support staff in Berlin, Durham, Hamburg, Heidelberg, Palaiseau, Paris, Saclay, and in Namibia in the construction and operation of the equipment.

References

- [1] Aharonian, F., et al. (HESS Collaboration) 2005, *A&A*, 441, 467
- [2] Aharonian, F., et al. (HESS Collaboration) 2006, *Nature*, 440, 1018
- [3] Aharonian, F., et al. (HESS Collaboration) 2006, *A&A*, 457, 899
- [4] Aharonian, F., et al. (HESS Collaboration) 2007, *A&A*, 470, 475
- [5] Aharonian, F., et al. (HESS Collaboration) 2007, *ApJ*, in press [arXiv:astro-ph/0706.0797]
- [6] Benbow, W. 2005, *Proceedings of Towards a Network of Atmospheric Cherenkov Detectors VII* (Palaiseau), 163
- [7] Feldman, G.J. & Cousins, R.D. 1998, *Phys Rev D*, 57, 3873
- [8] Gould, R.J., & Schröder, G.P. 1967, *Phys Rev*, 155, 1408
- [9] Hartman, R.C., et al. 1999, *ApJS*, 123, 79
- [10] Hauser, M.G. & Dwek, E. 2001, *ARA&A*, 39, 249
- [11] Hinton, J. 2004, *New Astron Rev*, 48, 331
- [12] Mazin, D., et al. 2005, *Proceedings of the 29th ICRC (Pune)*, 4, 331
- [13] Mitsuda, K., et al. 2007, *PASJ*, 59, 1



A search for Very High Energy γ -rayemission from Passive Super-massive Black Holes

G.PEDALETTI^{1,2}, S. WAGNER¹, W. BENBOW³, FOR THE H.E.S.S. COLLABORATION

¹Landessternwarte, Universität Heidelberg, Königstuhl, 69117 Heidelberg, Germany

²Max-Planck-Institut für Astronomie, Königstuhl, 69117 Heidelberg, Germany

³Max-Planck-Institut für Kernphysik, PO Box 103980, 69029 Heidelberg, Germany

gpedalet@lsw.uni-heidelberg.de

Abstract: Jets of Active Galactic Nuclei (AGN) are established emitters of very high energy (VHE; >100 GeV) γ -rays. VHE radiation is also expected to be emitted from the vicinity of super-massive black holes (SMBH), irrespective of their activity state. Accreting SMBH rotate and generate a dipolar magnetic field. In the magnetosphere of the spinning black hole, acceleration of particles can take place in the field gaps. VHE emission from these particles is feasible via leptonic or hadronic processes. Therefore quiescent systems, where the lack of a strong photon field allows the VHE emission to escape, are candidates for emission. The H.E.S.S. experiment has observed the passive SMBH in the nearby galaxy NGC 1399. No VHE γ -ray signal is observed from the galactic nucleus. Constraints set by the NGC 1399 observations are discussed in the context of different mechanisms for the production of VHE γ -rayemission.

Introduction

Spheroidal systems (such as elliptical galaxies, lenticular galaxies and early-type spiral galaxies with bulges) are commonly believed to host in the central region super-massive black holes with masses in the range $M_{\text{BH}} = 10^6 - 10^9 M_{\odot}$ [8]. During the early stages of galaxy evolution these SMBH accrete matter at high rates and are observed as bright QSOs. The radiative output at low energy (e.g. optical) decays from redshift $z>3$ to $z=0$ by almost 2 orders of magnitude. Therefore, the majority of SMBH in the local universe are not embedded in dense radiation fields. This enables VHE γ -rays to escape from the nuclear region without suffering from strong absorption via γ -photon pair absorption. Several models [1, 12, 6, 14] are proposed for the production of VHE γ -rayemission from these passive AGN. In all cases a large mass of the central object is the most important characteristic for generating a high VHE flux. H.E.S.S. has already observed nine nearby galaxies whose black hole mass is measured [5, 13]. Only the case of NGC 1399 is considered here. Constraints on the physical parameters

of the system (e.g. the magnetic field \mathbf{B}) are derived using several of the aforementioned models.

Acceleration Mechanism

If the central black hole is accreting matter from a disk that also carries magnetic flux, it will develop a magnetosphere similar to those surrounding neutron stars. If the charge density is not too high in the magnetosphere of the spinning black hole, it is possible to have a non-zero component of the electric field \mathbf{E} parallel to the magnetic field \mathbf{B} . In this configuration field gaps are created, where acceleration of particles can take place [14].

Various methods can be used to estimate the magnetic field B . For example, B is estimated:

- assuming equipartition

$$\frac{B^2}{8\pi} = \frac{1}{2} \rho(r_0) v_r^2(r_0), \quad (1)$$

where ρ is the mass density and v_r is the radial infall velocity of the accreting matter

(both being a function of r_0 , the distance to the inner edge of the disk);

- from the angular momentum as in [11]

$$B = 3.1 \times 10^3 \frac{\dot{m}^{1/2}}{M_{10}^{1/2}} \left(\frac{r}{r_g} \right)^{-5/4} \text{ Gauss},$$

where \dot{m} is the mass accretion rate in units of the Eddington mass accretion rate, r_g is the gravitational radius of the black hole and $M_{10} = (M_{\text{BH}}/10^{10} M_{\odot})$.

In the model of [14] protons accelerated in the outer part of the black hole magnetosphere will collide with other protons present in the accretion disk producing pions some of which decay into VHE γ -rays. The available power is

$$W_{\text{max}} \sim 10^{27} (M_{\text{BH}})^2 (B_4)^2 \text{ ergs s}^{-1}, \quad (2)$$

where $B_4 = (B/10^4 \text{ Gauss})$. Here it is assumed that the magnetic energy density is in equipartition with the accretion energy density, which depends on various properties of the accretion disk (see Eq. 1).

In other models [1, 12, 6] VHE γ -rays originate from electromagnetic processes such as synchrotron or curvature emission. Following the analogous arguments given in [1] for the Galactic Center, synchrotron emission is not feasible due to a cut-off for protons and electrons at $\epsilon_{\gamma, \text{max}} \simeq 0.3 \text{ TeV}$ and $\epsilon_{\gamma, \text{max}} \simeq 0.16 \text{ GeV}$ respectively. These cut-offs are independent of the magnetic field strength. The energy of curvature photons (when curvature losses are the dominant ones) does not depend on the mass of the particle, so it is the same for electron or proton originated photons. The emission spectrum from curvature radiation can extend up to VHE energies, with a cut-off at:

$$E_{\text{max}} \simeq 14 (M_{10})^{1/2} (B_4)^{3/4} \text{ TeV}. \quad (3)$$

VHE Observation of NGC 1399

The giant elliptical galaxy NGC 1399 is located in the central region of the Fornax cluster at a distance of 20.3 Mpc. An SMBH of $M_{\text{BH}} = 1.06 \times 10^9 M_{\odot}$ resides in the central region. The nucleus of this galaxy is well known for its low emissivity at all

wavelengths [7]. Considering also the visibility of candidate sources for H.E.S.S., NGC 1399 therefore emerged as the best candidate for this study.

NGC 1399 was observed with the H.E.S.S. array of imaging atmospheric-Cherenkov telescopes for a total of 22.4 h (53 runs of ~ 28 min each). After applying the standard H.E.S.S. data-quality selection criteria a total of 13.9 hours live time remain. The mean zenith angle is $Z_{\text{mean}} = 22^\circ$. The data were reduced using the standard analysis tools and selection cuts [2] and the Reflected-Region method [3] for the estimation of the background. This leads to a post-analysis threshold of 200 GeV at Z_{mean} . No significant excess (-29 events, -1σ) is detected from NGC 1399 (see Fig. 1 and Fig. 2). Results are consistent with independent analysis in the collaboration.

Assuming a photon index of $\Gamma=2.6$, the upper limit (99% confidence level; [10]) on the integral flux above 200 GeV is:

$$I(> 200 \text{ GeV}) < 2.3 \times 10^{-12} \text{ cm}^{-2} \text{ s}^{-1},$$

or 1% of the Crab Nebula flux.

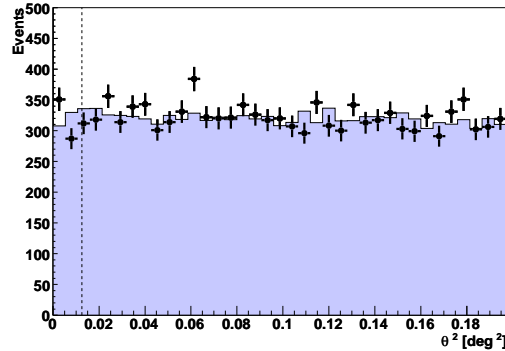


Figure 1: Distribution of squared angular distance from NGC 1399 for gamma-ray-like events in the ON region (dots) and in the OFF region (filled area, normalized). The dotted line represents the cut for point-like sources. Preliminary.

Constraints from NGC 1399 Observations

As can be seen from the spectral energy distribution (SED) of NGC 1399 in Fig. 3, the VHE frac-

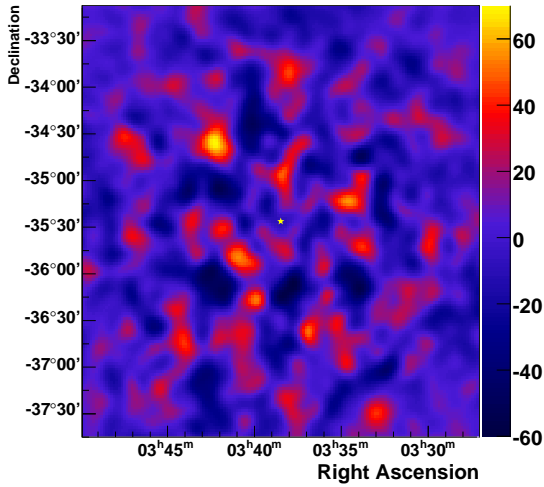


Figure 2: The smoothed (smoothing radius $r=0.09$) VHE excess in the region centered on NGC 1399. The yellow star indicates the position of the optical centre of NGC 1399. Preliminary.

tion of its total energy budget is potentially not-negligible. The H.E.S.S. limit on the isotropic VHE γ -ray luminosity is:

$$L_{\gamma} < 9.6 \times 10^{40} \text{ erg s}^{-1}.$$

Here it is assumed that the γ -ray emission originates solely from the nucleus, even though the entire galaxy is point-like considering the angular resolution of H.E.S.S.

In the case of NGC 1399 photon-photon pair absorption would not hide any possible VHE emission. The cross section $\sigma_{\gamma\gamma}$ of this process depends on the product of the energies of the colliding photons. In the case of VHE photons, the most effective interaction is with background photons of energy:

$$\epsilon_{\text{IR}} \approx (E/1\text{TeV})^{-1} \text{ eV}.$$

The optical depth resulting from this absorption, in a source of luminosity L and radius R , reads:

$$\begin{aligned} \tau(E, R_{\text{IR}}) &= \frac{L_{\text{IR}} \sigma_{\gamma\gamma}}{4\pi R_{\text{IR}} \epsilon_{\text{IR}}} \\ &\simeq 1 \left[\frac{L_{\text{IR}}(\epsilon)}{10^{-7} L_{\text{Edd}}} \right] \left[\frac{R_{\text{S}}}{R_{\text{IR}}} \right] \left[\frac{E}{1 \text{ TeV}} \right], \end{aligned}$$

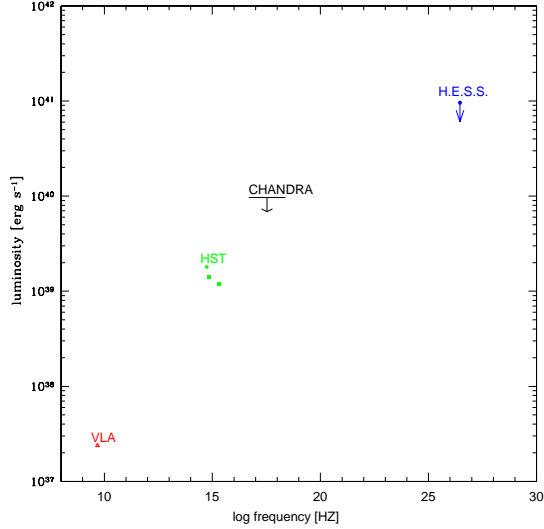


Figure 3: The SED of NGC 1399. All the data are for the core region. The archival points are VLA radio data (red triangles; [9]), HST optical data (green squares; [7]), and Chandra X-ray upper limits (solid line; [4]). The blue dot is the H.E.S.S. upper limit derived from the 2005 observations. Preliminary.

where R_{S} is the Schwarzschild radius of the black hole and L_{Edd} is the Eddington luminosity. In the system here presented, the visibility of a 200 GeV photon requires $L_{\text{IR}} < 7.9 \times 10^{40} \text{ ergs s}^{-1}$, a condition that seems to be satisfied.

In the p-p interaction scenario, assuming that all the available power (Eq. 2) will be radiated in the VHE domain, the following limit for the magnetic field is obtained from the H.E.S.S. result:

$$B < 92.6 \text{ Gauss}.$$

In order to maintain gaps in the magnetosphere, as is essential for particle acceleration, pair production should be avoided. Translating this condition into an upper limit for the magnetic field yields:

$$B < 3.6 \times 10^4 (M_{10})^{-2/7} = 6.8 \times 10^4 \text{ Gauss}.$$

Therefore the H.E.S.S. NGC 1399 data allow plausible values of the magnetic field. Considering the production of a 1 TeV photon via curvature emission (Eq. 3) requires in the case of NGC 1399:

$$B = 1.3 \times 10^3 \text{ Gauss}.$$

The non-detection of NGC 1399 does not constrain the magnetic field. In all the aforementioned scenarios, hadronic and/or leptonic, no clear constraints on the magnetic field are derived.

Conclusions

VHE emission from passive SMBH is plausible either via leptonic or hadronic processes. In order to detect this emission the giant elliptical galaxy NGC 1399 was observed by H.E.S.S. in 2005. NGC 1399 is not detected in these observations. The corresponding upper limit does not allow a firm estimation of the circumnuclear magnetic field.

Acknowledgments

The support of the Namibian authorities and of the University of Namibia in facilitating the construction and operation of H.E.S.S. is gratefully acknowledged, as is the support by the German Ministry for Education and Research (BMBF), the Max Planck Society, the French Ministry for Research, the CNRS-IN2P3 and the Astroparticle Interdisciplinary Programme of the CNRS, the U.K. Science and Technology Facilities Council (STFC), the IPNP of the Charles University, the Polish Ministry of Science and Higher Education, the South African Department of Science and Technology and National Research Foundation, and by the University of Namibia. We appreciate the excellent work of the technical support staff in Berlin, Durham, Hamburg, Heidelberg, Palaiseau, Paris, Saclay, and in Namibia in the construction and operation of the equipment.

This work has been supported by the International Max Planck Research School (IMPRS) for Astronomy & Cosmic Physics at the University of Heidelberg.

References

- [1] F. Aharonian and A. Neronov. High-Energy gamma rays from the massive black hole in the galactic center. *ApJ*, 619:306–313, 2005.
- [2] W. Benbow. The H.E.S.S. Standard Analysis Technique. *Proceedings of Towards a Network of Atmospheric Cherenkov Detectors VII (Palaiseau)*, page 163, 2005.
- [3] Berge D. et al. Background modelling in very-high-energy γ -ray astronomy. *A&A*, 466:1219, 2007.
- [4] Loewenstein M. et al. Chandra Limits on X-Ray Emission Associated with the Supermassive Black Holes in Three Giant Elliptical Galaxies. *ApJ*, 555:L21–29, 2001.
- [5] Magorrian A. et al. The demography of massive dark objects in galaxy centers. *ApJ*, 115:2285–2305, 1998.
- [6] Neronov A. et al. TeV signatures of compact UHECR accelerators. *J. Exp. Theor. Phys.*, 100:656–662, 2004.
- [7] O’Connell R. W. et al. UV/Optical Nuclear Activity in the gE Galaxy NGC 1399. *ApJ*, 635:305–310, 2005.
- [8] Richstone D. et al. Supermassive black holes and the evolution of galaxies. *Nature*, 395:A14, 1998.
- [9] Sadler E. M. et al. Low-luminosity radio sources in early-type galaxies. *MNRAS*, 240:591, 1989.
- [10] G. J. Feldman and R. D. Cousins. Unified approach to the classical statistical analysis of small signals. *Phys. Rev. D*, 57:3873, 1998.
- [11] Z. Kuncic and G. V. Bicknell. Dynamics and Energetics of Turbulent, Magnetized Disk Accretion around Black Holes: A First-Principles Approach to Disk-Corona-Outflow Coupling. *ApJ*, 616:669, 2004.
- [12] A. Levinson. Particle Acceleration and Curvature TeV Emission by Rotating, Supermassive Black Holes. *Phys. Rev. Lett.*, 85:912–915, 2000.
- [13] S. Pellegrini. Nuclear Accretion in Galaxies of the local Universe: Clues from CHANDRA Observations. *ApJ*, 624:155–161, 2005.
- [14] P. Slane and S. M. Wagh. TeV gamma-ray production in accreting black hole systems. *ApJ*, 364:198–202, 1990.



Wide-range multiwavelength observations of northern TeV blazars with MAGIC/HESS, Suzaku and KVA

M. HAYASHIDA^{1,*}, S. RÜGAMER², D. MAZIN³, R. FIRPO³, K. MANNHEIM², F. TAVECCHIO⁴, M. TESHIMA¹ ON BEHALF OF THE MAGIC COLLABORATION.

D. HORNS⁵, L. COSTAMANTE⁶, S. SCHWARZBURG⁵, S. WAGNER⁷ ON BEHALF OF THE HESS COLLABORATION.

T. TAKAHASHI⁸, J. KATAOKA⁹, G. MADEJSKI¹⁰, R. SATO⁸, M. USHIO⁸ FOR THE SUZAKU TEAM

¹Max-Planck-Institut für Physik, D-80805 München, Germany, ²Universität Würzburg, D-97074 Würzburg, Germany, ³Institut de Física d'Altes Energies, Edifici Cn., E-08193 Barcelona, Spain, ⁴INAF/Osservatorio Astronomico di Brera, Merate, Italy, ⁵Institut für Astronomie und Astrophysik Eberhard Karls Universität, D-72076 Tübingen, Germany, ⁶Max-Planck-Institut für Kernphysik, D-69029 Heidelberg, Germany, ⁷Landessternwarte, Universität Heidelberg, Königstuhl, D-69117 Heidelberg, Germany, ⁸Institute of Space and Astronautical Science/JAXA, Kanagawa, 229-8510, Japan, ⁹Tokyo Institute of Technology, Tokyo, 152-8551, Japan, ¹⁰Stanford Linear Accelerator Center, Stanford, CA, 943099-4349, USA

mahaya@mppmu.mpg.de

Abstract: We conducted multiwavelength observations of the northern TeV blazars, Mkn501 and Mkn421, employing the ground-based γ -ray telescopes MAGIC and HESS, the Suzaku X-ray satellite and the KVA optical telescope. The observations for Mkn501 were performed in July 2006. The source showed one of the lowest fluxes both in very high energy (VHE) γ -ray and X-ray. No significant flux variability could be found in the VHE band while an overall increase of about 50% on a 1-day time scale could be seen in the light curve of the X-ray flux. A one-zone synchrotron self-Compton model can well describe our simultaneous spectral data of the VHE γ -ray and the X-ray emissions of Mkn501 in the quiescent state. The simultaneous observations of Mkn421 were carried out in April 2006. The source was clearly detected in all observations and showed a high state of activity both in VHE γ -ray and X-ray.

Introduction

Blazars, a sub-class of active galactic nuclei (AGNs) characterized by small angles between the jet axis and the line of sight, can provide excellent opportunities for studying particle acceleration mechanism in the jet. One of the most successful models for the emission mechanism in the jet for TeV blazars is the synchrotron self-Compton (SSC) models [7], in which the radiation is originated from relativistic electrons. Models based on the acceleration of hadrons can also sufficiently describe the observed emission [12]. Blazars often show strong flux variability. Hence, simultaneous multiwavelength observations over a wide-energy range in different states are essential to studying the evolution of physical conditions and the shock

mechanism in the jet [e.g.] [13]. However, most of the previous simultaneous multiwavelength observations could only be conducted during flaring states due to the low sensitivity of the participating γ -ray telescopes.

Multiwavelength campaigns for several northern TeV blazars were coordinated in 2006. A new generation of Imaging Atmospheric Cherenkov Telescopes (IACTs) for very high energy (VHE; >100 GeV) γ -ray, the MAGIC and HESS telescopes, the Suzaku X-ray satellite and the KVA optical telescope were involved in those campaigns. In this paper we present the observational results of the campaigns for Mkn501 and Mkn421.

Involved Instruments

MAGIC

The MAGIC telescope is an IACT with a 17-m diameter dish, located on the Canary Island of La Palma (28.2° N, 17.8° W, 2225 m a.s.l.). The telescope is operating at a γ -ray trigger threshold of ~ 50 GeV and a spectral threshold of ~ 100 GeV. The telescope parameters and performance are described in detail in [3].

HESS

The HESS array consists of four IACTs, each with a tessellated 13-m diameter mirror, located in the Khomas highlands in Namibia (23.3° S, 16.5° E, 1800 m a.s.l.). Due to large zenith angle for northern objects, the observations with HESS array are sensitive to an energy range shifted towards higher energies. The telescope parameters and performance are described in detail in [9].

Suzaku

The joint Japanese-US satellite Suzaku [14], launched successfully into orbit on 10 July 2005, has four X-ray Imaging Spectrometers (XIS) and a separate Hard X-ray Detector (HXD). The XIS are sensitive in the 0.2-10 keV band with CCDs. The HXD's silicon PIN diode array is the most sensitive detector in the 10-70 keV band thanks to the good noise shielding. Its high sensitivity both in the soft and hard X-rays makes it an excellent instrument for studying the synchrotron component of TeV blazar emission, making the detection of the X-ray peak position feasible.

KVA

KVA¹ is a 35-cm optical telescope also situated on La Palma. Selected blazars are regularly observed with KVA as a part of the Tuorla Observatory blazar monitoring program. The KVA telescope can be fully committed to monitoring the target sources during the multiwavelength campaign.

Markarian 501

Mkn501 ($z = 0.034$) is the second established TeV blazar [18]. In 1997 this source went into a state of surprisingly high activity and strong variability, becoming 10 times brighter than the Crab Nebula in the TeV range [1]. In 1998-1999 the mean flux dropped by an order of magnitude [2]. Recently, rapid flux variability with flux-doubling times down to 2 minutes has been reported [4].

VHE γ -ray observations

Mkn501 was observed for 10.5 h with the MAGIC telescope in the night of 18th, 19th and 20th of July, 2006. The observations were performed in the so-called wobble mode [8], where the object is observed with an 0.4° offset from the camera center. After the data selection by the quality and zenith angle ($< 35^\circ$), the remaining data of 9.1 h were analyzed using the MAGIC standard analysis chain. The detailed information can be found in [3, 5]. An observed excess signal corresponding to 13.4σ excess was found.

The source was also observed with the HESS array during the campaign. The data analysis is currently ongoing.

X-ray observations

The X-ray observation window of Suzaku was between 53934.789 and 53935.727 in MJD time (from 18th to 19th of July, 2006). The net exposure times after screening are 35 ksec in both XIS and HXD detectors.

Light curves

Figure 1 shows the light curves in various energy bands. The source was rather quiet during the campaign. The fluxes in VHE γ -ray and optical R-band were consistent with constant levels, while the X-ray count rate was growing during the observations with an overall increase of about 50% on a 1-day time scale between the beginning and the end of the observations.

1. more information at <http://tur3.tur.iac.es/>

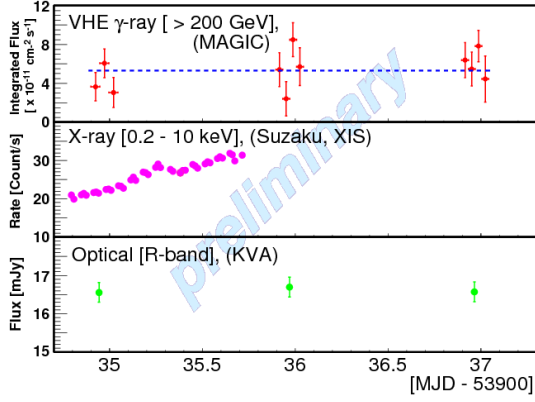


Figure 1: Light curves of Mkn501 in different energy bands during the campaign in 2006. **Top:** VHE γ -ray flux measured by the MAGIC telescope with 1-hour binning. A dotted horizontal line represents the average flux. **Middle:** The X-ray count rate recorded by the Suzaku XIS detectors. **Bottom:** Measured Optical R-band flux by KVA.

The average integrated flux above 200 GeV is $(5.3 \pm 0.5) \times 10^{-11} \text{ cm}^{-2} \text{ s}^{-1}$ ($\chi^2/\text{dof} = 12.7/10$), which corresponds to about 27% of the Crab Nebula flux as measured by the MAGIC telescope [3].

Spectra

The spectrum in the VHE band is well described by a simple power law from 85 GeV to 2 TeV with $dN/dE = (1.24 \pm 0.11) \times 10^{-10} (E/300 \text{ GeV})^{-2.85 \pm 0.14} [\text{TeV}^{-1} \text{ s}^{-1} \text{ cm}^{-2}]$. The flux level and the photon index of the measured spectrum are comparable to those in the lowest state among 2005 MAGIC observations ($dN/dE = (1.36 \pm 0.21) \times 10^{-10} (E/300 \text{ GeV})^{-2.73 \pm 0.29}$ [4]) for this object.

Spectral Modeling

Figure 2 shows the spectral energy distribution (SED) of Mkn501 with data of this multiwavelength campaign and some historical data [4, 21]. The "de-absorbed" data in blue points at the VHE band were corrected for the extra-galactic background light (EBL) absorption using the "Best" fit

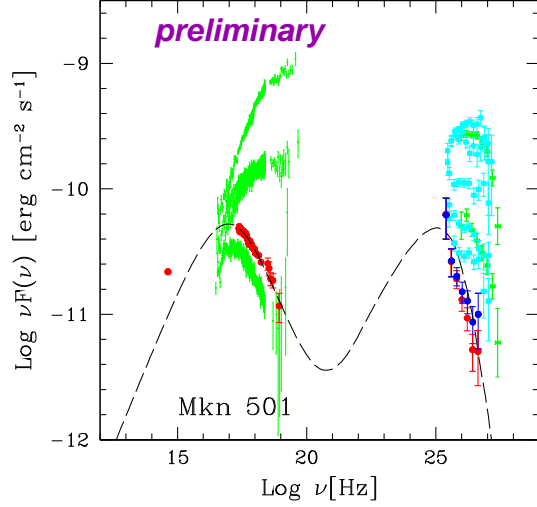


Figure 2: SED of Mkn501. The simultaneous spectral data in optical (KVA), X-ray (Suzaku) and VHE γ -ray (MAGIC) in the 2006 campaign are shown by red points. Blue points represent a "de-absorbed" spectrum corrected for the EBL absorption. The line describes the best fit to this campaign data with a one-zone SSC model developed by [20, 21]. See text for the fit parameters. For comparison, green points denote historical data taken by BeppoSAX for X-rays data from 1997 to 1999 and by CAT in the VHE γ -ray range in 1997 [21]. Flux levels from the MAGIC observations in 2005 are also denoted by cyan points [4].

model of [11]. In optical, the host galaxy contributions $(12.0 \pm 0.3) \text{ mJy}$ [15] has already been subtracted. Since systematic errors at soft X-ray energies are still under investigation, we use only X-ray data above 1 keV for the model fit.

Assuming a uniform injection of the electrons throughout a homogeneous emission region, we applied a one-zone SSC model for the campaign data to estimate the physical parameters of the emitting region using the code developed by [20, 21]. Briefly, a spherical shape (blob) is adopted for the emission region with radius R , filled with a tangled magnetic field with intensity B . An electron distribution is described by a smoothed broken power-law energy distribution with slopes s_1 from γ_{\min} to the break energy γ_b and s_2 up to the limit of γ_{\max} and with a normalization factor of

K . The relativistic effects are taken into account by the Doppler factor δ .

R is selected to be 1×10^{15} cm, which has been adopted in [4] for the SED during the rapid flare observed with MAGIC in 2005. Since no cut off can be seen both in the X-ray and VHE γ -ray spectra, γ_{\min} and γ_{\max} are fixed at 1 and 10^7 , respectively. The best fit was achieved with the following parameters: $\delta = 20$, $B = 0.26$ G, $K = 1 \times 10^5 \text{ cm}^{-3}$, $\gamma_b = 6.7 \times 10^4$, $s_1 = 2$ and $s_2 = 4$. This one-zone SSC model can reproduce well the obtained X-ray and VHE γ -ray fluxes in the low state of activity during the campaign. However, it is apparent that the model underestimates the optical flux. This can be explained by the assumption that the emission from radio to UV has another origin than the high energy emission. This interpretation has already been applied to previous SEDs of Mkn501 by [10]. Compared to historical measurements our data show one of the lowest states both in X-ray and VHE γ -ray. The historical data suggest a correlation between the peak positions and the source luminosity [21]. Following [13, 21] we can assume this feature is related to the evolution of γ_b . In that framework we can find our derived value of γ_b to be small compared to previous observation results [e.g.] [4, 10, 16, 21]. More details on the analysis and the results will be found in [6].

Markarian 421

Mkn421 ($z = 0.030$) is the closest known source and the first extragalactic one detected in the TeV energy range using IACTs [17], and it is one of the best studied TeV γ -ray blazar.

Observations and Results

The multiwavelength observations for this source were conducted in the night of April 28th, 2006. The X-ray observations with Suzaku were carried out between 53853.267 and 53854.271 in MJD time. The source was observed by the MAGIC telescope for 3.8 h and by the HESS array for 1.5 h. Both observations were performed during the Suzaku pointing to the source. Clear detections of signals can be found in all observations. The X-

ray spectrum is extracted from the data which are exactly coincident with the HESS or MAGIC observation times. The spectrum in the X-ray band as well as in the VHE γ -ray band indicates that the source showed a high state and a rather stable activity during the simultaneous observations. Details of the observational results of this campaign will be discussed in [19].

Acknowledgments

The MAGIC collaboration thanks the IAC for the excellent working conditions at the ORM. The MAGIC project is supported by the German BMBF and MPG, the Italian INFN, the Spanish CICYT, the Swiss ETH and the Polish MNiI.

References

- [1] F. Aharonian et al. *A&A*, 342:69, 1999.
- [2] F. Aharonian et al. *ApJ*, 546:898, 2001.
- [3] J. Albert et al. *ApJ*, 2007. submitted (astro-ph/0705.3244).
- [4] J. Albert et al. *ApJ*, 2007. in press (astro-ph/0702008).
- [5] J. Albert et al. *ApJ*, 663:125, 2007.
- [6] J. Albert et al. 2007. in preparation.
- [7] L. Costamante and G. Ghisellini. *A&A*, 384:56, 2002.
- [8] A. Daum et al. *AstroPart. Phys.*, 8:1, 1997.
- [9] J. A. Hinton et al. *New Astron. Rev.*, 48:331, 2004.
- [10] K. Katarzynski et al. *A&A*, 367:809, 2001.
- [11] T. M. Kneiske et al. *A&A*, 413:807, 2004.
- [12] K. Mannheim. *A&A*, 269:67, 1993.
- [13] A. Mastichiadis and J. G. Kiri. *ApJ*, 320:19, 1997.
- [14] K. Mitsuda et al. *PASJ*, 59:1, 2007.
- [15] K. Nilsson et al. *A&A*, 2007. submitted.
- [16] E. Pian et al. *ApJ*, 492:L17, 1998.
- [17] M. Punch et al. *Nature*, 358:477, 1992.
- [18] J. Quinn et al. *ApJ*, 456:L83, 1996.
- [19] T. Takahashi et al. 2007. in preparation.
- [20] F. Tavecchio et al. *ApJ*, 509:608, 1998.
- [21] F. Tavecchio et al. *ApJ*, 554:725, 2001.



Simultaneous observation of GRB060602B with the H.E.S.S. Air Cherenkov array

PAK-HIN TAM¹, KONRAD BERNLÖHR², PAULA CHADWICK³, JIM HINTON^{1,2,4}, DALIBOR NEDBAL², GERD PÜHLHOFER¹, STEFAN WAGNER¹ FOR THE H.E.S.S. COLLABORATION

¹*Landessternwarte, Universität Heidelberg, Königstuhl, D 69117 Heidelberg, Germany*

²*Max-Planck-Institut für Kernphysik, P.O. Box 103980, D 69029 Heidelberg, Germany*

³*University of Durham, Department of Physics, South Road, Durham DH1 3LE, U.K.*

⁴*School of Physics & Astronomy, University of Leeds, Leeds LS2 9JT, U.K.*

pham@lsw.uni-heidelberg.de

Abstract: On June 2, 2006, the *Swift* Burst Alert Telescope (BAT) triggered a bursting event in the 15–350 keV energy band. The burst position was being observed with the H.E.S.S. array of IACTs before the burst, throughout the duration of the burst, and after the burst. In particular, the burst position accidentally fell in the f.o.v. of the H.E.S.S. camera when the burst occurred. This is the first completely simultaneous observation of a soft gamma-ray bursting event with an IACT instrument. A search for VHE gamma-rays coincident with the burst event as well as that during the afterglow period was performed. No signal was found during the period covered by the H.E.S.S. observation. The *Swift* X-ray Telescope, which started observation 83 seconds after the BAT trigger, detected an X-ray counterpart of the event. No optical/infrared counterpart was found. Due to the very soft BAT spectrum (photon index $\Gamma \approx 5$) of the burst compared to other *Swift* GRBs and its proximity to the galactic center, the burst might have been caused by a galactic X-ray burster (e.g. a low-mass X-ray binary). However, the possibility of it being a cosmological GRB cannot be ruled out. Since the nature of the event is still unclear, we discuss the implications according to the two different bursting scenarios.

Introduction

The temporally and spatially unpredictable, and fast-fading nature of gamma-ray bursts (GRBs) makes it operationally rather difficult to study the prompt phase of GRBs simultaneously in other wavelengths. There are two operational techniques currently employed in the very-high-energy (VHE; 100 GeV – 100 TeV) γ -ray regime: (1) To slew quickly to the GRB position provided by a burst alert from satellites. This technique is suitable for IACTs such as H.E.S.S. which have a field of view (f.o.v.) of several degrees. However, there is always a delay in time for IACT operating in this GRB-follow-up mode, as long as the GRB position lies outside the camera f.o.v. at the GRB onset. The MAGIC telescope, operating in this mode, was able to slew to the position of GRB 050713a, 40 seconds after the GRB onset, while the prompt keV emission was still active. A total of 37-minute observation was made and no evidence of emission

above 175 GeV was obtained [1]; (2) To observe a large part of the sky continually, at the expense of a much lower sensitivity at the GRB position than the IACT technique. This technique is used, e.g. by the water Cherenkov detector Milagro [2].

Here we report on the first completely simultaneous observation of a soft γ -ray bursting event (a possible GRB) with H.E.S.S., an IACT instrument. The burst position accidentally fell in the f.o.v. (albeit with a large offset from the center of the f.o.v.) of the H.E.S.S. camera when the burst occurred.

GRB 060602B

At 23:54:33 UT on 2 June, 2006 (denoted by t_0), the Burst Alert Telescope (BAT) on board *Swift*, which operates in the 15–350 keV energy band, triggered a bursting event. This event was announced as a gamma-ray burst (GRB) and designated GRB 060602B (e.g. [3, 4,

5]). The refined BAT position was (RA,Dec) = ($17^{\text{h}}49^{\text{m}}28^{\text{s}}.2, -28^{\circ}7'15''.5$) (J2000, [6]). The BAT light curve showed a single-peaked structure lasting from $t_0 - 1.0$ s to $t_0 + 12.0$ s. The peak was the strongest in the 15-25 keV energy band among other bands and was absent above 50 keV. T_{90} (defined as the duration when 90% of the total fluence of the 15-350 keV was emitted) is 9.0 ± 2 sec. The time-averaged energy spectrum from $t_0 - 1.1$ s to $t_0 + 8.8$ s can best be fit by a simple power law (PL), with a photon index of 5.02 ± 0.52 (one of the softest among *Swift* GRBs). The fluence in the 15-150 keV band was $(1.8 \pm 0.2) \times 10^{-7}$ ergs cm^{-2} [6].

Although no counterpart was found in the optical/IR bands [4, 7, 8, 9], an X-ray counterpart was found using *Swift*/XRT and was fading as a PL with an index 1.05 ± 0.07 for at least 11 hours, after a small rise before $t_0 + 200$ s [10].

The time-averaged X-ray energy spectrum during 100s – 11.4ks after t_0 can be fit equally well by an absorbed PL or an absorbed blackbody (BB) model. A photon index of $2.6^{+1.0}_{-0.8}$ and a hydrogen column density of $3.8^{+2.1}_{-1.4} \times 10^{22} \text{cm}^{-2}$ were obtained for the PL model. For an absorbed BB model, a temperature of $0.90^{+0.23}_{-0.17}$ keV and a column density of $1.8^{+1.2}_{-0.8} \times 10^{22} \text{cm}^{-2}$ were obtained.

The galactic coordinates of the source were (lon, lat) = ($1.15^{\circ}, -0.30^{\circ}$). This position has raised up a possibility of the event originating from a galactic source (eg. an X-ray burster). The fact that the BAT spectrum was one of the softest *Swift* GRBs could be used to argue for this scenario [6].

The H.E.S.S. Observations

The H.E.S.S. array is a system of four 13m-diameter imaging atmospheric Cherenkov telescopes located in the Khomas Highland of Namibia. The system has a point source sensitivity above 100 GeV of $\sim 3.0 \times 10^{-13} \text{cm}^{-2} \text{s}^{-1}$ (1% of the flux from the Crab nebula) for a 5σ detection in a 25 h observation. Its has a f.o.v. of radius $\sim 2.6^{\circ}$ (at this radius the relative gamma-ray acceptance is about 10% of that at the targeting position of the telescopes), thus enabling it to detect serendipitous sources, as have been demonstrated in the galactic scan survey [11].

The position of GRB 060602B was being observed with H.E.S.S. before the burst, throughout the duration of the burst, and after the burst. The source offsets from the observation positions were large (up to $\sim 2.8^{\circ}$) in the beginning. A total of 4.9 hours of observation was obtained during the night of 2-3 June, 2006. This includes 1.7hr *pre-burst*, 9s *prompt*, and 3.2hr *afterglow* epochs. An additional 4.7 hours of observation at the burst position was obtained during the next 3 nights. All data were taken in good weather conditions and good hardware status. The observations were taken with the source position placed at different offsets relative to the center of the f.o.v. of the telescopes. This is because most observational runs were not dedicated to the position of the event GRB 060602B.

The source position fell into the H.E.S.S. f.o.v. during other H.E.S.S. observations (which targeted objects like Sgr A*) as well. This allows us to investigate a possible long-term emission of the source at VHE energies. It is of particular interest in the X-ray burst (XRB) scenario, which we will discuss later.

Data Analysis

Calibration of data, event reconstruction and rejection of the cosmic-ray background (i.e. γ -ray event selection criteria) were performed as described in [9]. On-source data were taken from a circular region of radius θ_{cut} centered at the source. The background was then estimated using the reflected-region model as described in [13], which makes use of the off-source data obtained during the same observation period.

Two sets of analysis cuts were applied to search for a signal. These include standard cuts (as described in [9]) and soft cuts (with lower-energy thresholds, as described in [11]). Furthermore, for the periods with large offsets, we also used larger θ_{cut} 's to match the larger point spread functions (PSFs).

Figure 1 shows the independent events observed within a circular region of radius $\theta_{\text{cut}} = 0.32^{\circ}$ (for $t < t_0 + 500$ s) and $\theta_{\text{cut}} = 0.2^{\circ}$ (for $t_0 + 600$ s $< t < t_0 + 2050$ s) centered at the source. The θ_{cut} values were chosen to match the different PSFs for observations with different source offsets.

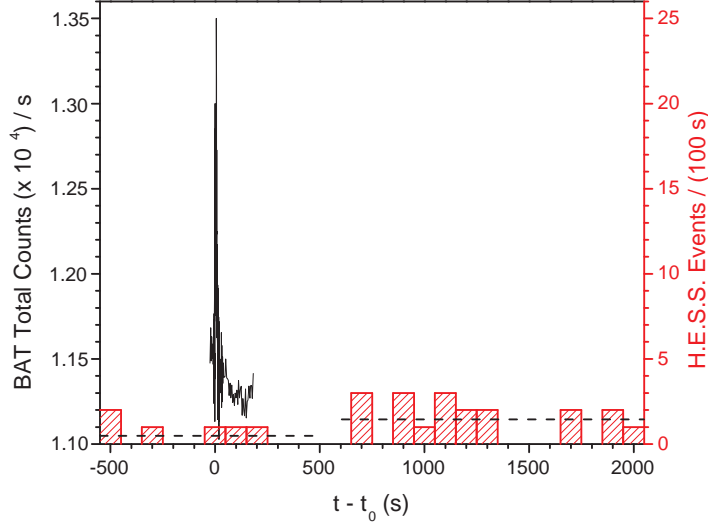


Figure 1: Shaded, red histogram: Events observed with H.E.S.S. within a circular region of radius $\theta_{\text{cut}} = 0.32^\circ$ (for $t < t_0 + 500\text{s}$) and $\theta_{\text{cut}} = 0.2^\circ$ (for $t > t_0 + 600\text{s}$) centered at the *Swift*/XRT position in 100-second bins. The dashed horizontal lines indicate the expected number of background events in the circular regions, using the reflected-region background model [13]. The difference in event rates is due to the different offsets, zenith angles, and θ_{cut} for different periods. The gap between 500s and 600s is due to the transition of observation runs. Solid, black curve: *Swift*/BAT light curve in the 15-150 keV band.

Results

No evidence of excess events as observed with H.E.S.S. in any time before, during, or after the soft-gamma-ray bursting event is seen. There was no hint of radiation in the next 3 nights as well.

We also looked into the H.E.S.S. observations from 2004 to 2006 containing the XRT position in the f.o.v. Again no emission was found and the 99% confidence level (c.l.) upper limits using the method of Feldman & Cousins [14] derived from 128.3 hours of observation using standard cuts is $1.06 \times 10^{-12} \text{ photons cm}^{-2} \text{ s}^{-1}$ above 200 GeV (i.e. 0.5% of the Crab flux).

Discussions

The nature of the bursting event that occurred at 23:54:33 UT on 2 June, 2006 is unclear. It was

firstly announced as a GRB by [3] and several other teams including [4, 5]. Thus the event has been designated GRB 060602B. However, its very soft spectrum (photon index $\Gamma \approx 5$) in the 15-150 keV band and its galactic position support a galactic origin of the event, as first suggested in [6]. A faint XMM-Newton source was detected on 23 September 2000 in the proximity of the *Swift*/XRT position, as first noticed by [16]. Whether this source is related to the bursting event on 2 June, 2006 is unclear. However, the possibility of the event as a cosmological GRB is not ruled out. Since the results are still not conclusive, we briefly discuss the implications of the H.E.S.S. observations according to these two scenarios.

The gamma-ray burst scenario

If GRB 060602B were a cosmological GRB, it would be a GRB with a very steep keV spec-

trum and happened to be to the direction next to the galactic center. Our observation with H.E.S.S. would be the first strictly simultaneous observation of a GRB with an IACT instrument during its prompt phase.

High-energy components from GRBs have been predicted (e.g. [17, 5]) and observed (e.g. in the case of GRB 940217 up to ~ 18 GeV [2]) in the prompt and afterglow phases. The H.E.S.S. data can be used to constrain the level of such a high-energy component of GRB 060602B at VHE energies.

The X-ray burst scenario

If GRB 060602B were a galactic XRB, it would be the first simultaneous observation of an XRB with an IACT instrument. Its galactic position suggests that it is quite near the galactic center and thus probably at a distance of ~ 8 kpc. Any optical emission would have been absorbed.

XRBs have only been detected from low-mass-X-ray binaries [20]. Early claims of persistent detections in the VHE regime of this class of objects were not confirmed with more sensitive experiments (see e.g. [21]). Our long-term upper limit of the burst position is among the most constraining ones. Possible models which suggest continual VHE emission from X-ray binaries were proposed [22] (see also [23] for a review).

Conclusions

For the first time, a strictly simultaneous observation of a soft γ -ray bursting event with an IACT instrument without time delay were obtained on 2 June, 2006.

The burst position was being observed with H.E.S.S. at VHE energies before the burst, throughout the duration of the burst, and after the burst. This was also the first time a soft γ -ray bursting event was observed with an IACT instrument before its onset. A search for TeV signal coincident with the burst event as well as that during the afterglow period was performed. No signal has been found during the period covered by the H.E.S.S. observation. The data analysis is still ongoing and final results will be published elsewhere [24].

References

- [1] Albert, J. et al. (MAGIC collaboration) 2006, *ApJ*, 641, L9
- [2] Saz Parkinson, P. M. et al. 30th Proc. ICRC, Mexico, 2007.
- [3] Jalinec, M., Kubánek, P., & Vítek, S. 2006, *GCN Circ.* 5198
- [4] Kubánek, P., Jalinec, M., & French, J. 2006, *GCN Circ.* 5199
- [5] Schady, P., Beardmore, A. P., Marshall, F. E. et al. 2006, *GCN Circ.* 5200
- [6] Palmer, D., Barbier, L., Barthelmy, S. et al. 2006, *GCN Circ.* 5208
- [7] Khamitov, I., Bikmaev, I. & Sakhbullin, N. 2006, *GCN Circ.* 5205
- [8] Blustin, A. J., Schady, P. & Pandey, S. B. 2006, *GCN Circ.* 5207
- [9] Melandri, A., Distefano, E., Covino, S. et al. 2006, *GCN Circ.* 5229
- [10] Beardmore, A. P., Godet, O., Sakamoto, T. et al. 2006, *GCN Circ.* 5209
- [11] Aharonian, F. A. et al. (HESS collaboration) 2005a, *Science*, 307, 1938
- [12] Aharonian, F. A. et al. (HESS collaboration) 2006a, *A&A*, 457, 899.
- [13] Berge, D., Funk, S. & Hinton, J. A. 2007, *A&A*, 466, 1219
- [14] Aharonian, F. A. et al. (HESS collaboration) 2006b, *A&A*, 448, L19
- [15] Feldman, G. J. & Cousins, R. D. 1998, *Phys. Rev. D.*, 57, 3873
- [16] Halpern, J. 2006, *GCN Circ.* 5210
- [17] Wang, X. Y., Dai, Z. G. & Lu, T. 2001, *ApJ*, 556, 1010
- [18] Pe'er, A. & Waxman, E. 2005, *ApJ*, 633, 1018
- [19] Hurley, K., Dingus, B. L., Mukherjee, R. et al. 1994, *Nature*, 372, 652
- [20] Lewin, W. H. G., Paradijs, J. van & Heuvel, E. P. J. van den 1995, *X-Ray Binaries* (Cambridge University Press, Cambridge) 178
- [21] Weekes, T. C., 1992, *Space Sci. Rev.*, 59, 315
- [22] Cheng, K. S. & Ruderman, M. 1991, *ApJ*, 373, 187
- [23] Moskalenko, I. V., 1995, *Space Sci. Rev.*, 72, 593
- [24] Aharonian, F. A. et al. (HESS collaboration), in preparation



Gamma-ray burst observations with the H.E.S.S. Air Cherenkov array

PAK-HIN TAM¹, PAULA CHADWICK², YVES GALLANT³, DIETER HORNS⁴, GERD PÜHLHOFFER¹, GAVIN ROWELL⁵, STEFAN WAGNER¹ FOR THE H.E.S.S. COLLABORATION

¹*Landessternwarte, Universität Heidelberg, Königstuhl, D 69117 Heidelberg, Germany*

²*University of Durham, Department of Physics, South Road, Durham DH1 3LE, U.K.*

³*Laboratoire de Physique Théorique et Astroparticules, IN2P3/CNRS, Université Montpellier II, CC 70, Place Eugène Bataillon, F-34095 Montpellier Cedex 5, France*

⁴*Institut für Astronomie und Astrophysik, Universität Tübingen, Sand 1, D 72076 Tübingen, Germany*

⁵*School of Chemistry & Physics, University of Adelaide, Adelaide 5005, Australia*

phitam@lsw.uni-heidelberg.de

Abstract: Gamma-ray bursts (GRBs) are among the potential very-high-energy (VHE) gamma-ray and cosmic-ray sources. Particles are accelerated to highly-relativistic speeds. This might give rise to emission of VHE gamma-ray and/or cosmic-ray particles with ultra-high energy $> 10^{19}$ eV. Despite its generally fast-fading behavior seen in many longer wavebands, the time evolution of any VHE radiation is still not clear. In order to probe the largely unexplored VHE spectra of GRBs, a GRB observing program has been set up by the H.E.S.S. collaboration. With the high sensitivity of the H.E.S.S. array and given favorable observational conditions, VHE flux levels predicted by GRB models are within reach. Extra-galactic background light (EBL) absorption is considered in cases where redshifts of the GRBs are reported. We present the H.E.S.S. VHE gamma-ray observations of and results from some of the reported GRB positions during the past few years, including recent observations in early 2007.

Introduction

Gamma-ray bursts (GRBs), being established as originating from highly-relativistic ejecta, are among potential VHE gamma-ray and cosmic-ray sources. First detected in late 1960s, the origin of GRBs is still not well understood, especially compared with other objects such as pulsars and quasars which were also detected in the same era but the origins of which are much more understood nowadays than GRBs. The main reason is that to obtain multi-wavelength information other than gamma-rays proves to be operationally very difficult. Two breakthroughs in understanding GRBs include the establishment of the isotropic spatial distribution by the BATSE experiment on board CGRO in the 1990s and the discovery of longer-wavelength counterparts after the launch of BeppoSAX in Feb 1997. Since then not only GRBs are confirmed to be of cosmological origin, but the theories of GRBs and their modeling have drawn a lot of attentions from the astrophysical community.

After the highly variable radiation seen in keV-MeV gamma-ray energies (known as the prompt GRB phase), fast-fading behavior is generally seen in counterparts in longer wavebands (known as the afterglow phase). It is believed that during the GRBs, particles are accelerated to highly-relativistic speeds. Highly-relativistic particles might give rise to emission of VHE gamma-ray and/or cosmic-ray particles with ultra-high energy $> 10^{19}$ eV (see e.g. [1]). Although VHE emission from GRBs during the prompt GRB phase or the afterglow phase is predicted, its flux level and temporal behavior is not clear, given that no emission in this energy range has ever been detected unambiguously by now. With the high sensitivity of the H.E.S.S. array and given favorable observational conditions, VHE flux levels predicted by GRB models are within reach.

VHE emission from GRBs

The highest energy radiation from GRBs ever detected firmly by any instrument was a ~ 18 GeV photon coming from GRB 940217, detected using EGRET about 1.5 hour after the onset of the GRB [2]. From the theoretical point of view, photons with energies up to ~ 10 TeV from GRBs are expected (for review, see e.g. [3] and references therein). In one case considered by [4] where electron IC emission dominates, an energy flux of about $5 \times 10^{-12} \text{ erg cm}^{-2} \text{ s}^{-1}$ at 1 TeV one day after GRB onset is predicted¹, if one assumes a redshift of 0.15. This is within H.E.S.S. detection limit. The detection of VHE photons (and its quantity) or upper limits (in cases of null detections) could be used to constrain GRB properties, eg. bulk Lorentz factor and ambient density [5, 6]. Currently, the most sensitive detectors in the VHE gamma-ray regime are air Cherenkov systems, including H.E.S.S., MAGIC, VERITAS, and Whipple. While still no detection using any of the instruments is established, results on upper limits have been reported by the MAGIC collaboration [7] and the Whipple collaboration [8]. In general, their results are consistent with power-law extrapolation of the keV spectra obtained with satellite data.

At cosmological distances, one has to take into account the absorption of VHE gamma-ray by extragalactic background light (EBL). For low-redshift GRBs and sub-TeV energies, the attenuation is less significant. Moreover, there is evidence from distant blazar spectra that the Universe is more transparent for VHE gamma-ray than previously thought [9]. Thus, current air Cherenkov systems are able to observe out to $z \sim 1$ at ~ 100 GeV.

H.E.S.S. GRB observing program

The H.E.S.S. array is a system of four 13m-diameter Imaging Atmospheric Cherenkov Telescopes (IACTs) located in the Khomas Highland of Namibia [21]. Since the completion of the whole array in late 2003, H.E.S.S. has proven to be very successful in VHE gamma-ray astronomy, thus opening a new era in astronomy in this observational window. The array is one of the most sensitive VHE gamma-ray detectors. For a point source

with integral flux $\sim 1.4 \times 10^{-11} \text{ ph cm}^{-2} \text{ s}^{-1}$ above 1 TeV and spectral index 2.6, only a 2-hour H.E.S.S. observation is required for a 5- σ detection.

We have been observing GRBs since early 2003. At the beginning of 2005, a GRB coordination team was set up and since then our GRB observation program has been fully established. An automated program is running on site to keep the shift crew alerted of any new detected GRBs in real-time.

We have followed on-board GRB triggers distributed by *Swift*, as well as triggers from INTEGRAL and HETE II confirmed by ground-based analysis. Upon the reception of a GRB Coordinates Network (GCN) notice from one of these satellites (with good indications that the source is a genuine GRB), we will observe the burst position as soon as possible, limited to $ZA < 45^\circ$ (to ensure a reasonably low energy threshold) and HESS dark time². We start observing the burst position up to 24 hours after the burst time. The nominal observation time is 2 hours (within the above observational constraints). If there are tentative positive signals indicated by a quick analysis, further observations will be carried out accordingly.

In Table 1, we show 17 GRBs which we have observed using H.E.S.S. during the period from March 2003 to April 2007. All GRB data shown were taken in good weather conditions and good hardware status, while data taken in non-optimal situations are not shown and not used in further analyzes. For each burst, the start observation time, live-time of the observation and the mean zenith angle (ZA) are presented.

Data Analysis and Results

Calibration of data, the event reconstruction and rejection of the cosmic-ray background (i.e. gamma-ray event selection criteria) were performed as described in [11]. Except for the case of GRB 030329, where a different analysis cut was

1. The attenuation factor due to EBL absorption is about 0.1 at 1 TeV for a GRB with $z = 0.15$ [9].

2. H.E.S.S. observations are taken in darkness and when the moon is below the horizon. The fraction of H.E.S.S. dark time is about 0.2.

used because only two telescopes were operating, standard analysis cuts as described in [6] were applied to each GRB to search for any possible signal. The background was then estimated using the reflected-region model as described in [13]. The energy threshold (E_{th}) after analysis cuts of each GRB observation (mainly depending on the zenith angle) is shown in Table 1.

No evidence of excess events for any GRB observed using H.E.S.S. was seen. The 99.9% confidence level (c.l.) integral photon flux upper limits above E_{th} using the method of [14] for each GRB are included in Table 1. For GRBs with reported redshifts < 1 , the EBL-corrected values using the P0.45 model as in [9] are also shown. For GRBs with redshifts > 1 , the attenuation of VHE gamma-ray by EBL is large, thus the EBL-corrected values are much higher (which are not shown here).

Acknowledgements

The support of the Namibian authorities and of the University of Namibia in facilitating the construction and operation of H.E.S.S. is gratefully acknowledged, as is the support by the German Ministry for Education and Research (BMBF), the Max Planck Society, the French Ministry for Research, the CNRS-IN2P3 and the Astroparticle Interdisciplinary Programme of the CNRS, the U.K. Science and Technology Facilities Council (STFC), the IPNP of the Charles University, the Polish Ministry of Science and Higher Education, the South African Department of Science and Technology and National Research Foundation, and by the University of Namibia. We appreciate the excellent work of the technical support staff in Berlin, Durham, Hamburg, Heidelberg, Palaiseau, Paris, Saclay, and in Namibia in the construction and operation of the equipment.

References

- [1] Waxman, E. 2006, Nuclear Physics B (Proc. Suppl.), 151, 46.
- [2] Hurley, K. et al. 1994, Nature, 372, 652.
- [3] Zhang, B. & Mészáros, P. 2004, Int. J. Mod. Phys. A., 19, 2385
- [4] Zhang, B. & Mészáros, P. 2001, ApJ, 559, 110.
- [5] Pe’er, A. & Waxman, E. 2005, ApJ, 633, 1018.
- [6] Wang X. Y. et al. 2005, A&A, 439, 957.
- [7] Albert, J. et al. 2007, submitted to ApJ
- [8] Horan, D. et al. 2007, ApJ, 655, 396.
- [9] Aharonian, F. A. et al. (HESS collaboration) 2006a, Nature, 440, 1018.
- [10] Hinton, J. A. 2004, New Astronomy Review, 48, 331.
- [11] Aharonian, F. A. et al. (HESS collaboration) 2006b, A&A, 457, 899.
- [12] Benbow, W. 2005, Proc. of Towards a Network of Atmospheric Cherenkov Detectors VII (Palaiseau), 163
- [13] Berge, D., Funk, S. & Hinton, J. A. 2007, A&A, 466, 1219.
- [14] Feldman, G. J. & Cousins, R. D. 1998, Phys. Rev. D., 57, 3873.
- [15] Berger, E. & Fox, D. 2007, GCN Circular, 6101.
- [16] Berger, E. & Gladders, M. 2006, GCN Circular, 5170.
- [17] Ofek, E. O. et al. 2007, ApJ, 662, 1129.
- [18] D’Elia, V. et al. 2005, GCN Circular 4044.
- [19] de Pasquale, M. et al. 2007, MNRAS, 377, 1638.
- [20] Soderberg, A. M. et al. 2006, ApJ, 636, 391.
- [21] Stanek, K. Z. et al. 2003, ApJ, 591, L17.

Table 1: GRBs observed with H.E.S.S. from March 2003 to April 2007. All GRB data shown were taken in good weather conditions and good hardware status. For each burst, start observation time, live-time, mean zenith angle (ZA), energy threshold (E_{th}) and 99.9% c.l. upper limit (UL) of the observation are presented.

GRB	Observation starts after GRB onset	live time (hrs)	mean ZA (deg)	E_{th} (GeV)	Flux ULs* ($\text{ph cm}^{-2} \text{s}^{-1}$)	redshift
070429A	64 min	0.5	21	310	1.06×10^{-12}	–
070419B	15.1 h	1.0	48	750	3.89×10^{-12}	–
070209	15.4 h	1.0	41	660	$4.49 \times 10^{-12}(1.70 \times 10^{-9})$	0.314 [†]
060526	4.7 h	1.9	25	200	5.90×10^{-12}	3.21 [16]
060505	19.4 h	2.0	42	450	$6.29 \times 10^{-12}(1.55 \times 10^{-11})$	0.089 [17]
060403	13.6 h	0.9	39	310	9.37×10^{-12}	–
050922C	52 min	0.7	23	200	1.22×10^{-11}	2.199 [18]
050801	16 min	0.5	43	370	3.40×10^{-12}	1.56 [‡]
050726	10.8 h	2.0	40	400	4.22×10^{-12}	–
050607	14.8 h	1.5	37	290	5.39×10^{-12}	–
050509C	21 h	1.0	22	220	1.08×10^{-11}	–
050209	20.2 h	2.5	48	520	3.32×10^{-12}	–
041211	9.5 h	2.0	46	420	4.00×10^{-12}	–
041006	4.7 h	1.4	27	220	$1.01 \times 10^{-11}(2.69 \times 10^{-8})$	0.716 [20]
040425	26 h	0.4	28	230	2.37×10^{-11}	–
030821	18 h	1.0	28	290	1.52×10^{-11}	–
030329	11.5 d	0.5	60	1400	$2.58 \times 10^{-12}(5.59 \times 10^{-11})$	0.169 [21]

* Flux upper limits ($> E_{\text{th}}$) are at the 99.9% c.l. using the method given in [14]. For GRBs with redshifts < 0.5 , the EBL-corrected values in the energy range $[E_{\text{th}}, 10 \text{ TeV}]$ are also given in the brackets. For GRB041006, the EBL-corrected value in the energy range $[E_{\text{th}}, 0.7 \text{ TeV}]$ is given.

[†] Redshift of a host galaxy candidate found by [15].

[‡] Photometric redshift according to [19].



Search for a Dark Matter annihilation signal from the Sagittarius dwarf galaxy with H.E.S.S.

E. MOULIN¹, C. FARNIER², J.-F. GLICENSTEIN¹, A. JACHOLKOWSKA², L. ROLLAND³, M. VIVIER¹,
FOR THE H.E.S.S. COLLABORATION

¹DAPNIA/DSM/CEA, CE Saclay, F-91191 Gif-sur-Yvette Cedex, France

²Laboratoire de Physique Théorique et Astroparticules, Université Montpellier II, CC 70, Place Eugène Bataillon, F-34095 Montpellier Cedex 5, France

³Laboratoire d'Annecy-le-Vieux de Physique des Particules, IN2P3/CNRS, 9 Chemin de Bellevue, BP 110 F-74941 Annecy-le-Vieux Cedex, France

emmanuel.moulin@cea.fr

Abstract: Dwarf Spheroidal galaxies are amongst the best targets to search for a Dark Matter (DM) annihilation signal. The annihilation of WIMPs in the center of Sagittarius dwarf spheroidal (Sgr dSph) galaxy would produce high energy γ -rays in the final state. Observations carried out with the H.E.S.S. array of Imaging Atmospheric Cherenkov telescopes are presented. A careful modelling of the Dark Matter halo profile of Sgr dwarf was performed using latest measurements on its structural parameters. Constraints on the velocity-weighted cross section of Dark Matter particles are derived in the framework of Supersymmetric and Kaluza-Klein models.

Introduction

Astrophysical and cosmological observations provide a substantial body of evidences for the existence of Cold Dark Matter (CDM) although its nature remains still unknown. It is commonly assumed that CDM is composed of yet undiscovered non-baryonic particles for which plausible candidates are Weakly Interacting Massive Particles (WIMPs). In most theories, candidates for CDM are predicted in theories beyond the Standard Model of particle physics [6]. The annihilation of WIMPs into γ -rays may lead to detectable very high energy (VHE, $E > 100$ GeV) γ -ray fluxes above background via continuum emission from the hadronization and decay of the cascading annihilation products, predominantly from π^0 's generated in the quark jets. Among the best-motivated CDM candidates are the lightest neutralino $\tilde{\chi}$ provided by R-parity conserving supersymmetric extensions of the Standard Model [12], and the lightest Kaluza-Klein particle (LKP) [19] in universal extra dimension theories which is most often the first KK mode of the hypercharge gauge boson,

$\tilde{B}^{(1)}$. The H.E.S.S. array of Imaging Atmospheric Cherenkov Telescopes (IACTs), designed for high sensitivity measurements in the 100 GeV - 10 TeV energy regime, is a suitable instrument to detect VHE γ -rays and investigate their possible origin. Dwarf Spheroidal galaxies such as Sagittarius or Canis Major, discovered recently in the Local Group, are among the most extreme DM-dominated environments. Indeed, measurements of roughly constant radial velocity dispersion of stars imply large mass to luminosity ratios [20]. The core of the Sgr dSph at $l=5.6^\circ$ and $b=-14^\circ$ in galactic coordinates at a distance of about 24 kpc from the Sun [14]. Latest velocity dispersion measurements on M giant stars with 2MASS yields a mass to light ratio of about 25 [13]. The luminous density profile of Sgr dSph has two components [16]. The compact component, namely the core, is characterized by a size of about 3 pc FWHM, which corresponds to a point-like region for H.E.S.S. This is the DM annihilation region from which γ -ray signal may be expected. A diffuse component is well fitted by a King model with a characteristic size of 1.6 kpc.

We present in this paper the observations of the Sgr dSph galaxy by the H.E.S.S. array of Imaging Atmospheric Cherenkov Telescopes. A careful modeling of the Dark Matter halo using the latest measurements on the structural parameters of Sagittarius is presented to derive constraints on the WIMP velocity-weighted annihilation rate.

Search for VHE γ -rays from observations of Sagittarius dwarf by H.E.S.S.

H.E.S.S. (High Energy Stereoscopic System) has observed the Sgr dSph in June 2006 with zenith angles ranging from 7° to 43° around an average value of 19° . A total of 11 hours of high quality data are available for the analysis after standard selection cuts. After calibration of the raw shower images from PMT signals [1], two independent reconstruction techniques were combined to select γ -ray events and reconstruct their direction and energy. The first one uses the Hillas moment method [2]. The second analysis referred hereafter as “Model Analysis”, is based on the pixel-per-pixel comparison of the shower image with a template generated by a semi-analytical shower development model [7, 8]. The separation between γ candidates and hadrons is done using a combination of the Model goodness-of-fit parameter [8] and the Hillas mean scaled width and length parameters, which results in an improved background rejection [3]. An additional cut on the primary interaction depth is used to improve background rejection.

The on-source signal is defined by integrating all the events with angular position θ in a circle around the target position with a radius of θ_{cut} . The target position is chosen according to the photometric measurements of the Sgr dSph luminous cusp showing that the position of the center corresponds to the center of the globular cluster M 54 [15]. The target position is thus found to be (RA = $18^h55^m59.9s$, Dec = $-30^d28'59.9''$) in equatorial coordinates (J2000.0). The signal coming from Sgr dSph is expected to come from a region of 1.5 pc, about $30''$, much smaller the H.E.S.S. point spread function (PSF). A θ_{cut} value of 0.14° suitable for a point-like source was therefore used in the analysis. In case of a Navarro-Frenk-White (NFW) density profile [17] for which ρ follows r^{-1}

or a cored profile [9] folded with the point spread function (PSF) of H.E.S.S., the integration region allows to retrieve a significant fraction of the expected signal. See Table 1.

No significant γ -ray excess is detected in the sky map. We thus derived the 95% confidence level upper limit on the observed number of γ -rays: $N_\gamma^{95\% \text{ C.L.}}$. The limit is computed knowing the numbers of events in the signal and background regions above the energy of 250 GeV using the Feldman & Cousins method [10] and we obtain: $N_\gamma^{95\% \text{ C.L.}} = 56$. Given the acceptance of the detector for the observations of the Sgr dSph, a 95% confidence level upper limit on the γ -ray flux is also derived:

$$\Phi_\gamma(E_\gamma > 250 \text{ GeV}) < 3.6 \times 10^{-12} \text{ cm}^{-2} \text{ s}^{-1} \quad (95\% \text{ C.L.}) \quad (1)$$

Predictions of γ -ray from Dark Matter annihilations

The γ -ray flux from annihilations of DM particles of mass m_{DM} accumulating in a spherical DM halo can be expressed in the form:

$$\frac{d\Phi(\Delta\Omega, E_\gamma)}{dE_\gamma} = \frac{1}{4\pi} \underbrace{\frac{\langle\sigma v\rangle}{m_{DM}^2} \frac{dN_\gamma}{dE_\gamma}}_{\text{Particle Physics}} \times \underbrace{\bar{J}(\Delta\Omega)\Delta\Omega}_{\text{Astrophysics}} \quad (2)$$

as a product of a particle physics component with an astrophysics component. The particle physics part contains $\langle\sigma v\rangle$, the velocity-weighted annihilation cross section, and dN_γ/dE_γ , the differential γ -ray spectrum summed over the whole final states with their corresponding branching ratios. The astrophysical part corresponds to the line-of-sight-integrated squared density of the DM distribution J , averaged over the instrument solid angle integration region for H.E.S.S. ($\Delta\Omega = 2 \times 10^{-5} \text{ sr}$):

$$\bar{J}(\Delta\Omega) = \frac{1}{\Delta\Omega} \int_{\Delta\Omega} \text{PSF} * \int_{l.o.s} \rho^2(r[s]) ds d\Omega \quad (3)$$

where PSF is the point spread function of H.E.S.S. The mass distribution of the DM halo of Sgr dwarf has been described by plausible models taking into account the best available measurements of the Sgr dwarf galactic structure parameters. We have used

Halo type	Parameters	J ($10^{24}\text{GeV}^2\text{cm}^{-5}$)	Fraction of signal in $\Delta\Omega = 2 \times 10^{-5}\text{sr}$
Cusped NFW halo	$r_s = 0.2\text{ kpc}$ $A = 3.3 \times 10^7 M_\odot$	2.2	93.6%
Cored halo	$r_c = 1.5\text{ pc}$ $v_a = 13.4\text{ km s}^{-1}$	75.0	99.9%

Table 1: Structural parameters for a cusped NFW (r_s , A) and a cored (r_c , v_a) DM halo model, respectively. The values of the solid-angle-averaged l.o.s integrated squared DM distribution are reported in both cases for the solid angle integration region $\Delta\Omega = 2 \times 10^{-5}\text{sr}$.

two widely different models. The first has a NFW cusped profile [17] with the mass density given by:

$$\rho_{\text{NFW}}(r) = \frac{A}{r(r+r_s)^2} \quad (4)$$

with A the normalization factor and r_s the scale radius taken from [9]. Using Eq. 3, the value of \bar{J} obtained with this model is reported in Table 1. We have also studied a core-type halo model as in [9] characterized by the mass density:

$$\rho_{\text{core}}(r) = \frac{v_a^2}{4\pi G} \frac{3r_c^2 + r^2}{(r_c^2 + r^2)^2} \quad (5)$$

where r_c is the core radius and v_a a velocity scale. However, we have tried to update the v_a and r_c values which were used in [9]. By inserting in the Jeans equation the luminosity profile of the Sgr dwarf core of the form:

$$\nu(r) = \frac{\nu_0 r_c^{2\alpha}}{(r_c^2 + r^2)^\alpha} \quad (6)$$

we estimated from the data of [15] $\alpha = 2.69 \pm 0.10$ and $r_c = 1.5\text{ pc}$. Note that the value of r_c is only an upper limit. The value of the central velocity dispersion of Sgr Dwarf is $\sigma = 8.2 \pm 0.3\text{ km s}^{-1}$ [21]. We have assumed that the velocity dispersion is independent of position. The value of v_a is then given by $v_a = \sqrt{\alpha}\sigma = 13.4\text{ km s}^{-1}$. The cored model gives a very large value of \bar{J} , which is reported in Table 1. The third column of Table 1 gives the amount of signal expected in the solid angle integration region $\Delta\Omega = 2 \times 10^{-5}\text{sr}$. Fig. 1 shows the limits in the case of a cored (green dashed line) and cusped NFW (red dotted line) profile using the value of \bar{J} computed above. Predictions for phenomenological MSSM (pMSSM)

models are displayed (grey points) as well as those satisfying in addition the WMAP constraints on the CDM relic density (blue points). The SUSY models are calculated with DarkSUSY4.1 [11]. In the case of a cusped NFW profile, the H.E.S.S. observations do not establish severe constraints on the velocity-weighted cross section. For a cored profile, due to a higher central density, stronger

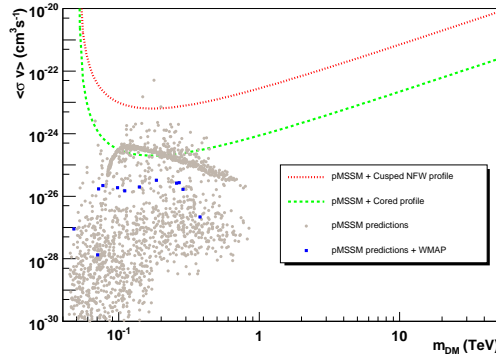


Figure 1: Upper limits at 95% C.L. on $\langle\sigma v\rangle$ versus the DM particle mass in the case of a cusped NFW (red dotted line) and a cored (green dashed line) DM halo profiles respectively. The pMSSM parameter space was explored with DarkSUSY 4.1 [11], each point on the plot corresponding to a specific model (grey point). Amongst these models, those satisfying in addition the WMAP constraints on the CDM relic density are overlaid as blue square. The limits in case of neutralino dark matter from pMSSM are derived using the parametrisation from [5] for a higgsino-type neutralino annihilation γ profiles.

constraints are derived and some pMSSM models can be excluded in the upper part of the pMSSM scanned region.

In the case of KK dark matter, the differential γ spectrum is parametrized using Pythia [18] simulations and branching ratios from [19]. Predictions for the velocity-weighted cross section of $B^{(1)}$ dark matter particle are performed using the formula given in [4]. In this case, the expression for $\langle\sigma v\rangle$ depends analytically on the $B^{(1)}$ mass

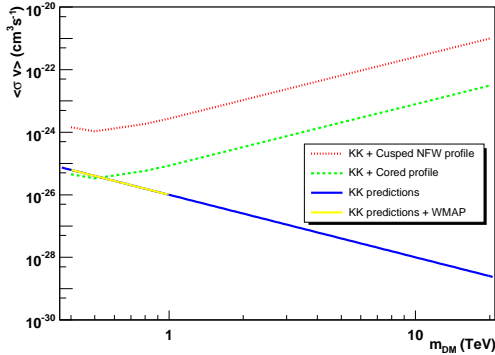


Figure 2: Upper limits at 95% C.L. on $\langle\sigma v\rangle$ versus the DM particle mass in the $B^{(1)}$ Kaluza-Klein scenarios for a cusped NFW (red dotted line) and a cored (green dashed line) DM halo profiles respectively. The blue line corresponds to Kaluza-Klein models [19]. Overlaid (yellow line) are the KK models satisfying WMAP constraints on the CDM relic density.

square. Fig. 2 shows the sensitivity of H.E.S.S. in the case of Kaluza-Klein models where the hypercharge boson $B^{(1)}$ is the LKP, for a cored (green solid line) and a cusped NFW (red solid line) profile respectively using the value of \bar{J} computed in section 3.2. With a NFW profile, no Kaluza-Klein models can be tested. In the case of a cored model, some models providing a LKP relic density compatible with WMAP constraints can be excluded. From the sensitivity of H.E.S.S., we exclude $B^{(1)}$ masses lying in the range 300 - 500 GeV.

Conclusions

The observations of Sgr dSph with H.E.S.S. reveal no significant γ -ray excess at the nominal target position. The Sagittarius dwarf DM halo profile has been modeled using latest measurements of its structure parameters. Constraints have been derived on the velocity-weighted cross section of the DM particle in the framework of supersymmetric and Kaluza-Klein models.

References

- [1] F. A. Aharonian *et al.* *A&A*, 22:109, 2004.
- [2] F. A. Aharonian *et al.* *A&A*, 430:865, 2005.
- [3] F. A. Aharonian *et al.* *A&A*, 457:899, 2006.
- [4] E. Baltz and D. Hopper. *JCAP*, 0507:001, 2005.
- [5] L. Bergström, P. Ullio, and J. Buckley. *Astroparticle Physics*, 9:137, 1998.
- [6] G. Bertone, D. Hooper, and J. Silk. *Physics Report*, 405:279, 2005.
- [7] M. de Naurois *et al.* In *International Cosmic Ray Conference*, 2003.
- [8] M. de Naurois *et al.* In *Towards a Network of Atmospheric Cherenkov Detectors*, 2005.
- [9] N. W. Evans, F. Ferrer, and S. Sarkar. *Phys. Rev. D*, 69:123501, 2004.
- [10] G. Feldman and R. Cousins. *Phys. Rev. D*, 57:3873, 1998.
- [11] P. Gondolo *et al.* *JCAP*, 0407:008, 2004.
- [12] G. Jungman, K. Kamionkowski, and K. Griest. *Phys. Rep.*, 276:195, 1996.
- [13] S. Majewski *et al.* In *IAU Symposium 220: Dark Matter in Galaxies*.
- [14] S. Majewski *et al.* *Astroparticle Journal*, 599:1082, 2003.
- [15] L. Monaco *et al.* *MNRAS*, 356:1396, 2005.
- [16] L. Monaco *et al.* *MNRAS*, 356:1396, 2006.
- [17] J. Navarro, C. Frenk, and S. White. *Astroparticle Journal*, 490:493, 1997.
- [18] PYTHIA package.
- [19] G. Servant and T. Tait. *Nucl. Phys. B*, 605:391, 2003.
- [20] M. I. Wilkinson *et al.* In *XXIst IAP Colloquium : Mass Profiles & Shapes of Cosmological Structures*.
- [21] S. Zaggia *et al.* *Mem. Soc. Astr. It. Suppl.*, 5:291, 2004.



The γ -radiation from the Galactic Center observed by H.E.S.S. and the possible dark matter interpretation

J. RIPKEN¹, G. HEINZELMANN¹, J. F. GLICENSTEIN², J. HINTON³, D. HORNS⁴, L. ROLLAND⁵, ON BEHALF OF THE H.E.S.S. COLLABORATION

¹*Institut für Experimentalphysik, Univ. Hamburg, Luruper Chaussee 149, D-22761 Hamburg, Germany*

²*DAPNIA/DSM/CEA, CE Saclay, F-91191 Gif-sur-Yvette, Cedex, France*

³*Max-Planck-Institut für Kernphysik, Saupfercheckweg 1, D-69117 Heidelberg, Germany*

⁴*Institut für Astronomie und Astrophysik, Eberhard Karls Universität Tübingen, Sand 1, D-72076 Tübingen*

⁵*LPNHE, IN2P3/CNRS, Universités Paris VI & VII, 4 Place Jussieu, F-75252 Paris Cedex 5, France*

ripkenj@mail.desy.de

Abstract: With the H.E.S.S. system of four Cherenkov telescopes a signal of very high energy γ -radiation from the direction of the Galactic center has been detected. The interpretation of the signal due to dark matter annihilation is discussed and limits on the annihilation cross sections and density profiles are given.

Introduction

The nature of the dark matter particles is still one of the outstanding problems of astrophysics. A possible candidate for a dark matter particle is provided by the R -parity conserving supersymmetric extension of the standard model of particle physics e.g. the neutralino χ . Another possible candidate is predicted by Kaluza Klein (KK) theories, the $B^{(1)}$ [1]. Both particles are neutral, stable, and could naturally match the measured matter density. Besides direct measurements of dark matter in underground experiments, indirect detections via measurement of the secondary particles produced in the self-annihilation in deep gravitational potential wells has been suggested. One product of the self-annihilation of dark matter particles is high energy γ -radiation. Regions of high mass accumulations such as the Galactic center (GC) could produce a detectable very high energy (VHE) γ -ray flux [2]. With the H.E.S.S. Cherenkov telescope array [3] the Galactic Center has been observed in 2003 and 2004 [4]. High energy γ -radiation has been observed with high significance. This radiation has been investigated in the framework of dark matter annihilation [5, 6, 7].

γ -rays from dark matter annihilation

Since the χ and the $B^{(1)}$ are Majorana particles, they can annihilate producing photons with energies up to the particle masses. Whereas the direct production of photons leading to monoenergetic γ -rays are loop suppressed most of the high energy photons are produced in decays of secondaries from the annihilation processes. These photons have a continuous energy spectrum up to the mass of the dark matter particle and are not easily distinguished from other astrophysical processes for VHE γ -rays. The calculation of the γ -ray flux leads to the formula

$$\begin{aligned}\Phi(E) &= 2.8 \cdot 10^{-10} \text{ cm}^{-2} \text{ s}^{-1} \\ &\times \frac{dN_\gamma}{dE} \left(\frac{\langle \sigma v \rangle}{\text{pb c}} \right) \left(\frac{100 \text{ GeV}}{m_{\text{DM}}} \right)^2 \\ &\times \bar{J}(\Delta\Omega) \Delta\Omega \\ \bar{J}(\Delta\Omega) \Delta\Omega &= \frac{1}{(0.3 \text{ GeV/cm}^3)^2 \cdot 8.5 \text{ kpc}} \\ &\times \int d\Omega \int_{\text{los}} dl \varrho^2\end{aligned}\quad (1)$$

where $\langle \sigma v \rangle$ denotes the mean of the annihilation cross section multiplied with the velocity of the particles and dN_γ/dE the photon energy spectrum per annihilation. The solid angle $\Delta\Omega$ denotes the

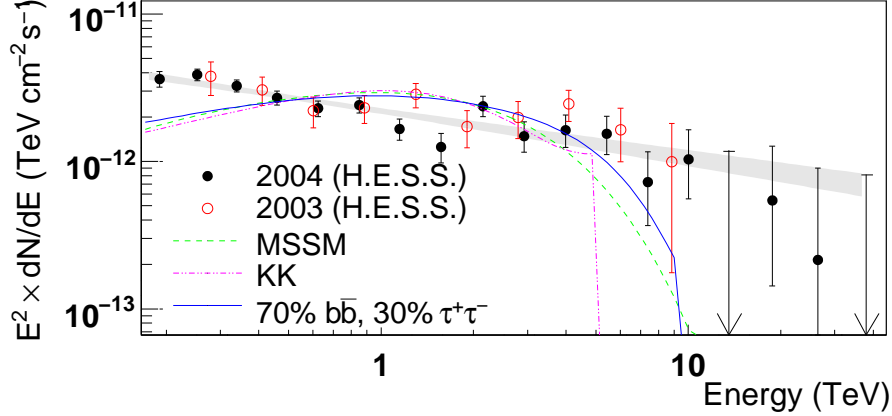


Figure 1: (Color online) Spectral energy density $E^2 \times dN/dE$ of γ -rays from the GC source, for the 2004 data (full points) and 2003 data (open points). Upper limits are 95% CL. The shaded area shows the power-law fit $dN/dE \sim E^{-\Gamma}$. The dashed line illustrates a typical spectrum of neutralino DM annihilation for best fit neutralino masses of 14 TeV. The dotted line shows the distribution predicted for KK DM with a mass of 5 TeV. The solid line gives the spectrum of a 10 TeV DM particle annihilating into $\tau^+\tau^-$ (30%) and $b\bar{b}$ (70%).

resolution of the detector or the investigated solid angle. ρ denotes the dark matter density along the line of sight (los).

The center of our Galaxy

The GC region containing the supermassive black hole Sgr A*, was observed with the H.E.S.S. telescopes in the years 2003 and 2004. High energy γ -radiation above 200 GeV was detected with a significance of 38 standard deviations (in 2004) without indications for variability. Further data have been collected in 2005 and 2006 not yet included in this analysis.

The central region of our Galaxy is due to its proximity (≈ 8.5 kpc) and the expectation of high mass concentration a target for the indirect search for dark matter. The scaling factor $\bar{J}(\Delta\Omega)\Delta\Omega$ depends strongly on the not well known density profile. We consider the results of N -body-simulations from Navarro, Frenk and White (NFW) predicting $\rho(r) \propto r^{-1}$ [8] and Moore et al. predicting $\rho(r) \propto r^{-1.5}$ [9].

The measured spectrum can be described by a powerlaw

$$\Phi(E) = \Phi_0 \left(\frac{E}{1 \text{ TeV}} \right)^{-\Gamma} \quad (2)$$

with an index of $\Gamma = 2.25 \pm 0.04_{\text{stat}} \pm 0.10_{\text{syst}}$. The integral flux above 1 TeV is $(1.87 \pm 0.10_{\text{stat}} \pm 0.30_{\text{syst}}) \cdot 10^{-12} \text{ cm}^{-2} \text{ s}^{-1}$.

In the following, two different assumptions are used to derive conclusions on dark matter annihilation from the observed radiation:

1. The flux results solely from dark matter annihilation as discussed in [5] and [10] exploring the consistency of the required mass density and cross section with other observations. This hypothesis explores the mass and cross section of the dark matter particle and the density profile of the dark matter halo in the central region of our Galaxy.
2. Only a part of the signal originates from dark matter annihilation, whereas the remaining part is produced by other processes and sources. This hypothesis can constrain either particle properties assuming a density profile of the factor $\bar{J}(\Delta\Omega)\Delta\Omega$ assuming in turn a range of cross sections.

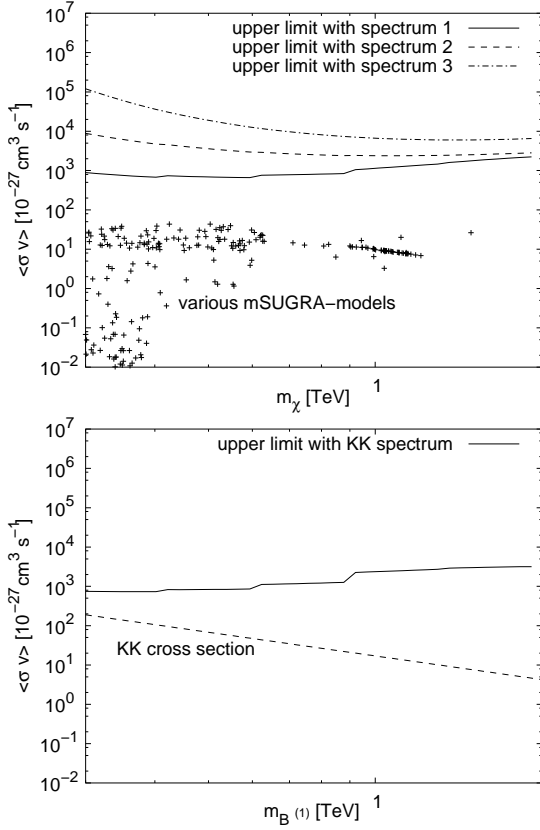


Figure 2: Upper limits (99% CL) on the annihilation cross section for neutralinos (upper panel) and KK particle (lower panel) as function of the dark matter particle mass assuming an NFW profile.

Hypothesis 1: 100 % dark matter annihilation radiation

Density profile: The density profile of the dark matter in the inner part of the halo can be approximated by $\rho \sim r^{-\alpha}$. Instead of the integration over the solid angle $\Delta\Omega$ in equation 1 we convolute the line of sight integral with the point spread function of the detector (the H.E.S.S. experiment). In the GC region are molecular clouds which lead to a diffuse radiation of γ -radiation [11] which has been subtracted for this investigation. The remaining signal from the Galactic Center is compatible with a point source. For α a lower limit of 1.2 with a confidence level of 95% was derived [7]. This is not compatible with an NFW profile, but with a Moore profile.

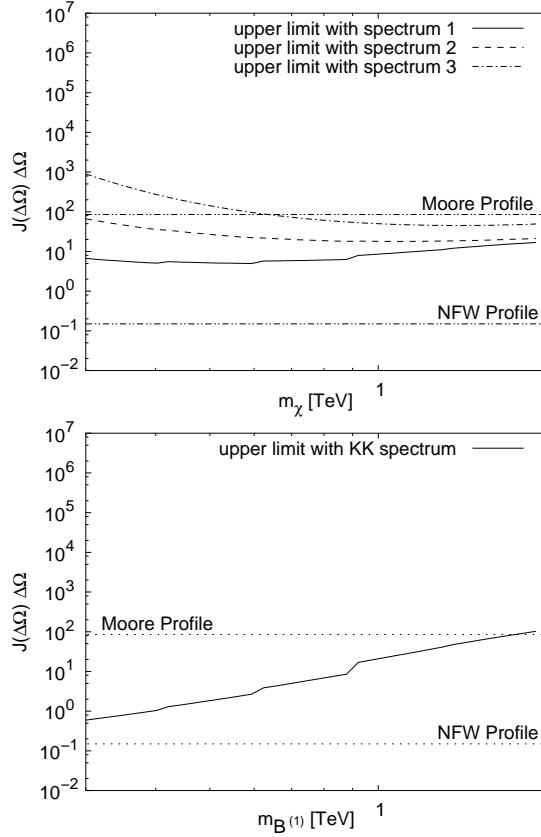


Figure 3: Upper limits on $\bar{J}(\Delta\Omega)\Delta\Omega$ assuming a cross section for neutralinos (upper panel) and KK particles (lower panel) as function of the dark matter particle mass.

Energy spectrum: The energy spectrum measured by H.E.S.S. reaches up to more than 10 TeV. This would require a very massive dark matter particle close to the unitarity limit [12]. The favored mass range of the dark matter particles is below 1 TeV [13] in the considered models, but such high masses, not violating the unitarity limit, cannot be ruled out completely.

In Figure 1 the spectral energy distribution measured by H.E.S.S. is shown together with fits of a neutralino annihilation spectrum parameterized according to [5] and a $B^{(1)}$ annihilation spectrum from [10]. Clearly, the expected curvature of the predicted energy spectra is not matching the data which is in reasonable agreement with a power law type function. With nonminimal SUSY models

flatter spectra can be obtained, but they also don't fit the measured spectrum well. Hypothesis 1 can therefore be ruled out.

Hypothesis 2: Background and dark matter annihilation radiation

In the GC region other processes may produce γ -radiation above 100 GeV. This may result in a γ -ray background to a hypothetical annihilation. The strength of the annihilation radiation (equation 1) for a given particle mass m_{DM} is proportional to $A = \langle \sigma v \rangle \cdot J(\Delta\Omega)\Delta\Omega$. Fitting the assumed background (a power law) plus the fixed annihilation component we get a function $\chi^2(A)$, which provides the upper limits on A . With this limits we can produce upper limits either on the cross section $\langle \sigma v \rangle$ of the annihilation by assuming a density profile or on $\bar{J}(\Delta\Omega)\Delta\Omega$ with a fixed cross section. In the Figures 2 and 3 these upper limits are shown as functions of the particle mass for neutralino dark matter and for KK dark matter. In the supersymmetric scenario the number of photons per annihilation depends on the parameter set used. Three spectra which are encompassing all probabilities are used. The mSUGRA model cross sections are calculated with DarkSUSY 4.1 [14]. The KK annihilation spectrum and its cross section is described in [10]. With an NFW profile no cross section neither from supersymmetric models (calculated with DarkSUSY 4.1 [14]) nor with KK dark matter can be ruled out. With a mean cross section for neutralinos or the expected cross section for KK particles a profile suggested by Moore can be ruled out for all considered neutralino masses.

Conclusion

We have investigated whether part or all of the high energy γ -radiation from the GC observed by H.E.S.S. could be attributed to dark matter annihilation. The energy spectrum can't be reconciled by either a neutralino annihilation spectrum or with a spectrum produced by KK dark matter only. Considering an additional background we can exclude a large line of sight integral of the squared density. For an NFW profile still no model, neither mSUGRA nor KK dark matter, can be ruled out.

Acknowledgements: The support of the Namibian authorities and of the University of Namibia in facilitating the construction and operation of

H.E.S.S. is gratefully acknowledged, as is the support by the German Ministry for Education and Research (BMBF), the Max Planck Society, the French Ministry for Research, the CNRS-IN2P3 and the Astroparticle Interdisciplinary Programme of the CNRS, the U.K. Particle Physics and Astronomy Research Council (PPARC), the IPNP of the Charles University, the South African Department of Science and Technology and National Research Foundation, and by the University of Namibia. We appreciate the excellent work of the technical support staff in Berlin, Durham, Hamburg, Heidelberg, Palaiseau, Paris, Saclay, and in Namibia in the construction and operation of the equipment.

References

- [1] G. Servant and T. M. P. Tait, Nucl.Phys. B, 650 (2003) 391-419
- [2] L. Bergström, P. Ullio and J. H. Buckley, Astroparticle Physics, 9 (1998) 137
- [3] K. Bernlöhner, O. Carrol and R. Cornils et al., Astroparticle Physics, 20 (2003) 111
- [4] F. Aharonian, et al. (H.E.S.S. collaboration), A&A, 425 (2004) 13
- [5] D. Horns, Phys.Lett. B, 607 (2005) 225
- [6] J. Ripken et al. (H.E.S.S. collaboration), Proceedings of 29th ICRC, 5 (2005) 151
- [7] F. Aharonian et al. (H.E.S.S. collaboration), Physical Review Letters, 97 (2006) 22, 221102
- [8] J. F. Navarro, C. S. Frenk and S. D. M. White, ApJ 490 (1997) 493
- [9] B. Moore, et al., MNRAS, 355 (1999) 794
- [10] L. Bergström, T. Bringmann, M. Eriksson and M. Gustafsson, Phys.Rev.Lett. 94 (2005) 131301
- [11] F. Aharonian et al. (H.E.S.S. collaboration), Nature, 439 (2006) 695
- [12] K. Griest, M. Kamionkowski, Phys. Rev. Lett. 61 (1990) 615
- [13] J. Ellis, K. A. Olive, Y. Santoso and V. C. Spanos, Phys.Lett. B565 (2003) 176-182
- [14] P. Gondolo, J. Edsjö, P. Ullio, L. Bergström, M. Schelke and E.A. Baltz, JCAP 0407 (2004) 008



Energy spectrum of cosmic iron nuclei measured by H.E.S.S.

R. BÜHLER¹ FOR THE H.E.S.S. COLLABORATION

¹Max-Planck-Institut für Kernphysik, P.O. Box 103980, D 69029 Heidelberg, Germany

rolf.buehler@mpi-hd.mpg.de

Abstract: A recently proposed novel technique for the detection of cosmic rays with arrays of *Imaging Atmospheric Cherenkov Telescopes* is applied to data from the High Energy Stereoscopic System (H.E.S.S.). The method relies on the ground based detection of Cherenkov light emitted from the primary particle prior to its first interaction in the atmosphere. The charge of the primary particle (Z) can be estimated from the intensity of this light, since it is proportional to Z^2 . Using H.E.S.S. data, an energy spectrum for cosmic-ray iron nuclei in the energy range 13–200 TeV is derived. The reconstructed spectrum is consistent with previous direct measurements and is the most precise measurement so far in this energy range.

Introduction

At present the best measurements of elemental composition of cosmic rays in the energy range 1 GeV to 0.5 PeV come from long duration balloon flights [10]. Because of the decreasing flux of cosmic rays and the limited collection area of these experiments ($\approx 1 \text{ m}^2$), it is hard to extend such measurements to higher energies. A further improvement in the accuracy and energy range of composition measurements of cosmic rays could however provide crucial information about the acceleration mechanism and propagation of these particles.

In 2001, Kieda et al. [2] proposed a new method for the measurement of cosmic rays with *Imaging Atmospheric Cherenkov Telescopes* (IACTs). The measurement from the ground takes advantage of the huge detection area ($\approx 10^5 \text{ m}^2$) of IACTs, in principle enabling the extension of spectral and composition measurements up to $\sim 1 \text{ PeV}$. Here we review this technique and describe its application to data from the *High Energy Stereoscopic System* (H.E.S.S.). We present the measurement of the iron spectrum and give an outlook on future applications of this method (a more detailed description of the analysis and the results can be found in [5]).

Technique

When cosmic rays enter the atmosphere they emit Cherenkov light (so called *Direct Cherenkov Light*) above an element-dependent energy threshold. The Cherenkov angle increases with the density of the surrounding medium. The emission angle of the DC-light therefore increases with increasing depth of the primary particle in the atmosphere, creating a light cone on the ground with a radius of roughly 100 m (see Fig. 1). At a typical height of 30 km the particle interacts and a particle cascade is induced (Extensive Air Shower, EAS). The Cherenkov light from these secondary particles creates a second, wider, light cone on the ground.

The intensity of the DC-light is proportional to the square of the charge Z of the emitting particle, and can therefore be used to identify the primary particle. The challenge for detecting DC-light is to distinguish it from the ≈ 100 times brighter EAS-light background. Because the DC-light is emitted higher in the atmosphere, it is emitted at a smaller angle than the EAS-light, and is therefore imaged closer to the shower direction in the camera plane. A typical emission angle for DC-light is 0.15° to 0.3° , whereas most of the EAS-light is emitted at angles greater 0.4° from the direction of the primary particle. The H.E.S.S. Cherenkov cameras,

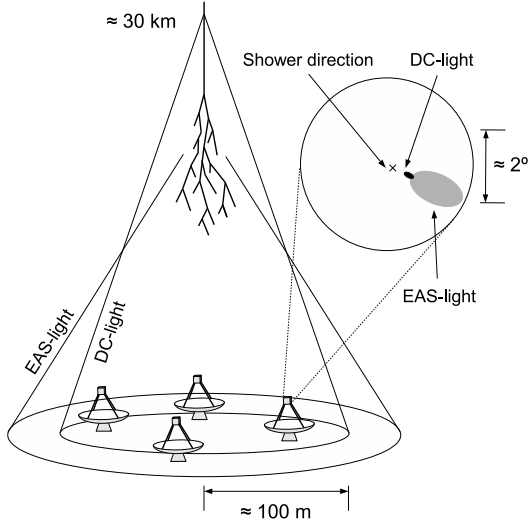


Figure 1: Schematic representation of the Cherenkov emission from a cosmic-ray primary particle and the light distribution on the ground and in the camera plane of an IACT.

with pixel sizes of 0.16° , are therefore able to resolve the DC-emission as a single bright pixel between the reconstructed shower direction and the *center of gravity* (cog) of the EAS-image in the camera plane (Fig. 1).

The energy range over which this technique can be applied depends on the charge of the primary particle [2]. At lower energies the limiting factor is that the primary particle momentum must exceed the Cherenkov threshold. At very high energies, the EAS-light outshines the DC-light, making the detection of the latter impossible. The reason for this is that the intensity of the EAS-light increases approximately linearly with energy, whereas the amount of emitted DC-photons remains basically constant above a certain energy. Because of their large atomic number and high flux compared to other heavy elements, iron nuclei are well suited for DC-light detection. The lower energy threshold for the detection of these nuclei is ~ 10 TeV.

H.E.S.S. Data

A total of 357 hours live time of H.E.S.S. data were considered for the analysis. The camera im-

ages were calibrated and the particle energy and direction were reconstructed using the standard H.E.S.S. analysis [3, 4]. Afterwards, the DC-Light is identified as a single high intensity pixel in the aforementioned angular area of the camera (Fig. 1). Once a DC-light pixel is found in a camera image, the DC-light intensity I_{DC} is reconstructed by subtracting the mean intensity of the neighboring pixels $I_{neighb.pixels}$ from the DC-pixel intensity:

$$I_{DC} = I_{DC-pixel} - \langle I_{neighb.pixels} \rangle \quad (1)$$

In total 1899 events with DC-light detection in at least two camera images were found in the data-set (events with DC-light detection in only one camera image were not considered in the analysis to minimize systematic uncertainties [5]). The elemental composition of these events is estimated using the Z dependence of the DC-light intensity. The reconstructed charge Z^* is defined as:

$$Z^* = d(E, \theta) \sqrt{I_{DC}}, \quad (2)$$

where θ is the zenith angle, E the reconstructed energy of the particle and $d(E, \theta)$ is a factor that normalizes the mean of the Z^* distribution from iron simulations to the atomic number Z of iron. The fraction k_{Fe} of iron events among the data is then measured by a two-component model fit to the Z^* distribution of the data. The first component of this model is the Z^* distribution of simulated iron nuclei. The second component is a sum of the Z^* distribution of lighter nuclei. The relative composition of the lighter charge bands (= all except the iron band, defined as $Z > 24$) is kept fixed to a reference composition, so that k_{Fe} is the single free parameter of the fit. The reference composition is taken from the elemental flux compilations given in [11, 1]. The flux errors of these compilations are afterwards propagated into the fit result.

Iron Flux

The iron fraction in the data was measured in five energy bins. The differential iron flux $\phi(E)$ can then be estimated in each bin as:

$$\phi(E) = \frac{N_{DC}(E)}{A_{eff}(E) \cdot \Delta E \cdot t} \cdot k_{Fe}, \quad (3)$$

where $N_{DC}(E)$ is the number of detected DC-events in the energy interval from E to $E + \Delta E$,

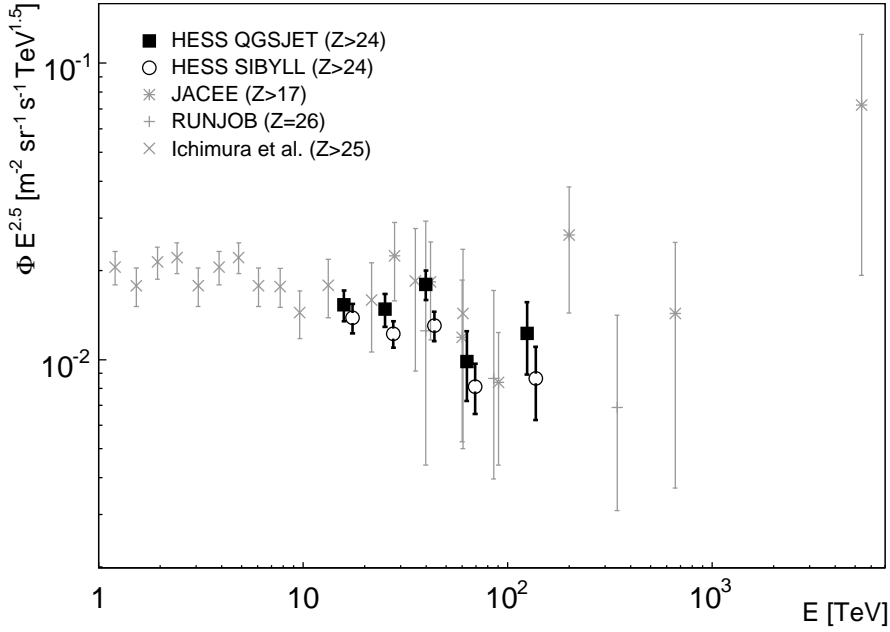


Figure 2: Differential iron energy spectrum measured with H.E.S.S. for the hadronic models QGSJET and SIBYLL multiplied by $E^{2.5}$ for better visibility of structures. The spectral points for both models are measured for the same energies. For better visibility the SIBYLL points were shifted 10% upwards in energy. The error bars show the statistical errors. The systematic flux error in each bin is 20%. The measurements from balloon experiments with data points at the highest energies are shown for comparison [8, 10, 9]. When comparing the measurements one should bear in mind that the experiments have different charge thresholds for their definition of the iron band (see legend).

t is the total live-time of the data-set and A_{eff} is the mean effective area times the field of view of the detector, averaged over the zenith angle of the observations, taking into account the efficiency of selection cuts.

A_{eff} is derived from atmospheric shower simulations of iron nuclei. These simulations rely on the detailed modeling of the hadronic interaction in EAS-showers at energies that are not accessible to current particle accelerators. To assess the systematic errors arising from uncertainties in these interactions, the analysis is performed with simulations based on two independent hadronic interaction models, SIBYLL 2.1 [9] and QGSJET 01f [14].

The resulting iron energy spectrum is shown in Fig. 2 for both hadronic models, together with the highest energy balloon measurements. The derived spectra agree well with these measurements for both models and are well fit by a power law $\phi(E) = \phi_0 (\frac{E}{\text{TeV}})^{-\gamma}$. The best fit values for the SIBYLL spectrum are given by $\phi_0 = (0.029 \pm 0.011) \text{ m}^{-2}\text{sr}^{-1} \text{ TeV}^{-1}$ and $\gamma = 2.76 \pm 0.11$ with an χ^2/ndf of 3.0/3. For the QGSJET spectrum the best fit values are $\phi_0 = (0.022 \pm 0.009) \text{ m}^{-2}\text{sr}^{-1} \text{ TeV}^{-1}$ and $\gamma = 2.62 \pm 0.11$ with χ^2/ndf of 5.3/3.

The difference between the two measured spectra gives an estimate of the systematic error introduced due to hadronic modeling. We note that, despite this uncertainty, the presented measurement is the most precise so far in its energy range. The result confirms the flux measurements from balloon ex-

periments with an independent technique, giving confidence in both results.

Outlook

Future improvements of the DC-light technique could extend the energy range of the measurement to an energy of ~ 1 PeV. Besides larger statistics, this extension requires additional separation power of the DC-light from the EAS-light. As shown in [2], additional separation power can be achieved using the time structure of the DC-light, since it arrives with a typical delay of 4 ns with respect to the EAS light. This fact could not be exploited in the analysis presented because the H.E.S.S. data used here were taken with the standard integration window of 16 ns. However, current and planned Cherenkov telescopes, which routinely store pulse timing information [6, 7], may take advantage of this characteristic.

Due to the strong dependence of the DC-light yield on the charge of the primary particle, the DC-light technique has great potential for composition measurements. The limiting factor in the charge resolution is currently the accuracy of shower reconstruction. However, future IACT's, with pixels of smaller angular size and more nearby telescopes could provide the needed reconstruction accuracy [5].

Acknowledgments

The support of the Namibian authorities and of the University of Namibia in facilitating the construction and operation of H.E.S.S. is gratefully acknowledged, as is the support by the German Ministry for Education and Research (BMBF), the Max Planck Society, the French Ministry for Research, the CNRS-IN2P3 and the Astroparticle Interdisciplinary Programme of the CNRS, the U.K. Science and Technology Facilities Council (STFC), the IPNP of the Charles University, the Polish Ministry of Science and Higher Education, the South African Department of Science and Technology and National Research Foundation, and by the University of Namibia. We appreciate the excellent work of the technical support staff in Berlin, Durham, Hamburg, Heidelberg, Palaiseau, Paris,

Saclay, and in Namibia in the construction and operation of the equipment.

References

- [1] H. Meyer B. Wiebel-Sooth, P. L. Biermann. Individual element spectra: prediction and data. *Astronomy & Astrophysics*, 330:389, 1998.
- [2] S.P. Swordy D. B. Kieda and S.P. Wakely. A high resolution method for measuring cosmic ray composition beyond 10 TeV. *Astroparticle Physics*, 15:287, 2001.
- [3] F. Aharonian et al. Calibration of cameras of the H.E.S.S. detector. *Astroparticle Physics*, 22:109, 2004.
- [4] F. Aharonian et al. Observations of the Crab Nebula with H.E.S.S. *Astronomy & Astrophysics*, 457:899, 2006.
- [5] F. Aharonian et al. First ground based measurement of atmospheric Cherenkov light from cosmic rays. *Phys. Rev. D*, 75:042004, 2007.
- [6] J. Cortina et al. Technical Performance of the MAGIC Telescope. *Proc. 29th ICRC, Pune*, 5:359, 2005.
- [7] J. Holder et al. The first VERITAS telescope. *Astroparticle Physics*, 25:391, 2006.
- [8] K. Asakimori et al. Energy Spectra and Elemental Composition of Nuclei above 100 TeV from a Series of the JACEE Balloon Flight. *Proc. 24th ICRC, Rome*, 2:707, 1995.
- [9] M. Ichimura et al. Observation of heavy cosmic-ray primaries over the wide energy range from ~ 100 GeV / particle to ~ 100 TeV / particle: Is the celebrated knee actually so prominent? *Phys. Rev. D*, 48:1949, 1993.
- [10] V. A. Derbina et al. Cosmic-ray spectra and composition in the energy range of 10-100 TeV per particle obtained by the RUNJOB experiment. *The Astrophysical Journal*, 628:L41, 2005.
- [11] J. R. Hörandel. On the knee in the energy spectrum of cosmic rays. *Astroparticle Physics*, 19:193, 2003.
- [12] A. I. Pavlov N. N. Kalmykov, S. S. Ostapchenko. Quark-gluon-string model and EAS simulation problems at ultra-high energies. *Nucl. Phys. B (Proc. Suppl.)*, 52, 1997.
- [13] P. Lipari T. Stanev R. S. Fletcher, T. K. Gaisser. SIBYLL: An event generator for simulation of high energy cosmic ray cascades. *Phys. Rev. D*, 50:5710, 1994.



Measurement of Cosmic Ray Electrons with H.E.S.S.

KATHRIN EGBERTS¹, CHRISTOPHER VAN ELDIK¹, JIM HINTON² FOR THE H.E.S.S. COLLABORATION

¹*Max-Planck-Institut für Kernphysik, P.O. Box 103980, D 69029 Heidelberg, Germany*

²*School of Physics & Astronomy, University of Leeds, Leeds LS2 9JT, UK*

kathrin.egberts@mpi-hd.mpg.de

Abstract: Due to energy losses in the interstellar medium, cosmic ray electrons at TeV energies carry information on local (within a few hundred parsecs) accelerators. However, measurements of the spectrum of the cosmic ray electrons beyond 1 TeV are extremely difficult due to the rapidly declining flux and the much more numerous background of nucleonic cosmic rays. The very large collection area of Cherenkov telescope arrays makes them promising instruments with which to measure these high energy electrons. While Cherenkov telescopes solve the problem of low fluxes of cosmic ray electrons in the TeV range, they still have to deal with the problem of distinguishing electrons from the nucleonic background. Here we report on first results towards a measurement of the cosmic ray electron spectrum with the High Energy Stereoscopic System (H.E.S.S.). The improved background suppression that is needed for such a measurement is achieved by an event classification with the “Random Forest” algorithm based on decision trees.

Introduction

Cosmic ray electrons are with about 1% of the flux in the GeV range a small but peculiar fraction of cosmic rays. In contrast to hadronic cosmic rays, they lose their energy rapidly via inverse Compton scattering and synchrotron radiation leading to a steep spectrum following a power law $dN/dE \propto E^{-\Gamma}$ with spectral index $\Gamma \approx 3.3$, which is observed in the GeV range by various balloon and satellite experiments as shown in Fig. 1. Furthermore, at high energies, the energy of the electron limits its lifetime, $t \propto 1/E$, and hence its propagation distance. Therefore, at TeV energies, distinct features of single nearby sources can be expected in the electron spectrum [2][12]. At these energies, however, no measurements exist, as the rapidly declining electron flux calls for larger detector areas than balloon and satellite experiments can provide. Thus, while interesting theoretical predictions for the TeV range of the spectrum exist, it has been impossible so far to measure.

J. Nishimura proposed an alternative approach using imaging atmospheric Cherenkov telescopes (IACTs) [13]. They use the earth’s atmosphere as detector and therefore provide an order of 10^5

larger collection areas. Designed for the measurement of γ -rays, they can be used to study cosmic ray electrons, which, like γ -rays, produce electromagnetic showers. The High Energy Stereoscopic System (H.E.S.S.) is an array of four imaging atmospheric Cherenkov telescopes in the Khomas highlands in Namibia [11]. Its sensitivity and its large field of view make such a measurement of cosmic ray electrons in the TeV range now possible.

Measuring cosmic ray electrons with H.E.S.S.

For the analysis of cosmic ray electrons, all data that were taken by the complete four telescope array, targeting extragalactic fields to avoid contamination of diffuse γ -ray emission from the galactic plane, were used. Any known or potential γ -ray source was excluded.

While the big advantage of IACTs is their large collection area, the challenge that is posed by such a cosmic ray electron measurement is the discrimination of the electrons from the much more numerous hadronic background. Therefore, a sophis-

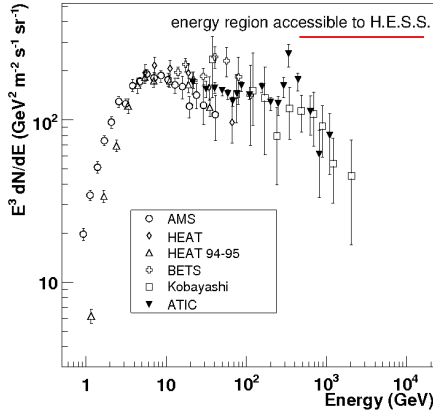


Figure 1: The electron spectrum measured with balloon and satellite experiments. Data are taken from [1][3][8][6][15]. The energy region accessible to H.E.S.S. with sufficient statistics, assuming a spectral index of 3.3, is indicated by the red bar. Systematic effects may limit the results.

ticated machine learning algorithm was chosen to separate electron and hadron events. The “Random Forest” program [5][4] is based on decision trees and was trained using Monte Carlo simulations of electrons and off-source data. The input parameters for the training contain camera image information like the width and length of the elliptical image scaled to the expected width and length defined by simulations, and intensity information. Only those events are used that triggered all four telescopes in order to assure that only the best measured events are chosen for analysis. As the input parameters are partially energy dependent, an improved performance was achieved by training in five energy bands. The zenith angle dependence was taken into account by restricting the data set to zenith angles smaller than 28° , thus approximately matching the simulations at 20° .

The Random Forest converts the input parameters into an output ζ between zero and one, denoting the electron-likeness of the respective event. A large ζ represents an electron-like event, while $\zeta = 0$ stands for background events. The Random Forest method allows for an improved background rejection shown in Fig. 2. Only about 0.5 – 2.0%, depending on energy, of all proton events passing

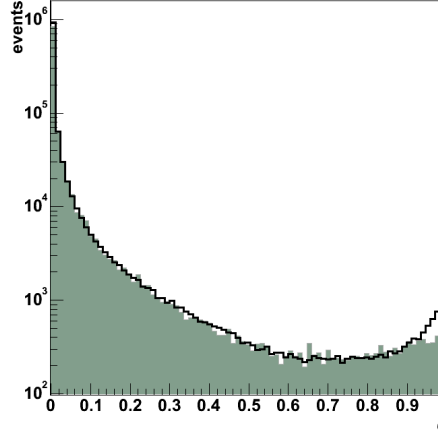


Figure 2: The distribution of the Random Forest output ζ for data with energy 0.4-1.0 TeV (solid line) and background simulation consisting of contributions from protons, helium, nitrogen, silicon and iron. A clear excess of electron events can be seen at higher values of ζ that cannot be explained by background simulations.

the four-telescope cut end up in the electron signal region of $\zeta > 0.6$. This large suppression of hadronic background events makes a measurement of cosmic ray electrons possible in the first place. In Fig. 2 the ζ distribution of data is shown together with a Monte Carlo simulation of the background, showing the good agreement at low values of ζ and a clear signal of an electromagnetic showers at $\zeta = 1$.

In order to estimate the remaining background and extract the number of electrons from the data, simulated electrons and protons are fitted to the data in the ζ distribution. The simulations are produced using CORSIKA [10] with SIBYLL as hadronic interaction model [9]. Modeling the background with simulated protons only is possible because heavier nuclei contained in the hadronic background show an even better classification power than protons and therefore, background in the signal region is completely dominated by protons. This method of fitting electron and proton simulations to the data is demonstrated in Fig. 3 exemplarily for the energy between 0.7 and 1.0 TeV. A good match between data and electron-proton combination is observed.

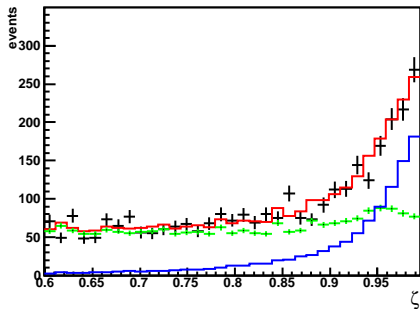


Figure 3: The distribution of ζ in the signal region of $\zeta > 0.6$ for data (black) with a reconstructed energy between 0.7 and 1 TeV and the fitted proton (green) and electron (blue) simulations in this energy range. The best fit model of electrons and protons is shown in red.

This method has the potential to extend the spectrum of cosmic ray electrons to energies of several TeV. While statistical errors are small compared to direct measurements, systematic effects have to be taken into account. Prime source of systematic uncertainties is the usage of proton simulations to model the data. To quantify this effect, two different hadronic interaction models, SIBYLL [9] and QGSJET [14] are compared. Additionally, confusion with γ -rays might occur as γ -rays and electrons produce very similar air showers in the atmosphere. They can be separated on a statistical basis by the height of their shower maximum X_{max} , which occurs half a radiation length higher in the atmosphere for electrons than for γ -rays. As X_{max} is not measured precisely enough, a contribution of extragalactic γ -rays can experimentally not be excluded. However, theoretical predictions for diffuse extragalactic γ -ray flux lie far below the electron flux [7].

Ongoing work concerns the in-depth study of systematic errors and model-dependence of the results with the goal to derive a reliable electron spectrum.

Conclusion

For the first time, cosmic ray electrons have been measured with IACTs. A clear signal of electrons can be seen in the H.E.S.S. data. Therefore, IACTs seem to be able to extend the measured spectrum

of cosmic ray electrons into the TeV range, where the shape of the spectrum is completely unknown, but expected to give information on the existence of nearby cosmic ray accelerators.

References

- [1] M. Aguilar, J. Alcaraz, J. Allaby, B. Alpat, G. Ambrosi, and H. Anderhub. The Alpha Magnetic Spectrometer (AMS) on the International Space Station: Part I - results from the test flight on the space shuttle. *Physics Reports*, 366:331–405, 2002.
- [2] F. A. Aharonian, A. M. Atoyan, and H. J. Völk. High energy electrons and positrons in cosmic rays as an indicator of the existence of a nearby cosmic tevatron. *Astron. & Astrophys.*, 294:L41–L44, 1995.
- [3] S. W. Barwick, J. J. Beatty, C. R. Bower, C. J. Chaput, S. Coutu, G. A. de Nolfo, M. A. Duvernois, D. Ellithorpe, D. Ficenec, J. Knapp, D. M. Lowder, S. McKee, D. Mueller, J. A. Musser, S. L. Nutter, E. Schneider, S. P. Swordy, G. Tarle, A. D. Tomasch, and E. Torbet. The Energy Spectra and Relative Abundances of Electrons and Positrons in the Galactic Cosmic Radiation. *Astrophys. J.*, 498:779–789, May 1998.
- [4] R. K. Bock, A. Chilingarian, M. Gaug, F. Hakl, T. Hengstebeck, M. Jirina, J. Klaschka, E. Kotrc, P. Savicky, S. Towers, A. Vaiciulis, and W. Wittek. Methods for multidimensional event classification: a case study using images from a Cherenkov gamma-ray telescope. *NIM A 516*, 2-3:511–528, 2004.
- [5] L. Breiman and A. Cutler. <http://www.stat.berkeley.edu/users/breiman/RandomForests/>.
- [6] J. Chang and et al. The Electron Spectrum above 20 GeV Measured by ATIC-2. In *International Cosmic Ray Conference*, volume 3 of *International Cosmic Ray Conference*, page 1, 2005.
- [7] P. S. Coppi and F. A. Aharonian. Constraints on the Very High Energy Emissivity of the Universe from the Diffuse GeV Gamma-Ray Background. *Astrophys. J.*, 487:L9+, September 1997.

- [8] M. A. DuVernois, S. W. Barwick, J. J. Beatty, A. Bhattacharyya, C. R. Bower, C. J. Chaput, S. Coutu, G. A. de Nolfo, D. M. Lowder, S. McKee, D. Müller, J. A. Musser, S. L. Nutter, E. Schneider, S. P. Swordy, G. Tarlé, A. D. Tomasch, and E. Torbet. Cosmic-Ray Electrons and Positrons from 1 to 100 GeV: Measurements with HEAT and Their Interpretation. *Astrophys. J.*, 559:296–303, September 2001.
- [9] R. S. Fletcher, T. K. Gaisser, P. Lipari, and T. Stanev. Sibyll: An event generator for simulation of high energy cosmic ray cascades. *Physical Review D*, 50:5710–5731, November 1994.
- [10] D. Heck, J. Knapp, J.N. Capdevielle, and T. Thouw. CORSIKA: A Monte Carlo Code to Simulate Extensive Air Showers. *Forschungszentrum Karlsruhe Report, FZKA 6019*, 1998.
- [11] J. A. Hinton (H.E.S.S. Collaboration). The status of the HESS project. *New Astronomy Review*, 48:331–337, April 2004.
- [12] T. Kobayashi, Y. Komori, K. Yoshida, and J. Nishimura. The Most Likely Sources of High-Energy Cosmic-Ray Electrons in Supernova Remnants. *Astrophys. J.*, 601:340–351, January 2004.
- [13] J. Nishimura. Opening talk for the meeting of the TeV gamma rays, Proc. *Towards a Major Cherenkov Detector III. Universal Academy Press, Tokyo*, pages 1–10, 1994.
- [14] S. Ostapchenko, T. Thouw, and K. Werner. On the Semihard Hadronic Interactions in Extensive Air Shower. *Nuclear Physics B Proceedings Supplements*, 52:113–115, February 1997.
- [15] S. Torii, T. Tamura, N. Tateyama, K. Yoshida, J. Nishimura, T. Yamagami, H. Murakami, T. Kobayashi, Y. Komori, K. Kasahara, and T. Yuda. The Energy Spectrum of Cosmic-Ray Electrons from 10 to 100 GeV Observed with a Highly Granulated Imaging Calorimeter. *Astrophys. J.*, 559:973–984, October 2001.



H.E.S.S. observations of galaxy clusters

W. DOMAINKO¹, W. BENBOW¹, J. A. HINTON², O. MARTINEAU-HUYNH³, M. DE NAUROIS³, D. NEDBAL⁴, G. PEDALETTI⁵, G. ROWELL⁶ FOR THE H.E.S.S. COLLABORATION.

¹*Max-Planck-Institut für Kernphysik, Heidelberg, Germany*

²*School of Physics & Astronomy University of Leeds, UK*

³*Laboratoire de Physique Nucléaire et de Hautes Energies, Universités Paris VI & VII, France*

⁴*Institute of Particle and Nuclear Physics, Charles University, Prague, Czech Republic*

⁵*Landessternwarte, Universität Heidelberg, Germany*

⁶*School of Chemistry & Physics, University of Adelaide, Australia*

wilfried.domainko@mpi-hd.mpg.de

Abstract: Clusters of galaxies, the largest gravitationally bound objects in the universe, are expected to contain a significant population of hadronic and leptonic cosmic rays. Potential sources for these particles are merger and accretion shocks, starburst driven galactic winds and radio galaxies. Furthermore, since galaxy clusters confine cosmic ray protons up to energies of at least 1 PeV for a time longer than the Hubble time they act as storehouses and accumulate all the hadronic particles which are accelerated within them. Consequently clusters of galaxies are potential sources of VHE (> 100 GeV) gamma rays. Motivated by these considerations, promising galaxy clusters are observed with the H.E.S.S. experiment as part of an ongoing campaign. Here, upper limits for the VHE gamma ray emission for the Abell 496 and Coma cluster systems are reported.

Introduction

Galaxy clusters are the largest non-thermal sources in the universe. Radio [20], [15] and hard X-ray [29], [16] observations show the presence of accelerated electrons in these systems. It is understood that hadronic cosmic rays accelerated within the cluster volume will be confined there (with energies of up to 10^{15} eV) for timescales longer than the Hubble time [32], [7]. Hence clusters of galaxies act as storehouses for such particles, and therefore a large component of cosmic rays is expected in these systems.

Several sources of cosmic rays can be found in galaxy clusters. Accretion and merger shocks driven by large-scale structure formation have the ability to accelerate cosmic rays [10], [23], [31]. Supernova remnant shocks and galactic winds can also produce high-energy particles [32]. Additionally AGN outbursts can distribute non-thermal particles in the cluster volume [13], [1], [22].

Due to the expected large component of non-thermal particles, galaxy clusters are potential sources for gamma-ray emission (see [8] for a recent review). Various processes can lead to the production of gamma-ray radiation in these objects. Inelastic collisions between cosmic ray protons and thermal nuclei from the intra-cluster medium (ICM) will lead to gamma-ray emission through π^0 -decay [11], [32]. Electrons with sufficiently high energies can up-scatter cosmic microwave background (CMB) photons to the gamma-ray range in inverse Compton processes [5], [17], [18]. Despite the arguments for potential gamma-ray emission given above, no galaxy cluster has firmly been established as a source of high-energy and very high-energy electromagnetic radiation [27], [26].

The H.E.S.S. experiment

The H.E.S.S. experiment is an array of imaging atmospheric Cherenkov telescopes located in the

Khomas highlands, Namibia [21]. It observes in the VHE gamma-ray regime and has a field of view of $\sim 5^\circ$. Due to the large field of view it is possible to detect extended sources such as supernova remnants [2], [3]. Galaxy clusters are expected to feature extended VHE gamma-ray emission. The H.E.S.S. experiment is well suited to search for such a signal (see e.g. [2]).

Targets

Abell 496

Abell 496 is a nearby ($z = 0.033$), relaxed cluster of galaxies with a mean temperature of 4.7 keV. It features a cooling core at its center [24]. It is located in the Southern Hemisphere [9] and is therefore well suited for observations with H.E.S.S. Data taking was performed during moonless nights in the time period from October to December 2005, and in October 2006. In total 23.4 hours of data were taken, with 15.9 hours passing standard data-quality selection (live time 14.6 hours). The mean zenith angle is 27.6° which results in an energy threshold of 0.31 TeV for standard cuts and 0.57 TeV for hard cuts. H.E.S.S. standard data analysis (described in [6]) was performed using different geometrical size cuts to account for the extended nature of the target. No significant excess of VHE gamma-ray emission is found at the position of Abell 496 (see Fig. 1). Upper limits for this object for two different size cuts are derived. All upper limits are obtained following [14] assuming a power law spectral index of -2.1 and are given at the 99.9% confidence level. The first radial size cut, 0.1° , is applied to test gamma-ray emission associated with the high density core region of the cluster. This is of particular interest for a hadronic scenario, since the gamma-ray emission should be enhanced in regions with higher density of target material. In this region an upper limit of $F_{UL}(> 0.31 \text{ TeV}) = 1.0 \times 10^{-12} \text{ ph cm}^{-2} \text{ s}^{-1}$ (0.8% Crab flux) is determined. A radial size cut of 0.6° is also applied, which covers the entire cluster [28]. For this extended region an upper limit of $F_{UL}(> 0.57 \text{ TeV}) = 2.4 \times 10^{-12} \text{ ph cm}^{-2} \text{ s}^{-1}$ (4.5% Crab flux) is found. It should be noted that the H.E.S.S. upper limits scale approximately with r/r_0 with r and r_0 being geometrical size cuts and

this relation can be used to convert the presented upper limits to other sizes.

Coma cluster

The Coma cluster is a prominent hot ($T = 8.25 \text{ keV}$, [4]), nearby ($z = 0.023$) galaxy cluster which shows a merger signature in the X-ray gas ([25]). It features a hard X-ray excess ([29], [16] but see [30] for a different interpretation) and a radio halo [19]. The Coma cluster is often considered as a "standard cluster", and, due to the wealth of data on this object, it is very important for theoretical interpretations. It is located in the Northern Hemisphere which makes it less accessible for H.E.S.S. This cluster was observed during moonless nights in April and May 2006. 7.9 hours of good data were obtained resulting in 7.3 hours live time. The mean zenith angle of these observation is 53.5° which results in an energy threshold of 1.0 TeV for standard cuts and 2.0 TeV for hard cuts. No significant signal is found in these observations using various geometrical size cuts (see Fig. 2). Upper limits on the VHE gamma ray emission of the Coma cluster for the core region and for the entire cluster are derived. Applying a radial size cut of 0.2° (core region) an upper limit of $F_{UL}(> 1.0 \text{ TeV}) = 8.3 \times 10^{-13} \text{ ph cm}^{-2} \text{ s}^{-1}$ (3.7% Crab flux) is found. For the entire cluster, with a radial size cut of 1.4° , an upper limit of $F_{UL}(> 2.0 \text{ TeV}) = 4.8 \times 10^{-12} \text{ ph cm}^{-2} \text{ s}^{-1}$ (65.6% Crab flux) is obtained. For the latter, very extended analysis, only data with a live time of 6.4 hours are used due to an insufficient number of OFF-source runs with such a large zenith angle for the background estimation.

Summary & outlook

Clusters of galaxies are the most massive gravitationally bound structures in the universe and as such they are believed to be representatives for the universe as a whole. Therefore they are important tools for cosmology. The detection of gamma-ray emission from these objects will give important information about structure formation and supernova activity over the entire history of the universe. No gamma-ray excess has been found with H.E.S.S. from any cluster, with observation times in the range of 10 – 20 hours. As a next step, one

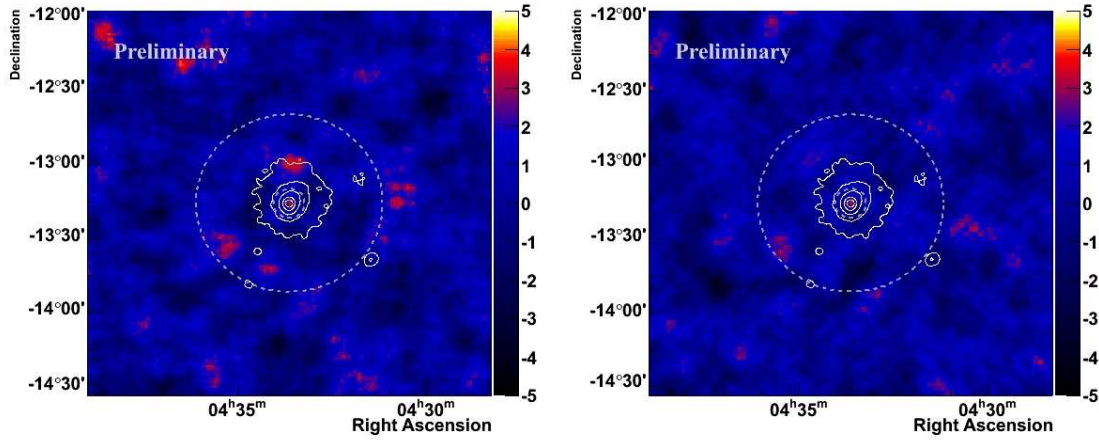


Figure 1: Significance map of the cluster Abell 496 seen by H.E.S.S. with standard cuts (left panel) and hard cuts (right panel). No signal is detected from this region of the sky. The dashed circles show the two size cuts and the white contours correspond to *ROSAT* X-ray contours [12].

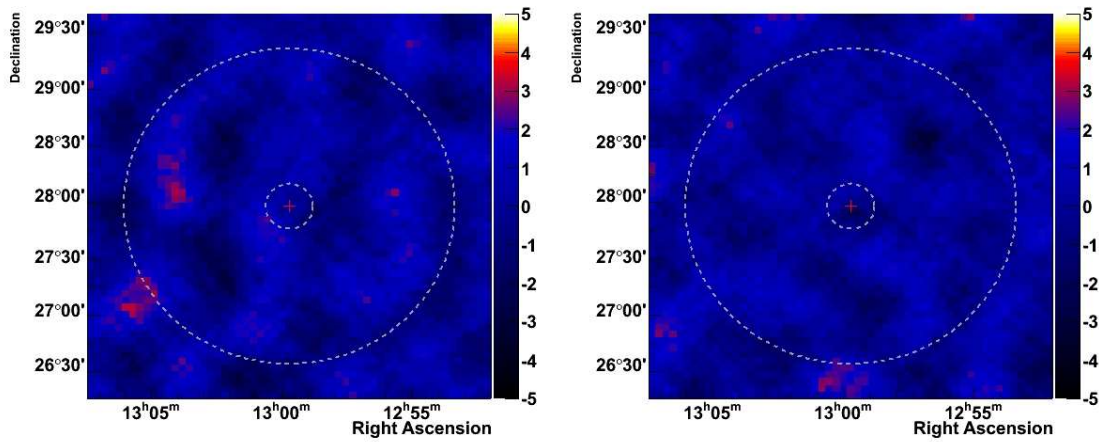


Figure 2: Significance map with standard cuts (left) and hard cuts (right) of the Coma cluster. No signal is found in the data. The two dashed circles correspond to the two size cuts.

promising galaxy cluster will be given a very deep H.E.S.S. exposure of at least 50 hours.

Acknowledgments

The support of the Namibian authorities and of the University of Namibia in facilitating the construction and operation of H.E.S.S. is gratefully acknowledged, as is the support by the German Ministry for Education and Research (BMBF), the Max Planck Society, the French Ministry for Research, the CNRS-IN2P3 and the Astroparticle Interdisciplinary Programme of the CNRS, the U.K. Science and Technology Facilities Council (STFC), the IPNP of the Charles University, the Polish Ministry of Science and Higher Education, the South African Department of Science and Technology and National Research Foundation, and by the University of Namibia. We appreciate the excellent work of the technical support staff in Berlin, Durham, Hamburg, Heidelberg, Palaiseau, Paris, Saclay, and in Namibia in the construction and operation of the equipment.

References

- [1] Aharonian, F. A. 2002, MNRAS, 332, 215
- [2] Aharonian, F. A., Akhperjanian, A. G., Aye, K.-M. et al. 2004, Nature, 432, 75
- [3] Aharonian, F., Akhperjanian, A. G., Bazer-Bachi, A. R. et al. 2007, ApJ, 661, 236
- [4] Arnaud, M., Aghanim, N., Gastaud, R., et al. 2001, A&A, 365, L67
- [5] Atoyan, A. M. & Völk, H. J. 2000, ApJ, 535, 45
- [6] Benbow, W. 2005 in Towards a Network of Atmospheric Cherenkov Detectors VII ed. B. Degrange & G Fontain (Palaiseau: Ecole Polytechnique), 163
- [7] Berezhinsky, V. S., Blasi, P. & Ptuskin, V. S. 1997, ApJ, 487, 529
- [8] Blasi, P., Gabici, S. & Brunetti, G. 2007, Int.J.Mod.Phys. A22, 681
- [9] Böhringer, H., Schuecker, P., Guzzo, L., et al. 2004, A&A, 425, 367
- [10] Colafrancesco, S. & Blasi, P. 1998, APh, 9, 227
- [11] Dennison, B. 1980, ApJ, 239, L93
- [12] Durret, F., Adami, C., Gerbal, D. & Pislak, V. 2000, A&A, 356, 815
- [13] EnSS 2883lin, T. A., Biermann, P. L., Kronberg, P. P. & Wu, X.-P. 1997, ApJ, 477, 560
- [14] Feldman, G. J. & Cousins, R. D. 1998, Phys. Rev. D, 57, 3873
- [15] Feretti, L., Brunetti, G., Giovannini, G., et al. 2004, JKAS, 37, 315
- [16] Fusco-Femiano, R. Orlandini, M., Brunetti, G., et al. 2004, ApJ, 602, 73
- [17] Gabici, S. & Blasi, P. 2003, APh, 19, 679
- [18] Gabici, S. & Blasi, P. 2004, APh, 20, 579
- [19] Giovannini, G., Feretti, L., Venturi, T., Kim, K.-T. & Kronberg, P. P. 1993, ApJ, 406, 399
- [20] Giovannini, G. & Feretti, L. 2000, NewA, 5, 335
- [21] Hinton, J. A., 2004, New Astron. Rev., 48, 331
- [22] Hinton, J. A., Domainko, W. & Pope, E. C. D. 2007, MNRAS submitted, astro-ph/0701033
- [23] Loeb, A. & Waxman, E. 2000, Nature, 405, 156
- [24] Markevitch, M., Vikhlinin, A., Forman, W. R. & Sarazin, C. L. 1999, ApJ, 527, 545
- [25] Neumann, D. M., Lumb, D. H., Pratt, G. W. & Briel, U. G. 2003, A&A, 400, 811
- [26] Perkins, J. S., Badran, H. M., Blaylock, G., et al. 2006, ApJ, 644, 148
- [27] Reimer, O., Pohl, M., Sreekumar, P. & Mattox, J. R. 2003, ApJ, 588, 155
- [28] Reiprich, T. H. & Böhringer, H. 2002, ApJ, 567, 716
- [29] Rephaeli, Y. & Gruber, D. 2002, ApJ, 597, 587
- [30] Rossetti, M. & Molendi, S. 2004, A&A, 414, L41
- [31] Ryu, D., Kang, H., Hallman, E. & Jones, T. W. 2003, ApJ, 593, 599
- [32] Völk, H. J., Aharonian, F. A., Breitschwerdt, D. 1996, SSRv, 75, 279



VHE γ -ray observations of starburst galaxies with H.E.S.S.

D. NEDBAL¹, W. BENBOW², K. BERNLÖHR^{2,3}, J. HINTON⁴, M. LEMOINE-GOUMARD⁵ FOR THE H.E.S.S. COLLABORATION.

¹*Institute of Particle and Nuclear Physics, Charles University, V Holesovickach 2, 180 00, Prague 8, Czech Republic*

²*Max-Planck-Institut für Kernphysik, P.O. Box 103980, D 69029 Heidelberg, Germany*

³*Institut für Physik, Humboldt-Universität zu Berlin, Newtonstr. 15, D 12489 Berlin, Germany*

⁴*School of Physics and Astronomy, University of Leeds, U.K.*

⁵*CENBG - CNRS - IN2P3, France*

nedbal@ipnp.troja.mff.cuni.cz

Abstract: Starburst galaxies are characterized by extremely high star-formation rates and, as a consequence, very high supernova rates. These rates, as well as the gas density, are orders of magnitude higher than in the Milky Way. Starburst galaxies contain both a high cosmic-ray flux and high density of target material for proton-proton and inverse-Compton interactions. These objects are therefore viable candidates for observable levels of VHE γ -ray emission. Nearby starburst galaxies, such as NGC 253 and M83, allow a study of general processes during galaxy formation and evolution of high redshift galaxies. These two galaxies were observed with H.E.S.S. stereoscopic array of atmospheric-Cherenkov telescopes. Upper limits from these observations are presented here.

Introduction

Starburst galaxies are galaxies with very intense star formation rate in the central region. The starburst activity could be triggered by mechanisms such as a galaxy merger, causing compression of the interstellar gas. Consequent high star formation is responsible for a high supernovae explosion rate in this region. Supernovae then provide shocks necessary for accelerating cosmic-ray particles.

Detectable levels of VHE γ -ray emission are predicted for starburst galaxies such as M82 [14] and NGC 253 [1], [6]. Gas densities in the starburst regions reach values 100 times larger than in the Milky Way. Such high densities provide enough target material for inelastic proton-proton collisions of cosmic-ray protons. Resulting π^0 mesons decay into high energetic γ -ray photons, that can be detected by earthbound Cherenkov imaging telescopes.

Despite encouraging predictions no significant detection of VHE γ -rays has been confirmed from starburst galaxies so far.

Results of M83 observations and re-observations of NGC 253 with the full array of four H.E.S.S. telescopes are presented here.

H.E.S.S. experiment

The H.E.S.S. Collaboration operates an array of four imaging atmospheric-Cherenkov telescopes (IACTs), located in Namibia. Each telescope has 107 m² mirror area and a camera consisting of 960 pixels providing a wide field-of-view of 5°. Images of γ -ray showers are analysed in order to reconstruct the direction and energy of the primary γ photon. Background suppression is based on a system of cuts on the image parameters (e.g. width). All results presented here are obtained using the standard Hillas-based H.E.S.S. analysis. For further details see [2]. All upper limits are calculated assuming a power-law spectrum with the photon index $\Gamma = 2.1$ of the γ rays, at the 99.9% confidence level (CL) [7]. Not included in the upper limits is a 20% systematic error on flux.

Observed targets

NGC 253

NGC 253 is the closest ($D \sim 2.5$ Mpc [5]) starburst galaxy viewed edge-on. It is considered to be, along with M 82, an archetypal starburst galaxy [12].

The object is very well studied in all wavelengths from radio to X-rays. Chandra X-ray observations [15] show, that the central region of size ~ 100 pc exhibits very intense starburst activity. The central region is surrounded by a torus of dense gas collimating a galactic wind driven by the starburst [11]. NGC 253 is suggested as a possible source of detectable VHE γ -ray flux (see for example [6]).

Several instruments have already published upper limits on γ -ray emission from NGC 253. CANGAROO III published results of 12.5 hours on-source observations [10]. The outcome was a 2σ upper limit of 3.4×10^{-12} ph. cm $^{-2}$ s $^{-1}$ above 450 GeV, corresponding to 4.5% of Crab flux. H.E.S.S. observed NGC 253 for 24.6 hours with 2 telescopes and for 3.4 hours using 3 telescopes. The result was an upper limit of 1.9×10^{-12} ph. cm $^{-2}$ s $^{-1}$ above 300 GeV (1.4% of Crab flux using Crab spectrum of [2]) at 99% CL. [1]. Upper limits were also determined by the HEGRA experiment [8] at 11% Crab units at 99% CL. EGRET set an upper limit at lower energies of $F(> 100\text{MeV}) < 3.4 \times 10^{-8}$ ph. cm $^{-2}$ s $^{-1}$ [3].

H.E.S.S. observed NGC 253 in several campaigns during 2003 and 2005. The total live time used for analysis (after applying current data selection criteria) is 21.3 hours taken with only two telescopes and 14.2 hours performed using the full array of four telescopes.

No VHE significant signal is found. The angular distribution of on-source and off-source events shows no hint of a γ -ray excess (see Figure 1) from the NGC 253 region. The 99.9% upper limit on the integral flux is $I_{\text{ul}}(> 270\text{GeV}) = 1.2 \times 10^{-12}$ ph. cm $^{-2}$ s $^{-1}$, corresponding to 0.7% of the Crab Nebula flux. The upper limits are considerably lower than all the previously published limits [1], [10].

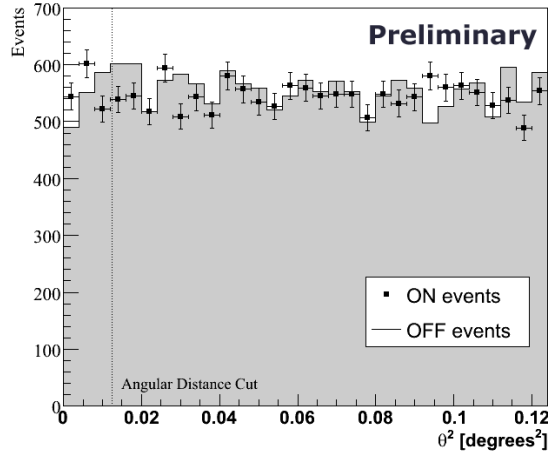


Figure 1: Angular distribution of on-source and off-source events of the H.E.S.S. observations of NGC 253

M 83

M83 is a nearly face-on spiral galaxy with high metallicity around twice the solar value [4]. The central ~ 300 pc is shown to host a starburst nucleus [9]. M83 is slightly further away ($D \sim 4.5$ Mpc [13]) and the FIR flux is also lower than in the case of NGC 253. This makes M83 a slightly worse VHE candidate with respect to NGC 253. On the other hand, M83 does not show any sign of a galactic wind, contrary to NGC 253. The convective losses of high-energy cosmic rays may thus be considerably lower than in the case of NGC 253, implying a detectable γ -ray flux as well.

M83 was observed by H.E.S.S. in July 2006. The total live time used for analysis is 8.2 hours of good-quality data. No significant VHE γ -ray emission is found. The angular distribution of on-source and off-source events (see Figure 2) does not show any hint of an excess. The resulting upper limit on the integral flux is $I(> 330\text{GeV}) = 2.2 \times 10^{-12}$ cm $^{-2}$ s $^{-1}$ at the 99.9% confidence level. These are the first VHE γ -ray upper limits to be presented for M83. The integral flux upper limits are also shown in the Figure 2.

In addition, no other significant signal is found in the field-of-view of M83.

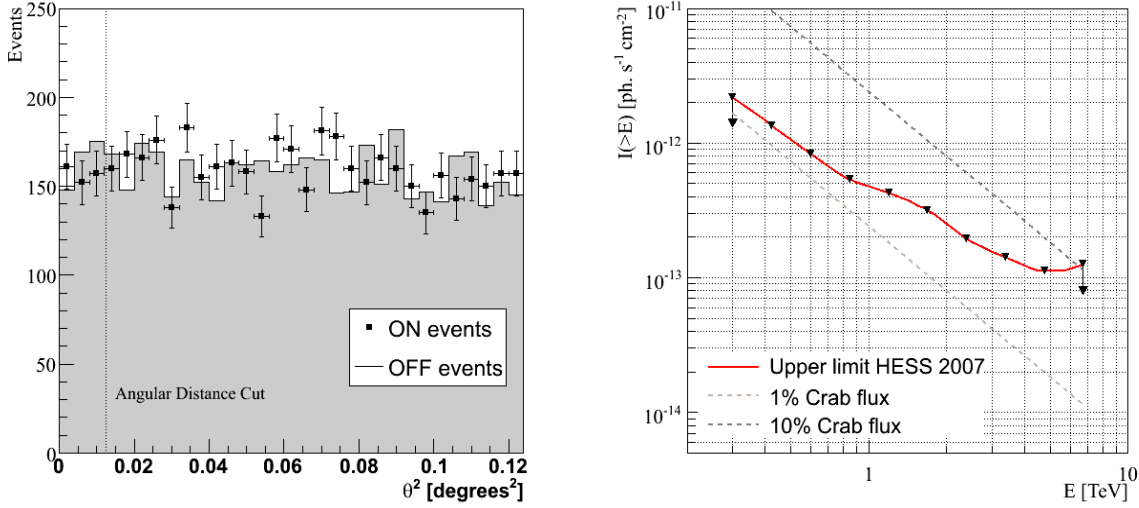


Figure 2: Left panel: Angular distribution of on-source and off-source events for M83. Right panel: Upper limit on the M83 integral flux above the energy, E . The H.E.S.S. results are compared to 1% and 10% of Crab integral flux according to [2].

Summary and conclusions

No significant VHE γ -ray signal was found in the H.E.S.S. follow-up observations of NGC 253 or in the observations of M83. Upper limits from these observations are presented. These limits are already very close to the theoretical predictions. Since there is only limited space for uncertainties in the flux-prediction models, the detection of starburst galaxies by the current or future generation of γ -ray experiments seems to be inevitable. Starburst galaxies thus remain very good candidates for future observations.

Acknowledgements

The support of the Namibian authorities and of the University of Namibia in facilitating the construction and operation of H.E.S.S. is gratefully acknowledged, as is the support by the German Ministry for Education and Research (BMBF), the Max Planck Society, the French Ministry for Research, the CNRS-IN2P3 and the Astroparticle Interdisciplinary Programme of the CNRS, the U.K. Science and Technology Facilities Council (STFC),

the IPNP of the Charles University, the Polish Ministry of Science and Higher Education, the South African Department of Science and Technology and National Research Foundation, and by the University of Namibia. We appreciate the excellent work of the technical support staff in Berlin, Durham, Hamburg, Heidelberg, Palaiseau, Paris, Saclay, and in Namibia in the construction and operation of the equipment.

References

- [1] F. Aharonian et al. A search for very high energy gamma-ray emission from the starburst galaxy NGC 253 with HESS. *A&A*, 442:177–183, 2005.
- [2] F. Aharonian et al. Observations of the Crab nebula with HESS. *A&A*, 457:899–915, October 2006.
- [3] J. J. Blom, T. A. D. Paglione, and A. Carrañana. Diffuse Gamma-Ray Emission from Starburst Galaxies and M31. *ApJ*, 516:744–749, May 1999.
- [4] F. Bresolin and R. C. Kennicutt, Jr. Optical Spectroscopy of Metal-rich H II Regions and

- Circumnuclear Hot Spots in M83 and NGC 3351. *ApJ*, 572:838–860, June 2002.
- [5] G. de Vaucouleurs. The extragalactic distance scale. IV - Distances of nearest groups and field galaxies from secondary indicators. *ApJ*, 224:710–717, September 1978.
- [6] E. Domingo-Santamaría and D. F. Torres. High energy γ -ray emission from the starburst nucleus of NGC 253. *A&A*, 444:403–415, December 2005.
- [7] G. J. Feldman and R. D. Cousins. Unified approach to the classical statistical analysis of small signals. *Phys. Rev. D*, 57:3873–3889, April 1998.
- [8] N. Götting. Nachweis von tev- γ -strahlung aus der richtung der blazare h 1426+428 und 1es 1959+650 sowie der radiogalaxie m 87 mit den hegra-cherenkov-teleskopen. *PhD Thesis, Universität Hamburg*, 2007.
- [9] J. Harris, D. Calzetti, J. S. Gallagher, III, C. J. Conselice, and D. A. Smith. Young Clusters in the Nuclear Starburst of M83. *AJ*, 122:3046–3064, December 2001.
- [10] C. Itoh et al. Evidence of TeV gamma-ray emission from the nearby starburst galaxy NGC 253. *A&A*, 462:67–71, January 2007.
- [11] P. J. McCarthy, W. van Breugel, and T. Heckman. Evidence for large-scale winds from starburst galaxies. I - The nature of the ionized gas in M82 and NGC 253. *Astronomical Journal*, 93:264–275, February 1987.
- [12] G. H. Rieke et al. The nature of the nuclear sources in M82 and NGC 253. *ApJ*, 238:24–40, May 1980.
- [13] F. Thim et al. The Cepheid Distance to NGC 5236 (M83) with the ESO Very Large Telescope. *ApJ*, 590:256–270, June 2003.
- [14] H. J. Völk, F. A. Aharonian, and D. Breitschwerdt. The Nonthermal Energy Content and Gamma-Ray Emission of Starburst Galaxies and Clusters of Galaxies. *Space Science Reviews*, 75:279–297, January 1996.
- [15] K. A. Weaver, T. M. Heckman, D. K. Strickland, and M. Dahlem. Chandra Observations of the Evolving Core of the Starburst Galaxy NGC 253. *ApJL*, 576:L19–L23, September 2002.